

Triple, Mutually Orthogonal Cycloadditions Through the Design of Electronically Activated SNO-OCTs

Yun Hu, Jessica M. Roberts, Henry R. Kilgore, Amirah Mat Lani, Ronald Raines, Jennifer Schomaker

Submitted date: 22/06/2020 • Posted date: 24/06/2020

Licence: CC BY-NC-ND 4.0

Citation information: Hu, Yun; Roberts, Jessica M.; Kilgore, Henry R.; Lani, Amirah Mat; Raines, Ronald; Schomaker, Jennifer (2020): Triple, Mutually Orthogonal Cycloadditions Through the Design of Electronically Activated SNO-OCTs. ChemRxiv. Preprint. <https://doi.org/10.26434/chemrxiv.12543254.v1>

Interest in mutually exclusive pairs of bioorthogonal labeling reagents continues to drive the design of new compounds capable of fast and predictable reactions. The ability to easily modify heterocyclic strained cyclooctynes containing sulfamate backbones (SNO-OCTs) enables electronic tuning of the relative rates of reactions of SNO-OCTs in cycloadditions with Type I–III dipoles. As opposed to optimizations based on just one specific dipole class, the electrophilicity of the alkynes in SNO-OCTs can be manipulated to achieve divergent reactivities and furnish mutually orthogonal dual ligation systems. Significant rate enhancements for reactions of a difluorinated SNO-OCT derivative compared to the parent scaffold were noted, with the second-order rate constant in cycloadditions with diazoacetamides exceeding $1 \text{ M}^{-1} \text{ s}^{-1}$. Computational and experimental studies were employed to inform the design of triple ligation systems that encompass three orthogonal reactivities. Finally, polar SNO-OCTs are rapidly internalized by mammalian cells and remain functional in the cytosol for live-cell labeling, highlighting their potential for diverse in vitro and in vivo applications.

File list (4)

Triple, Mutually Orthogonal Cycloadditions Through the D... (10.98 MiB)	view on ChemRxiv • download file
Jennifer Schomaker - Triple, Mutually Orthogonal Cycload... (1.44 MiB)	view on ChemRxiv • download file
Triple, Mutually Orthogonal Cycloadditions Through the De... (1.09 MiB)	view on ChemRxiv • download file
Triple, Mutually Orthogonal Cycloadditions Through the D... (25.71 MiB)	view on ChemRxiv • download file

Triple, Mutually Orthogonal Cycloadditions Through the Design of Electronically Activated SNO-OCTs

Yun Hu,^{†,‡} Jessica M. Roberts,^{†,‡} Henry R. Kilgore,^{§,†} Amirah S. Mat Lani,[†] Ronald T. Raines,^{*,§} and Jennifer M. Schomaker^{*,†}

¹Department of Chemistry, University of Wisconsin, Madison, Wisconsin 53706, United States

²Department of Chemistry, Massachusetts Institute of Technology, Cambridge, Massachusetts 02139, United States

ABSTRACT: Interest in mutually exclusive pairs of bioorthogonal labeling reagents continues to drive the design of new compounds capable of fast and predictable reactions. The ability to easily modify heterocyclic strained cyclooctynes containing sulfamate backbones (SNO-OCTs) enables electronic tuning of the relative rates of reactions of SNO-OCTs in cycloadditions with Type I-III dipoles. As opposed to optimizations based on just one specific dipole class, the electrophilicity of the alkynes in SNO-OCTs can be manipulated to achieve divergent reactivities and furnish mutually orthogonal dual ligation systems. Significant rate enhancements for reactions of a difluorinated SNO-OCT derivative compared to the parent scaffold were noted, with the second-order rate constant in cycloadditions with diazoacetamides exceeding $1\text{ M}^{-1}\text{s}^{-1}$. Computational and experimental studies were employed to inform the design of triple ligation systems that encompass three orthogonal reactivities. Finally, polar SNO-OCTs are rapidly internalized by mammalian cells and remain functional in the cytosol for live-cell labeling, highlighting their potential for diverse *in vitro* and *in vivo* applications.

INTRODUCTION

Bioorthogonal chemistry represents a powerful strategy to monitor individual molecules in biological systems; indeed, within the past two decades, a multitude of reactions have been developed to fulfill this function.¹ Nonetheless, a larger challenge involves the identification of mutually orthogonal pairs of bioorthogonal reagents with the potential to simultaneously observe the behavior of multiple biomolecules in a cell.² The ready availability of convenient, inexpensive, and electronically tunable “orthogonal bioorthogonal” reagent pairs remains a topic of intense interest, as new labeling tools are critical in efforts to push the boundaries of our understanding of complex biological systems.^{2d,3}

The 1,3-dipolar cycloadditions are popular reactions in bioorthogonal chemistry, particularly strain-promoted azide-alkyne cycloadditions (SPAAC; Figure 1a).^{1c,3b,4} Bertozzi and co-workers addressed issues with the slow kinetics of unfunctionalized cyclooctynes by electronically activating the alkyne via installation of fluorine atoms at the propargyl carbon. Moving from monofluorinated (MOFO) to difluorinated alkyne (DIFO) resulted in nearly two orders of magnitude increase in the rate of reaction with BnN_3 , from 0.0043 to $0.076\text{ M}^{-1}\text{s}^{-1}$.⁵ The popular

bioorthogonal reagent DBCO utilizes benzene rings fused to the cycloalkyne to further accelerate the reaction with BnN_3 ; however, further electronic tuning of this scaffold is challenging, due to limited derivatization sites.⁶ Other reported modifications to the parent compound yield reaction rates with BnN_3 spanning less than an order of magnitude (0.31 – $0.90\text{ M}^{-1}\text{s}^{-1}$).⁷ In addition to the lack of modularity, the strain-activated nature of this alkyne leads to issues with stability and chemoselectivity, limiting opportunities to develop mutually orthogonal reactions involving DBCO derivatives.⁸

Recently, we developed a unique class of strained cycloalkynes containing S-, N-, and O-heteroatoms embedded in the ring (SNO-OCTs).⁹ Our previous kinetic studies of the sulfamate-containing SNO-OCTs **1-2** (Figure 1a) show second-order kinetic rate constants (k_2) with BnN_3 ranging from 0.0014 to $0.087\text{ M}^{-1}\text{s}^{-1}$, with polar protic solvents further enhancing the rate of **2** to $0.13\text{ M}^{-1}\text{s}^{-1}$.^{1k,9} Despite the relaxed alkyne angles and reduced ring strain in **1-2**, these SNO-OCTs exhibit a significant rate-increase for cycloadditions, comparable to strain-activated DIBONE and DBCO. Density functional theory (DFT) calculations indicated these SNO-OCTs benefit from unique electronic activation of the

alkyne *via* tailored anomeric effects and hybridization, resulting in robust stability at high pH and in the presence of glutathione.^{2b,9} Furthermore, the presence of the sulfonyl group increases the polarity in the transition state, which has been shown to enhance the rates of cycloadditions.⁹

The tunability of SNO-OCTs begs the question of whether these scaffolds can be tailored for divergent reactivity with diverse coupling partners. The Prescher group developed several mutually orthogonal dual ligation systems, particularly a series of cyclopropenes that could be sterically tuned to achieve mutually orthogonal Type I and Type III cycloadditions (Figure 1b).^{2c-d,3c} Sterically encumbered 3,3-cyclopropenes prefer nitrile imines, while shifting the bulk in 1,3-cyclopropenes favors reaction with tetrazines. Similarly, Franzini and co-workers designed sterically differentiated isonitriles, which display chemoselective reaction with various tetrazine derivatives.¹⁰ Increasing the steric bulk on the tetrazine resulted in successful dual orthogonal labeling of a protein in the presence of *trans*-cyclooctene (TCO) and DBCO. Computational analysis indicated bulky tetrazines benefit from dispersion forces that favor reaction with isonitriles. Though steric tuning has proven successful for multiple ligation systems, the ability to tune SNO-OCT alkyne electronics in a predictable manner could tailor the chemoselectivity to achieve mutual orthogonality across diverse coupling partners without rate reductions often seen with steric-driven strategies.

a. Strain-pror

Previous wc

Figure 1. Previous work and design of new mutually “orthogonal bioorthogonal” reactions for multicomponent labeling.

This paper reports on the electronic tuning of SNO-OCTs to achieve chemoselective reactions with Type I, Type II, and Type III dipoles with fast kinetics. Frontier molecular orbital (FMO) and natural bond orbital (NBO) analyses were used to rationalize how derivatization influenced alkyne electronics,¹¹ while distortion/interaction analysis shed insight into how electronics and strain impacted reactivity trends. Computational insights guided the identification of potentially orthogonal SNO-OCT/dipole pairs; for example, the electron-deficient alkyne of difluorinated SNO-OCT **3** (dF-SNO-OCT) was expected to display divergent reactivity relative to the parent **1** (Figure 1c). Successes in developing new dual and triple ligation systems highlight the versatility of SNO-OCTs for chemoselective reactions with diverse dipoles by modifying the alkyne electronics. Finally, the use of a novel triple ligation system for protein labeling is demonstrated, and the application of SNO-OCTs as efficient cell-surface visualization agents is described.

RESULTS AND DISCUSSION

Computational Methods Development to Predict SNO-OCT Cycloaddition Reaction Rates. To facilitate rational design of promising SNO-OCT

derivatives (see Figure S1), we sought to develop a computational approach capable of accurately predicting reaction rates and reactivity trends. As numerous SNO-OCT derivatizations can be envisaged, DFT calculations were needed to rapidly identify potential mutually orthogonal reactions and streamline experimental efforts. Initial computations conducted at the M06-2X level of theory¹² with a 6-311++G(d,p) basis set using Gaussian 16¹³ showed predicted rates that deviated significantly from experimental values (Table 1). For example, previous studies showed that **1** reacts with BnN₃ in CH₃CN with $k_2 = 2.60 \times 10^{-2} \text{ M}^{-1}\text{s}^{-1}$ (Table 1, entry 1); however, DFT calculations predicted a k_2 value that was ~3 orders of magnitude lower, at $6.21 \times 10^{-5} \text{ M}^{-1}\text{s}^{-1}$. M06-2X has been previously shown to overestimate activation barriers, with Houk applying a correction factor to computed values to bring them into better quantitative agreement.¹⁴ Unfortunately, this correction factor is based on experimental second-order rate constants for similar cycloadditions; because our goal was to utilize computational methods to predict relative rates of derivatized SNO-OCT scaffolds, a different level of theory was required. Zuilhof also reported that M06-2X overestimates activation barriers in strain-promoted oxidation-controlled quinone (SPOCQ) cycloadditions and found that switching to the B97D functional gave calculated rates that aligned better with experimental data.¹⁵ SNO-OCT rates were calculated at the B97D level of theory using a Conductor-like Polarizable Continuum Model for the solvent (see the SI for details).¹⁶ B97D improved the agreement between computed and experimental k_2 values (within ~1 order of magnitude) and gave more accurate k_{rel} ratios for the experimental:predicted rates in reactions of **1/4:2** with the corresponding azides. In contrast, calculations at the M06-2X level of theory predict a slower rate of reaction for **2** with BnN₃ as compared to **4** (Table 1, entry 2), which is not manifested experimentally. Thus, the B97D functional furnishes calculated rates that are much more predictive of experimental values than does M06-2X. Accordingly, further computational analyses were conducted utilizing the B97D level of theory to predict potential mutual orthogonality of SNO-OCT derivatives.

Table 1. Experimental and calculated k_2 values for cycloadditions of SNO-OCTs with alkyl azides.

entry	R ¹ R ²	Experimental ^a		R ¹ R ²	Calculated				
		rate (M ⁻¹ s ⁻¹)	k_{rel}		M06-2X ^b		B97D ^c		
					rate (M ⁻¹ s ⁻¹)	k_{rel}	rate (M ⁻¹ s ⁻¹)	k_{rel}	
1	C ₆ H ₁₁ (1) CH ₂ Ph	0.0260	1.00	Me (4) Me	6.21×10^{-5} (5.88×10^{-5})	1.00	0.00407 (0.00395)	1.00	
2	CH ₂ OH (2) CH ₂ Ph	0.0870 (0.130)	3.3	CH ₂ OH (2) Me	4.90×10^{-5} (5.24×10^{-5})	0.79 (0.89)	0.0143 (0.0140)	3.5 (3.5)	

^aExperimental rates determined in CD₃CN or 2:1 D₂O:CD₃CN. ^bM06-2X/6-311++G(d,p); IEFPCM solvent model (H₂O or CH₃CN). ^cB97D/6-311++G(d,p); CPCM solvent model (H₂O or CH₃CN).

SNO-OCT derivatization to increase reaction rates.

Our ability to readily change the substitution pattern of the SNO-OCT scaffold stimulated efforts to electronically tune the alkyne to: 1) improve rates of dipolar cycloadditions, 2) achieve mutually exclusive orthogonal reactivities of SNO-OCTs with Type I-III dipoles in [3+2] and [4+2] cycloadditions, and 3) highlight the ability to install multiple functional handles for appending dyes and reporter molecules to SNO-OCTs for biological applications. As Type I-III cycloadditions can be designed based on FMO considerations, the potential for mutually orthogonal reactivity may be realized if effective orbital matching can be achieved. We hypothesized an electron-poor, electrophilic SNO-OCT derivative might engage in chemoselective reaction with a nucleophilic diazoacetamide dipole; furthermore, the reaction should be orthogonal to an inverse electron-demand Diels-Alder (IEDDA) reaction between a more electron rich SNO-OCT and dipyrindyl tetrazine. Azide cycloadditions were also studied computationally to determine if a triple SNO-OCT ligation system might transcend all three dipole classes.

NBO analyses¹¹ of geometry-optimized SNO-OCTs **2-4** in water were used to study the effects of derivatization on alkyne electronics. Multiple orbital interactions exist within the SNO-OCT scaffold; these may differ greatly in their contributions to the alkyne electronics, depending on the nature of the substitution in the alkyl side chain or the propargylic substitution (Figures 2a and S1-2). The predicted SNO-OCT alkyne electrophilicities were determined based on the 2nd-order perturbation energies of the relevant orbital interactions (Figure 2b, Table S1-1). As might be expected, SNO-OCT **4** and its hydroxylated counterpart **2**, which lack fluorine at the propargylic site, contain electron-rich alkynes. Introduction of a single propargyl fluorine (**3a**) yields a less electron-rich alkyne, while a second fluorination to furnish dF-SNO-OCT **3** contains the most electrophilic alkyne of the series. It is important to note the calculations suggest modification of the R group in **2** and **4**

minimally impacts the π system of the alkyne, whereas modifications at the propargylic site adjacent to the reactive center lead to dramatic changes in electrophilicity.

Identifying Potential Orthogonal Reactivity via Computed Reaction Rates. While qualitative predictions of SNO-OCT/Type I-III dipoles likely to yield mutually orthogonal systems might be gleaned from Figure 2, reaction modeling could help select optimal cycloaddition partners. Transition state (TS) modeling of reactions between SNO-OCTs **2-4** and an example from each dipole class (Type I, methyl diazoacetamide **D1**; Type II, methyl azide **D4**; Type III, dipyridyltetrazine **D3**) were carried out to assess potential orthogonality (Figure 3). Cycloadditions of nucleophilic Type I dipoles should be accelerated with electron-deficient alkynes, due to a lowering of the LUMO and a reduced FMO energy gap.¹⁷ Indeed, difluorination in dF-SNO-OCT **3** was predicted to give a ~ 300 -fold increase in reaction with **D1**, as compared to **2** and **4** (Figure 3a,e). Distortion/interaction¹⁸ or activation strain¹⁹ analysis on calculated transition state models shed further insight into the key features of the SNO-OCT driving reactivity. Computed reactivities of **2-4** in reactions with methyl diazoacetamide correlate with the total distortion energy required to reach the transition state geometry (Figure 3d, $E_{\text{dis,SNO-OCT}}$ and $E_{\text{dis,dipole}}$; Figure S1-4); **TS2a** and **TS4a** require further distortion of the dipole, as evidenced by the reduced bond angles (1.3–2.1° contraction, Figure 3a). Furthermore, dF-SNO-OCT **3** benefits from pre-distortion of the alkynyl bond angles and requires only a 6.34°-bond contraction of the distal alkynyl angle, whereas **2** and **4** require over 8.5°. These reactions also show excellent correlation to the interaction energy (Figure 3d, E_{int}) and the calculated alkyne electrophilicity, with dF-SNO-OCT **3** showing the largest

a. Orbital interactions leading to changes in alkyne electronics



b. Fluorination leads to substantial alkyne electrophilicity enhancement

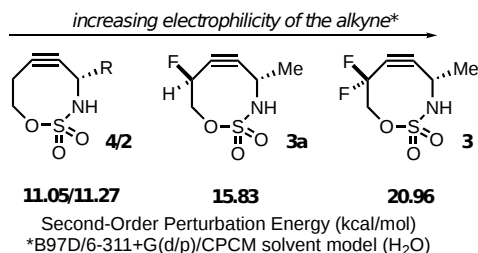


Figure 2. NBO analysis of orbital interactions contributing to predicted alkyne electrophilicity of SNO-OCTs.¹¹

stabilizing interaction energy between coupling partners (+3.1 kcal·mol⁻¹ relative to **4**). This distinction is explicable by FMO considerations, as the most electron-deficient alkynes benefit from lower-lying LUMO levels; the presence of the propargylic fluorines stabilizes the LUMO (**3**, -2.22 eV compared to **2**, -1.45 eV; **4**, -1.39 eV; Figure S1-3). Overall, Type I cycloadditions appear to be influenced by both strain and electronic components of the SNO-OCT (Figure S1-4).

Type III cycloadditions, as exemplified by IEDDA, should display faster reaction kinetics with electron-rich alkynes, due to destabilization of the HOMO. Previous computational studies on these systems investigated the transition states for either the cycloaddition²⁰ alone or both the cycloaddition and N₂ evolution.²¹ The cycloaddition TS is expected to be the kinetically relevant barrier, and the values reported herein correspond to the cycloaddition TS. Dipyridyl tetrazine **D3** (Figure 3b) was modeled, as the electron-withdrawing pyridyl groups enhance cycloaddition rates due to LUMO+1 stabilization of the dipole.²⁰ As predicted, electron-rich SNO-OCTs **2** and **4** (HOMO levels -6.42 eV and -6.44 eV respectively) exhibit the fastest kinetics, whereas dF-SNO-OCT **3** shows significantly lower reactivity due to HOMO stabilization (-7.03 eV). Furthermore, dipole distortion energy for reaction with dF-SNO-OCT **3** is elevated relative to **2** and **4**, likely due to the 0.2 Å shortening of the distal C-C bond, yielding increased steric interactions with the elongated C-F bonds (~ 0.3 Å). Hydroxylated SNO-OCT **2** was predicted to display a five-fold rate enhancement as compared to **4**. Reactivity trends showed moderate-to-excellent correlation to both distortion and interaction energies (Figures 3d and S1-5). Based on reactions of SNO-OCTs with Type I and III dipoles, the potential for mutually orthogonal double ligation appeared promising. The next challenge was to identify a third orthogonal reaction, ideally between a SNO-OCT and a Type II dipole. Thus, reactions of **2-4** with azide **D4** were modeled for comparison (Figure 3c). In Type II cycloadditions, reaction can occur via HOMO_{dipolarophile}-LUMO_{dipole} or HOMO_{dipole}-LUMO_{dipolarophile} interactions, depending on the corresponding FMO energy gaps. This dichotomy makes it challenging to correlate reactivity with alkyne electrophilicity; thus, reactivity trends in SNO-OCT reactions with azides were instead proposed to track with the relevant energy gaps. Switching the alkyl side chain from R = Me in **4** to R = CH₂OH in **2** was predicted to double the reaction rate with **D4**. dF-SNO-OCT **3** was expected to react even more quickly, with a k_2 value

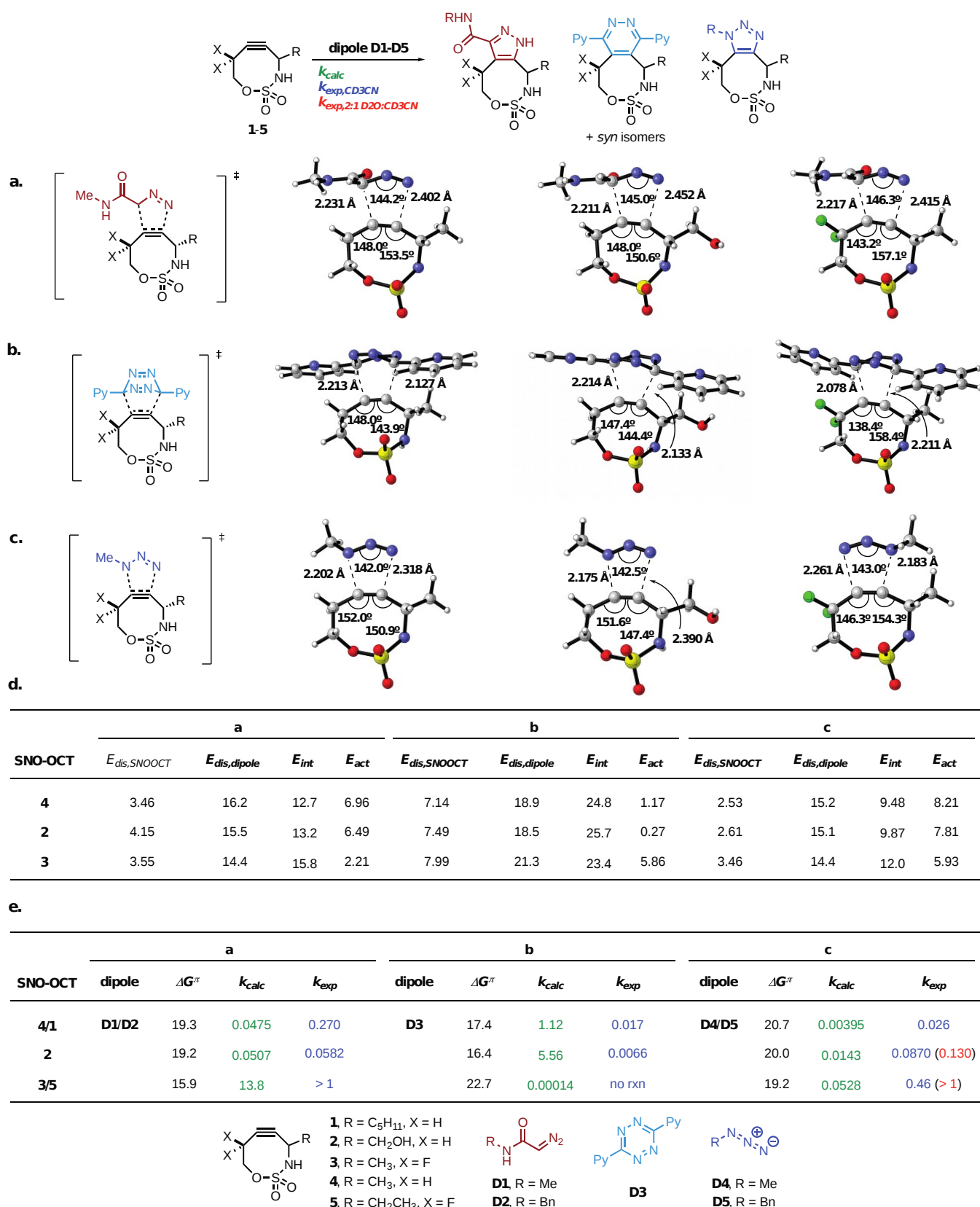


Figure 3. B97D/6-311+G(d,p) calculated transition state models for reactions of SNO-OCTs with (a) diazoacetamide, (b) tetrazine, and (c) azide. (d) Distortion/interaction analysis indicating the influence of distortion energy (ΔE_{dis}) and interaction energy (ΔE_{int}) on activation barriers for cycloadditions of Type I-III dipoles with various SNO-OCT derivatives. (e) Calculated and experimental second-order rate constants. Truncated SNO-OCTs **3** and **4** and dipoles **D1** and **D4** were used for computations; analogous SNO-OCTs **1** and **5** and dipoles **D2** and **D5** were used for experiments. Energies ($E_{dis,SNOOCT}$, $E_{dis,dipole}$, E_{int} , E_{act} , and ΔG^\ddagger) are reported in kcal/mol and second-order rate constants (k_{calc} and k_{exp}) are in $M^{-1}s^{-1}$.

predicted to be an order of magnitude higher than with **2**. Indeed, this reactivity trend can be predicted by assessing FMO gaps for each SNO-OCT/azide pair. Higher electron density in **2** and **4** leads to HOMO destabilization, and as such, these SNO-OCTs react *via* a reduced HOMO_{dipolarophile}-LUMO_{dipole} gap. Conversely, the presence of the fluoro groups in dF-SNO-OCT **3** increases this gap through HOMO stabilization, thus the **3**/MeN₃ reaction proceeds through a more favorable LUMO_{dipolarophile}-HOMO_{dipole} interaction. Though dF-SNO-OCT **3** exhibits reduced dipole distortion energy (−0.72 kcal·mol^{−1} relative to **4**), consistent with bond relaxation (+1.0°), the corresponding alkyne distortion energy is elevated in comparison to parent SNO-OCT **4** (+0.93 kcal mol^{−1}). Thus, the predicted acceleration for cycloadditions of azides with dF-SNO-OCT **3** is attributable to this pair having the highest stabilizing interaction energy (12.0 kcal mol^{−1}). Indeed, the activation barriers show improved correlation with the interaction energies relative to the distortion energies (Figure S1-6).

Experimental Observations Validate Computational Trends. To determine the extent to which SNO-OCT substitution impacts the value of k_2 in reactions with Type I-III dipoles, the reactivities of **2–4** were investigated experimentally and compared to predicted values. SNO-OCTs **1** and **2** were prepared as previously reported,⁹ while **5** required a modified synthetic route, affording the product in 34% yield from propionaldehyde (see Scheme S2-1 for details). Computational results were corroborated in selected instances through experimental kinetic data using ¹H NMR spectroscopy and plate-reader techniques (Figure 3e). It is important to note that the plate reader was utilized for dipyrindyl tetrazine reactions, due to solubility issues encountered in NMR kinetic experiments.

Calculated and experimental results of reactions between SNO-OCTs and alkyl diazoacetamides were particularly promising with respect to chemselectivity and accelerated reaction rates (Figure 3e). Although computed models utilized truncated versions of the substrates, the predicted k_2 ratio of **4** with azide **D4** and diazoalkane **D1** (12:1) was in excellent agreement with the experimental k_2 ratio of **1** with **D5** and **D2** (10:1) (Figure 3e).⁹ A *gem*-difluorination led to a predicted rate enhancement of ~300-fold moving from **4** to **3** in reaction with diazoacetamides (**D1**). Experimental determination of k_2 for the cycloaddition of **5** and **D2** proved difficult; the reaction at rt was too fast to accurately determine k_2 by NMR. VT-NMR showed formation of **5a** with 80% conversion within 2 min at −32 °C (Figure S2-17). Despite the lack of accurate rate data, the fact this reaction is faster than the NMR timescale suggests that $k_2 > 1 \text{ M}^{-1}\text{s}^{-1}$.

Predicted reactions of **2–4** with dipyrindyltetrazine **D3** indicate ~8000-fold rate enhancement in moving from electron-poor dF-SNO-OCT **3** to electron-rich parent **4**; indeed, experimental observations corroborated this prediction, and no reaction was noted between **5** and **D3**. Though calculated rates for IEDDA with **D3** showed a 2–3 orders of magnitude deviation from experimental rates, the computational method was successful in identifying two promising, mutually orthogonal reactions of SNO-OCTs. Further computational investigation into the origin of this deviation is underway to predict more accurate rates in IEDDA with **D3** for future studies.

Calculated rates between azides and SNO-OCTs fall within one order of magnitude from experimental values, when conducting measurements in CD₃CN (Figure 3e).⁹ The predicted value of $k_{\text{rel,azide}}$ between **2:4** (3.6:1) was in excellent agreement with the experimental value of $k_{\text{rel,azide}}$ between **2:1** (3.3:1). Furthermore, calculations indicated a 13× rate-enhancement moving from parent **4** to dF-SNO-OCT **3**, compared to the experimentally observed 18× rate-enhancement in moving from **1** to **5**, accurately predicting relevant experimental reactivity trends. Modified SNO-OCTs **4** and **1** also show predictable trends for azide/SNO-OCT cycloadditions. To our surprise, the computed $k_{\text{rel,azide}}$ between **3:2** (3.7:1) showed a better agreement with experimental results for **5:2** (3.5:1) when more water was used (2:1 D₂O:CD₃CN), suggesting a potential hydrophobic effect contributing to rate acceleration.²²

The inability of DFT methods to accurately model solvents is well-known. Zuilhof and coworkers also point out that their solvent model does not account for rate increases dependent on solvent identity.¹⁵ In our case, the B97D functional is sufficient to predict how electronic fine-tuning of the SNO-OCT influences cycloaddition rates, particularly in [3+2] cycloadditions.

Development of Dual and Triple Ligation Systems with Custom SNO-OCTs. With initial experimental and computational data in hand, we wanted to develop mutually exclusive bioorthogonal dual or triple ligations of SNO-OCTs with various dipoles, as dual ligation has been shown to be effective in probing complex native biological environments and details of subcellular mechanisms.²³ Success would effectively expand the tool box available for multiple ligation of biologically relevant functionalities and also enable fine-tuning of the properties of the SNO-OCT for specific applications.

As predicted by DFT, SNO-OCT **5** gave excellent yields in reactions with diazoalkane **D2** (94%) and azide **D5** (96%); no reaction was noted with **D3** (Scheme 1a). In validation of our

initial hypothesis that a dual ligation system comprised of orthogonal SNO-OCTs and Type I/Type III dipoles could be achieved, a competition experiment using SNO-OCTs **1** and **5** and dipoles **D2** and **D3** (Schemes 1b, S2-2a, and S2-2b; Figure S2-23) showed complete mutual orthogonality.^{2g,4d,24} Indeed, the excellent chemoselectivity supported the large rate enhancement predicted in moving from parent **4** to dF-SNO-OCT **3**. In contrast, a dual ligation system with azide **D5** instead of **D3** gave significantly reduced chemoselectivity (Scheme S2-2c); this also matches computed reaction rates (Figure 3e).

The development of a triple ligation system using only custom SNO-OCTs proved challenging, as predicted by the computational rate data. Ideally, the three mutually exclusive pairs of reagents should display k_2 values differing by at least two orders of magnitude. Based on calculated relative rates of dF-SNO-OCT **3/D1** and parent **4/D1** (Figure 3e), this condition cannot be explicitly met with our current SNO-OCT derivatives.¹⁴ Thus, a commercially available non-SPAAC boronic acid/hydrazine pair was introduced. Bane and co-workers have shown that boronic acid and hydrazine/hydrazide pairs are competent in fast bioorthogonal labeling of biologically relevant molecules; furthermore, the boronic acid system shows orthogonality to both IEDDA and SPAAC.^{2h,25} The orthogonality of these reactions was verified by LC-MS analysis, which is more reliable than NMR methods when significant peak overlap occurs in complex mixtures.^{2g} To our delight, the orthogonality in Scheme 1b translated to the triple ligation (Scheme 1c, Figure S2-17), with mutual orthogonality observed amongst all three reaction pairs by LC-MS.

Protein Triple Ligation and Mammalian Cell-Labeling Assays. Simultaneous multitarget *in vitro* and *in vivo* labeling is of considerable interest for advancing modern biotherapeutics, biological assay development, and basic science investigations.²⁶ We sought to demonstrate the mutual orthogonality of our SNO-OCT bioorthogonal pairs in biological settings, as well as their capacity to enable triple-orthogonal ligations as suggested by LC-MS assays (Scheme 1c). To that end, SNO-DF-Rho and SNO-C343 were synthesized from **5** and **1**, employing either carboxylic acid or primary amine handles, as they are easily derivatizable with other biologically relevant functionalities (Scheme S2-3). Additionally, a previously reported cysteine-hydrazide Texas Red derivative^{2h} was also adapted (Figure 4a, see the SI for more details). Based on the LC-MS experiment in Scheme 1c, these reagents should form the basis of a tripartite mutually orthogonal set, appropriate for demonstrating translatability to biologically relevant conditions. Indeed, one-pot labeling of three

different proteins functionalized to present a diazoacetamide (Cytoc-AcDz), tetrazine (RNase A-Tez), and boronic acid-aldehyde (RNase A-BA) showed excellent chemoselectivity in agreement with small-molecule triple ligation results (Figure 4a). As anticipated, *in situ* gel fluorescence images revealed some bleed over between dyes, but minimal cross reactivity across orthogonal pairs, demonstrating the chemoselectivity of the reagents (Figure S2-18).

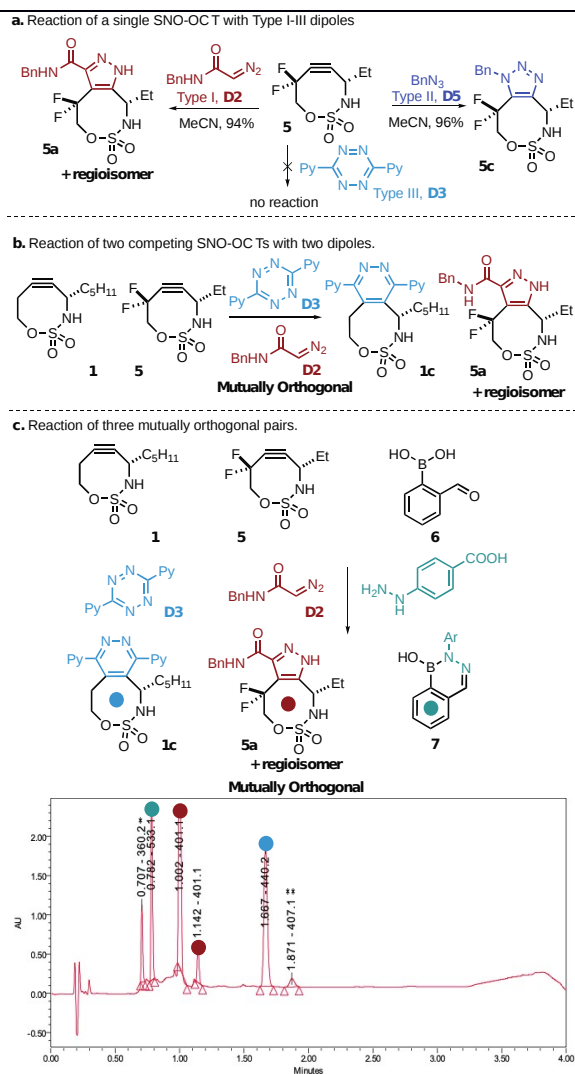
*Next, we sought to explore potential applications in cellulo. The cellular uptake properties of SNO-C343, SNO-DF-Rho, and three DBCO-derivatives were compared to assess internalization and localization of these molecules within Chinese hamster ovary (CHO)-K1 cells. We observed the rapid internalization of SNO-C343 and SNO-DF-Rho (Figures 4b, S2-19, and S2-20). Colocalization analysis of SNO-DF-Rho with MitoTracker GreenTM revealed robust mitochondrial trafficking as shown by a Pearson's correlation coefficient of $R = 0.90 \pm 0.01$ (Figure S2-21). Comparison to an in-house synthesized DBCO-C343 derivative as well as two commercial conjugates, DBCO-PEG₄-Rho110 and DBCO-Cy5, revealed enhanced internalization of SNO-OCT-dye conjugates relative to the commercial reagents upon incubation with CHO-K1 cells (Figure 4b). Internalization of DBCO-C343 occurred at comparable concentrations and gave staining patterns similar to those observed for SNO-C343 (Figure 4B, Figure S2-23). Internalization experiments with DBCO-PEG₄-Rho110 and DBCO-Cy5 conjugates illustrated indirect internalization of DBCO-PEG₄-Rho110, and ablation of internalization in the case of DBCO-Cy5, even at concentrations 5-fold greater than the maximum explored with SNO-OCT reagents (Figure 4b and Figure S2-22). In addition to the orthogonality of SNO-DF-Rho and SNO-C343 reactivity with Type-I and Type-II dipoles, these unconjugated reagents are taken-up robustly by mammalian cells and thus have potential for *in cellulo* applications.*

The mammalian glycocalyx forms a protective anionic coating anchored to the lipid bilayer.²⁷ The structure and chemical properties of this bilayer play important roles in both normal and pathological biological processes, including cellular recognition, organismal development, cancer, and infectivity.²⁸ In pioneering investigations, Reutter, Bertozzi, and their coworkers labeled the glycocalyx of live cells metabolically with synthetic carbohydrates.²⁹ We sought to enlarge the tool-kit for glycocalyx analyses with the new SNO-OCT reagents.

We used metabolic labelling with Ac₄ManDiaz²² to assess the reactivity of SNO-DF-Rho in a biological context. We began by assessing the concentration-dependent uptake and distribution of Ac₄ManDiaz in CHO-K1 cells, identifying optimal concentrations for resolving the glycocalyx upon reaction with SNO-DF-Rho at 1 μ M (Figure S2-24). Side-by-side comparison of staining patterns in CHO-K1 cells cultured in the absence or presence of Ac₄ManDiaz revealed a difference in the distribution of the label. Specifically, SNO-DF-Rho when cells were metabolically labeled with Ac₄ManDiaz (Figure

4d and 4e). In analogous flow-cytometry experiments, the robust labeling and internalization of cells metabolically

Scheme 1. Successful mutually orthogonal ligation systems using SNO-OCTs and Type I/III dipoles. (a) SNO-OCT **5** shows distinct chemoselectivity for **D2** and **D5** over **D3**. (b) Successful development of a dual SNO-OCT ligation system. (c) Triple ligation system assessed by LC-MS analysis (at 210 nm). *By-product from cycloaddition between **4** and **D3**. ****5** and **D2** product observed at high sample concentration (see the SI for more information).



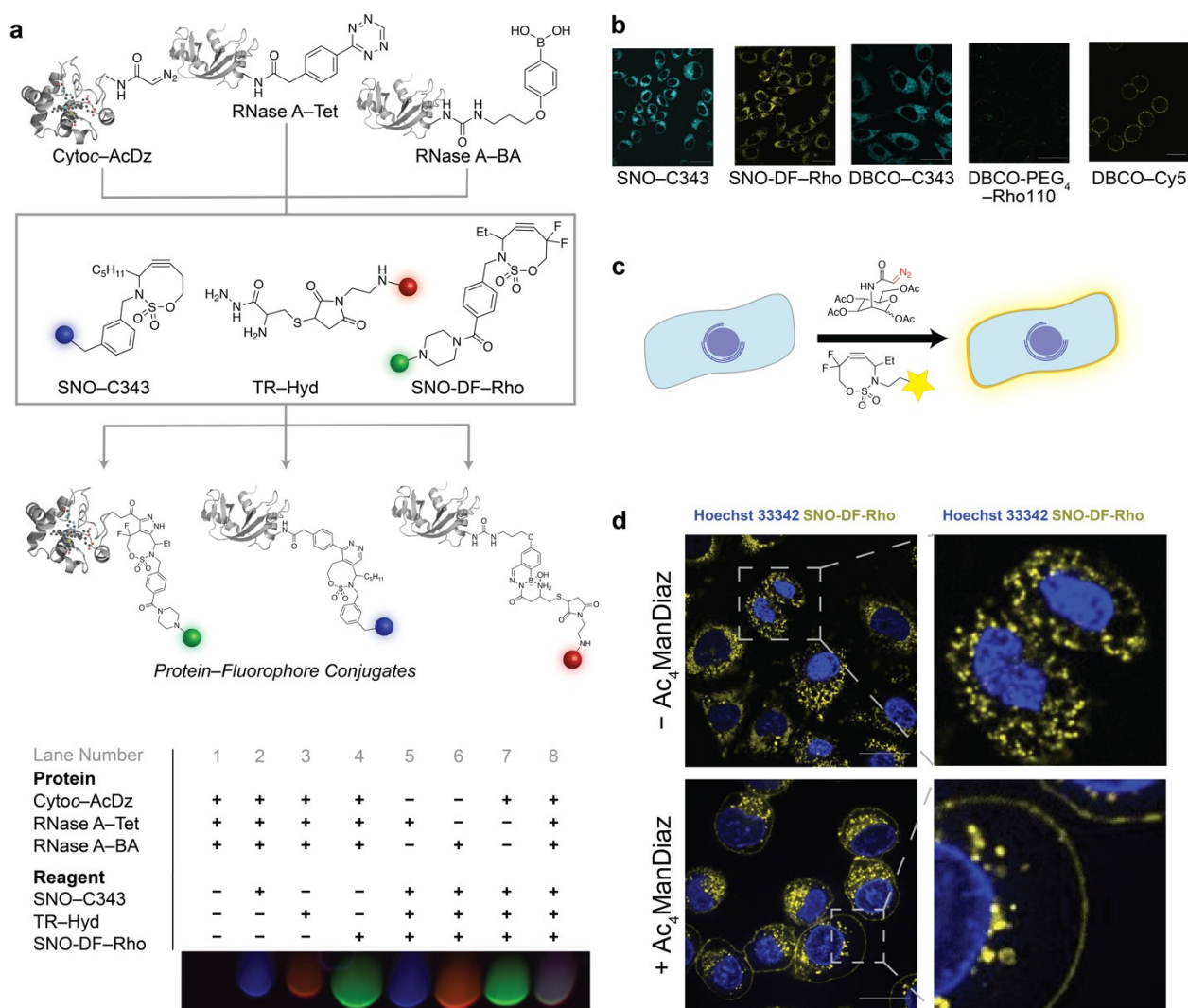


Figure 4. Triple ligation and *in cellulo* activity of SNO-OCT-dye conjugates. (a) Co-incubation of proteins that were labeled with reactive functional groups and fluorescent reagents. (b) Internalization of cyclooctyne-dye conjugates (1 μ M) into CHO-K1 cells. Scale: 10 μ m. (c) Scheme of the metabolic labeling experiments. (d) Visualization of metabolically labeled CHO-K1 cells grown with (bottom) or without (top) $\text{Ac}_4\text{ManDiaz}$ (20 μ M) then incubated with SNO-DF-Rho (1 μ M) for 1 h. Scale: 10 μ m.

labeled with $\text{Ac}_4\text{ManDiaz}$ was again observed, and without significant cell death (Figure S2-25). Together, these data demonstrate the reactivity of SNO-DF-Rho *in cellulo* and highlight the potential of SNO-OCT reagents for biological assays in living cells.

CONCLUSIONS

The integration of computational and experimental studies led to custom heterocyclic cycloalkynes (SNO-OCTs) that display orthogonal reactivities with Type I and III dipoles. The cooperative effects of the propargylic and homopropargylic heteroatoms, which are separated by a sulfonyl bridge, enable tuning of the alkyne electronics and alkyne distortion via remote hybridization and stereoelectronic effects. The addition of a *gem*-difluoro group to the propargylic carbon of the SNO-OCT has several beneficial features, including a significant increase in the value of

k_2 for reactions with Type I-II dipoles and a greatly decreased preference for participation in IEDDA-type reactions. Inspired by computational investigations, experimental validation of a new mutually orthogonal dual ligation was realized through successful electronic fine-tuning of the SNO-OCT alkyne. The inclusion of a previously reported boronic acid/hydrazine bioorthogonal pair furnished a triple ligation system demonstrated to be mutually orthogonal. The development of highly chemoselective, bioorthogonal labeling reactions for double and triple ligations provides useful new tools for future *in cellulo* investigations. The utility of SNO-OCTs for biological applications was demonstrated through a series of protein and cellular labeling assays. The full synthetic potential of these strained alkynes is an area of ongoing investigation in our research groups, with the goal of creating easily accessible and robust

bioorthogonal reagents to accelerate biological discovery.

ASSOCIATED CONTENT

Characterization data, optimization tables, and additional substrates/catalysts are included in the supplementary materials, which are available free of charge via the Internet at <http://pubs.acs.org>.

AUTHOR INFORMATION

*schomakerj@chem.wisc.edu

*rtraines@mit.edu

Author Contributions

The manuscript was written by J.M.S., R.T.R., J.M.R., Y.H., and H.R.K. Experimental work was conducted by Y.H., H.R.K., and A.S.M.L. Computational work was conducted by J.M.R. Biological work was conducted by H.R.K. All authors have given approval to the final version of the manuscript.

Funding Sources

J.M.S. is grateful to the Wisconsin Alumni Research Foundation for financial support of this research. H.R.K. and R.T.R. were supported by grant NIH R01 GM044783. The Paul Bender Chemistry Instrumentation Center includes: Thermo Q ExactiveTM Plus by NIH 1S10 OD020022-1; Bruker Avance-500 by a generous gift from Paul J. and Margaret M. Bender; Bruker Avance-600 by NIH S10 OK012245; Bruker Avance-400 by NSF CHE-1048642; Bruker D8 VENTURE Photon III by NSF CHE-1919350 and the University of Wisconsin-Madison; Varian Mercury-300 by NSF CHE-0342998.

ACKNOWLEDGMENT

Dr. Charles G. Fry and Dr. Heike Hofstetter at UW-Madison are thanked for help with NMR techniques. Dr. Martha M. Vestling at UW-Madison is thanked for mass spectrometry characterization.

REFERENCES

(1) For reviews: (a) Agard, N. J.; Prescher, J. A.; Bertozzi, C. R. A Strain-Promoted [3 + 2] Azide-Alkyne Cycloaddition for Covalent Modification of Biomolecules in Living Systems. *J. Am. Chem. Soc.* **2004**, *126*, 15046–15047. (b) Sletten, E. M.; Bertozzi, C. R. Bioorthogonal Chemistry: Fishing for Selectivity in a Sea of Functionality. *Angew. Chem., Int. Ed.* **2009**, *48*, 6974–6998. (c) Sletten, E. M.; Bertozzi, C. R. From Mechanism to Mouse: A Tale of Two Bioorthogonal Reactions. *Acc. Chem. Res.* **2011**, *44*, 666–676. (d) Ngo, J. T.; Tirrell, D. A. Noncanonical Amino Acids in the Interrogation of Cellular Protein Synthesis. *Acc. Chem. Res.* **2011**, *44*, 677–685. (e) Willems, L. I.; Van Der Linden, W. A.; Li, N.; Li, K. Y.; Liu, N.; Hoogendoorn, S.; Van Der Marel, G. A.; Florea, B. I.; Overkleeft, H. S. Bioorthogonal Chemistry: Applications in Activity-Based Protein Profiling. *Acc. Chem. Res.* **2011**, *44*, 718–729. (f) Best, M. D.; Rowland, M. M.; Bostic, H. E. Exploiting Bioorthogonal Chemistry to Elucidate Protein-Lipid Binding Interactions and Other Biological Roles of Phospholipids. *Acc. Chem. Res.* **2011**, *44*, 686–698. (g) Hang, H. C.; Wilson, J. P.; Charron, G. Bioorthogonal Chemical Reporters for Analyzing Protein Lipidation and Lipid Trafficking. *Acc. Chem. Res.* **2011**, *44*, 699–708. (h) Hao, Z.; Hong, S.; Chen,

X.; Chen, P. R. Introducing Bioorthogonal Functionalities into Proteins in Living Cells. *Acc. Chem. Res.* **2011**, *44*, 742–751. (i) Chen, Y. X.; Triola, G.; Waldmann, H. Bioorthogonal Chemistry for Site-Specific Labeling and Surface Immobilization of Proteins. *Acc. Chem. Res.* **2011**, *44*, 762–773. (j) Jing, C.; Cornish, V. W. Chemical Tags for Labeling Proteins inside Living Cells. *Acc. Chem. Res.* **2011**, *44*, 784–792. (k) Debets, M. F.; Van Berkel, S. S.; Dommerholt, J.; Dirks, A. J.; Rutjes, F. P. J. T.; Van Delft, F. L. Bioconjugation with Strained Alkenes and Alkynes. *Acc. Chem. Res.* **2011**, *44*, 805–815. (l) Devaraj, N. K.; Weissleder, R. Biomedical Applications of Tetrazine Cycloadditions. *Acc. Chem. Res.* **2011**, *44*, 816–827. (m) Lang, K.; Chin, J. W. Bioorthogonal Reactions for Labeling Proteins. *ACS Chem. Biol.* **2014**, *9*, 16–20. (n) Oliveira, B. L.; Guo, Z.; Bernardes, G. J. L. Inverse Electron Demand Diels-Alder Reactions in Chemical Biology. *Chem. Soc. Rev.* **2017**, *46*, 4895–4950.

(2) For reviews: (a) Liang, Y.; Mackey, J. L.; Lopez, S. A.; Liu, F.; Houk, K. N. Control and Design of Mutual Orthogonality in Bioorthogonal Cycloadditions. *J. Am. Chem. Soc.* **2012**, *134*, 17904–17907. (b) Patterson, D. M.; Nazarova, L. A.; Prescher, J. A. Finding the Right (Bioorthogonal) Chemistry. *ACS Chem. Biol.* **2014**, *9*, 592–605. (c) Patterson, D. M.; Prescher, J. A. Orthogonal Bioorthogonal Chemistries. *Curr. Opin. Chem. Biol.* **2015**, *28*, 141–149. (d) David Row, R.; Prescher, J. A. Constructing New Bioorthogonal Reagents and Reactions. *Acc. Chem. Res.* **2018**, *51*, 1073–1081. (e) Devaraj, N. K. The Future of Bioorthogonal Chemistry. *ACS Cent. Sci.* **2018**, *4*, 952–959. Recent publications: (f) Karver, M. R.; Weissleder, R.; Hilderbrand, S. A. Bioorthogonal Reaction Pairs Enable Simultaneous, Selective, Multi-Target Imaging. *Angew. Chem., Int. Ed.* **2012**, *51*, 920–922. (g) Kamber, D. N.; Nguyen, S. S.; Liu, F.; Briggs, J. S.; Shih, H. W.; Row, R. D.; Long, Z. G.; Houk, K. N.; Liang, Y.; Prescher, J. A. Isomeric Triazines Exhibit Unique Profiles of Bioorthogonal Reactivity. *Chem. Sci.* **2019**, *10*, 9109–9114. (h) Chio, T. I.; Gu, H.; Mukherjee, K.; Tumey, N.; Bane, S. L. Site-Specific Bioconjugation and Multi-Bioorthogonal Labeling via Rapid Formation of Boron-Nitrogen Heterocycle. *Bioconjugate Chem.* **2019**, *30*, 1554–1564. (i) Schäfer, R. J. B.; Monaco, M. R.; Li, M.; Tirla, A.; Rivera-Fuentes, P.; Wennemers, H. The Bioorthogonal Isonitrile-Chloroimine Ligation. *J. Am. Chem. Soc.* **2019**, *141*, 18644–18648.

(3) (a) Chen, W.; Wang, D.; Dai, C.; Hamelberg, D.; Wang, B. Clicking 1,2,4,5-Tetrazine and Cyclooctynes with Tunable Reaction Rates. *Chem. Commun.* **2012**, *48*, 1736–1738. (b) MacKenzie, D. A.; Sherratt, A. R.; Chigrinova, M.; Cheung, L. L. W.; Pezacki, J. P. Strain-Promoted Cycloadditions Involving Nitrones and Alkynes-Rapid Tunable Reactions for Bioorthogonal Labeling. *Curr. Opin. Chem. Biol.* **2014**, *21*, 81–88. (c) Kamber, D. N.; Nazarova, L. A.; Liang, Y.; Lopez, S. A.; Patterson, D. M.; Shih, H.-W.; Houk, K. N.; Prescher, J. A. Isomeric Cyclopropenes Exhibit Unique Bioorthogonal Reactivities. *J. Am. Chem. Soc.* **2013**, *135*, 13680.

(4) For reviews: (a) Debets, M. F.; Van Berkel, S. S.; Dommerholt, J.; Dirks, J.; Rutjes, F. P. J. T.; Van Delft, F. L. Bioconjugation with Strained Alkenes and Alkynes. *Acc. Chem. Res.* **2011**, *44*, 805–815. (b) Huber, T.; Sakmar, T. P. Chemical Biology Methods for Investigating G Protein-Coupled Receptor Signaling. *Chem. Biol.* **2014**, *21*, 1224–1237. (c) Dommerholt,

- J.; Rutjes, F. P. J. T.; Van Delft, F. L. Strain-Promoted 1,3-Dipolar Cycloaddition of Cycloalkynes and Organic Azides. *Top. Curr. Chem.* **2016**, *374*, 16–36. Recent publications: (d) Reddington, S. C.; Tippmann, E. M.; Dafydd Jones, D. Residue Choice Defines Efficiency and Influence of Bioorthogonal Protein Modification via Genetically Encoded Strain Promoted Click Chemistry. *Chem. Commun.* **2012**, *48*, 8419–8421. (e) Aronoff, M. R.; Gold, B.; Raines, R. T. 1,3-Dipolar Cycloadditions of Diazo Compounds in the Presence of Azides. *Org. Lett.* **2016**, *18*, 1538–1541. f) Kaneda, K.; Naruse, R.; Yamamoto, S. 2-Aminobenzenesulfonamide-Containing Cyclononyne as Adjustable Click Reagent for Strain-Promoted Azide-Alkyne Cycloaddition. *Org. Lett.* **2017**, *19*, 1096–1099.
- (5) Baskin, J. M.; Prescher, J. A.; Laughlin, S. T.; Agard, N. J.; Chang, P. V.; Miller, I. A.; Lo, A.; Codelli, J. A.; Bertozzi, C. R. Copper-Free Click Chemistry for Dynamic in Vivo Imaging. *Proc. Natl. Acad. Sci. USA* **2007**, *104*, 16793–16797.
- (6) (a) Golkowski, M.; Ziegler, T. Synthesis of Tetra(2-Hydroxyethoxy)-Substituted Dibenzocyclooctyne Derivatives as Novel, Highly Hydrophilic Tool Compounds for Strain-Promoted Alkyne-Azide Cycloaddition Applications. *Synthesis*. **2013**, *45*, 1207–1214. (b) Debets, M. F.; Prins, J. S.; Merks, D.; Van Berkel, S. S.; Van Delft, F. L.; Van Hest, J. C. M.; Rutjes, F. P. J. T. Synthesis of DIBAC Analogues with Excellent SPAAC Rate Constants. *Org. Biomol. Chem.* **2014**, *12*, 5031–5037. (c) Chadwick, R. C.; Van Gyzen, S.; Liogier, S.; Adronov, A. Scalable Synthesis of Strained Cyclooctyne Derivatives. *Synthesis*. **2014**, *46*, 669–677.
- (7) Debets, M. F.; Van Berkel, S. S.; Schoffelen, S.; Rutjes, F. P. J. T.; Van Hest, J. C. M.; Van Delft, F. L. Aza-Dibenzocyclooctynes for Fast and Efficient Enzyme PEGylation via Copper-Free [3+2] Cycloaddition. *Chem. Commun.* **2010**, *46*, 97–99.
- (8) (a) McKay, C. S.; Finn, M. G. Click Chemistry in Complex Mixtures: Bioorthogonal Bioconjugation. *Chem. Biol.* **2014**, *21*, 1075–1101. (b) Bakum, T.; Van Leeuwen, T.; Sarris, A. J. C.; Van Elsdand, D. M.; Poulcharidis, D.; Overkleeft, H. S.; Van Kasteren, S. I. Quantification of Bioorthogonal Stability in Immune Phagocytes Using Flow Cytometry Reveals Rapid Degradation of Strained Alkynes. *ACS Chem. Biol.* **2018**, *13*, 1173–1179.
- (9) Burke, E. G.; Gold, B.; Hoang, T. T.; Raines, R. T.; Schomaker, J. M. Fine-Tuning Strain and Electronic Activation of Strain-Promoted 1,3-Dipolar Cycloadditions with Endocyclic Sulfamates in SNO-OCTs. *J. Am. Chem. Soc.* **2017**, *139*, 8029–8037.
- (10) Tu, J.; Svatoněk, D.; Parvez, S.; Liu, A. C.; Levandowski, B. J.; Eckvahl, H. J.; Peterson, R. T.; Houk, K. N.; Franzini, R. M. Stable, Reactive and Orthogonal Tetrazines: Dispersion Forces Promote the Cycloaddition with Isonitriles. *Angew. Chem., Int. Ed.* **2019**, *58*, 9043–9048.
- (11) Glendening, E. D.; Badenhoop, J. K.; Reed, A. E.; Carpenter, J. E.; Bohmann, J. A.; Morales, C. M.; Landis, C. R.; Weinhold, F. NBO 6.0, Theoretical Chemistry Institute, University of Wisconsin, Madison, 2013.
- (12) (a) Hohenstein, E. G.; Chill, S. T.; Sherrill, C. D. Assessment of the Performance of the M05-2X and M06-2X Exchange-Correlation Functionals for Noncovalent Interactions in Biomolecules. *J. Chem. Theory Comput.* **2008**, *4*, 1996–2000. (b) Walker, M.; Harvey, A. J. A.; Sen, A.; Dessent, C. E. H. Performance of M06, M06-2X, and M06-HF Density Functionals for Conformationally Flexible Anionic Clusters: M06 Functionals Perform Better than B3LYP for a Model System with Dispersion and Ionic Hydrogen-Bonding Interactions. *J. Phys. Chem. A* **2013**, *117*, 12590–12600.
- (13) Frisch, M. J.; Trucks, G. W.; Schlegel, H. B.; Scuseria, G. E.; Robb, M. A.; Cheeseman, J. R.; Scalmani, G.; Barone, V.; Petersson, G. A.; Nakatsuji, H.; Li, X.; Caricato, M.; Marenich, A. V.; Bloino, J.; Janesko, B. G.; Gomperts, R.; Mennucci, B.; Hratch, D. J. Gaussian 16, Revision B.01. Gaussian, Inc.: Wallingford, CT **2016**.
- (14) Liu, F.; Liang, Y.; Houk, K. Bioorthogonal Cycloadditions: Computational Analysis with the Distortion/Interaction Model and Predictions of Reactivities. *Acc. Chem. Res.* **2017**, *50*, 2297–2308.
- (15) (a) Garcia-Hartjes, J.; Dommerholt, J.; Wennekes, T.; Van Delft, F. L.; Zuilhof, H. Electronic Effects versus Distortion Energies during Strain-Promoted Alkyne-Azide Cycloadditions: A Theoretical Tool to Predict Reaction Kinetics. *European J. Org. Chem.* **2013**, *6*, 3712–3720. (b) Escorihuela, J.; Das, A.; Looijen, W. J. E.; Van Delft, F. L.; Aquino, A. J. A.; Lischka, H.; Zuilhof, H. Kinetics of the Strain-Promoted Oxidation-Controlled Cycloalkyne-1,2-Quinone Cycloaddition: Experimental and Theoretical Studies. *J. Org. Chem.* **2018**, *83*, 244–252.
- (16) (a) Barone, V.; Cossi, M. Quantum Calculation of Molecular Energies and Energy Gradients in Solution by a Conductor Solvent Model. *J. Phys. Chem. A* **1998**, *102*, 1995–2001. (b) Cossi, M.; Rega, N.; Scalmani, G.; Barone, V. Energies, Structures, and Electronic Properties of Molecules in Solution with the C-PCM Solvation Model. *J. Comput. Chem.* **2003**, *24*, 669–681. (c) Takano, Y.; Houk, K. N. Benchmarking the Conductor-like Polarizable Continuum Model (CPCM) for Aqueous Solvation Free Energies of Neutral and Ionic Organic Molecules. *J. Chem. Theory Comput.* **2005**, *1*, 70–77. (d) Grimme, S. Semiempirical GGA-Type Density Functional Constructed with a Long-Range Dispersion Correction. *J. Comput. Chem.* **2006**, *27*, 1787–1799. (e) Grimme, S.; Ehrlich, S.; Goerigk, L. Effect of the Damping Function in Dispersion Corrected Density Functional Theory. *J. Comput. Chem.* **2011**, *32*, 1456–1465.
- (17) Fleming, I. *Molecular Orbitals and Organic Chemistry Reactions: Student Edition*; Wiley: West Sussex, UK, 2009.
- (18) (a) Ess, D. H.; Houk, K. N. Distortion/Interaction Energy Control of 1,3-Dipolar Cycloaddition Reactivity. *J. Am. Chem. Soc.* **2007**, *129*, 10646–10647. (b) Ess, D. H.; Houk, K. N. Theory of 1,3-Dipolar Cycloadditions: Distortion/Interaction and Frontier Molecular Orbital Models. *J. Am. Chem. Soc.* **2008**, *130*, 10187–10198.
- (19) (a) Fernández, I.; Bickelhaupt, F. M. The Activation Strain Model and Molecular Orbital Theory: Understanding and Designing Chemical Reactions. *Chem. Soc. Rev.* **2014**, *43*, 4953–4967. (b) Wolters, L. P.; Bickelhaupt, F. M. The Activation Strain Model and Molecular Orbital Theory. *Wiley Interdiscip. Rev. Comput. Mol. Sci.* **2015**, *5*, 324–343.
- (20) Liu, F.; Liang, Y.; Houk, K. N. Theoretical Elucidation of the Origins of Substituent and Strain Effects on the Rates of Diels-Alder Reactions of 1,2,4,5-Tetrazines. *J. Am. Chem. Soc.* **2014**, *136*,

11483-11493.

(21) Sadasivam, D. V.; Prasad, E.; Flowers, R. A.; Birney, D. M. Stopped-Flow Kinetics of Tetrazine Cycloadditions; Experimental and Computational Studies toward Sequential Transition States. *J. Phys. Chem. A* **2006**, *110*, 1288-1294.

(22) Andersen, K. A.; Aronoff, M. R.; Mcgrath, N. A.; Raines, R. T. Diazo Groups Endure Metabolism and Enable Chemoselectivity in *Cellulo*. *J. Am. Chem. Soc.* **2015**, *137*, 2412-2415

(23) (a) Huang, L. L.; Liu, K.; Zhang, Q.; Xu, J.; Zhao, D.; Zhu, H.; Xie, H. Y. Integrating Two Efficient and Specific Bioorthogonal Ligation Reactions with Natural Metabolic Incorporation in One Cell for Virus Dual Labeling. *Anal. Chem.* **2017**, *89*, 11620-11627. (b) Das, D. K.; Govindan, R.; Nikić-Spiegel, I.; Krammer, F.; Lemke, E. A.; Munro, J. B. Direct Visualization of the Conformational Dynamics of Single Influenza Hemagglutinin Trimers. *Cell* **2018**, *174*, 926-937.e12. (c) Reisacher, U.; Ploschik, D.; Röncke, F.; Cserép, G. B.; Kele, P.; Wagenknecht, H.-A. Copper-Free Dual Labeling of DNA by Triazines and Cyclopropanes as Minimal Orthogonal and Bioorthogonal Functions. *Chem. Sci.* **2019**, *10*, 4032-4037.

(24) Dommerholt, J.; Van Rooijen, O.; Borrmann, A.; Fonseca Guerra, C.; Bickelhaupt, F. M.; Van Delft, F. L. Highly Accelerated Inverse Electron-Demand Cycloaddition of Electron-Deficient Azides with Aliphatic Cyclooctynes. *Nat. Commun.* **2014**, *5*, 5378.

(25) (a) Dilek, O.; Lei, Z.; Bane, S. Rapid Formation of a Stable Boron-Nitrogen Heterocycle in Dilute, Neutral Aqueous Solution for Bioorthogonal Coupling Reactions. *Chem. Commun.* **2015**, 16992-16995. (b) Gu, H.; Ghosh, S.; Staples, R. J.; Bane, S. L. β -Hydroxy-Stabilized Boron-Nitrogen Heterocycles Enable Rapid and Efficient C-Terminal Protein Modification. *Bioconjugate Chem.* **2019**, *30*, 2604-2613. For reviews: (c) Akgun, B.; Hall, D. G. Boronic Acids as Bioorthogonal Probes for Site-Selective Labeling of Proteins. *Angew. Chem., Int. Ed.* **2018**, *57*, 13028-13044.

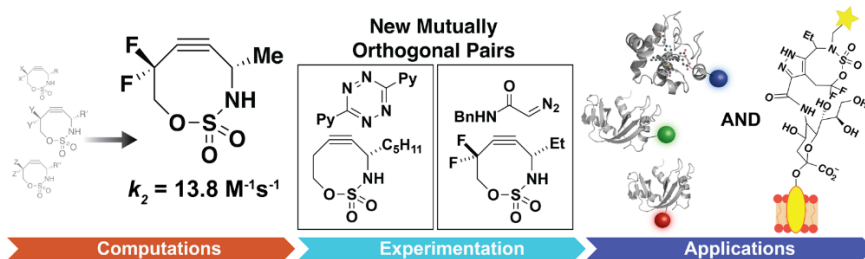
(26) (a) Kolb, H. C.; Finn, M. G.; Sharpless, B. K. Click Chemistry: Diverse Chemical Function from a Few Good Reactions. *Angew. Chem., Int. Ed.* **2001**, *40*, 2004-2021. (b) Cravatt, B. F.; Wright, A. T.; Kozarich, J. W. Activity-Based Protein Profiling: From Enzyme Chemistry to Proteomic Chemistry. *Annu. Rev. Biochem.* **2008**, *77*, 383-414. (c) Laughlin, S. T.; Bertozzi, C. R. Imaging the Glycome. *Proc. Natl. Acad. Sci. U.S.A.* **2009**, *106*, 12-17. (d) Signore, G.; Nifosi, R.; Albertazzi, L.; Storti, B.; Bizzarri, R. Polarity-Sensitive Coumarins Tailored to Live Cell Imaging. *J. Am. Chem. Soc.* **2010**, *132*, 1276-1288. (e) Dennler, P.; Fischer, E.; Schibli, R. Antibody Conjugates: From Heterogenous Populations to Defined Reagents. *Antibodies* **2015**, *4*, 197-224. (f) Beck, A.; Goetsch,

L.; Dumontet, C.; Corvaia, N. Strategies and Challenges for the next Generation of Antibody-Drug Conjugates. *Nat. Rev. Drug Discov.* **2017**, *16*, 315-337. (g) Rudra, A.; Li, J.; Shakur, R.; Bhagchandani, S.; Langer, R. Trends in Therapeutic Conjugates: Bench to Clinic. *Bioconjugate Chem.* **2020**, *31*, 462-473.

(27) (a) Letschert, S.; Gohler, A.; Franke, N.; Bertleff-Zieschang, N.; Memmel, E.; Doose, S.; Siebel, J.; Sauer, M. Super-Resolution Imaging of Plasma Membrane Glycans. *Angew. Chem., Int. Ed.* **2014**, *126*, 11101-11104. (b) Chen, J.; Gao, J.; Wu, M.; Zhang, M.; Cai, H.; Xu, J.; Jiang, Z.; Tian, Z.; Wang, H. Revealing the Carbohydrate Pattern on a Cell Surface by Super-Resolution Imaging. *Nanoscale* **2015**, *7*, 3373-3380. (c) Hegermann, J.; Lunsdorf, H.; Ochs, M.; Haller, H. Visualization of the Glomerular Endothelial Glycocalyx by Electron Microscopy Using Cationic Colloidal Thorium Dioxide. *Histochem. Cell Biol.* **2016**, *145*, 41-51. (d) Mockl, L.; Pedram, K.; Roy, A. R.; Krishnan, V.; Gustavsson, A. K.; Dorigo, O.; Bertozzi, C. R. Quantitative Super-Resolution Microscopy of the Mammalian Glycocalyx. *Dev. Cell* **2019**, *50*, 57-72.

(28) (a) Esko, J. D.; Rostand, K. S.; Weinke, J. L. Tumor Formation Dependent on Proteoglycan Biosynthesis. *Science*. **1988**, *241*, 1092-1096. (b) Matrosovich, M. N.; Matrosovich, T. Y.; Gray, T.; Roberts, N. A.; Klenk, H. D. Neuraminidase in Important for the Initiation of Influenza Virus Infection in Human Airway Epithelium. *J. Virol.* **2004**, *78*, 12655-12667. (c) Hudak, J. E.; Canham, S. M.; Bertozzi, C. R. Glycocalyx Engineering Reveals a Siglec-Based Mechanism for NK Cell Immune evasion. *Nat. Chem. Biol.* **2014**, *10*, 69-75. (d) Constantinou, P. E.; Morgado, M.; Carson, D. Transmembrane Mucin Expression and Function in Embryo Implantation and Placentation in *Regulation of Implantation and Establishment of Pregnancy in Mammals*, Bazer, F. W., Geisert, R. D., Eds.; Springer: New York, NY, 2015. (e) Gandhi, J. G.; Kock, D. L.; Paszek, M. J. Equilibrium Modeling of the Mechanics and Structure of the Cancer Glycocalyx. *Biophys. J.* **2019**, *116*, 694-708.

(29) (a) Kayser, H.; Zeitler, R.; Kannicht, C.; Grunow, D.; Nuck, R.; Reutter, W. Biosynthesis of a Nonphysiological Sialic Acid in Different Rat Organs, Using *N*-Propanoyl-D-Hexosamines as Precursors. *J. Biol. Chem.* **1992**, *267*, 16934-16938. (b) Mahal, L. K.; Yarema, K. J.; Bertozzi, C. R. Engineering Chemical Reactivity on Cell Surfaces Through Oligosaccharide Biosynthesis. *Science*. **1997**, *276*, 1125-1128. (c) Saxon, E.; Bertozzi, C. R. Cell Surface Engineering by a Modified Staudinger Reaction. *Science*. **2000**, *287*, 2007-2010.



Triple, Mutually Orthogonal Cycloadditions Through the D... (10.98 MiB) [view on ChemRxiv](#) • [download file](#)

Triple, Mutually Orthogonal Cycloadditions Through the Design of Electronically Activated SNO-OCTs

Yun Hu,^{†,‡} Jessica M. Roberts,^{†,‡} Henry R. Kilgore,^{§,†} Amirah S. Mat Lani,[†] Ronald T. Raines,^{*,§} and Jennifer M. Schomaker^{*,†}

¹Department of Chemistry, University of Wisconsin, Madison, Wisconsin 53706, United States

²Department of Chemistry, Massachusetts Institute of Technology, Cambridge, Massachusetts 02139, United States

ABSTRACT: Interest in mutually exclusive pairs of bioorthogonal labeling reagents continues to drive the design of new compounds capable of fast and predictable reactions. The ability to easily modify heterocyclic strained cyclooctynes containing sulfamate backbones (SNO-OCTs) enables electronic tuning of the relative rates of reactions of SNO-OCTs in cycloadditions with Type I–III dipoles. As opposed to optimizations based on just one specific dipole class, the electrophilicity of the alkynes in SNO-OCTs can be manipulated to achieve divergent reactivities and furnish mutually orthogonal dual ligation systems. Significant rate enhancements for reactions of a difluorinated SNO-OCT derivative compared to the parent scaffold were noted, with the second-order rate constant in cycloadditions with diazoacetamides exceeding $1\text{ M}^{-1}\text{s}^{-1}$. Computational and experimental studies were employed to inform the design of triple ligation systems that encompass three orthogonal reactivities. Finally, polar SNO-OCTs are rapidly internalized by mammalian cells and remain functional in the cytosol for live-cell labeling, highlighting their potential for diverse *in vitro* and *in vivo* applications.

INTRODUCTION

Bioorthogonal chemistry represents a powerful strategy to monitor individual molecules in biological systems; indeed, within the past two decades, a multitude of reactions have been developed to fulfill this function.¹ Nonetheless, a larger challenge involves the identification of mutually orthogonal pairs of bioorthogonal reagents with the potential to simultaneously observe the behavior of multiple biomolecules in a cell.² The ready availability of convenient, inexpensive, and electronically tunable “orthogonal bioorthogonal” reagent pairs remains a topic of intense interest, as new labeling tools are critical in efforts to push the boundaries of our understanding of complex biological systems.^{2d,3}

The 1,3-dipolar cycloadditions are popular reactions in bioorthogonal chemistry, particularly strain-promoted azide–alkyne cycloadditions (SPAAC; Figure 1a).^{1c,3b,4} Bertozzi and co-workers addressed issues with the slow kinetics of unfunctionalized cyclooctynes by electronically activating the alkyne via installation of fluorine atoms at the propargyl carbon. Moving from monofluorinated (MOFO) to difluorinated alkyne (DIFO) resulted in nearly two orders of magnitude increase in the rate of reaction with BnN_3 , from 0.0043 to $0.076\text{ M}^{-1}\text{s}^{-1}$.⁵ The popular bioorthogonal reagent DBCO utilizes benzene rings fused to the cycloalkyne to further accelerate the reaction with BnN_3 ; however, further electronic tuning of this scaffold is challenging, due to limited derivatization sites.⁶ Other reported modifications to the parent compound yield reaction rates with BnN_3 spanning less than an order of magnitude (0.31 – $0.90\text{ M}^{-1}\text{s}^{-1}$).⁷ In addition to the lack of modularity, the strain-activated nature of this alkyne leads to issues with stability and chemoselectivity, limiting opportunities to develop mutually orthogonal reactions involving DBCO derivatives.⁸

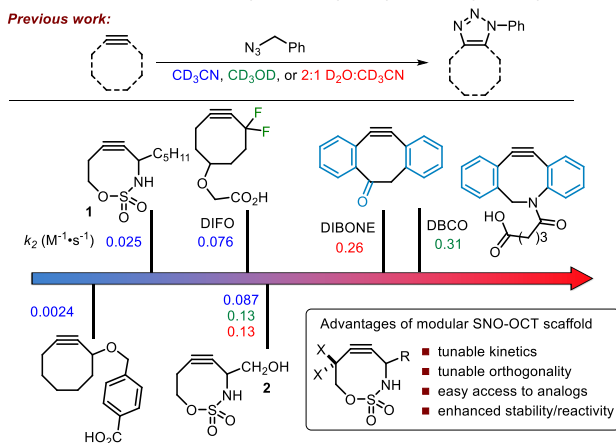
Recently, we developed a unique class of strained cycloalkynes containing *S*-, *N*-, and *O*-heteroatoms embedded in the ring (SNO-OCTs).⁹ Our previous kinetic studies of the

sulfamate-containing SNO-OCTs **1–2** (Figure 1a) show second-order kinetic rate constants (k_2) with BnN_3 ranging from 0.0014 to $0.087\text{ M}^{-1}\text{s}^{-1}$, with polar protic solvents further enhancing the rate of **2** to $0.13\text{ M}^{-1}\text{s}^{-1}$.^{1k,9} Despite the relaxed alkyne angles and reduced ring strain in **1–2**, these SNO-OCTs exhibit a significant rate-increase for cycloadditions, comparable to strain-activated DIBONE and DBCO. Density functional theory (DFT) calculations indicated these SNO-OCTs benefit from unique electronic activation of the alkyne *via* tailored anomeric effects and hybridization, resulting in robust stability at high pH and in the presence of glutathione.^{2b,9} Furthermore, the presence of the sulfonyl group increases the polarity in the transition state, which has been shown to enhance the rates of cycloadditions.⁹

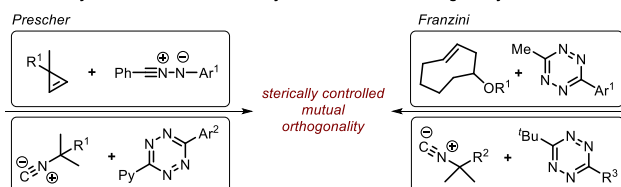
The tunability of SNO-OCTs begs the question of whether these scaffolds can be tailored for divergent reactivity with diverse coupling partners. The Prescher group developed several mutually orthogonal dual ligation systems, particularly a series of cyclopropenes that could be sterically tuned to achieve mutually orthogonal Type I and Type III cycloadditions (Figure 1b).^{2c–d,3c} Sterically encumbered 3,3-cyclopropenes prefer nitrile imines, while shifting the bulk in 1,3-cyclopropenes favors reaction with tetrazines. Similarly, Franzini and co-workers designed sterically differentiated isonitriles, which display chemoselective reaction with various tetrazine derivatives.¹⁰ Increasing the steric bulk on the tetrazine resulted in successful dual orthogonal labeling of a protein in the presence of *trans*-cyclooctene (TCO) and DBCO. Computational analysis indicated bulky tetrazines benefit from dispersion forces that favor reaction with isonitriles. Though steric tuning has proven successful for multiple ligation systems, the ability to tune SNO-OCT alkyne electronics in a predictable manner could tailor the chemoselectivity to achieve mutual orthogonality across diverse coupling partners without rate reductions often seen with steric-driven strategies.

a. Strain-promoted and electronically activated cycloalkynes in benzyl azide cycloadditions.

Previous work:



b. Sterically controlled chemoselectivity to achieve mutual orthogonality.



c. Tuning alkyne electronics in SNO-OCTs to afford divergent reactivity.

This work:

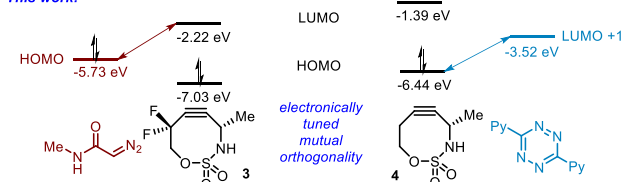


Figure 1. Previous work and design of new mutually “orthogonal bioorthogonal” reactions for multicomponent labeling.

This paper reports on the electronic tuning of SNO-OCTs to achieve chemoselective reactions with Type I, Type II, and Type III dipoles with fast kinetics. Frontier molecular orbital (FMO) and natural bond orbital (NBO) analyses were used to rationalize how derivatization influenced alkyne electronics,¹¹ while distortion/interaction analysis shed insight into how electronics and strain impacted reactivity trends. Computational insights guided the identification of potentially orthogonal SNO-OCT/dipole pairs; for example, the electron-deficient alkyne of difluorinated SNO-OCT **3** (dF-SNO-OCT) was expected to display divergent reactivity relative to the parent **1** (Figure 1c). Successes in developing new dual and triple ligation systems highlight the versatility of SNO-OCTs for chemoselective reactions with diverse dipoles by modifying the alkyne electronics. Finally, the use of a novel triple ligation system for protein labeling is demonstrated, and the application of SNO-OCTs as efficient cell-surface visualization agents is described.

RESULTS AND DISCUSSION

Computational Methods Development to Predict SNO-OCT Cycloaddition Reaction Rates. To facilitate rational design of promising SNO-OCT derivatives (see Figure S1), we sought to develop a computational approach capable of accurately predicting reaction rates and reactivity trends. As numerous SNO-OCT derivatizations can be envisaged, DFT calculations were needed to rapidly identify potential mutually

orthogonal reactions and streamline experimental efforts. Initial computations conducted at the M06-2X level of theory¹² with a 6-311++G(d,p) basis set using Gaussian 16¹³ showed predicted rates that deviated significantly from experimental values (Table 1). For example, previous studies showed that **1** reacts with BnN₃ in CH₃CN with $k_2 = 2.60 \times 10^{-2} \text{ M}^{-1}\text{s}^{-1}$ (Table 1, entry 1); however, DFT calculations predicted a k_2 value that was ~3 orders of magnitude lower, at $6.21 \times 10^{-5} \text{ M}^{-1}\text{s}^{-1}$. M06-2X has been previously shown to overestimate activation barriers, with Houk applying a correction factor to computed values to bring them into better quantitative agreement.¹⁴ Unfortunately, this correction factor is based on experimental second-order rate constants for similar cycloadditions; because our goal was to utilize computational methods to predict relative rates of derivatized SNO-OCT scaffolds, a different level of theory was required. Zuilhof also reported that M06-2X overestimates activation barriers in strain-promoted oxidation-controlled quinone (SPOCQ) cycloadditions and found that switching to the B97D functional gave calculated rates that aligned better with experimental data.¹⁵ SNO-OCT rates were calculated at the B97D level of theory using a Conductor-like Polarizable Continuum Model for the solvent (see the SI for details).¹⁶ B97D improved the agreement between computed and experimental k_2 values (within ~1 order of magnitude) and gave more accurate k_{rel} ratios for the experimental:predicted rates in reactions of **1/4:2** with the corresponding azides. In contrast, calculations at the M06-2X level of theory predict a slower rate of reaction for **2** with BnN₃ as compared to **4** (Table 1, entry 2), which is not manifested experimentally. Thus, the B97D functional furnishes calculated rates that are much more predictive of experimental values than does M06-2X. Accordingly, further computational analyses were conducted utilizing the B97D level of theory to predict potential mutual orthogonality of SNO-OCT derivatives.

Table 1. Experimental and calculated k_2 values for cycloadditions of SNO-OCTs with alkyl azides.

entry	R ¹ R ²	rate (M ⁻¹ s ⁻¹)	k_{rel}	Calculated			
				M06-2X ^b		B97D ^c	
				rate (M ⁻¹ s ⁻¹)	k_{rel}	rate (M ⁻¹ s ⁻¹)	k_{rel}
1	C ₅ H ₁₁ (1) CH ₂ Ph	0.0260	1.00	Me (4) Me	6.21×10^{-5} (5.88×10^{-5})	1.00 (0.00395)	0.00407 (0.00395)
2	CH ₂ OH (2) CH ₂ Ph	0.0870 (0.130)	3.3	CH ₂ OH (2) Me	4.90×10^{-5} (5.24×10^{-5})	0.79 (0.89)	0.0143 (0.0140)
							3.5 (3.5)

^aExperimental rates determined in CD₃CN or 2:1 D₂O:CD₃CN. ^bM06-2X/6-311++G(d,p); IEFFPCM solvent model (H₂O or CH₃CN). ^cB97D/6-311+G(d,p); CPCM solvent model (H₂O or CH₃CN).

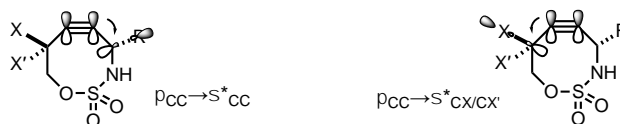
SNO-OCT derivatization to increase reaction rates. Our ability to readily change the substitution pattern of the SNO-OCT scaffold stimulated efforts to electronically tune the alkyne to: 1) improve rates of dipolar cycloadditions, 2) achieve mutually exclusive orthogonal reactivities of SNO-OCTs with Type I–III dipoles in [3+2] and [4+2] cycloadditions, and 3) highlight the ability to install multiple functional handles for appending dyes and reporter molecules to SNO-OCTs for biological applications. As Type I–III cycloadditions can be designed based on FMO considerations, the potential for

mutually orthogonal reactivity may be realized if effective orbital matching can be achieved. We hypothesized an electron-poor, electrophilic SNO-OCT derivative might engage in chemoselective reaction with a nucleophilic diazoacetamide dipole; furthermore, the reaction should be orthogonal to an inverse electron-demand Diels–Alder (IEDDA) reaction between a more electron rich SNO-OCT and dipyrindyl tetrazine. Azide cycloadditions were also studied computationally to determine if a triple SNO-OCT ligation system might transcend all three dipole classes.

NBO analyses¹¹ of geometry-optimized SNO-OCTs **2–4** in water were used to study the effects of derivatization on alkyne electronics. Multiple orbital interactions exist within the SNO-OCT scaffold; these may differ greatly in their contributions to the alkyne electronics, depending on the nature of the substitution in the alkyl side chain or the propargylic substitution (Figures 2a and S1-2). The predicted SNO-OCT alkyne electrophilicities were determined based on the 2nd-order perturbation energies of the relevant orbital interactions (Figure 2b, Table S1-1). As might be expected, SNO-OCT **4** and its hydroxylated counterpart **2**, which lack fluorine at the propargylic site, contain electron-rich alkynes. Introduction of a single propargyl fluorine (**3a**) yields a less electron-rich alkyne, while a second fluorination to furnish dF-SNO-OCT **3** contains the most electrophilic alkyne of the series. It is important to note the calculations suggest modification of the R group in **2** and **4** minimally impacts the π system of the alkyne, whereas modifications at the propargylic site adjacent to the reactive center lead to dramatic changes in electrophilicity.

Identifying Potential Orthogonal Reactivity via Computed Reaction Rates. While qualitative predictions of SNO-OCT/Type I–III dipoles likely to yield mutually orthogonal systems might be gleaned from Figure 2, reaction modeling could help select optimal cycloaddition partners. Transition state (TS) modeling of reactions between SNO-OCTs **2–4** and an example from each dipole class (Type I, methyl diazoacetamide **D1**; Type II, methyl azide **D4**; Type III, dipyrindyltetrazine **D3**) were carried out to assess potential orthogonality (Figure 3). Cycloadditions of nucleophilic Type I dipoles should be accelerated with electron-deficient alkynes, due to a lowering of the LUMO and a reduced FMO energy gap.¹⁷ Indeed, difluorination in dF-SNO-OCT **3** was predicted to give a ~300-fold increase in reaction with **D1**, as compared to **2** and **4** (Figure 3a,e). Distortion/ interaction¹⁸ or activation strain¹⁹ analysis on calculated transition state models shed further insight into the key features of the SNO-OCT driving reactivity. Computed reactivities of **2–4** in reactions with methyl diazoacetamide correlate with the total distortion energy required to reach the transition state geometry (Figure 3d, $E_{\text{dis,SNO-OCT}}$ and $E_{\text{dis,dipole}}$; Figure S1-4); **TS2a** and **TS4a** require further distortion of the dipole, as evidenced by the reduced bond angles (1.3–2.1° contraction, Figure 3a). Furthermore, dF-SNO-OCT **3** benefits from pre-distortion of the alkynyl bond angles and requires only a 6.34°-bond contraction of the distal alkynyl angle, whereas **2** and **4** require over 8.5°. These reactions also show excellent correlation to the interaction energy (Figure 3d, E_{int}) and the calculated alkyne electrophilicity, with dF-SNO-OCT **3** showing the largest

a. Orbital interactions leading to changes in alkyne electronics



b. Fluorination leads to substantial alkyne electrophilicity enhancement

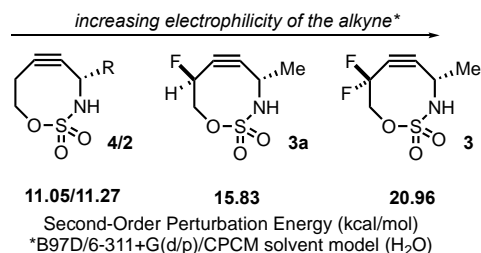


Figure 2. NBO analysis of orbital interactions contributing to predicted alkyne electrophilicity of SNO-OCTs.¹¹

stabilizing interaction energy between coupling partners (+3.1 kcal·mol^{−1} relative to **4**). This distinction is explicable by FMO considerations, as the most electron-deficient alkynes benefit from lower-lying LUMO levels; the presence of the propargylic fluorines stabilizes the LUMO (**3**, −2.22 eV compared to **2**, −1.45 eV; **4**, −1.39 eV; Figure S1-3). Overall, Type I cycloadditions appear to be influenced by both strain and electronic components of the SNO-OCT (Figure S1-4).

Type III cycloadditions, as exemplified by IEDDA, should display faster reaction kinetics with electron-rich alkynes, due to destabilization of the HOMO. Previous computational studies on these systems investigated the transition states for either the cycloaddition²⁰ alone or both the cycloaddition and N₂ evolution.²¹ The cycloaddition TS is expected to be the kinetically relevant barrier, and the values reported herein correspond to the cycloaddition TS. Dipyrindyl tetrazine **D3** (Figure 3b) was modeled, as the electron-withdrawing pyridyl groups enhance cyclo-addition rates due to LUMO+1 stabilization of the dipole.²⁰ As predicted, electron-rich SNO-OCTs **2** and **4** (HOMO levels −6.42 eV and −6.44 eV respectively) exhibit the fastest kinetics, whereas dF-SNO-OCT **3** shows significantly lower reactivity due to HOMO stabilization (−7.03 eV). Furthermore, dipole distortion energy for reaction with dF-SNO-OCT **3** is elevated relative to **2** and **4**, likely due to the 0.2 Å shortening of the distal C–C bond, yielding increased steric interactions with the elongated C–F bonds (~0.3 Å). Hydroxylated SNO-OCT **2** was predicted to display a five-fold rate enhancement as compared to **4**. Reactivity trends showed moderate-to-excellent correlation to both distortion and interaction energies (Figures 3d and S1-5).

Based on reactions of SNO-OCTs with Type I and III dipoles, the potential for mutually orthogonal double ligation appeared promising. The next challenge was to identify a third orthogonal reaction, ideally between a SNO-OCT and a Type II dipole. Thus, reactions of **2–4** with azide **D4** were modeled for comparison (Figure 3c). In Type II cycloadditions, reaction can occur *via* HOMO_{dipolarophile}–LUMO_{dipole} or HOMO_{dipole}–LUMO_{dipolarophile} interactions, depending on the corresponding FMO energy gaps. This dichotomy makes it challenging to correlate reactivity with alkyne electrophilicity; thus, reactivity trends in SNO-OCT reactions with azides were instead proposed to track with the relevant energy gaps. Switching the alkyl side chain from R = Me in **4** to R = CH₂OH in **2** was predicted to double the reaction rate with **D4**. dF-SNO-OCT **3** was expected to react even more quickly, with a k_2 value

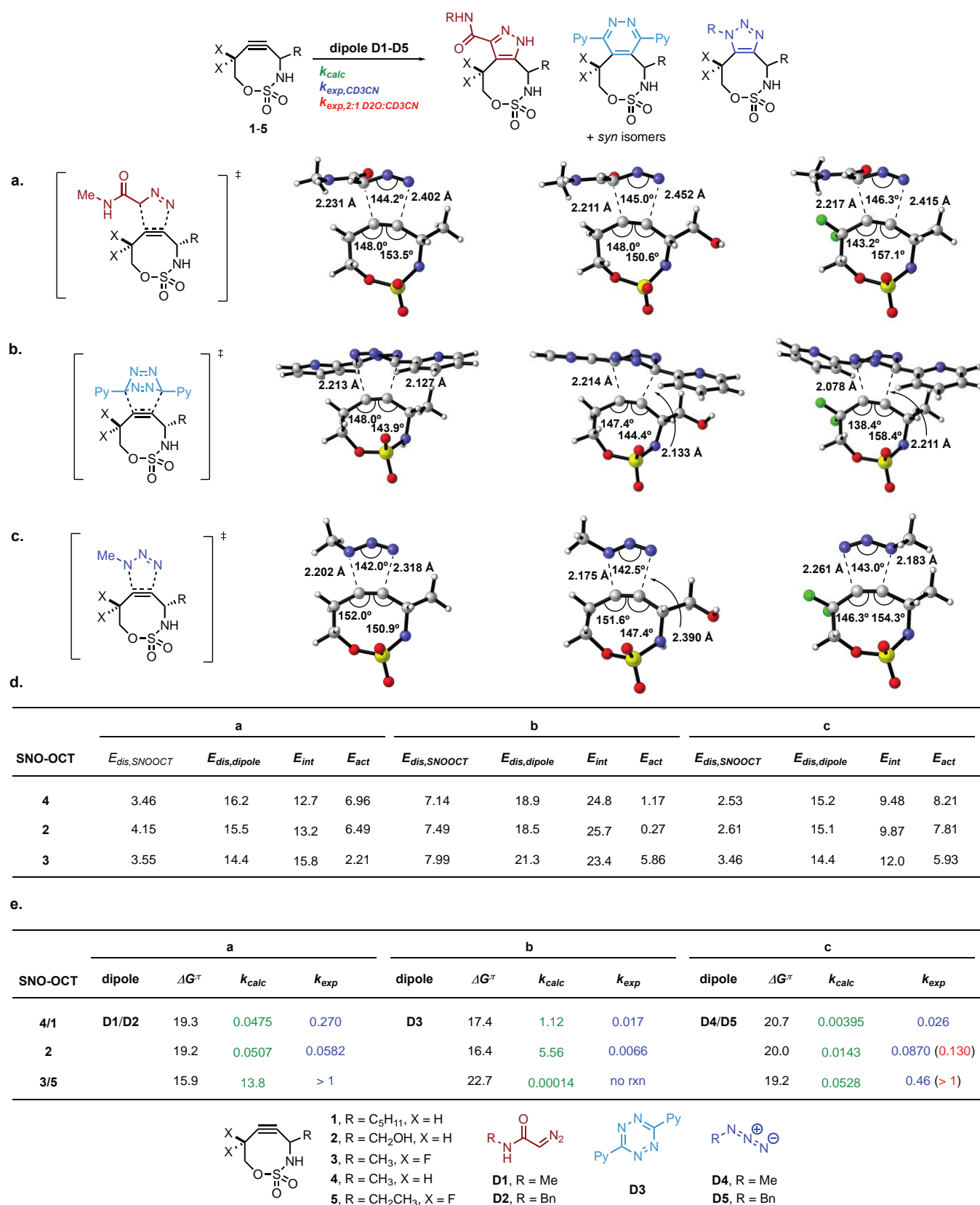


Figure 3. B97D/6-311+G(d,p) calculated transition state models for reactions of SNO-OCTs with (a) diazoacetamide, (b) tetrazine, and (c) azide. (d) Distortion/interaction analysis indicating the influence of distortion energy (ΔE_{dis}) and interaction energy (ΔE_{int}) on activation barriers for cycloadditions of Type I–III dipoles with various SNO-OCT derivatives. (e) Calculated and experimental second-order rate constants for cycloadditions of Type I–III dipoles with various SNO-OCT derivatives; analogous SNO-OCTs **1** and **5** and dipoles **D1** and **D4** were used for computations; analogous SNO-OCTs **1** and **5** and dipoles **D2** and **D5** were used for experiments. Energies ($E_{dis,SNO-OCT}$, $E_{dis,dipole}$, E_{int} , E_{act} , and ΔG^\ddagger) are reported in kcal/mol and second-order rate constants (k_{calc} and k_{exp}) are in M⁻¹s⁻¹.

predicted to be an order of magnitude higher than with **2**. Indeed, this reactivity trend can be predicted by assessing FMO gaps for each SNO-OCT/azide pair. Higher electron density in **2** and **4** leads to HOMO destabilization, and as such, these SNO-OCTs react *via* a reduced HOMO_{dipolarophile}–LUMO_{dipole} gap. Conversely, the presence of the fluoro groups in dF-SNO-OCT **3** increases this gap through HOMO stabilization, thus the 3/MeN₃ reaction proceeds through a more favorable LUMO_{dipolarophile}–HOMO_{dipole} interaction. Though dF-SNO-OCT **3** exhibits reduced dipole distortion energy (−0.72 kcal·mol^{−1} relative to **4**), consistent with bond relaxation (+1.0°), the corresponding alkyne distortion energy is elevated in comparison to parent SNO-OCT **4** (+0.93 kcal mol^{−1}). Thus, the predicted acceleration for cycloadditions of azides with dF-SNO-OCT **3** is attributable to this pair having the highest stabilizing interaction energy (12.0 kcal mol^{−1}). Indeed, the activation barriers show improved correlation with the interaction energies relative to the distortion energies (Figure S1–6).

Experimental Observations Validate Computational Trends. To determine the extent to which SNO-OCT substitution impacts the value of k_2 in reactions with Type I–III dipoles, the reactivities of **2–4** were investigated experimentally and compared to predicted values. SNO-OCTs **1** and **2** were prepared as previously reported,⁹ while **5** required a modified synthetic route, affording the product in 34% yield from propionaldehyde (see Scheme S2-1 for details). Computational results were corroborated in selected instances through experimental kinetic data using ¹H NMR spectroscopy and plate-reader techniques (Figure 3e). It is important to note that the plate reader was utilized for dipyrindyl tetrazine reactions, due to solubility issues encountered in NMR kinetic experiments.

Calculated and experimental results of reactions between SNO-OCTs and alkyl diazoacetamides were particularly promising with respect to chemoselectivity and accelerated reaction rates (Figure 3e). Although computed models utilized truncated versions of the substrates, the predicted k_2 ratio of **4** with azide **D4** and diazoalkane **D1** (12:1) was in excellent agreement with the experimental k_2 ratio of **1** with **D5** and **D2** (10:1) (Figure 3e).⁹ A *gem*-difluorination led to a predicted rate enhancement of ~300-fold moving from **4** to **3** in reaction with diazoacetamides (**D1**). Experimental determination of k_2 for the cycloaddition of **5** and **D2** proved difficult; the reaction at rt was too fast to accurately determine k_2 by NMR. VT-NMR showed formation of **5a** with 80% conversion within 2 min at −32 °C (Figure S2-17). Despite the lack of accurate rate data, the fact this reaction is faster than the NMR timescale suggests that $k_2 > 1 \text{ M}^{-1}\text{s}^{-1}$.

Predicted reactions of **2–4** with dipyrindyltetrazine **D3** indicate ~8000-fold rate enhancement in moving from electron-poor dF-SNO-OCT **3** to electron-rich parent **4**; indeed, experimental observations corroborated this prediction, and no reaction was noted between **5** and **D3**. Though calculated rates for IEDDA with **D3** showed a 2–3 orders of magnitude deviation from experimental rates, the computational method was successful in identifying two promising, mutually orthogonal reactions of SNO-OCTs. Further computational investigation into the origin of this deviation is underway to predict more accurate rates in IEDDA with **D3** for future studies.

Calculated rates between azides and SNO-OCTs fall within one order of magnitude from experimental values, when conducting measurements in CD₃CN (Figure 3e).⁹ The predicted value of $k_{\text{rel,azide}}$ between **2:4** (3.6:1) was in excellent agreement with the experimental value of $k_{\text{rel,azide}}$ between **2:1** (3.3:1). Furthermore, calculations indicated a 13× rate-enhancement moving from parent **4** to dF-SNO-OCT **3**, compared to the experimentally observed 18× rate-enhancement in moving from **1** to **5**, accurately predicting relevant experimental reactivity trends. Modified SNO-OCTs **4** and **1** also show predictable trends for azide/SNO-OCT cycloadditions. To our surprise, the computed $k_{\text{rel,azide}}$ between **3:2** (3.7:1) showed a better agreement with experimental results for **5:2** (3.5:1) when more water was used (2:1 D₂O:CD₃CN), suggesting a potential hydrophobic effect contributing to rate acceleration.²²

The inability of DFT methods to accurately model solvents is well-known. Zuilhof and coworkers also point out that their solvent model does not account for rate increases dependent on solvent identity.¹⁵ In our case, the B97D functional is sufficient to predict how electronic fine-tuning of the SNO-OCT influences cycloaddition rates, particularly in [3+2] cycloadditions.

Development of Dual and Triple Ligation Systems with Custom SNO-OCTs. With initial experimental and computational data in hand, we wanted to develop mutually exclusive bioorthogonal dual or triple ligations of SNO-OCTs with various dipoles, as dual ligation has been shown to be effective in probing complex native biological environments and details of subcellular mechanisms.²³ Success would effectively expand the tool box available for multiple ligation of biologically relevant functionalities and also enable fine-tuning of the properties of the SNO-OCT for specific applications.

As predicted by DFT, SNO-OCT **5** gave excellent yields in reactions with diazoalkane **D2** (94%) and azide **D5** (96%); no reaction was noted with **D3** (Scheme 1a). In validation of our initial hypothesis that a dual ligation system comprised of orthogonal SNO-OCTs and Type I/Type III dipoles could be achieved, a competition experiment using SNO-OCTs **1** and **5** and dipoles **D2** and **D3** (Schemes 1b, S2-2a, and S2-2b; Figure S2-23) showed complete mutual orthogonality.^{2g,4d,24} Indeed, the excellent chemoselectivity supported the large rate enhancement predicted in moving from parent **4** to dF-SNO-OCT **3**. In contrast, a dual ligation system with azide **D5** instead of **D3** gave significantly reduced chemoselectivity (Scheme S2-2c); this also matches computed reaction rates (Figure 3e).

The development of a triple ligation system using only custom SNO-OCTs proved challenging, as predicted by the computational rate data. Ideally, the three mutually exclusive pairs of reagents should display k_2 values differing by at least two orders of magnitude. Based on calculated relative rates of dF-SNO-OCT **3/D1** and parent **4/D1** (Figure 3e), this condition cannot be explicitly met with our current SNO-OCT derivatives.¹⁴ Thus, a commercially available non-SPAAC boronic acid/hydrazine pair was introduced. Bane and coworkers have shown that boronic acid and hydrazine/hydrazide pairs are competent in fast bioorthogonal labeling of biologically relevant molecules; furthermore, the boronic acid system shows orthogonality to both IEDDA and SPAAC.^{2h,25} The orthogonality of these reactions was verified by LC-MS analysis, which is more reliable than NMR methods when

significant peak overlap occurs in complex mixtures.²⁸ To our delight, the orthogonality in Scheme 1b translated to the triple ligation (Scheme 1c, Figure S2-17), with mutual orthogonality observed amongst all three reaction pairs by LC-MS.

Protein Triple Ligation and Mammalian Cell-Labeling Assays. Simultaneous multitarget *in vitro* and *in vivo* labeling is of considerable interest for advancing modern biotherapeutics, biological assay development, and basic science investigations.²⁶ We sought to demonstrate the mutual orthogonality of our SNO-OCT bioorthogonal pairs in biological settings, as well as their capacity to enable triple-orthogonal ligations as suggested by LC-MS assays (Scheme 1c). To that end, SNO-DF-Rho and SNO-C343 were synthesized from **5** and **1**, employing either carboxylic acid or primary amine handles, as they are easily derivatizable with other biologically relevant functionalities (Scheme S2-3). Additionally, a previously reported cysteine-hydrazide Texas Red derivative^{2h} was also adapted (Figure 4a, see the SI for more details). Based on the LC-MS experiment in Scheme 1c, these reagents should form the basis of a tripartite mutually orthogonal set, appropriate for demonstrating translatability to biologically relevant conditions. Indeed, one-pot labeling of three different proteins functionalized to present a diazoacetamide (Cytoc-AcDz), tetrazine (RNase A-Tez), and boronic acid-aldehyde (RNase A-BA) showed excellent chemoselectivity in agreement with small-molecule triple ligation results (Figure 4a). As anticipated, *in situ* gel fluorescence images revealed some bleed over between dyes, but minimal cross reactivity across orthogonal pairs, demonstrating the chemoselectivity of the reagents (Figure S2-18).

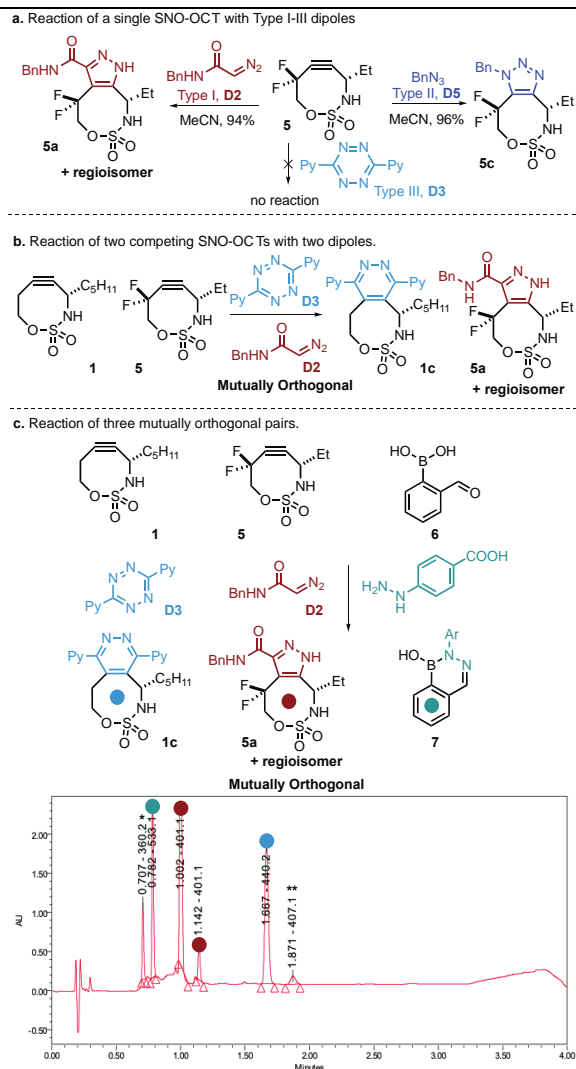
Next, we sought to explore potential applications *in cellulo*. The cellular uptake properties of SNO-C343, SNO-DF-Rho, and three DBCO-derivatives were compared to assess internalization and localization of these molecules within Chinese hamster ovary (CHO)-K1 cells. We observed the rapid internalization of SNO-C343 and SNO-DF-Rho (Figures 4b, S2-19, and S2-20). Colocalization analysis of SNO-DF-Rho with MitoTracker Green™ revealed robust mitochondrial trafficking as shown by a Pearson's correlation coefficient of $R = 0.90 \pm 0.01$ (Figure S2-21). Comparison to an in-house synthesized DBCO-C343 derivative as well as two commercial conjugates, DBCO-PEG₄-Rho110 and DBCO-Cy5, revealed enhanced internalization of SNO-OCT-dye conjugates relative to the commercial reagents upon incubation with CHO-K1 cells (Figure 4b). Internalization of DBCO-C343 occurred at comparable concentrations and gave staining patterns similar to those observed for SNO-C343 (Figure 4B, Figure S2-23). Internalization experiments with DBCO-PEG₄-Rho110 and DBCO-Cy5 conjugates illustrated indirect internalization of DBCO-PEG₄-Rho110, and ablation of internalization in the case of DBCO-Cy5, even at concentrations 5-fold greater than the maximum explored with SNO-OCT reagents (Figure 4b and Figure S2-22). In addition to the orthogonality of SNO-DF-Rho and SNO-C343 reactivity with Type-I and Type-II dipoles, these unconjugated reagents are taken-up robustly by mammalian cells and thus have potential for *in cellulo* applications.

The mammalian glycocalyx forms a protective anionic coating anchored to the lipid bilayer.²⁷ The structure and chemical properties of this bilayer play important roles in both normal and pathological biological processes, including cellular

recognition, organismal development, cancer, and infectivity.²⁸ In pioneering investigations, Reutter, Bertozzi, and their coworkers labeled the glycocalyx of live cells metabolically with synthetic carbohydrates.²⁹ We sought to enlarge the toolkit for glycocalyx analyses with the new SNO-OCT reagents.

We used metabolic labelling with Ac₄ManDiaz²² to assess the reactivity of SNO-DF-Rho in a biological context. We began by assessing the concentration-dependent uptake and distribution of Ac₄ManDiaz in CHO-K1 cells, identifying optimal concentrations for resolving the glycocalyx upon reaction with SNO-DF-Rho at 1 μ M (Figure S2-24). Side-by-side comparison of staining patterns in CHO-K1 cells cultured in the absence or presence of Ac₄ManDiaz revealed a difference in the distribution of the label. Specifically, SNO-DF-Rho when cells were metabolically labeled with Ac₄ManDiaz (Figure 4d and 4e). In analogous flow-cytometry experiments, the robust labeling and internalization of cells metabolically

Scheme 1. Successful mutually orthogonal ligation systems using SNO-OCTs and Type I/III dipoles. (a) SNO-OCT **5** shows distinct chemoselectivity for **D2** and **D5** over **D3**. (b) Successful development of a dual SNO-OCT ligation system. (c) Triple ligation system assessed by LC-MS analysis (at 210 nm). *By-product from cycloaddition between **4** and **D3**. ****5** and **D2** product observed at high sample concentration (see the SI for more information).



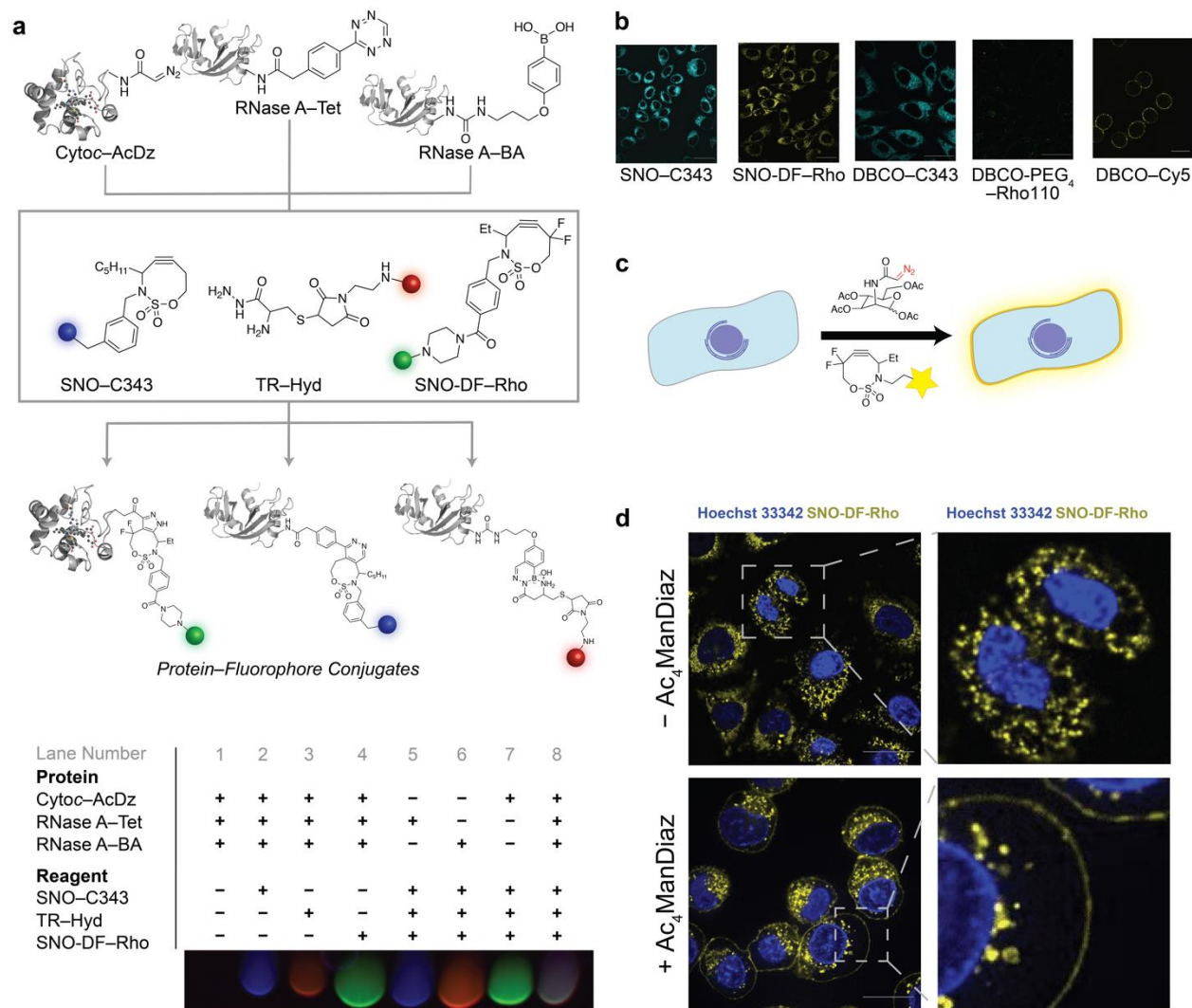


Figure 4. Triple ligation and *in cellulo* activity of SNO-OCT-dye conjugates. (a) Co-incubation of proteins that were labeled with reactive functional groups and fluorescent reagents. (b) Internalization of cyclooctyne-dye conjugates (1 μ M) into CHO-K1 cells. Scale: 10 μ m. (c) Scheme of the metabolic labeling experiments. (d) Visualization of metabolically labeled CHO-K1 cells grown with (bottom) or without (top) Ac₄ManDiaz (20 μ M) then incubated with SNO-DF-Rho (1 μ M) for 1 h. Scale: 10 μ m.

labeled with Ac₄ManDiaz was again observed, and without significant cell death (Figure S2-25). Together, these data demonstrate the reactivity of SNO-DF-Rho *in cellulo* and highlight the potential of SNO-OCT reagents for biological assays in living cells.

CONCLUSIONS

The integration of computational and experimental studies led to custom heterocyclic cycloalkynes (SNO-OCTs) that display orthogonal reactivities with Type I and III dipoles. The cooperative effects of the propargylic and homopropargylic heteroatoms, which are separated by a sulfonyl bridge, enable tuning of the alkyne electronics and alkyne distortion via remote hybridization and stereoelectronic effects. The addition of a *gem*-difluoro group to the propargylic carbon of the SNO-OCT has several beneficial features, including a significant increase in the value of k_2 for reactions with Type I-II dipoles and a greatly decreased preference for participation in IEDDA-type reactions. Inspired by computational investigations, experimental validation of a new mutually orthogonal dual ligation was realized through successful electronic fine-tuning

of the SNO-OCT alkyne. The inclusion of a previously reported boronic acid/hydrazine bioorthogonal pair furnished a triple ligation system demonstrated to be mutually orthogonal. The development of highly chemoselective, bioorthogonal labeling reactions for double and triple ligations provides useful new tools for future *in cellulo* investigations. The utility of SNO-OCTs for biological applications was demonstrated through a series of protein and cellular labeling assays. The full synthetic potential of these strained alkynes is an area of ongoing investigation in our research groups, with the goal of creating easily accessible and robust bioorthogonal reagents to accelerate biological discovery.

ASSOCIATED CONTENT

Characterization data, optimization tables, and additional substrates/catalysts are included in the supplementary materials, which are available free of charge via the Internet at <http://pubs.acs.org>.

AUTHOR INFORMATION

*schomakerj@chem.wisc.edu

Author Contributions

The manuscript was written by J.M.S., R.T.R., J.M.R., Y.H., and H.R.K. Experimental work was conducted by Y.H., H.R.K., and A.S.M.L. Computational work was conducted by J.M.R. Biological work was conducted by H.R.K. All authors have given approval to the final version of the manuscript.

Funding Sources

J.M.S. is grateful to the Wisconsin Alumni Research Foundation for financial support of this research. H.R.K. and R.T.R. were supported by grant NIH R01 GM044783. The Paul Bender Chemistry Instrumentation Center includes: Thermo Q ExactiveTM Plus by NIH 1S10 OD020022-1; Bruker Avance-500 by a generous gift from Paul J. and Margaret M. Bender; Bruker Avance-600 by NIH S10 OK012245; Bruker Avance-400 by NSF CHE-1048642; Bruker D8 VENTURE Photon III by NSF CHE-1919350 and the University of Wisconsin-Madison; Varian Mercury-300 by NSF CHE-0342998.

ACKNOWLEDGMENT

Dr. Charles G. Fry and Dr. Heike Hofstetter at UW-Madison are thanked for help with NMR techniques. Dr. Martha M. Vestling at UW-Madison is thanked for mass spectrometry characterization.

REFERENCES

(1) For reviews: (a) Agard, N. J.; Prescher, J. A.; Bertozzi, C. R. A Strain-Promoted [3 + 2] Azide-Alkyne Cycloaddition for Covalent Modification of Biomolecules in Living Systems. *J. Am. Chem. Soc.* **2004**, *126*, 15046–15047. (b) Sletten, E. M.; Bertozzi, C. R. Bioorthogonal Chemistry: Fishing for Selectivity in a Sea of Functionality. *Angew. Chem., Int. Ed.* **2009**, *48*, 6974–6998. (c) Sletten, E. M.; Bertozzi, C. R. From Mechanism to Mouse: A Tale of Two Bioorthogonal Reactions. *Acc. Chem. Res.* **2011**, *44*, 666–676. (d) Ngo, J. T.; Tirrell, D. A. Noncanonical Amino Acids in the Interrogation of Cellular Protein Synthesis. *Acc. Chem. Res.* **2011**, *44*, 677–685. (e) Willems, L. I.; Van Der Linden, W. A.; Li, N.; Li, K. Y.; Liu, N.; Hoogendoorn, S.; Van Der Marel, G. A.; Florea, B. I.; Overkleeft, H. S. Bioorthogonal Chemistry: Applications in Activity-Based Protein Profiling. *Acc. Chem. Res.* **2011**, *44*, 718–729. (f) Best, M. D.; Rowland, M. M.; Bostic, H. E. Exploiting Bioorthogonal Chemistry to Elucidate Protein-Lipid Binding Interactions and Other Biological Roles of Phospholipids. *Acc. Chem. Res.* **2011**, *44*, 686–698. (g) Hang, H. C.; Wilson, J. P.; Charron, G. Bioorthogonal Chemical Reporters for Analyzing Protein Lipidation and Lipid Trafficking. *Acc. Chem. Res.* **2011**, *44*, 699–708. (h) Hao, Z.; Hong, S.; Chen, X.; Chen, P. R. Introducing Bioorthogonal Functionalities into Proteins in Living Cells. *Acc. Chem. Res.* **2011**, *44*, 742–751. (i) Chen, Y. X.; Triola, G.; Waldmann, H. Bioorthogonal Chemistry for Site-Specific Labeling and Surface Immobilization of Proteins. *Acc. Chem. Res.* **2011**, *44*, 762–773. (j) Jing, C.; Cornish, V. W. Chemical Tags for Labeling Proteins inside Living Cells. *Acc. Chem. Res.* **2011**, *44*, 784–792. (k) Debets, M. F.; Van Berkel, S. S.; Dommerholt, J.; Dirks, A. J.; Rutjes, F. P. J. T.; Van Delft, F. L. Bioconjugation with Strained Alkenes and Alkynes. *Acc. Chem. Res.* **2011**, *44*, 805–815. (l) Devaraj, N. K.; Weissleder, R. Biomedical Applications of Tetrazine Cycloadditions. *Acc. Chem. Res.* **2011**, *44*, 816–827. (m) Lang, K.; Chin, J. W. Bioorthogonal Reactions for Labeling Proteins. *ACS Chem. Biol.* **2014**, *9*, 16–20. (n) Oliveira, B. L.; Guo, Z.; Bernardes, G. J. L. Inverse Electron Demand Diels–Alder Reactions in Chemical Biology. *Chem. Soc. Rev.* **2017**, *46*, 4895–4950.

(2) For reviews: (a) Liang, Y.; Mackey, J. L.; Lopez, S. A.; Liu, F.; Houk, K. N. Control and Design of Mutual Orthogonality in Bioorthogonal Cycloadditions. *J. Am. Chem. Soc.* **2012**, *134*, 17904–17907. (b) Patterson, D. M.; Nazarova, L. A.; Prescher, J. A. Finding the Right (Bioorthogonal) Chemistry. *ACS Chem. Biol.* **2014**, *9*, 592–605. (c) Patterson, D. M.; Prescher, J. A. Orthogonal Bioorthogonal

Chemistries. *Curr. Opin. Chem. Biol.* **2015**, *28*, 141–149. (d) David Row, R.; Prescher, J. A. Constructing New Bioorthogonal Reagents and Reactions. *Acc. Chem. Res.* **2018**, *51*, 1073–1081. (e) Devaraj, N. K. The Future of Bioorthogonal Chemistry. *ACS Cent. Sci.* **2018**, *4*, 952–959. Recent publications: (f) Karver, M. R.; Weissleder, R.; Hilderbrand, S. A. Bioorthogonal Reaction Pairs Enable Simultaneous, Selective, Multi-Target Imaging. *Angew. Chem., Int. Ed.* **2012**, *51*, 920–922. (g) Kamber, D. N.; Nguyen, S. S.; Liu, F.; Briggs, J. S.; Shih, H. W.; Row, R. D.; Long, Z. G.; Houk, K. N.; Liang, Y.; Prescher, J. A. Isomeric Triazines Exhibit Unique Profiles of Bioorthogonal Reactivity. *Chem. Sci.* **2019**, *10*, 9109–9114. (h) Chio, T. I.; Gu, H.; Mukherjee, K.; Tumey, N.; Bane, S. L. Site-Specific Bioconjugation and Multi-Bioorthogonal Labeling via Rapid Formation of Boron–Nitrogen Heterocycle. *Bioconjugate Chem.* **2019**, *30*, 1554–1564. (i) Schäfer, R. J. B.; Monaco, M. R.; Li, M.; Tirla, A.; Rivera-Fuentes, P.; Wennemers, H. The Bioorthogonal Isonitrile–Chlorooxime Ligation. *J. Am. Chem. Soc.* **2019**, *141*, 18644–18648.

(3) (a) Chen, W.; Wang, D.; Dai, C.; Hamelberg, D.; Wang, B. Clicking 1,2,4,5-Tetrazine and Cyclooctynes with Tunable Reaction Rates. *Chem. Commun.* **2012**, *48*, 1736–1738. (b) MacKenzie, D. A.; Sherratt, A. R.; Chigrinova, M.; Cheung, L. L. W.; Pezacki, J. P. Strain-Promoted Cycloadditions Involving Nitrones and Alkynes–Rapid Tunable Reactions for Bioorthogonal Labeling. *Curr. Opin. Chem. Biol.* **2014**, *21*, 81–88. (c) Kamber, D. N.; Nazarova, L. A.; Liang, Y.; Lopez, S. A.; Patterson, D. M.; Shih, H.-W.; Houk, K. N.; Prescher, J. A. Isomeric Cyclopropanes Exhibit Unique Bioorthogonal Reactivities. *J. Am. Chem. Soc.* **2013**, *135*, 13680.

(4) For reviews: (a) Debets, M. F.; Van Berkel, S. S.; Dommerholt, J.; Dirks, J.; Rutjes, F. P. J. T.; Van Delft, F. L. Bioconjugation with Strained Alkenes and Alkynes Bioconjugation with Strained Alkenes and Alkynes. *Acc. Chem. Res.* **2011**, *44*, 805–815. (b) Huber, T.; Sakmar, T. P. Chemical Biology Methods for Investigating G Protein-Coupled Receptor Signaling. *Chem. Biol.* **2014**, *21*, 1224–1237. (c) Dommerholt, J.; Rutjes, F. P. J. T.; Van Delft, F. L. Strain-Promoted 1,3-Dipolar Cycloaddition of Cycloalkynes and Organic Azides. *Top. Curr. Chem.* **2016**, *374*, 16–36. Recent publications: (d) Reddington, S. C.; Tippmann, E. M.; Dafydd Jones, D. Residue Choice Defines Efficiency and Influence of Bioorthogonal Protein Modification via Genetically Encoded Strain Promoted Click Chemistry. *Chem. Commun.* **2012**, *48*, 8419–8421. (e) Aronoff, M. R.; Gold, B.; Raines, R. T. 1,3-Dipolar Cycloadditions of Diazo Compounds in the Presence of Azides. *Org. Lett.* **2016**, *18*, 1538–1541. (f) Kaneda, K.; Naruse, R.; Yamamoto, S. 2-Aminobenzenesulfonamide-Containing Cyclononyne as Adjustable Click Reagent for Strain-Promoted Azide–Alkyne Cycloaddition. *Org. Lett.* **2017**, *19*, 1096–1099.

(5) Baskin, J. M.; Prescher, J. A.; Laughlin, S. T.; Agard, N. J.; Chang, P. V.; Miller, I. A.; Lo, A.; Codelli, J. A.; Bertozzi, C. R. Copper-Free Click Chemistry for Dynamic in Vivo Imaging. *Proc. Natl. Acad. Sci. USA* **2007**, *104*, 16793–16797.

(6) (a) Golkowski, M.; Ziegler, T. Synthesis of Tetra(2-Hydroxyethoxy)-Substituted Dibenzocyclooctyne Derivatives as Novel, Highly Hydrophilic Tool Compounds for Strain-Promoted Alkyne–Azide Cycloaddition Applications. *Synthesis* **2013**, *45*, 1207–1214. (b) Debets, M. F.; Prins, J. S.; Merkx, D.; Van Berkel, S. S.; Van Delft, F. L.; Van Hest, J. C. M.; Rutjes, F. P. J. T. Synthesis of DIBAC Analogues with Excellent SPAAC Rate Constants. *Org. Biomol. Chem.* **2014**, *12*, 5031–5037. (c) Chadwick, R. C.; Van Gyzen, S.; Liogier, S.; Adronov, A. Scalable Synthesis of Strained Cyclooctyne Derivatives. *Synthesis* **2014**, *46*, 669–677.

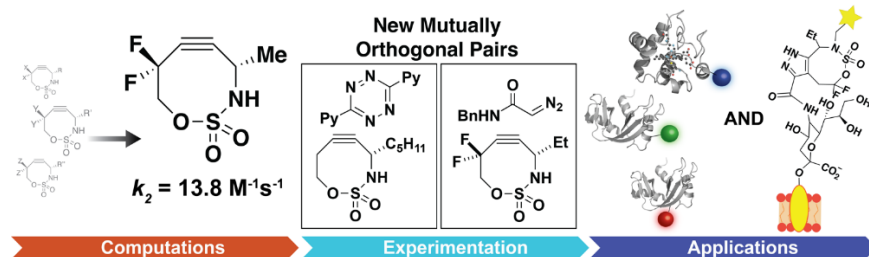
(7) Debets, M. F.; Van Berkel, S. S.; Schoffelen, S.; Rutjes, F. P. J. T.; Van Hest, J. C. M.; Van Delft, F. L. Aza-Dibenzocyclooctynes for Fast and Efficient Enzyme PEGylation via Copper-Free [3+2] Cycloaddition. *Chem. Commun.* **2010**, *46*, 97–99.

(8) (a) McKay, C. S.; Finn, M. G. Click Chemistry in Complex Mixtures: Bioorthogonal Bioconjugation. *Chem. Biol.* **2014**, *21*, 1075–1101. (b) Bakum, T.; Van Leeuwen, T.; Sarris, A. J. C.; Van Elstrand, D. M.; Poulcharidis, D.; Overkleeft, H. S.; Van Kasteren, S. I. Quantification of Bioorthogonal Stability in Immune Phagocytes Using Flow Cytometry Reveals Rapid Degradation of Strained Alkynes. *ACS*

- (9) Burke, E. G.; Gold, B.; Hoang, T. T.; Raines, R. T.; Schomaker, J. M. Fine-Tuning Strain and Electronic Activation of Strain-Promoted 1,3-Dipolar Cycloadditions with Endocyclic Sulfamates in SNO-OCTs. *J. Am. Chem. Soc.* **2017**, *139*, 8029–8037.
- (10) Tu, J.; Svatunek, D.; Parvez, S.; Liu, A. C.; Levandowski, B. J.; Eckvahl, H. J.; Peterson, R. T.; Houk, K. N.; Franzini, R. M. Stable, Reactive and Orthogonal Tetrazines: Dispersion Forces Promote the Cycloaddition with Isonitriles. *Angew. Chem., Int. Ed.* **2019**, *58*, 9043–9048.
- (11) Glendening, E. D.; Badenhop, J. K.; Reed, A. E.; Carpenter, J. E.; Bohmann, J. A.; Morales, C. M.; Landis, C. R.; Weinhold, F. NBO 6.0, Theoretical Chemistry Institute, University of Wisconsin, Madison, 2013.
- (12) (a) Hohenstein, E. G.; Chill, S. T.; Sherrill, C. D. Assessment of the Performance of the M05-2X and M06-2X Exchange-Correlation Functionals for Noncovalent Interactions in Biomolecules. *J. Chem. Theory Comput.* **2008**, *4*, 1996–2000. (b) Walker, M.; Harvey, A. J. A.; Sen, A.; Dessent, C. E. H. Performance of M06, M06-2X, and M06-HF Density Functionals for Conformationally Flexible Anionic Clusters: M06 Functionals Perform Better than B3LYP for a Model System with Dispersion and Ionic Hydrogen-Bonding Interactions. *J. Phys. Chem. A* **2013**, *117*, 12590–12600.
- (13) Frisch, M. J.; Trucks, G. W.; Schlegel, H. B.; Scuseria, G. E.; Robb, M. A.; Cheeseman, J. R.; Scalmani, G.; Barone, V.; Petersson, G. A.; Nakatsuji, H.; Li, X.; Caricato, M.; Marenich, A. V.; Bloino, J.; Janesko, B. G.; Gomperts, R.; Mennucci, B.; Hratch, D. J. Gaussian 16, Revision B.01. Gaussian, Inc.: Wallingford, CT **2016**.
- (14) Liu, F.; Liang, Y.; Houk, K. Bioorthogonal Cycloadditions: Computational Analysis with the Distortion/Interaction Model and Predictions of Reactivities. *Acc. Chem. Res.* **2017**, *50*, 2297–2308.
- (15) (a) Garcia-Hartjes, J.; Dommerholt, J.; Wennekes, T.; Van Delft, F. L.; Zuilhof, H. Electronic Effects versus Distortion Energies during Strain-Promoted Alkyne-Azide Cycloadditions: A Theoretical Tool to Predict Reaction Kinetics. *European J. Org. Chem.* **2013**, *6*, 3712–3720. (b) Escorihuela, J.; Das, A.; Looijen, W. J. E.; Van Delft, F. L.; Aquino, A. J. A.; Lischka, H.; Zuilhof, H. Kinetics of the Strain-Promoted Oxidation-Controlled Cycloalkyne-1,2-Quinone Cycloaddition: Experimental and Theoretical Studies. *J. Org. Chem.* **2018**, *83*, 244–252.
- (16) (a) Barone, V.; Cossi, M. Quantum Calculation of Molecular Energies and Energy Gradients in Solution by a Conductor Solvent Model. *J. Phys. Chem. A* **1998**, *102*, 1995–2001. (b) Cossi, M.; Rega, N.; Scalmani, G.; Barone, V. Energies, Structures, and Electronic Properties of Molecules in Solution with the C-PCM Solvation Model. *J. Comput. Chem.* **2003**, *24*, 669–681. (c) Takano, Y.; Houk, K. N. Benchmarking the Conductor-like Polarizable Continuum Model (CPCM) for Aqueous Solvation Free Energies of Neutral and Ionic Organic Molecules. *J. Chem. Theory Comput.* **2005**, *1*, 70–77. (d) Grimme, S. Semiempirical GGA-Type Density Functional Constructed with a Long-Range Dispersion Correction. *J. Comput. Chem.* **2006**, *27*, 1787–1799. (e) Grimme, S.; Ehrlich, S.; Goerigk, L. Effect of the Damping Function in Dispersion Corrected Density Functional Theory. *J. Comput. Chem.* **2011**, *32*, 1456–1465.
- (17) Fleming, I. *Molecular Orbitals and Organic Chemistry Reactions: Student Edition*; Wiley: West Sussex, UK, 2009.
- (18) (a) Ess, D. H.; Houk, K. N. Distortion/Interaction Energy Control of 1,3-Dipolar Cycloaddition Reactivity. *J. Am. Chem. Soc.* **2007**, *129*, 10646–10647. (b) Ess, D. H.; Houk, K. N. Theory of 1,3-Dipolar Cycloadditions: Distortion/Interaction and Frontier Molecular Orbital Models. *J. Am. Chem. Soc.* **2008**, *130*, 10187–10198.
- (19) (a) Fernández, I.; Bickelhaupt, F. M. The Activation Strain Model and Molecular Orbital Theory: Understanding and Designing Chemical Reactions. *Chem. Soc. Rev.* **2014**, *43*, 4953–4967. (b) Wolters, L. P.; Bickelhaupt, F. M. The Activation Strain Model and Molecular Orbital Theory. *Wiley Interdiscip. Rev. Comput. Mol. Sci.* **2015**, *5*, 324–343.
- (20) Liu, F.; Liang, Y.; Houk, K. N. Theoretical Elucidation of the Origins of Substituent and Strain Effects on the Rates of Diels–Alder Reactions of 1,2,4,5-Tetrazines. *J. Am. Chem. Soc.* **2014**, *136*, 11483–11493.
- (21) Sadasivam, D. V.; Prasad, E.; Flowers, R. A.; Birney, D. M. Stopped-Flow Kinetics of Tetrazine Cycloadditions; Experimental and Computational Studies toward Sequential Transition States. *J. Phys. Chem. A* **2006**, *110*, 1288–1294.
- (22) Andersen, K. A.; Aronoff, M. R.; Mcgrath, N. A.; Raines, R. T. Diazo Groups Endure Metabolism and Enable Chemoselectivity in Cellulo. *J. Am. Chem. Soc.* **2015**, *137*, 2412–2415.
- (23) (a) Huang, L. L.; Liu, K.; Zhang, Q.; Xu, J.; Zhao, D.; Zhu, H.; Xie, H. Y. Integrating Two Efficient and Specific Bioorthogonal Ligation Reactions with Natural Metabolic Incorporation in One Cell for Virus Dual Labeling. *Anal. Chem.* **2017**, *89*, 11620–11627. (b) Das, D. K.; Govindan, R.; Nikić-Spiegel, I.; Krammer, F.; Lemke, E. A.; Munro, J. B. Direct Visualization of the Conformational Dynamics of Single Influenza Hemagglutinin Trimers. *Cell* **2018**, *174*, 926–937.e12. (c) Reisacher, U.; Ploschik, D.; Röncke, F.; Cserép, G. B.; Kele, P.; Wagenknecht, H.-A. Copper-Free Dual Labeling of DNA by Triazines and Cyclopropenes as Minimal Orthogonal and Bioorthogonal Functions. *Chem. Sci.* **2019**, *10*, 4032–4037.
- (24) Dommerholt, J.; Van Rooijen, O.; Borrmann, A.; Fonseca Guerra, C.; Bickelhaupt, F. M.; Van Delft, F. L. Highly Accelerated Inverse Electron-Demand Cycloaddition of Electron-Deficient Azides with Aliphatic Cyclooctynes. *Nat. Commun.* **2014**, *5*, 5378.
- (25) (a) Dilek, O.; Lei, Z.; Bane, S. Rapid Formation of a Stable Boron–Nitrogen Heterocycle in Dilute, Neutral Aqueous Solution for Bioorthogonal Coupling Reactions. *Chem. Commun.* **2015**, 16992–16995. (b) Gu, H.; Ghosh, S.; Staples, R. J.; Bane, S. L. β -Hydroxy-Stabilized Boron–Nitrogen Heterocycles Enable Rapid and Efficient C-Terminal Protein Modification. *Bioconjugate Chem.* **2019**, *30*, 2604–2613. For reviews: (c) Akgun, B.; Hall, D. G. Boronic Acids as Bioorthogonal Probes for Site-Selective Labeling of Proteins. *Angew. Chem., Int. Ed.* **2018**, *57*, 13028–13044.
- (26) (a) Kolb, H. C.; Finn, M. G.; Sharpless, B. K. Click Chemistry: Diverse Chemical Function from a Few Good Reactions. *Angew. Chem., Int. Ed.* **2001**, *40*, 2004–2021. (b) Cravatt, B. F.; Wright, A. T.; Kozarich, J. W. Activity-Based Protein Profiling: From Enzyme Chemistry to Proteomic Chemistry. *Annu. Rev. Biochem.* **2008**, *77*, 383–414. (c) Laughlin, S. T.; Bertozzi, C. R. Imaging the Glycome. *Proc. Natl. Acad. Sci. U.S.A.* **2009**, *106*, 12–17. (d) Signore, G.; Nifosi, R.; Albertazzi, L.; Storti, B.; Bizzarri, R. Polarity-Sensitive Coumarins Tailored to Live Cell Imaging. *J. Am. Chem. Soc.* **2010**, *132*, 1276–1288. (e) Dennler, P.; Fischer, E.; Schibli, R. Antibody Conjugates: From Heterogenous Populations to Defined Reagents. *Antibodies* **2015**, *4*, 197–224. (f) Beck, A.; Goetsch, L.; Dumontet, C.; Corvaia, N. Strategies and Challenges for the next Generation of Antibody-Drug Conjugates. *Nat. Rev. Drug Discov.* **2017**, *16*, 315–337. (g) Rudra, A.; Li, J.; Shakur, R.; Bhagchandani, S.; Langer, R. Trends in Therapeutic Conjugates: Bench to Clinic. *Bioconjugate Chem.* **2020**, *31*, 462–473.
- (27) (a) Letschert, S.; Gohler, A.; Franke, N.; Bertleff-Zieschang, N.; Memmel, E.; Doose, S.; Siebel, J.; Sauer, M. Super-Resolution Imaging of Plasma Membrane Glycans. *Angew. Chem., Int. Ed.* **2014**, *126*, 11101–11104. (b) Chen, J.; Gao, J.; Wu, M.; Zhang, M.; Cai, H.; Xu, J.; Jiang, Z.; Tian, Z.; Wang, H. Revealing the Carbohydrate Pattern on a Cell Surface by Super-Resolution Imaging. *Nanoscale* **2015**, *7*, 3373–3380. (c) Hegermann, J.; Lunsdorf, H.; Ochs, M.; Haller, H. Visualization of the Glomerular Endothelial Glycocalyx by Electron Microscopy Using Cationic Colloidal Thorium Dioxide. *Histochem. Cell Biol.* **2016**, *145*, 41–51. (d) Mockl, L.; Pedram, K.; Roy, A. R.; Krishnan, V.; Gustavsson, A. K.; Dorigo, O.; Bertozzi, C. R. Quantitative Super-Resolution Microscopy of the Mammalian Glycocalyx. *Dev. Cell* **2019**, *50*, 57–72.
- (28) (a) Esko, J. D.; Rostand, K. S.; Weinke, J. L. Tumor Formation Dependent on Proteoglycan Biosynthesis. *Science*. **1988**, *241*, 1092–1096. (b) Matrosovich, M. N.; Matrosovich, T. Y.; Gray, T.; Roberts, N. A.; Klenk, H. D. Neuraminidase is Important for the Initiation of

Influenza Virus Infection in Human Airway Epithelium. *J. Virol.* **2004**, 78, 12655–12667. (c) Hudak, J. E.; Canham, S. M.; Bertozzi, C. R. Glycocalyx Engineering Reveals a Siglec-Based Mechanism for NK Cell Immune Evasion. *Nat. Chem. Biol.* **2014**, 10, 69–75. (d) Constantinou, P. E.; Morgado, M.; Carson, D. Transmembrane Mucin Expression and Function in Embryo Implantation and Placentation in *Regulation of Implantation and Establishment of Pregnancy in Mammals*, Bazer, F. W., Geisert, R. D., Eds.; Springer: New York, NY, 2015. (e) Gandhi, J. G.; Kock, D. L.; Paszek, M. J. Equilibrium Modeling of the Mechanics and Structure of the Cancer Glycocalyx. *Biophys. J.* **2019**, 116, 694–708.

(29) (a) Kayser, H.; Zeitler, R.; Kannicht, C.; Grunow, D.; Nuck, R.; Reutter, W. Biosynthesis of a Nonphysiological Sialic Acid in Different Rat Organs, Using *N*-Propanoyl-D-Hexosamines as Precursors. *J. Biol. Chem.* **1992**, 267, 16934–16938. (b) Mahal, L. K.; Yarema, K. J.; Bertozzi, C. R. Engineering Chemical Reactivity on Cell Surfaces Through Oligosaccharide Biosynthesis. *Science*. **1997**, 276, 1125–1128. (c) Saxon, E.; Bertozzi, C. R. Cell Surface Engineering by a Modified Staudinger Reaction. *Science*. **2000**, 287, 2007–2010.



Jennifer Schomaker - Triple, Mutually Orthogonal Cycload... (1.44 MiB)

[view on ChemRxiv](#) • [download file](#)

Supplementary Materials Part 1 for

Triple, Mutually Orthogonal Cycloadditions Through the Design of Electronically Activated SNO-OCTs

Yun Hu,^{†,‡} Jessica M. Roberts,^{†,‡} Henry R. Kilgore,^{§,‡} Amirah S. Mat Lani,[†]
Ronald T. Raines,^{*,§} and Jennifer M. Schomaker^{*,†}

[†]Department of Chemistry, University of Wisconsin, Madison, Wisconsin 53706, United States

[§]Department of Chemistry, Massachusetts Institute of Technology, Cambridge, Massachusetts 02139, United States

[‡]These authors contributed equally to this work.

*Corresponding authors: schomakerj@chem.wisc.edu, rtraines@mit.edu

Table of Contents.....	S1-1
I. Computational Methods.....	S1-2
II. Alkyne electrophilicity calculations.....	S1-3
III. Frontier molecular orbital calculations.....	S1-6
IV. Free energies of activation and calculated reaction rates.....	S1-8
V. Distortion/interaction analyses.....	S1-13
VI. References.....	S1-16
VII. Cartesian coordinates.....	S1-17

I. Computational Methods

All calculations were conducted using the Gaussian 16 software package.¹ Computational models were visualized using CYLView.²

Ground state geometry optimizations. Initial geometry optimizations for reported SNO-OCTs and dipoles were performed using M06-2X level of theory and 6-311++G(d,p) basis set with the integral equation formalism variant polarizable continuum model (IEFPCM) for specified solvents.³⁻⁵ These structures were also optimized using B97D level of theory and 6-311+G(d,p) basis set with the conductor-like polarizable continuum model (CPCM) for specified solvents.⁶ Frequency calculations were conducted to ensure no negative frequencies were observed for geometry optimized structures, indicating that the stationary points are minima.

Transition state geometry optimizations. All transition state models were calculated using the OPT=(TS,NoEigenTest,CalcFc) keywords. Frequency calculations were conducted to ensure one negative frequency is obtained for each transition state model. In addition, IRC calculations were conducted in the forward and reverse direction along the negative bond frequency in order to confirm that the transition state model obtained is along the reaction path between the reactant complex and the product complex. All reported ΔE and ΔE^\ddagger values are reported with zero-point correction. Activation energies were determined by energy differences between the transition state and a summation of the reactants.

Distortion/interaction analyses. Distortion/interaction analysis⁷ involved obtaining the dipole and SNO-OCT structures from the transition state optimization and performing individual single point calculations. Activation barriers were determined by the difference in energy between the transition state and the summation of starting materials.

Calculated regioselectivity. Regioselectivity is defined herein as the difference in Gibbs free energy of activation between two regioisomers.

Frontier molecular orbital (FMO) and natural bond orbital (NBO) analyses. Frontier molecular orbital energy levels were obtained from geometry optimization calculations conducted in Gaussian 16.¹ Natural bond orbital analysis was conducted using the NBO 6 software package in Gaussian 16.^{1,8}

II. Alkyne electrophilicity calculations

Figure S1-1. Investigated SNO-OCT derivatives.

A variety of substitution patterns were investigated in order to determine advantageous tuning of the alkyne electronics for use as a dienophile in 1,3-dipolar cycloadditions (**Figure S1-1**). NBO analysis⁸ was conducted on geometry optimized SNO-OCTs in water to investigate the effects of scaffold derivatization on alkyne electronics. Numerous orbital interactions can be envisaged within the SNO-OCT, with variations on the impact of reactivity depending on the nature of X and R (**Figure S1-2**).⁹ The resultant calculations illustrated minimal changes to alkyne electronics based on perturbations of the exocyclic side chain (R), with alterations of the propargylic position (X) and the heteroatoms in the ring (Y) having more profound impacts.

Alkyne electrophilicity was determined using similar methodology reported in our previous work⁹ and was used as an initial indicator of potential dipole coupling partners to target for each SNO-OCT. Second-order perturbation energies of orbital interactions were classified into two categories – enhancing electrophilic or nucleophilic character – and the difference between the two sums was deemed as the predicted alkyne electrophilicity.

Figure S1-2. Predicted alkyne electrophilicity based on second-order perturbation energies from NBO analysis.^{8,9}

Table S1-1. Second-order perturbation energies for various orbital interactions influencing alkyne electronics in the SNO-OCT derivatives.

III. Frontier molecular orbital considerations.

The reactivity of 1,3-dipolar cycloadditions can be categorized using on frontier molecular orbital (FMO) theory (see generalized FMO diagram, **Figure S1-3a**).¹⁰ Type I involves interaction between the lowest unoccupied molecular orbital (LUMO) of the dipolarophile and the highest occupied molecular orbital (HOMO) of the dipole. Introduction of electron withdrawing functionalities into the alkyne scaffold lead to LUMO stabilization, effectively decreasing the energy gap and accelerating reaction kinetics. The ambiphilic Type II cycloadditions have similar energy gaps between FMOs and have reaction rates that have a parabolic relationship with alkyne ionization potential.¹⁷ Type III cycloadditions often involve interaction between LUMO_{dipole} and HOMO_{dipolarophile}; it is important to note that inverse electron demand Diels Alder (IEDDA) reactions involving tetrazine, as described in this work, involves the LUMO+1 of the tetrazine and the HOMO of the SNO-OCT coupling partner. Scaffold modifications leading to electron donation into the alkyne can destabilize the HOMO and are expected to enhance reactivity. Electronic activation can be guided by these principles, with changes to the scaffold affecting chemoselectivity. Three different coupling partners were investigated in this work: methyl diazoacetamide (Type I), methyl azide (Type II), and dipyrityl tetrazine (Type III) (**Figure S1-3b**). SNO-OCT derivatives were designed with varied substitution patterns to tune the alkyne electronics appropriately for specific Type I, II, or III dipoles. These modifications did lead to varied HOMO and LUMO energy levels, allowing for selective reactivity across different dipoles (**Figure S1-3c**).

(a) Frontier mol

Figure S1-3. (a) Applying frontier molecular orbital theory to help pair (b) Type I-III coupling partners with (c) electronically tuned SNO-OCT derivatives for Type I-III cycloadditions.

IV. Free energies of activation, calculated reaction rates, and regioselectivities

Table S1-2. Free energies of activation (kcal/mol) and reaction rates with methyl diazoacetamide. Geometry optimizations conducted at the M06-2X level of theory with 6-311++ (d,p) basis set and IEFPCM solvent model for water.

Table S1-3. Free energies of activation (kcal/mol) and reaction rates with methyl diazoacetamide. Geometry optimizations conducted at the B97D level of theory with 6-311+(d,p) basis set and CPCM solvent model for water.

Table S1-4. Free energies of activation (kcal/mol) and reaction rates with methyl azide. Geometry optimizations conducted at the M06-2X level of theory with 6-311++(d,p) basis set and IEFCPM solvent model for water.

Table S1-5. Free energies of activation (kcal/mol) and reaction rates with methyl azide. Geometry optimizations conducted at the B97D level of theory with 6-311+(d,p) basis set and CPCM solvent model for water.

Table S1-6. Free energies of activation (kcal/mol) and reaction rates with dipyrityl tetrazine. Geometry optimizations conducted at the B97D level of theory with 6-311+(d,p) basis set and CPCM solvent model for water.

V. Distortion/interaction analyses

(a)

Figure S1-4. (a) Distortion energies, interaction energies, and activation barriers for reaction of various SNO-OCTs with methyl diazoacetamide. (b) Distortion energy and (c) interaction energy trends with respect to activation barrier. Geometry optimizations conducted at the B97D level of theory with 6-311+(d,p) basis set and CPCM solvent model for water.

(a)

Figure S1-5. (a) Distortion energies, interaction energies, and activation barriers for reaction of various SNO-OCTs with dipyrityl tetrazine. (b) Distortion energy and (c) interaction energy trends with respect to activation barrier. Geometry optimizations conducted at the B97D level of theory with 6-311+(d,p) basis set and CPCM solvent model for water.

(c)

Figure S1-6. (a) Distortion energies, interaction energies, and activation barriers for reaction of various SNO-OCTs with methyl azide. (b) Distortion energy and (c) interaction energy trends with respect to activation barrier. Geometry optimizations conducted at the B97D level of theory with 6-311+(d,p) basis set and CPCM solvent model for water.

VI. References

1. Frisch, M. J.; Trucks, G. W.; Schlegel, H. B.; Scuseria, G. E.; Robb, M. A.; Cheeseman, J. R.; Scalmani, G.; Barone, V.; Petersson, G. A.; Nakatsuji, H.; Li, X.; Caricato, M.; Marenich, A. V.; Bloino, J.; Janesko, B. G.; Gomperts, R.; Mennucci, B.; Hratch, D. J. Gaussian 16, Revision B.01. Gaussian, Inc.: Wallingford, CT **2016**.
2. Legault, C.Y.; CYLview, 1.0b, Université de Sherbrooke, **2009**.
3. (a) Hohenstein, E. G.; Chill, S. T.; Sherrill, C. D. Assessment of the Performance of the M05-2X and M06-2X Exchange-Correlation Functionals for Noncovalent Interactions in Biomolecules. *J. Chem. Theory Comput.* **2008**, *4*, 1996–2000. (b) Walker, M.; Harvey, A. J. A.; Sen, A.; Dessent, C. E. H. Performance of M06, M06-2X, and M06-HF Density Functionals for Conformationally Flexible Anionic Clusters: M06 Functionals Perform Better than B3LYP for a Model System with Dispersion and Ionic Hydrogen-Bonding Interactions. *J. Phys. Chem. A*. **2013**, *117*, 12590–12600.
4. (a) Grimme, S. Semiempirical GGA-Type Density Functional Constructed with a Long-Range Dispersion Correction. *J. Comput. Chem.* **2006**, *27*, 1787–1799. (b) Grimme, S.; Ehrlick, S.; Goerigk, L. Effect of the Damping Function in Dispersion Corrected Density Functional Theory. *J. Comput. Chem.* **2011**, *32*, 1456–1465.
5. (a) Miertuš, S.; Scrocco, E.; Tomasi, J. Electrostatic Interaction of a Solute with a Continuum. A Direct Utilization of *ab Initio* Molecular Potentials for the Prevision of Solvent Effects. *Chem. Phys.* **1981**, *55*, 117–129. (b) Tomasi, J.; Mennucci, B.; Cancès, E. The IEF Version of the PCM Solvation Method: An Overview of a New Method Addressed to Study Molecular Solutes at the QM *ab Initio* Level. *J. Mol. Struct.: THEOCHEM* **1999**, *464*, 211–226. (c) Tomasi, J.; Mennucci, B.; Cammi, R. Quantum Mechanical Continuum Solvation Models. *Chem. Rev.* **2005**, *105*, 2999–3094.
6. (a) Barone, V.; Cossi, M. Quantum Calculation of Molecular Energies and Energy Gradients in Solution by a Conductor Solvent Model. *J. Phys. Chem. A* **1998**, *102*, 1995–2001. (b) Cossi, M.; Rega, N.; Scalmani, G.; Barone, V. Energies, Structures, and Electronic Properties of Molecules in Solution with the C-PCM Solvation Model. *J. Comput. Chem.* **2003**, *24*, 669–681. (c) Takano, Y.; Houk, K. N. Benchmarking the Conductor-like Polarizable Continuum Model (CPCM) for Aqueous Solvation Free Energies of Neutral and Ionic Organic Molecules. *J. Chem. Theory Comput.* **2005**, *1*, 70–77.
7. (a) Ess, D. H.; Houk, K. N. Distortion/Interaction Energy Control of 1,3-Dipolar Cycloaddition Reactivity. *J. Am. Chem. Soc.* **2007**, *129*, 10646–10647. (b) Ess, D. H.; Houk, K. N. Theory of 1,3-Dipolar Cycloadditions: Distortion/Interaction and Frontier Molecular Orbital Models. *J. Am. Chem. Soc.* **2008**, *130*, 10187–10198.

8. Glendening, E. D.; Badenhop, J. K.; Reed, A. E.; Carpenter, J. E.; Bohmann, J. A.; Morales, C. M.; Landis, C. R.; Weinhold, F. NBO 6.0. Theoretical Chemistry Institute, University of Wisconsin, Madison. **2013**.
9. Burke, E. G.; Gold, B.; Hoang, T. T.; Raines, R. T.; Schomaker, J. M. Fine-Tuning Strain and Electronic Activation of Strain-Promoted 1,3-Dipolar Cycloadditions with Endocyclic Sulfamates in SNO-OCTs. *J. Am. Chem. Soc.* **2017**, *139*, 8029–8037.
10. Fleming, I. *Molecular Orbitals and Organic Chemistry Reactions: Student Edition*; Wiley: West Sussex, **2009**.

VII. Cartesian coordinates

VIIa. Ground state geometry optimizations

2 using M06-2X/6-311++G(d,p) and IEFPCM solvent model (water)

C	0.45267	1.61443	0.27140
C	-0.63102	2.08950	0.05968
C	-2.05855	2.10537	-0.24460
H	-2.62812	2.78682	0.38960
H	-2.22947	2.38385	-1.28585
C	1.45245	0.54449	0.38497
C	-2.52683	0.66672	0.02078
H	-3.52908	0.49582	-0.36754
H	-2.49585	0.44291	1.08603
N	0.92002	-0.66591	-0.28379
S	-0.59200	-1.21204	0.05479
O	-0.71654	-2.47870	-0.62156
O	-0.78092	-1.09460	1.48162
C	2.79586	0.90893	-0.25146
H	3.15653	1.82072	0.23248
H	2.64763	1.12113	-1.31239
H	1.60728	0.29231	1.43732
H	1.12155	-0.72236	-1.27971
O	-1.67681	-0.27432	-0.68726
O	3.73231	-0.13975	-0.17030
H	4.00957	-0.24476	0.74531

HF: -987.6859524

Sum of electronic and zero-point Energies=	-987.524356
Sum of electronic and thermal Energies=	-987.512912
Sum of electronic and thermal Enthalpies=	-987.511968
Sum of electronic and thermal Free Energies=	-987.561644

2 using M06-2X/6-311++G(d,p) and IEFPCM solvent model (acetonitrile)

C	0.45250	1.61373	0.27484
---	---------	---------	---------

C	-0.63061	2.08934	0.06150
C	-2.05738	2.10563	-0.24618
H	-2.62842	2.78651	0.38734
H	-2.22561	2.38531	-1.28756
C	1.45262	0.54417	0.38855
C	-2.52635	0.66655	0.01630
H	-3.52753	0.49615	-0.37513
H	-2.49863	0.44191	1.08147
N	0.92089	-0.66681	-0.27921
S	-0.59206	-1.21231	0.05550
O	-0.71541	-2.47872	-0.62104
O	-0.78494	-1.09346	1.48158
C	2.79491	0.91023	-0.24947
H	3.15757	1.81957	0.23774
H	2.64397	1.12770	-1.30897
H	1.60827	0.29269	1.44099
H	1.12821	-0.72889	-1.27349
O	-1.67428	-0.27348	-0.68987
O	3.73067	-0.13941	-0.17661
H	4.00658	-0.25358	0.73828

HF: -987.6854308

Sum of electronic and zero-point Energies=	-987.523892
Sum of electronic and thermal Energies=	-987.512413
Sum of electronic and thermal Enthalpies=	-987.511469
Sum of electronic and thermal Free Energies=	-987.561304

2 using B97D/6-311+G(d,p) and CPCM solvent model (water)

C	0.49671	1.64799	0.22023
C	-0.59524	2.14270	0.02180
C	-2.03381	2.16534	-0.22719
H	-2.57783	2.88038	0.40694
H	-2.25311	2.41350	-1.27507
C	1.46365	0.54887	0.33914
C	-2.53803	0.73940	0.11026
H	-3.58103	0.60713	-0.19867
H	-2.43670	0.53854	1.18189
N	0.91524	-0.66531	-0.34878
S	-0.62137	-1.24326	0.05077
O	-0.76598	-2.49709	-0.68725
O	-0.74302	-1.17599	1.50914
C	2.84896	0.87654	-0.26949
H	3.18559	1.82145	0.18349
H	2.74524	1.02599	-1.35186
H	1.59733	0.28144	1.39603
H	0.99072	-0.60076	-1.36548
O	-1.79672	-0.27790	-0.65250
O	3.80478	-0.16526	-0.09041
H	4.01897	-0.21337	0.85154

HF: -987.5676955

Sum of electronic and zero-point Energies=	-987.413680
Sum of electronic and thermal Energies=	-987.401587
Sum of electronic and thermal Enthalpies=	-987.400643

Sum of electronic and thermal Free Energies= -987.451441

2 using B97D/6-311+G(d,p) and CPCM solvent model (acetonitrile)

C	0.49654	1.64791	0.22067
C	-0.59529	2.14281	0.02206
C	-2.03379	2.16531	-0.22734
H	-2.57807	2.88012	0.40685
H	-2.25276	2.41379	-1.27524
C	1.46351	0.54881	0.33968
C	-2.53785	0.73901	0.10934
H	-3.58079	0.60677	-0.19997
H	-2.43699	0.53800	1.18101
N	0.91546	-0.66547	-0.34795
S	-0.62128	-1.24358	0.05100
O	-0.76564	-2.49718	-0.68708
O	-0.74369	-1.17535	1.50920
C	2.84875	0.87701	-0.26885
H	3.18547	1.82145	0.18518
H	2.74473	1.02789	-1.35100
H	1.59710	0.28153	1.39665
H	0.99203	-0.60211	-1.36459
O	-1.79606	-0.27752	-0.65328
O	3.80458	-0.16495	-0.09171
H	4.01663	-0.21694	0.85049

HF: -987.5673519

Sum of electronic and zero-point Energies= -987.413341

Sum of electronic and thermal Energies= -987.401245

Sum of electronic and thermal Enthalpies= -987.400300

Sum of electronic and thermal Free Energies= -987.451113

3 using M06-2X/6-311++G(d,p) and IEFPCM solvent model (water)

C	0.01994	1.60569	0.34415
C	-1.13341	1.29101	0.23204
C	-2.15800	0.28258	-0.02595
C	1.48679	1.53087	0.37537
C	-1.51838	-1.10232	0.13286
H	-2.19575	-1.85899	-0.26246
H	-1.31952	-1.27561	1.19036
N	1.87219	0.28466	-0.33136
S	1.16237	-1.14658	0.04544
O	1.88433	-2.16350	-0.66853
O	0.99171	-1.18344	1.47659
C	2.19706	2.70686	-0.28196
H	1.95215	3.62138	0.25657
H	3.27459	2.54973	-0.24580
H	1.87836	2.81498	-1.31990
H	1.80831	1.42711	1.41315
H	2.00156	0.38841	-1.33565
O	-0.31664	-1.17485	-0.63873

F	-3.21545	0.35464	0.82330
F	-2.66701	0.42001	-1.28080

HF: -1110.9497004

Sum of electronic and zero-point Energies=	-1110.809738
Sum of electronic and thermal Energies=	-1110.797886
Sum of electronic and thermal Enthalpies=	-1110.796942
Sum of electronic and thermal Free Energies=	-1110.847499

3 using B97D/6-311+G(d,p) and CPCM solvent model (water)

C	-0.02192	1.63786	0.30929
C	-1.18530	1.30747	0.19567
C	-2.17835	0.26547	-0.02391
C	1.44281	1.58420	0.36184
C	-1.52457	-1.12491	0.18837
H	-2.21979	-1.90339	-0.14628
H	-1.30136	-1.24197	1.25429
N	1.87793	0.34214	-0.36093
S	1.21621	-1.15485	0.05196
O	1.96082	-2.14504	-0.71664
O	1.10438	-1.19780	1.50973
C	2.16689	2.78503	-0.26650
H	1.88441	3.69401	0.27678
H	3.25020	2.63921	-0.19017
H	1.88259	2.89794	-1.32019
H	1.75568	1.46774	1.40691
H	1.86272	0.45165	-1.37688
O	-0.33595	-1.27140	-0.62240
F	-3.26080	0.34789	0.84254
F	-2.71148	0.34772	-1.30514

HF: -1110.8107373

Sum of electronic and zero-point Energies=	-1110.678026
Sum of electronic and thermal Energies=	-1110.665418
Sum of electronic and thermal Enthalpies=	-1110.664473
Sum of electronic and thermal Free Energies=	-1110.716531

3a using M06-2X/6-311++G(d,p) and IEFPCM solvent model (water)

C	-0.06138	1.67074	0.15002
C	-1.21620	1.41715	-0.06483
C	-2.31204	0.52932	-0.44006
C	1.37838	1.45860	0.35929
C	-1.82638	-0.89868	-0.12803
H	-2.50891	-1.63714	-0.54499
H	-1.75128	-1.01790	0.95302
N	1.71969	0.14988	-0.25434
S	0.83700	-1.19365	0.08644
O	1.53859	-2.29954	-0.50934
O	0.52040	-1.15924	1.49323
C	2.28160	2.52528	-0.24474
H	2.06619	3.48525	0.22299

H	3.32574	2.26907	-0.06695
H	2.10637	2.61324	-1.31843
H	1.56838	1.36859	1.43028
H	1.95277	0.19872	-1.24393
O	-0.55196	-1.12887	-0.75239
F	-3.45866	0.73467	0.31267
H	-2.58113	0.64418	-1.49053

HF=-1011.701895

Sum of electronic and zero-point Energies=	-1011.553347
Sum of electronic and thermal Energies=	-1011.542214
Sum of electronic and thermal Enthalpies=	-1011.541270
Sum of electronic and thermal Free Energies=	-1011.590087

3a using B97D/6-311+G(d,p) and CPCM solvent model (water)

C	-0.11779	1.70157	0.12747
C	-1.27883	1.41236	-0.08432
C	-2.33776	0.47987	-0.44004
H	-2.61325	0.54943	-1.50001
C	1.32307	1.52575	0.35198
C	-1.83371	-0.94595	-0.07514
H	-2.53478	-1.70257	-0.44396
H	-1.72874	-1.02146	1.01273
N	1.72786	0.22349	-0.28134
S	0.89902	-1.20183	0.08943
O	1.64461	-2.27009	-0.56965
O	0.63723	-1.19336	1.52919
C	2.22246	2.62911	-0.22558
H	1.96117	3.58338	0.24635
H	3.27333	2.39798	-0.01684
H	2.07326	2.71799	-1.30953
H	1.50885	1.42158	1.42826
H	1.82512	0.29965	-1.29573
O	-0.57082	-1.23042	-0.74177
F	-3.53301	0.68374	0.30542

HF=-1011.5841257

Sum of electronic and zero-point Energies=	-1011.442862
Sum of electronic and thermal Energies=	-1011.431052
Sum of electronic and thermal Enthalpies=	-1011.430108
Sum of electronic and thermal Free Energies=	-1011.480251

4 using M06-2X/6-311++G(d,p) and IEFPCM solvent model (water)

C	0.96101	1.50044	0.24461
C	-0.06317	2.10035	0.05294
C	-1.48461	2.27710	-0.23067
H	-1.96487	3.01866	0.41022
H	-1.63877	2.57380	-1.26957
C	1.84107	0.32778	0.35707
C	-2.11088	0.90201	0.04307

H	-3.13161	0.84615	-0.33074
H	-2.09001	0.67505	1.10798
N	1.16057	-0.81409	-0.31047
S	-0.40171	-1.18510	0.05125
O	-0.67968	-2.42920	-0.62183
O	-0.55586	-1.05089	1.48092
C	3.21661	0.49443	-0.27517
H	3.74887	1.30068	0.22856
H	3.78852	-0.42781	-0.17333
H	3.12283	0.74807	-1.33289
H	1.94687	0.05828	1.40937
H	1.32246	-0.86012	-1.31442
O	-1.38460	-0.13057	-0.67572

HF: -912.4683389

Sum of electronic and zero-point Energies: -912.311954

Sum of electronic and thermal Energies= -912.301686

Sum of electronic and thermal Enthalpies= -912.300742

Sum of electronic and thermal Free Energies= -912.347195

4 using M06-2X/6-311++G(d,p) and IEFPCM solvent model (acetonitrile)

C	0.96101	1.50107	0.24328
C	-0.06315	2.10100	0.05165
C	-1.48492	2.27714	-0.23069
H	-1.96469	3.01894	0.41032
H	-1.64026	2.57323	-1.26961
C	1.84055	0.32811	0.35675
C	-2.11031	0.90180	0.04432
H	-3.13168	0.84555	-0.32780
H	-2.08769	0.67528	1.10931
N	1.16038	-0.81369	-0.31085
S	-0.40180	-1.18561	0.05131
O	-0.67956	-2.42896	-0.62274
O	-0.55552	-1.05138	1.48089
C	3.21689	0.49401	-0.27399
H	3.74885	1.30044	0.22978
H	3.78838	-0.42836	-0.17097
H	3.12457	0.74713	-1.33198
H	1.94507	0.05895	1.40928
H	1.32174	-0.85945	-1.31484
O	-1.38474	-0.13028	-0.67520

HF: -912.4679546

Sum of electronic and zero-point Energies= -912.311559

Sum of electronic and thermal Energies= -912.301292

Sum of electronic and thermal Enthalpies= -912.300348

Sum of electronic and thermal Free Energies= -912.346800

4 using B97D/6-311+G(d,p) and CPCM solvent model (water)

C	1.03270	1.50665	0.22409
C	0.01724	2.14459	0.02784

C	-1.40462	2.35421	-0.23361
H	-1.85800	3.13164	0.39857
H	-1.57932	2.63376	-1.28204
C	1.86318	0.30061	0.35092
C	-2.09547	1.00619	0.09071
H	-3.14215	1.01017	-0.23413
H	-2.03743	0.79237	1.16306
N	1.15800	-0.84141	-0.33349
S	-0.44817	-1.20611	0.05370
O	-0.75079	-2.43479	-0.67956
O	-0.57407	-1.11763	1.51077
C	3.27153	0.40363	-0.25579
H	3.82226	1.19982	0.25890
H	3.80525	-0.54558	-0.12798
H	3.21322	0.65097	-1.32409
H	1.94242	0.02100	1.40902
H	1.24507	-0.79031	-1.35043
O	-1.48190	-0.09901	-0.66380

HF: -912.3698172

Sum of electronic and zero-point Energies=	-912.220776
Sum of electronic and thermal Energies=	-912.209834
Sum of electronic and thermal Enthalpies=	-912.208889
Sum of electronic and thermal Free Energies=	-912.256660

4 using B97D/6-311+G(d,p) and CPCM solvent model (acetonitrile)

C	1.03270	1.50685	0.22357
C	0.01730	2.14489	0.02742
C	-1.40469	2.35427	-0.23349
H	-1.85791	3.13167	0.39887
H	-1.57984	2.63381	-1.28188
C	1.86290	0.30065	0.35075
C	-2.09515	1.00598	0.09099
H	-3.14207	1.00993	-0.23322
H	-2.03654	0.79222	1.16334
N	1.15794	-0.84131	-0.33364
S	-0.44826	-1.20646	0.05381
O	-0.75080	-2.43475	-0.67978
O	-0.57395	-1.11746	1.51079
C	3.27154	0.40343	-0.25537
H	3.82218	1.19974	0.25926
H	3.80511	-0.54581	-0.12719
H	3.21369	0.65056	-1.32377
H	1.94164	0.02119	1.40894
H	1.24471	-0.79011	-1.35058
O	-1.48175	-0.09868	-0.66383

HF: -912.3695642

Sum of electronic and zero-point Energies=	-912.220516
Sum of electronic and thermal Energies=	-912.209575
Sum of electronic and thermal Enthalpies=	-912.208631
Sum of electronic and thermal Free Energies=	-912.256398

8 using M06-2X/6-311++G(d,p) and IEFPCM solvent model (water)

C	0.82910	1.56463	0.30272
C	-0.24236	2.07048	0.10313
C	-1.66315	2.13815	-0.22039
H	-2.22338	2.81195	0.42988
H	-1.80891	2.45753	-1.25340
C	1.78577	0.45978	0.35614
C	-2.17765	0.70649	-0.00906
H	-3.16320	0.56735	-0.44726
H	-2.19597	0.45405	1.04955
O	1.15221	-0.65624	-0.37939
S	-0.28556	-1.19321	0.05023
O	-0.39103	-2.47143	-0.59082
O	-0.45027	-1.05280	1.47467
C	3.10799	0.69687	-0.33951
H	3.63577	1.50051	0.17479
H	3.71370	-0.20776	-0.30290
H	2.94006	0.98670	-1.37658
H	1.92600	0.12303	1.38448
O	-1.32256	-0.24708	-0.70702
HF: -932.3305297			
Sum of electronic and zero-point Energies=			-932.186816
Sum of electronic and thermal Energies=			-932.176727
Sum of electronic and thermal Enthalpies=			-932.175783
Sum of electronic and thermal Free Energies=			-932.221992

8 using B97D/6-311+G(d,p) and CPCM solvent model (water)

C	0.92828	1.56330	0.29075
C	-0.13033	2.12112	0.08322
C	-1.54945	2.24693	-0.22844
H	-2.07843	2.96660	0.41250
H	-1.69953	2.55286	-1.27278
C	1.82656	0.41805	0.35871
C	-2.16019	0.84578	0.02484
H	-3.17404	0.77856	-0.38240
H	-2.16297	0.61010	1.09311
O	1.14235	-0.70987	-0.40051
S	-0.35279	-1.21320	0.05581
O	-0.50702	-2.48280	-0.64050
O	-0.50363	-1.10282	1.50729
C	3.17958	0.57027	-0.32634
H	3.74406	1.34999	0.20104
H	3.73627	-0.37212	-0.27237
H	3.04803	0.86941	-1.37265
H	1.93980	0.06585	1.39130
O	-1.41612	-0.20486	-0.70468
HF: -932.2292445			
Sum of electronic and zero-point Energies=			-932.092887
Sum of electronic and thermal Energies=			-932.082068
Sum of electronic and thermal Enthalpies=			-932.081124

Sum of electronic and thermal Free Energies= -932.128727

9 using M06-2X/6-311++G(d,p) and IEFPCM solvent model (water)

C	-0.19825	-1.41322	0.43612
C	0.99245	-1.45425	0.29205
C	2.26286	-0.81290	-0.03978
C	-1.57526	-0.91000	0.46940
C	2.07031	0.70618	0.05457
H	2.92398	1.20426	-0.40473
H	1.98105	0.98136	1.10517
N	-1.59765	0.38379	-0.24513
S	-0.47783	1.53904	0.04964
O	-0.89216	2.70568	-0.67993
O	-0.23785	1.56045	1.47120
C	-2.56969	-1.86584	-0.20206
H	-2.24649	-2.05374	-1.22781
H	-1.87275	-0.72996	1.50548
H	-1.86727	0.33998	-1.22490
O	0.91053	1.09874	-0.68361
F	3.27833	-1.15951	0.79146
F	2.66138	-1.15621	-1.29460
H	-2.54897	-2.81085	0.34665
O	-3.86074	-1.31491	-0.27253
H	-4.25091	-1.30024	0.60730

HF: -1186.1664438

Sum of electronic and zero-point Energies= -1186.021145

Sum of electronic and thermal Energies= -1186.008154

Sum of electronic and thermal Enthalpies= -1186.007210

Sum of electronic and thermal Free Energies= -1186.060874

9 using B97D/6-311+G(d,p) and CPCM solvent model (water)

C	-0.20644	-1.45887	0.31077
C	1.00025	-1.51790	0.18797
C	2.27612	-0.84777	-0.02533
C	-1.56994	-0.92623	0.36541
C	2.09833	0.67737	0.19753
H	3.00760	1.19525	-0.12866
H	1.91813	0.85209	1.26376
N	-1.58813	0.38096	-0.35920
S	-0.48639	1.58935	0.05227
O	-0.87260	2.76099	-0.72421
O	-0.37127	1.59821	1.51025
C	-2.63443	-1.87015	-0.25591
H	-2.43697	-1.98367	-1.32887
H	-1.83819	-0.72444	1.41083
H	-1.61577	0.27450	-1.37476
O	1.02240	1.19948	-0.61607
F	3.27191	-1.27822	0.84040
F	2.75587	-1.08740	-1.30672

H	-2.51862	-2.85079	0.22873
O	-3.95690	-1.36589	-0.12939
H	-4.22334	-1.44965	0.79670
HF: -1186.0077627			
Sum of electronic and zero-point Energies=			-1185.870125
Sum of electronic and thermal Energies=			-1185.856363
Sum of electronic and thermal Enthalpies=			-1185.855419
Sum of electronic and thermal Free Energies=			-1185.910480

10 using M06-2X/6-311++G(d,p) and IEFPCM solvent model (water)

C	-0.16337	-1.42515	0.44121
C	1.02762	-1.43130	0.30324
C	2.28381	-0.76242	-0.03300
C	-1.53538	-0.92209	0.43709
C	2.04376	0.75226	0.04408
H	2.87118	1.27230	-0.43652
H	1.95574	1.04077	1.09079
O	-1.50514	0.30916	-0.35375
S	-0.51557	1.49658	0.04294
O	-1.01473	2.63420	-0.66241
O	-0.30827	1.50013	1.46577
C	-2.53910	-1.83952	-0.25140
H	-2.48530	-2.81561	0.23893
H	-2.24639	-1.95441	-1.29560
H	-1.85613	-0.66890	1.45022
O	0.86033	1.10085	-0.69001
F	3.30242	-1.06635	0.80659
F	2.69260	-1.10832	-1.28092
O	-3.83540	-1.29933	-0.22884
H	-4.22353	-1.43804	0.64079
HF: -1206.025134			
Sum of electronic and zero-point Energies=			-1205.892379
Sum of electronic and thermal Energies=			-1205.879669
Sum of electronic and thermal Enthalpies=			-1205.878725
Sum of electronic and thermal Free Energies=			-1205.931717

10 using B97D/6-311+G(d,p) and CPCM solvent model (water)

C	-0.17111	-1.44775	0.41002
C	1.03433	-1.47013	0.27741
C	2.28941	-0.79455	-0.02757
C	-1.53807	-0.94724	0.41588
C	2.07826	0.74018	0.08852
H	2.94030	1.25327	-0.35070
H	1.96931	0.99789	1.14658
O	-1.52210	0.31472	-0.38965
S	-0.52212	1.54851	0.04977
O	-1.02382	2.68031	-0.70679
O	-0.35078	1.57078	1.49978
C	-2.56589	-1.87027	-0.26831

H	-2.46791	-2.85967	0.20480
H	-2.31171	-1.95773	-1.33067
H	-1.85881	-0.69133	1.43420
O	0.92797	1.17573	-0.68523
F	3.31987	-1.13236	0.83195
F	2.72668	-1.11860	-1.30242
O	-3.89157	-1.36762	-0.18741
H	-4.21534	-1.51272	0.71244
HF: -1205.8635998			
Sum of electronic and zero-point Energies=			-1205.738546
Sum of electronic and thermal Energies=			-1205.724984
Sum of electronic and thermal Enthalpies=			-1205.724040
Sum of electronic and thermal Free Energies=			-1205.778750

D1 using M06-2X/6-311++G(d,p) and IEFPCM solvent model (water)

C	2.74658	0.12617	-0.00051
N	1.49433	-0.60902	0.00058
C	0.30784	0.03671	0.00027
C	-0.87109	-0.83131	0.00031
N	-2.02562	-0.22403	-0.00011
N	-2.99887	0.33184	-0.00049
O	0.22137	1.26469	0.00037
H	3.56558	-0.58910	0.00397
H	2.82556	0.75494	-0.88904
H	1.51368	-1.61667	-0.00212
H	-0.88650	-1.90944	0.00067
H	2.82199	0.76188	0.88328
HF: -356.7294236			
Sum of electronic and zero-point Energies=			-356.640212
Sum of electronic and thermal Energies=			-356.632435
Sum of electronic and thermal Enthalpies=			-356.631491
Sum of electronic and thermal Free Energies=			-356.672830

D1 using B97D/6-311+G(d,p) and CPCM solvent model (water)

C	-2.78913	0.07680	0.00045
N	-1.49680	-0.60692	-0.00073
C	-0.31522	0.07601	-0.00008
C	0.87646	-0.79891	-0.00003
N	2.05679	-0.24042	0.00008
N	3.06629	0.29146	0.00025
O	-0.25215	1.31707	-0.00025
H	-3.57495	-0.68471	-0.00508
H	-2.89841	0.70467	0.89551
H	-1.48880	-1.61809	0.00108
H	0.85724	-1.88424	-0.00011
H	-2.89447	0.71360	-0.88863
HF: -356.651195			
Sum of electronic and zero-point Energies=			-356.565775
Sum of electronic and thermal Energies=			-356.558597

Sum of electronic and thermal Enthalpies=	-356.557652
Sum of electronic and thermal Free Energies=	-356.597300

D3 using B97D/6-311+G(d,p) and CPCM solvent model (water)

C	1.29187	0.01333	0.33078
C	-1.29187	-0.01328	0.33078
N	-0.66566	1.17462	0.49536
N	0.65197	1.19619	0.51882
N	-0.65195	-1.19613	0.51890
N	0.66565	-1.17457	0.49545
C	-2.74884	-0.01231	0.05545
C	-5.43402	-0.08577	-0.49888
C	-3.52774	1.12760	0.33212
N	-3.25766	-1.14480	-0.47819
C	-4.57146	-1.16601	-0.74611
C	-4.89639	1.08295	0.05089
H	-3.06672	2.01180	0.76284
H	-4.95773	-2.08744	-1.18423
H	-5.52864	1.94383	0.25921
H	-6.49276	-0.16570	-0.73581
C	2.74883	0.01232	0.05543
C	5.43403	0.08572	-0.49887
C	3.52771	-1.12762	0.33210
N	3.25770	1.14480	-0.47819
C	4.57150	1.16598	-0.74608
C	4.89636	-1.08300	0.05088
H	3.06665	-2.01180	0.76280
H	4.95779	2.08740	-1.18420
H	5.52858	-1.94390	0.25920
H	6.49277	0.16561	-0.73578

HF=-790.1523328

Sum of electronic and zero-point Energies=	-789.969607
Sum of electronic and thermal Energies=	-789.956030
Sum of electronic and thermal Enthalpies=	-789.955085
Sum of electronic and thermal Free Energies=	-790.012275

D4 using M06-2X/6-311++G(d,p) and IEFPCM solvent model (water)

H	-2.42898	0.31125	-0.00119
C	-1.52808	-0.29467	-0.00007
H	-1.51582	-0.92230	0.89312
H	-1.51473	-0.92397	-0.89207
N	-0.38893	0.64670	-0.00012
N	0.71303	0.11151	0.00054
N	1.76562	-0.28635	-0.00034

HF: -204.0628864

Sum of electronic and zero-point Energies=	-204.012019
Sum of electronic and thermal Energies=	-204.007584
Sum of electronic and thermal Enthalpies=	-204.006640

Sum of electronic and thermal Free Energies= -204.038578

D4 using M06-2X/6-311++G(d,p) and IEFPCM solvent model (acetonitrile)

H	-2.42913	0.31066	-0.00009
C	-1.52767	-0.29456	0.00001
H	-1.51548	-0.92336	0.89265
H	-1.51531	-0.92340	-0.89261
N	-0.38918	0.64682	0.00006
N	0.71287	0.11128	-0.00012
N	1.76574	-0.28617	0.00007

HF: -204.0627687

Sum of electronic and zero-point Energies= -204.011897

Sum of electronic and thermal Energies= -204.007470

Sum of electronic and thermal Enthalpies= -204.006526

Sum of electronic and thermal Free Energies= -204.038433

D4 using B97D/6-311+G(d,p) and CPCM solvent model (water)

H	-2.45053	0.36086	-0.00052
C	-1.56612	-0.28126	-0.00001
H	-1.57089	-0.91331	0.89928
H	-1.57042	-0.91412	-0.89872
N	-0.38627	0.62587	-0.00004
N	0.71946	0.09426	0.00007
N	1.80804	-0.26954	-0.00004

HF: -204.033061

Sum of electronic and zero-point Energies= -203.984252

Sum of electronic and thermal Energies= -203.979741

Sum of electronic and thermal Enthalpies= -203.978797

Sum of electronic and thermal Free Energies= -204.010846

D4 using B97D/6-311+G(d,p) and CPCM solvent model (acetonitrile)

H	2.45053	-0.36086	-0.00052
C	1.56612	0.28126	-0.00001
H	1.57089	0.91331	0.89928
H	1.57042	0.91412	-0.89872
N	0.38627	-0.62587	-0.00004
N	-0.71946	-0.09426	0.00007
N	-1.80804	0.26954	-0.00004

HF: -204.0329772

Sum of electronic and zero-point Energies= -203.984168

Sum of electronic and thermal Energies= -203.979656

Sum of electronic and thermal Enthalpies= -203.978712

Sum of electronic and thermal Free Energies= -204.010763

VIIb. Transition state optimizations

Coupling with D1 (*anti* TS)

2 using M06-2X/6-311++G(d,p) and IEFPCM solvent model (water)

C	0.14838	0.66405	0.43778
C	-0.58981	-0.32677	0.45046
C	-0.75855	-1.77689	0.20455
H	-1.46672	-2.23729	0.89763
H	-1.14515	-1.93927	-0.80573
C	1.41502	1.37381	0.18892
C	0.57793	-2.48472	0.37677
H	0.50272	-3.53714	0.10742
H	0.94150	-2.39139	1.39931
N	2.42493	0.54161	-0.50426
S	2.75749	-0.97806	-0.02987
O	3.89491	-1.41239	-0.80395
O	2.78579	-0.99201	1.41499
C	1.19314	2.61780	-0.68467
H	0.51805	3.29132	-0.15505
H	0.71615	2.31259	-1.61901
H	1.85113	1.68173	1.14420
H	2.46849	0.65128	-1.51352
O	1.56086	-1.92979	-0.53039
O	2.40116	3.25583	-1.03757
H	2.78816	3.65309	-0.25088
C	-4.82768	-1.27390	-1.35023
N	-4.06403	-0.94764	-0.15703
C	-3.38734	0.21117	-0.06514
C	-2.54471	0.33428	1.16218
N	-2.10563	1.57049	1.40135
N	-1.22449	2.28255	1.31711
O	-3.38701	1.06743	-0.93994
H	-5.24472	-2.27066	-1.23072
H	-5.63814	-0.55828	-1.49803
H	-4.08654	-1.57806	0.62974
H	-2.76387	-0.24666	2.05148
H	-4.18033	-1.25666	-2.22801

HF: -1344.4009427

Sum of electronic and zero-point Energies= -1344.148511

Sum of electronic and thermal Energies= -1344.128820

Sum of electronic and thermal Enthalpies= -1344.127876

Sum of electronic and thermal Free Energies= -1344.198078

Frequency: -463.11

2 using B97D/6-311+G(d,p) and CPCM solvent model (water)

C	0.17641	0.81557	0.48867
---	---------	---------	---------

C	-0.62915	-0.12507	0.64357
C	-0.85403	-1.58790	0.71057
H	-1.50386	-1.86187	1.55518
H	-1.35841	-1.94300	-0.19979
C	1.54036	1.30561	0.20283
C	0.47005	-2.33457	0.90377
H	0.30263	-3.41705	0.94122
H	0.97976	-2.00986	1.81742
N	2.30190	0.37475	-0.68828
S	2.69999	-1.16439	-0.16498
O	3.56756	-1.73343	-1.19626
O	3.12812	-1.04983	1.23270
C	1.56804	2.70333	-0.46924
H	0.99964	3.38479	0.17483
H	1.07054	2.64850	-1.44629
H	2.10841	1.36785	1.14159
H	1.91102	0.32488	-1.63009
O	1.35580	-2.13955	-0.25331
O	2.88787	3.19340	-0.70984
H	3.29424	3.37799	0.14805
C	-4.79344	-1.59692	-1.13280
N	-4.11360	-0.89563	-0.04343
C	-3.42894	0.25998	-0.24602
C	-2.65214	0.70870	0.96238
N	-2.25191	1.99375	0.95845
N	-1.35526	2.70405	0.80659
O	-3.37101	0.84263	-1.33569
H	-5.18596	-2.53861	-0.73819
H	-5.62098	-0.99282	-1.52910
H	-4.16403	-1.28985	0.88651
H	-2.94190	0.34852	1.94985
H	-4.08841	-1.80581	-1.94807

HF: -1344.2085547

Sum of electronic and zero-point Energies= -1343.967216

Sum of electronic and thermal Energies= -1343.946616

Sum of electronic and thermal Enthalpies= -1343.945671

Sum of electronic and thermal Free Energies= -1344.018115

Frequency: -378.12

3 using M06-2X/6-311++G(d,p) and IEFPCM solvent model (water)

C	0.39591	1.10648	0.23315
C	-0.32906	0.12054	0.38758
C	-0.40608	-1.34455	0.30103
C	1.64318	1.82786	-0.08017
C	0.94361	-2.01857	0.50593
H	0.83723	-3.08978	0.33569
H	1.29090	-1.82437	1.52042
N	2.64944	0.95116	-0.73027
S	3.05266	-0.48697	-0.07921
O	4.19226	-0.98111	-0.80506
O	3.07044	-0.33420	1.35542
C	1.44002	3.02775	-1.00239
H	0.78966	3.75429	-0.52005

H	2.40170	3.49477	-1.21494
H	0.97695	2.71172	-1.93945
H	2.08101	2.16254	0.86333
H	2.58579	0.90353	-1.74461
O	1.87311	-1.53677	-0.46290
F	-1.25231	-1.87489	1.24029
F	-0.92634	-1.71714	-0.90739
C	-4.52552	-1.27050	-1.18826
N	-3.79494	-0.75539	-0.04205
C	-3.18945	0.44202	-0.09549
C	-2.30442	0.73487	1.07740
N	-1.89609	2.00006	1.14653
N	-1.06797	2.75007	0.96296
O	-3.29159	1.22208	-1.03236
H	-5.00036	-2.20580	-0.90275
H	-5.29100	-0.55695	-1.49202
H	-3.58741	-1.37688	0.72549
H	-2.46206	0.25699	2.03743
H	-3.85305	-1.44694	-2.03081

HF: -1467.6739851

Sum of electronic and zero-point Energies= -1467.442723

Sum of electronic and thermal Energies= -1467.422861

Sum of electronic and thermal Enthalpies= -1467.421917

Sum of electronic and thermal Free Energies= -1467.491534

Frequency: -405.38

3 using B97D/6-311+G(d,p) and CPCM solvent model (water)

C	0.38975	1.10984	0.22311
C	-0.34916	0.11734	0.37731
C	-0.37540	-1.34863	0.31880
C	1.62950	1.84246	-0.08031
C	0.99146	-2.01025	0.56788
H	0.88053	-3.09567	0.46559
H	1.32796	-1.75699	1.57893
N	2.65817	0.98308	-0.76274
S	3.14296	-0.46520	-0.08690
O	4.27024	-0.94290	-0.88156
O	3.22469	-0.27792	1.36261
C	1.42812	3.07063	-0.98855
H	0.75551	3.77755	-0.49449
H	2.39471	3.55373	-1.17342
H	0.98259	2.76712	-1.94516
H	2.07899	2.16377	0.86829
H	2.47436	0.85322	-1.75886
O	1.95455	-1.61290	-0.42968
F	-1.23387	-1.90070	1.28184
F	-0.88444	-1.77651	-0.90769
C	-4.60776	-1.36475	-1.15967
N	-3.87233	-0.77530	-0.04052
C	-3.28322	0.44343	-0.13421
C	-2.37108	0.74845	1.03049
N	-1.99241	2.02936	1.15596
N	-1.15091	2.80017	0.99808

O	-3.42473	1.21533	-1.08861
H	-5.12340	-2.25869	-0.79658
H	-5.34286	-0.64535	-1.53764
H	-3.61505	-1.38237	0.72737
H	-2.51789	0.23722	1.98076
H	-3.92686	-1.64077	-1.97830
HF: -1467.4584083			
Sum of electronic and zero-point Energies=			-1467.238204
Sum of electronic and thermal Energies=			-1467.217264
Sum of electronic and thermal Enthalpies=			-1467.216320
Sum of electronic and thermal Free Energies=			-1467.288501
Frequency: -343.14			

3a using M06-2X/6-311++G(d,p) and IEFPCM solvent model (water)

C	0.29928	1.00018	0.22800
C	-0.37802	-0.02717	0.31949
C	-0.42868	-1.48702	0.14040
C	1.52188	1.77876	-0.04604
C	0.94686	-2.09859	0.39846
H	0.92157	-3.17444	0.23218
H	1.26416	-1.88135	1.41854
N	2.55808	0.96531	-0.73198
S	3.01560	-0.48446	-0.13909
O	4.16848	-0.90335	-0.89374
O	3.05043	-0.38080	1.30015
C	1.28058	3.00937	-0.91650
H	0.59425	3.68548	-0.41053
H	2.22304	3.52664	-1.09726
H	0.84030	2.71690	-1.87228
H	1.95070	2.08762	0.91015
H	2.48214	0.94813	-1.74631
O	1.88305	-1.56640	-0.54923
F	-1.29127	-2.09421	1.06062
C	-4.48771	-1.35184	-1.41830
N	-3.72396	-0.95559	-0.24657
C	-3.24228	0.29323	-0.12789
C	-2.36858	0.50175	1.06823
N	-1.98649	1.76355	1.24696
N	-1.16752	2.53691	1.11261
O	-3.44077	1.18167	-0.94652
H	-4.81234	-2.38076	-1.28552
H	-5.36237	-0.71083	-1.53182
H	-3.46026	-1.65270	0.43438
H	-2.50470	-0.07080	1.97758
H	-3.87953	-1.27838	-2.32196
H	-0.79543	-1.74844	-0.85477
HF=-1368.4236136			
Sum of electronic and zero-point Energies=			-1368.184023
Sum of electronic and thermal Energies=			-1368.164847
Sum of electronic and thermal Enthalpies=			-1368.163903
Sum of electronic and thermal Free Energies=			-1368.232256
Frequency: -419.88			

3a using B97D/6-311+G(d,p) and CPCM solvent model (water)

C	0.29711	1.02577	0.26402
C	-0.39466	-0.00571	0.37662
C	-0.41495	-1.46901	0.24051
H	-0.79330	-1.77856	-0.74260
C	1.52621	1.78905	-0.01754
C	0.97121	-2.08229	0.51793
H	0.91927	-3.17305	0.43100
H	1.31316	-1.79954	1.51957
N	2.54178	0.97565	-0.77355
S	3.08226	-0.49010	-0.17546
O	4.18279	-0.90839	-1.04058
O	3.23692	-0.34821	1.27383
C	1.30288	3.06644	-0.84827
H	0.63214	3.73689	-0.30287
H	2.26174	3.56955	-1.02091
H	0.84265	2.81690	-1.81383
H	1.99937	2.05659	0.93613
H	2.30963	0.87519	-1.76302
O	1.91834	-1.65744	-0.49820
F	-1.28528	-2.08476	1.20524
C	-4.45962	-1.51703	-1.43006
N	-3.77761	-0.98360	-0.25049
C	-3.30484	0.28867	-0.20856
C	-2.45301	0.55948	1.00571
N	-2.11207	1.84136	1.20758
N	-1.27829	2.63179	1.09902
O	-3.49568	1.12937	-1.09513
H	-4.86120	-2.50210	-1.17443
H	-5.28067	-0.85036	-1.71870
H	-3.49181	-1.63442	0.47030
H	-2.61025	-0.01102	1.91925
H	-3.76703	-1.61294	-2.27916

HF=-1368.22975

Sum of electronic and zero-point Energies= -1368.001192

Sum of electronic and thermal Energies= -1367.981007

Sum of electronic and thermal Enthalpies= -1367.980063

Sum of electronic and thermal Free Energies= -1368.051162

Frequency: -356.04

4 using M06-2X/6-311++G(d,p) and IEFPCM solvent model (water)

C	-0.19887	0.93986	-0.29284
C	0.43859	-0.10100	-0.48751
C	0.47191	-1.58048	-0.51320
H	1.10025	-1.96471	-1.32114
H	0.88458	-1.96330	0.42479
C	-1.41158	1.69666	0.08268
C	-0.93417	-2.12087	-0.72754

H	-0.95193	-3.20826	-0.67141
H	-1.33874	-1.79518	-1.68521
N	-2.40903	0.84566	0.78346
S	-2.93798	-0.54878	0.11481
O	-4.04019	-1.00602	0.92541
O	-3.09801	-0.31870	-1.30282
C	-1.14247	2.88463	1.00366
H	-0.50840	3.60830	0.49643
H	-2.08360	3.36307	1.27591
H	-0.63238	2.55218	1.91090
H	-1.89754	2.05009	-0.82961
H	-2.23294	0.73184	1.77919
O	-1.80912	-1.67226	0.33647
C	4.50706	-1.78097	1.11285
N	3.80992	-1.16953	-0.00649
C	3.26936	0.05755	0.10326
C	2.46435	0.48323	-1.07939
N	2.14761	1.77852	-1.08592
N	1.33372	2.54108	-0.86792
O	3.35564	0.74692	1.11160
H	4.82701	-2.77687	0.81719
H	5.38034	-1.18932	1.39188
H	3.75008	-1.66764	-0.88116
H	2.63928	0.05521	-2.06026
H	3.84444	-1.85632	1.97637

HF: -1269.1827118

Sum of electronic and zero-point Energies= -1268.935516

Sum of electronic and thermal Energies= -1268.917052

Sum of electronic and thermal Enthalpies= -1268.916108

Sum of electronic and thermal Free Energies= -1268.983182

Frequency: -467.01

4 using B97D/6-311+G(d,p) and CPCM solvent model (water)

C	-0.21633	0.96730	-0.26236
C	0.44451	-0.07498	-0.43907
C	0.47268	-1.55562	-0.46522
H	1.14423	-1.94492	-1.24406
H	0.84140	-1.94968	0.49328
C	-1.44457	1.70959	0.07819
C	-0.92432	-2.11510	-0.75951
H	-0.91163	-3.21112	-0.75756
H	-1.30081	-1.75291	-1.72240
N	-2.45452	0.84955	0.79398
S	-3.01715	-0.56881	0.09956
O	-4.11118	-1.03182	0.95437
O	-3.21129	-0.31117	-1.33068
C	-1.22046	2.93217	0.98774
H	-0.56100	3.64261	0.48075
H	-2.18040	3.41568	1.20608
H	-0.74612	2.62360	1.92944
H	-1.93386	2.03793	-0.84796
H	-2.18966	0.66408	1.76285

O	-1.87411	-1.76213	0.30457
C	4.60326	-1.87839	1.01612
N	3.89021	-1.17233	-0.04824
C	3.35806	0.06480	0.13583
C	2.51403	0.52302	-1.01965
N	2.23187	1.83798	-1.06304
N	1.41012	2.62732	-0.86953
O	3.47512	0.71386	1.18290
H	4.80179	-2.89866	0.67474
H	5.55425	-1.37981	1.25038
H	3.81891	-1.61625	-0.95408
H	2.65537	0.07419	-2.00311
H	3.98876	-1.90802	1.92490

HF: -1269.0099286

Sum of electronic and zero-point Energies= -1268.773769

Sum of electronic and thermal Energies= -1268.754265

Sum of electronic and thermal Enthalpies= -1268.753321

Sum of electronic and thermal Free Energies= -1268.823272

Frequency: -383.87

8 using M06-2X/6-311++G(d,p) and IEFPCM solvent model (water)

C	-0.22704	0.91530	-0.27106
C	0.43106	-0.11610	-0.43874
C	0.48387	-1.59430	-0.39160
H	1.12880	-2.01284	-1.16801
H	0.88448	-1.92213	0.57187
C	-1.42788	1.65930	0.10600
C	-0.91288	-2.15974	-0.60363
H	-0.92968	-3.23877	-0.46408
H	-1.29537	-1.90631	-1.59118
O	-2.38828	0.75973	0.79795
S	-2.92395	-0.54139	0.07618
O	-4.09103	-0.92438	0.81913
O	-2.99019	-0.32460	-1.34789
C	-1.20265	2.77802	1.10460
H	-0.57886	3.54444	0.64683
H	-2.15835	3.21763	1.38865
H	-0.69961	2.39158	1.99166
H	-1.94071	2.02404	-0.78632
O	-1.82416	-1.64134	0.40450
C	4.59665	-1.70726	1.05390
N	3.84900	-1.12013	-0.04608
C	3.26853	0.08633	0.08070
C	2.42508	0.48723	-1.08530
N	2.09041	1.77743	-1.09963
N	1.28809	2.54982	-0.88838
O	3.34652	0.77509	1.08936
H	4.92602	-2.69939	0.75610
H	5.46653	-1.09607	1.30012
H	3.81448	-1.60228	-0.93125
H	2.57855	0.05153	-2.06630
H	3.96293	-1.78782	1.93804

HF: -1289.0482777
Sum of electronic and zero-point Energies= -1288.813825
Sum of electronic and thermal Energies= -1288.795517
Sum of electronic and thermal Enthalpies= -1288.794572
Sum of electronic and thermal Free Energies= -1288.861365
Frequency: -445.19

8 using B97D/6-311+G(d,p) and CPCM solvent model (water)

C	0.23619	0.93930	0.24675
C	-0.44011	-0.09511	0.40423
C	-0.47512	-1.57512	0.35846
H	-1.15108	-2.00185	1.11271
H	-0.83806	-1.91679	-0.62183
C	1.42691	1.69128	-0.10180
C	0.91835	-2.15196	0.63710
H	0.91316	-3.24311	0.54293
H	1.27482	-1.86506	1.63152
O	2.44416	0.77123	-0.81698
S	3.00862	-0.54733	-0.06157
O	4.17438	-0.94196	-0.84397
O	3.10240	-0.31644	1.38241
C	1.23399	2.81852	-1.11272
H	0.59056	3.58064	-0.65873
H	2.20172	3.26728	-1.36541
H	0.75076	2.43795	-2.02060
H	1.94800	2.04653	0.79565
O	1.89400	-1.71398	-0.37885
C	-4.66799	-1.81396	-0.98745
N	-3.91146	-1.14180	0.06936
C	-3.35264	0.08266	-0.11192
C	-2.47837	0.50955	1.03768
N	-2.18468	1.81975	1.09810
N	-1.38847	2.63131	0.91256
O	-3.46726	0.74702	-1.14825
H	-4.87768	-2.83609	-0.65885
H	-5.61434	-1.29190	-1.18667
H	-3.84766	-1.59135	0.97313
H	-2.60669	0.04698	2.01646
H	-4.07791	-1.83856	-1.91211

HF: -1288.8725786
Sum of electronic and zero-point Energies= -1288.649147
Sum of electronic and thermal Energies= -1288.629779
Sum of electronic and thermal Enthalpies= -1288.628834
Sum of electronic and thermal Free Energies= -1288.697910
Frequency: -366.75

9 using M06-2X/6-311++G(d,p) and IEFPCM solvent model (water)

C	0.37942	0.84381	0.42752
C	-0.45910	-0.05995	0.44297

C	-0.70431	-1.47813	0.13918
C	1.69030	1.46819	0.20179
C	0.54971	-2.33396	0.25726
H	0.32818	-3.33934	-0.10035
H	0.86720	-2.35931	1.29917
N	2.66094	0.55853	-0.44350
S	2.83808	-0.98386	0.01728
O	3.96905	-1.51437	-0.69723
O	2.75248	-1.03615	1.45697
C	1.55783	2.70554	-0.70251
H	1.06184	2.41301	-1.63033
H	2.10798	1.76871	1.16762
H	2.84083	0.71124	-1.43174
O	1.57406	-1.81063	-0.58560
F	-1.63610	-2.03408	0.97562
F	-1.22670	-1.59928	-1.11861
H	0.93414	3.43840	-0.18831
O	2.81220	3.23548	-1.06391
H	3.21781	3.64479	-0.29266
C	-4.75967	-0.72042	-1.35440
N	-3.99967	-0.45446	-0.14406
C	-3.24721	0.65182	-0.03654
C	-2.36507	0.68120	1.17542
N	-1.82334	1.87277	1.42023
N	-0.91859	2.54880	1.35407
O	-3.22183	1.54919	-0.86751
H	-5.44205	0.10514	-1.55583
H	-4.09291	-0.84449	-2.21050
H	-3.90565	-1.18437	0.54654
H	-2.60266	0.10397	2.06151
H	-5.33320	-1.63203	-1.20769

HF: -1542.8918312

Sum of electronic and zero-point Energies= -1542.655404

Sum of electronic and thermal Energies= -1542.634320

Sum of electronic and thermal Enthalpies= -1542.633376

Sum of electronic and thermal Free Energies= -1542.705969

Frequency: -398.61

9 using B97D/6-311+G(d,p) and CPCM solvent model (water)

C	0.37031	0.86006	0.36459
C	-0.48994	-0.04142	0.41710
C	-0.68610	-1.48483	0.22456
C	1.69669	1.45115	0.14358
C	0.58574	-2.32453	0.43815
H	0.34928	-3.37533	0.23635
H	0.91992	-2.20352	1.47414
N	2.63784	0.54124	-0.58351
S	2.92530	-1.00389	-0.03135
O	4.01021	-1.54575	-0.84322
O	2.98143	-0.95354	1.43036
C	1.62220	2.77527	-0.67133
H	1.21845	2.55897	-1.66877

H	2.15336	1.66528	1.11981
H	2.49966	0.53175	-1.59447
O	1.61778	-1.96050	-0.50097
F	-1.63083	-2.01333	1.11576
F	-1.20459	-1.73619	-1.04530
H	0.92860	3.44326	-0.14704
O	2.89396	3.38495	-0.86972
H	3.19344	3.73305	-0.01861
C	-4.86623	-0.86082	-1.30778
N	-4.08466	-0.46864	-0.13459
C	-3.34595	0.66854	-0.11246
C	-2.43155	0.75376	1.08875
N	-1.92104	1.96713	1.34865
N	-1.00273	2.65849	1.28658
O	-3.36441	1.53166	-0.99588
H	-5.49751	-0.02400	-1.62737
H	-4.20914	-1.14933	-2.14133
H	-3.93192	-1.16303	0.58563
H	-2.66199	0.17594	1.98254
H	-5.49676	-1.71034	-1.02887

HF: -1542.6563046

Sum of electronic and zero-point Energies= -1542.431335

Sum of electronic and thermal Energies= -1542.409115

Sum of electronic and thermal Enthalpies= -1542.408171

Sum of electronic and thermal Free Energies= -1542.484377

Frequency: -338.00

10 using M06-2X/6-311++G(d,p) and IEFPCM solvent model (water)

C	0.39084	0.85026	0.40055
C	-0.46901	-0.03168	0.44528
C	-0.73252	-1.45716	0.18480
C	1.71816	1.40044	0.15555
C	0.51704	-2.31768	0.32283
H	0.29000	-3.33244	-0.00103
H	0.84857	-2.30789	1.36032
O	2.55572	0.43952	-0.58611
S	2.80282	-1.00881	-0.00485
O	3.93333	-1.51878	-0.71877
O	2.76248	-0.98129	1.43380
C	1.70815	2.64665	-0.72705
H	1.05305	3.38300	-0.25694
H	1.29527	2.37902	-1.70069
H	2.22199	1.60096	1.10498
O	1.53893	-1.83095	-0.55347
F	-1.65896	-1.97819	1.04493
F	-1.26101	-1.61183	-1.06442
O	3.00363	3.15198	-0.94319
H	3.29277	3.62702	-0.15810
C	-4.78277	-0.71635	-1.32814
N	-4.01350	-0.41584	-0.13161
C	-3.24215	0.67985	-0.06991
C	-2.35939	0.74409	1.14198

N	-1.81435	1.94258	1.34478
N	-0.93381	2.64242	1.27496
O	-3.19864	1.54201	-0.93593
H	-5.37163	-1.61097	-1.14289
H	-5.45086	0.11266	-1.56087
H	-3.94266	-1.11259	0.59493
H	-2.60321	0.20464	2.05003
H	-4.12073	-0.88694	-2.17975
HF: -1562.7545535			
Sum of electronic and zero-point Energies=			-1562.530902
Sum of electronic and thermal Energies=			-1562.509995
Sum of electronic and thermal Enthalpies=			-1562.509051
Sum of electronic and thermal Free Energies=			-1562.581657
Frequency: -363.11			

10 using B97D/6-311+G(d,p) and CPCM solvent model (water)

C	0.38677	0.84109	0.37272
C	-0.48342	-0.04820	0.42039
C	-0.68987	-1.48419	0.18078
C	1.68507	1.43867	0.14185
C	0.58443	-2.33090	0.35982
H	0.36132	-3.36583	0.08015
H	0.90399	-2.27623	1.40514
O	2.59455	0.48214	-0.61757
S	2.90803	-0.98304	0.00310
O	4.04764	-1.47011	-0.75652
O	2.90180	-0.94339	1.46489
C	1.65122	2.69541	-0.75470
H	0.93445	3.39210	-0.29957
H	1.29053	2.41014	-1.74957
H	2.18981	1.65479	1.09269
O	1.63311	-1.90048	-0.54101
F	-1.62780	-2.03862	1.05669
F	-1.21092	-1.68804	-1.09429
O	2.93233	3.29130	-0.92620
H	3.16309	3.74474	-0.10389
C	-4.88063	-0.83550	-1.28273
N	-4.08705	-0.45512	-0.11333
C	-3.33882	0.67461	-0.09215
C	-2.42191	0.75053	1.11045
N	-1.90155	1.95703	1.36816
N	-1.01401	2.68163	1.31983
O	-3.34901	1.53978	-0.97250
H	-5.51471	-1.68198	-1.00293
H	-5.50833	0.00738	-1.59328
H	-3.94421	-1.15005	0.60834
H	-2.64689	0.17011	2.00380
H	-4.23127	-1.12432	-2.12200
HF: -1562.5163987			
Sum of electronic and zero-point Energies=			-1562.303996
Sum of electronic and thermal Energies=			-1562.282018
Sum of electronic and thermal Enthalpies=			-1562.281074

Sum of electronic and thermal Free Energies= -1562.355968
 Frequency: -305.32

Coupling with D1 (syn TS)

2 using M06-2X/6-311++G(d,p) and IEFPCM solvent model (water)

C	0.16237	0.54231	-0.75733
C	-0.35721	1.66189	-0.71679
C	-1.51199	2.56023	-0.54722
H	-1.21120	3.55349	-0.20560
H	-2.02669	2.68511	-1.50341
C	0.00448	-0.92361	-0.67102
C	-2.47194	1.97549	0.48170
H	-3.37278	2.58027	0.56742
H	-1.99807	1.87777	1.45750
N	-1.43176	-1.26450	-0.61538
S	-2.34600	-0.69174	0.62511
O	-3.47477	-1.58473	0.73665
O	-1.54121	-0.38629	1.78917
C	0.55481	-1.66254	-1.89441
H	1.62972	-1.49091	-1.97268
H	0.07000	-1.27673	-2.79202
H	0.51456	-1.29409	0.22846
H	-1.59577	-2.26266	-0.73702
O	-2.94382	0.67364	0.04987
O	0.25562	-3.04355	-1.82406
H	0.86167	-3.46834	-1.20824
C	3.58762	-1.63756	1.73965
N	3.28452	-0.91162	0.51672
C	2.76573	0.33137	0.56273
C	2.39429	0.88989	-0.77138
N	2.17852	2.20591	-0.77609
N	1.38156	3.01696	-0.74552
O	2.52796	0.92564	1.60521
H	3.90699	-2.64219	1.47407
H	4.38074	-1.14183	2.30243
H	3.58474	-1.29508	-0.36641
H	2.84596	0.50955	-1.68100
H	2.69703	-1.69621	2.36625

HF: -1344.4014438

Sum of electronic and zero-point Energies= -1344.148520
 Sum of electronic and thermal Energies= -1344.129212
 Sum of electronic and thermal Enthalpies= -1344.128268
 Sum of electronic and thermal Free Energies= -1344.196581
 Frequency: -456.52

2 using B97D/6-311+G(d,p) and CPCM solvent model (water)

C	0.14767	0.59797	-0.78376
C	-0.41734	1.70660	-0.73795

C	-1.60471	2.55936	-0.56869
H	-1.34718	3.57233	-0.22682
H	-2.13666	2.66589	-1.52576
C	0.02923	-0.87135	-0.71952
C	-2.54941	1.95040	0.48070
H	-3.46119	2.54981	0.57493
H	-2.05883	1.86282	1.45579
N	-1.41374	-1.26471	-0.69369
S	-2.36303	-0.76748	0.61278
O	-3.48057	-1.71270	0.67138
O	-1.56297	-0.47335	1.81045
C	0.64460	-1.58643	-1.94553
H	1.69758	-1.29043	-2.03161
H	0.11127	-1.27922	-2.85211
H	0.54151	-1.24230	0.18305
H	-1.51150	-2.27993	-0.77312
O	-3.04058	0.62887	0.05916
O	0.51036	-3.00894	-1.85126
H	1.12157	-3.31925	-1.16808
C	3.54148	-1.75878	1.64605
N	3.26885	-0.89538	0.49673
C	2.76853	0.36313	0.63624
C	2.40800	0.99857	-0.67585
N	2.20506	2.32819	-0.66124
N	1.38927	3.14800	-0.65114
O	2.53000	0.89001	1.72887
H	3.71661	-2.77353	1.27598
H	4.42485	-1.41393	2.20242
H	3.56080	-1.21503	-0.41745
H	2.86789	0.63970	-1.59640
H	2.67737	-1.75781	2.32117

HF: -1344.2083773

Sum of electronic and zero-point Energies= -1343.966798

Sum of electronic and thermal Energies= -1343.946499

Sum of electronic and thermal Enthalpies= -1343.945555

Sum of electronic and thermal Free Energies= -1344.016084

Frequency: -371.31

3 using M06-2X/6-311++G(d,p) and IEFPCM solvent model (water)

C	-0.26797	0.32280	0.72407
C	0.42069	1.29089	0.38415
C	1.71524	1.80809	-0.05937
C	-0.40656	-1.13175	1.00437
C	2.47566	0.81739	-0.93203
H	3.44398	1.24254	-1.19525
H	1.89503	0.60267	-1.82904
N	0.89181	-1.83341	0.94083
S	1.86282	-1.72026	-0.36363
O	2.84265	-2.76840	-0.25921
O	1.02357	-1.57343	-1.52783
C	-1.00022	-1.44340	2.37590
H	-2.01772	-1.06589	2.44891

H	-1.02242	-2.52249	2.52683
H	-0.40333	-0.97893	3.16316
H	-1.03615	-1.57016	0.22545
H	1.41861	-1.85718	1.81028
O	2.74556	-0.37131	-0.19013
F	1.59795	2.95478	-0.79434
F	2.48627	2.14237	1.02052
C	-4.24315	-1.66460	-1.06432
N	-3.69360	-0.76719	-0.05972
C	-2.94419	0.29020	-0.41995
C	-2.35300	1.05175	0.72771
N	-1.94924	2.28223	0.40349
N	-1.07846	2.95513	0.13774
O	-2.67575	0.57200	-1.57853
H	-3.44304	-2.03064	-1.70805
H	-4.71041	-2.50474	-0.55705
H	-3.99044	-0.86717	0.89915
H	-2.77316	0.97867	1.72477
H	-4.98474	-1.15328	-1.68075

HF: -1467.6702901

Sum of electronic and zero-point Energies= -1467.439141

Sum of electronic and thermal Energies= -1467.419219

Sum of electronic and thermal Enthalpies= -1467.418274

Sum of electronic and thermal Free Energies= -1467.488226

Frequency: -415.32

3 using B97D/6-311+G(d,p) and CPCM solvent model (water)

C	-0.26656	0.38176	0.76169
C	0.43869	1.34558	0.39833
C	1.72858	1.81743	-0.08386
C	-0.39294	-1.05822	1.11262
C	2.43846	0.81282	-1.01240
H	3.38711	1.24756	-1.34657
H	1.79247	0.60142	-1.87162
N	0.90557	-1.78900	1.03082
S	1.82559	-1.76846	-0.36552
O	2.81110	-2.83696	-0.23420
O	0.91280	-1.67739	-1.50598
C	-0.92879	-1.29823	2.53656
H	-1.91498	-0.83930	2.65032
H	-1.01406	-2.37495	2.72154
H	-0.25272	-0.85055	3.27654
H	-1.06444	-1.53638	0.38947
H	1.50516	-1.65256	1.84543
O	2.79769	-0.39604	-0.30894
F	1.63098	3.00054	-0.82631
F	2.56914	2.13218	0.98925
C	-4.13877	-1.81771	-1.03573
N	-3.63080	-0.83372	-0.07793
C	-2.95055	0.27251	-0.47507
C	-2.38661	1.06878	0.68019
N	-2.04252	2.33622	0.38794

N	-1.18247	3.05513	0.12891
O	-2.71522	0.55635	-1.65284
H	-3.34454	-2.08773	-1.74164
H	-4.45303	-2.70472	-0.47803
H	-3.89145	-0.93761	0.89390
H	-2.81570	0.95557	1.67516
H	-4.99277	-1.41614	-1.59922

HF: -1467.4560385

Sum of electronic and zero-point Energies= -1467.235693

Sum of electronic and thermal Energies= -1467.214778

Sum of electronic and thermal Enthalpies= -1467.213834

Sum of electronic and thermal Free Energies= -1467.285982

Frequency: -351.21

3a using M06-2X/6-311++G(d,p) and IEFPCM solvent model (water)

C	-0.21443	0.37501	0.82474
C	0.37236	1.43294	0.56774
C	1.60704	2.13845	0.22530
C	-0.17206	-1.10006	1.01726
C	2.42846	1.30985	-0.76143
H	3.33203	1.84640	-1.04660
H	1.83615	1.07126	-1.64524
N	1.20865	-1.62387	0.94444
S	2.16866	-1.32404	-0.34176
O	3.27340	-2.24493	-0.26692
O	1.32557	-1.24689	-1.51063
C	-0.74172	-1.56693	2.35411
H	-1.79577	-1.30828	2.43193
H	-0.64438	-2.64919	2.43912
H	-0.21182	-1.08925	3.18069
H	-0.72423	-1.57401	0.20153
H	1.72767	-1.60017	1.81866
O	2.87434	0.11051	-0.11029
F	1.36651	3.35751	-0.41080
C	-3.81452	-2.00568	-1.26565
N	-3.42966	-1.10159	-0.19320
C	-2.80463	0.05912	-0.46316
C	-2.36420	0.82059	0.74867
N	-2.12083	2.11327	0.51281
N	-1.33673	2.91011	0.33191
O	-2.52914	0.43491	-1.59356
H	-2.93963	-2.26885	-1.86118
H	-4.23289	-2.90625	-0.82350
H	-3.74563	-1.29280	0.74533
H	-2.81647	0.63115	1.71592
H	-4.55698	-1.54226	-1.91771
H	2.19384	2.35519	1.12037

HF=-1368.420337

Sum of electronic and zero-point Energies= -1368.181034

Sum of electronic and thermal Energies= -1368.161706

Sum of electronic and thermal Enthalpies= -1368.160761

Sum of electronic and thermal Free Energies= -1368.229598

Frequency: -432.13

3a using B97D/6-311+G(d,p) and CPCM solvent model (water)

C	-0.23261	0.41794	0.81817
C	0.37885	1.47630	0.56261
C	1.62292	2.15454	0.22737
H	2.22890	2.35354	1.12184
C	-0.17895	-1.05532	1.03369
C	2.43592	1.33623	-0.79807
H	3.32117	1.90115	-1.10944
H	1.81954	1.08613	-1.66885
N	1.21729	-1.58329	1.00204
S	2.20367	-1.35019	-0.33195
O	3.32537	-2.27430	-0.18295
O	1.35094	-1.34430	-1.52233
C	-0.77378	-1.51333	2.37764
H	-1.82432	-1.21549	2.44541
H	-0.70996	-2.60441	2.45994
H	-0.23159	-1.04948	3.21199
H	-0.71443	-1.55320	0.21642
H	1.74137	-1.39224	1.85681
O	2.96436	0.13364	-0.17220
F	1.41271	3.43152	-0.39648
C	-3.74143	-2.16764	-1.18958
N	-3.37684	-1.17502	-0.17744
C	-2.85137	0.03327	-0.50833
C	-2.40368	0.83183	0.69152
N	-2.23207	2.15027	0.47939
N	-1.47633	3.00051	0.30883
O	-2.65818	0.40888	-1.66880
H	-3.95572	-3.11111	-0.67925
H	-4.62734	-1.84707	-1.75559
H	-3.60671	-1.37166	0.78786
H	-2.82593	0.60917	1.67062
H	-2.90738	-2.30752	-1.88786

HF=-1368.2279347

Sum of electronic and zero-point Energies= -1367.999279

Sum of electronic and thermal Energies= -1367.979087

Sum of electronic and thermal Enthalpies= -1367.978143

Sum of electronic and thermal Free Energies= -1368.048692

Frequency: -357.53

4 using M06-2X/6-311++G(d,p) and IEFPCM solvent model (water)

C	-0.18279	0.55402	0.73990
C	0.29420	1.65070	0.42932
C	1.40975	2.51213	0.00259
H	1.06242	3.37566	-0.56984

H	1.94643	2.89351	0.87520
C	-0.00140	-0.89897	0.98502
C	2.35872	1.70713	-0.87444
H	3.22663	2.29623	-1.16647
H	1.85359	1.32961	-1.76313
N	1.42691	-1.29285	0.95740
S	2.38800	-0.91997	-0.31262
O	3.58933	-1.70485	-0.16559
O	1.58237	-1.00310	-1.50901
C	-0.54743	-1.37553	2.32848
H	-1.62351	-1.22302	2.37814
H	-0.34202	-2.43840	2.45690
H	-0.08559	-0.81671	3.14528
H	-0.48852	-1.45477	0.17909
H	1.91662	-1.17159	1.84063
O	2.90291	0.59101	-0.12626
C	-3.60060	-2.20831	-1.14595
N	-3.29238	-1.22482	-0.12044
C	-2.79778	-0.01568	-0.45060
C	-2.41891	0.83471	0.71681
N	-2.25436	2.12597	0.42180
N	-1.48254	2.93030	0.19258
O	-2.58730	0.33445	-1.60430
H	-4.40942	-1.86003	-1.79096
H	-2.71838	-2.39409	-1.75949
H	-3.56947	-1.40852	0.83168
H	-2.84102	0.65273	1.69868
H	-3.90017	-3.13263	-0.65849

HF: -1269.1818345

Sum of electronic and zero-point Energies= -1268.934302

Sum of electronic and thermal Energies= -1268.915995

Sum of electronic and thermal Enthalpies= -1268.915051

Sum of electronic and thermal Free Energies= -1268.980916

Frequency: -466.29

4 using B97D/6-311+G(d,p) and CPCM solvent model (water)

C	-0.19129	0.59124	0.76174
C	0.30302	1.69408	0.45808
C	1.42580	2.54151	0.02499
H	1.08682	3.42842	-0.53020
H	1.99681	2.90363	0.89304
C	-0.00656	-0.85902	1.01408
C	2.35278	1.74267	-0.90357
H	3.19798	2.35669	-1.23482
H	1.80956	1.35983	-1.77471
N	1.43689	-1.26259	1.00636
S	2.42095	-0.93688	-0.31411
O	3.63941	-1.72161	-0.11149
O	1.60296	-1.08027	-1.52202
C	-0.56823	-1.33861	2.36480
H	-1.64243	-1.13786	2.41306
H	-0.40265	-2.41640	2.47836

H	-0.08097	-0.80420	3.19126
H	-0.48558	-1.42716	0.20696
H	1.92591	-0.99908	1.86284
O	2.98689	0.62387	-0.19150
C	-3.55094	-2.33360	-1.07244
N	-3.27950	-1.26485	-0.11104
C	-2.83105	-0.03943	-0.49757
C	-2.46442	0.84789	0.65753
N	-2.34885	2.16052	0.37986
N	-1.57941	2.99953	0.17150
O	-2.64301	0.28007	-1.67772
H	-4.44292	-2.10884	-1.67457
H	-2.69314	-2.45374	-1.74529
H	-3.52856	-1.42076	0.85658
H	-2.87275	0.64544	1.64698
H	-3.71188	-3.26095	-0.51451

HF: -1269.0097541

Sum of electronic and zero-point Energies= -1268.773434

Sum of electronic and thermal Energies= -1268.754068

Sum of electronic and thermal Enthalpies= -1268.753124

Sum of electronic and thermal Free Energies= -1268.821585

Frequency: -380.09

8 using M06-2X/6-311++G(d,p) and IEFPCM solvent model (water)

C	-0.16475	0.57391	0.71841
C	0.32591	1.66047	0.39877
C	1.46152	2.50120	-0.01324
H	1.14037	3.36363	-0.60191
H	1.98391	2.88181	0.86803
C	0.01257	-0.86123	0.99550
C	2.41477	1.67433	-0.86512
H	3.31445	2.23279	-1.11512
H	1.93168	1.31961	-1.77453
O	1.45001	-1.19284	0.98353
S	2.32560	-0.93856	-0.31465
O	3.45370	-1.81433	-0.17427
O	1.49026	-0.98352	-1.48852
C	-0.45134	-1.31669	2.36540
H	-1.53143	-1.20284	2.44701
H	-0.20100	-2.36739	2.50805
H	0.02581	-0.71725	3.14106
H	-0.45020	-1.45841	0.20550
O	2.89817	0.52811	-0.10873
C	-3.58855	-2.21931	-1.08919
N	-3.27170	-1.21716	-0.08423
C	-2.78777	-0.01165	-0.44048
C	-2.40018	0.85771	0.71090
N	-2.22094	2.13942	0.39599
N	-1.45537	2.94287	0.14846
O	-2.58965	0.32301	-1.60021
H	-4.41719	-1.89230	-1.72001
H	-2.71737	-2.39967	-1.71969

H	-3.53648	-1.38538	0.87439
H	-2.80652	0.69162	1.70224
H	-3.86256	-3.14109	-0.58231

HF: -1289.0470574

Sum of electronic and zero-point Energies= -1288.812192

Sum of electronic and thermal Energies= -1288.794079

Sum of electronic and thermal Enthalpies= -1288.793135

Sum of electronic and thermal Free Energies= -1288.858839

Frequency: -446.90

8 using B97D/6-311+G(d,p) and CPCM solvent model (water)

C	-0.17041	0.61139	0.75023
C	0.33444	1.70314	0.42735
C	1.47956	2.52724	0.01064
H	1.16917	3.41536	-0.55860
H	2.03671	2.88410	0.88941
C	0.00404	-0.81275	1.05494
C	2.41045	1.70844	-0.89611
H	3.29367	2.29059	-1.17880
H	1.88947	1.35746	-1.79278
O	1.47728	-1.17093	1.03336
S	2.35061	-0.95842	-0.32844
O	3.49775	-1.84023	-0.15462
O	1.49110	-1.04116	-1.51090
C	-0.43479	-1.24187	2.45341
H	-1.51417	-1.08389	2.55355
H	-0.21876	-2.30561	2.60473
H	0.08082	-0.64341	3.21366
H	-0.46936	-1.43700	0.28729
O	2.97979	0.54981	-0.17881
C	-3.55858	-2.33857	-1.01715
N	-3.27430	-1.25359	-0.07737
C	-2.82170	-0.03926	-0.49069
C	-2.44839	0.86878	0.64841
N	-2.31040	2.17074	0.34658
N	-1.54104	3.00285	0.11607
O	-2.63493	0.25845	-1.67575
H	-4.45334	-2.11890	-1.61689
H	-2.70601	-2.47565	-1.69327
H	-3.52011	-1.38858	0.89450
H	-2.85223	0.68788	1.64386
H	-3.72102	-3.25435	-0.44100

HF: -1288.8714909

Sum of electronic and zero-point Energies= -1288.647917

Sum of electronic and thermal Energies= -1288.628643

Sum of electronic and thermal Enthalpies= -1288.627699

Sum of electronic and thermal Free Energies= -1288.696522

Frequency: -367.49

9 using M06-2X/6-311++G(d,p) and IEFPCM solvent model (water)

C	-0.18963	-0.39059	-0.67323
C	0.62378	-1.30655	-0.51023
C	1.99533	-1.71733	-0.20279
C	-0.50306	1.06020	-0.71863
C	2.67242	-0.79816	0.80623
H	3.69831	-1.13284	0.95824
H	2.11986	-0.81867	1.74540
N	0.68614	1.90391	-0.52771
S	1.71204	1.69118	0.71139
O	2.54251	2.86350	0.78556
O	0.94826	1.21979	1.84111
C	-1.13751	1.47490	-2.05488
H	-0.44802	1.23430	-2.86685
H	-1.19812	1.29372	0.09432
H	1.13079	2.26914	-1.36473
O	2.75313	0.52489	0.27895
F	2.06059	-2.97705	0.32170
F	2.74164	-1.75739	-1.34853
H	-2.05200	0.89852	-2.20634
O	-1.38115	2.85902	-2.12078
H	-2.09395	3.08510	-1.51383
C	-4.26362	0.86515	1.50524
N	-3.67081	0.16788	0.37387
C	-2.78833	-0.82943	0.56732
C	-2.17894	-1.36571	-0.69258
N	-1.61127	-2.56596	-0.55327
N	-0.64933	-3.14966	-0.42627
O	-2.42478	-1.21471	1.66818
H	-3.47709	1.26285	2.14711
H	-4.86783	1.68520	1.12566
H	-4.03577	0.34006	-0.55071
H	-2.66758	-1.22636	-1.65095
H	-4.89082	0.19220	2.09252

HF: -1542.8875197

Sum of electronic and zero-point Energies= -1542.651186

Sum of electronic and thermal Energies= -1542.630025

Sum of electronic and thermal Enthalpies= -1542.629081

Sum of electronic and thermal Free Energies= -1542.702364

Frequency: -412.68

9 using B97D/6-311+G(d,p) and CPCM solvent model (water)

C	-0.17557	0.42063	0.74781
C	0.65014	1.33876	0.56475
C	2.00504	1.70906	0.18159
C	-0.45997	-1.02913	0.88964
C	2.58015	0.81900	-0.93918
H	3.58059	1.18207	-1.19970
H	1.91805	0.86694	-1.81067
N	0.72451	-1.88971	0.62870
S	1.61967	-1.73426	-0.77293
O	2.44965	-2.93008	-0.87706
O	0.71626	-1.30767	-1.84206

C	-0.96255	-1.37105	2.32102
H	-0.13951	-1.22367	3.03173
H	-1.23495	-1.31994	0.16903
H	1.34561	-1.99673	1.43093
O	2.77291	-0.54123	-0.49434
F	2.09590	3.01949	-0.30084
F	2.85816	1.67196	1.28928
H	-1.76609	-0.66903	2.57898
O	-1.38458	-2.72338	2.45461
H	-2.20584	-2.82943	1.95458
C	-4.12710	-0.97258	-1.65299
N	-3.59680	-0.23067	-0.50739
C	-2.74522	0.81596	-0.66012
C	-2.20516	1.34057	0.65446
N	-1.71076	2.59083	0.60230
N	-0.76719	3.24070	0.50150
O	-2.35656	1.24207	-1.75053
H	-3.30879	-1.21970	-2.33920
H	-4.58601	-1.89294	-1.27987
H	-3.97911	-0.43280	0.40743
H	-2.73528	1.11746	1.57978
H	-4.87820	-0.38037	-2.19474
HF: -1542.6538148			
Sum of electronic and zero-point Energies=			-1542.428367
Sum of electronic and thermal Energies=			-1542.406331
Sum of electronic and thermal Enthalpies=			-1542.405387
Sum of electronic and thermal Free Energies=			-1542.480438
Frequency: -348.51			

10 using M06-2X/6-311++G(d,p) and IEFPCM solvent model (water)

C	0.15440	0.42382	-0.68597
C	-0.69737	1.29836	-0.50599
C	-2.08704	1.63072	-0.18687
C	0.50670	-1.00631	-0.75231
C	-2.69207	0.67339	0.83430
H	-3.73803	0.93226	0.99234
H	-2.13402	0.73125	1.76809
O	-0.69328	-1.82568	-0.60679
S	-1.57441	-1.73310	0.70972
O	-2.26481	-2.98319	0.79285
O	-0.78296	-1.22414	1.79837
C	1.09749	-1.44245	-2.09088
H	1.94738	-0.79793	-2.32687
H	0.33984	-1.30923	-2.86413
H	1.18224	-1.26869	0.06745
O	-2.69164	-0.65994	0.31034
F	-2.22168	2.88336	0.33586
F	-2.84655	1.61741	-1.32198
O	1.46088	-2.80070	-2.08310
H	2.28083	-2.90580	-1.58998
C	4.24145	-0.77468	1.45916
N	3.63280	-0.06903	0.34114

C	2.73831	0.91302	0.55414
C	2.11775	1.45902	-0.69650
N	1.50209	2.62924	-0.53251
N	0.53359	3.19389	-0.38679
O	2.37079	1.27613	1.66061
H	3.46350	-1.18295	2.10474
H	4.84576	-1.58751	1.06463
H	3.99454	-0.22254	-0.58816
H	2.60228	1.35041	-1.66080
H	4.87125	-0.10439	2.04664
HF: -1562.7501196			
Sum of electronic and zero-point Energies=			-1562.526165
Sum of electronic and thermal Energies=			-1562.505372
Sum of electronic and thermal Enthalpies=			-1562.504427
Sum of electronic and thermal Free Energies=			-1562.576401
Frequency: -381.92			

10 using B97D/6-311+G(d,p) and CPCM solvent model (water)

C	-0.14879	0.43293	0.72252
C	0.69310	1.33192	0.52856
C	2.06510	1.66393	0.16866
C	-0.45763	-0.99517	0.87838
C	2.64360	0.73969	-0.92268
H	3.67582	1.03952	-1.13078
H	2.02937	0.81663	-1.82548
O	0.75590	-1.83232	0.63945
S	1.55128	-1.73873	-0.78426
O	2.26526	-2.99986	-0.88640
O	0.67168	-1.24537	-1.84168
C	-0.88884	-1.36703	2.31409
H	-1.66601	-0.65549	2.62650
H	-0.02478	-1.25238	2.97817
H	-1.21925	-1.31573	0.15637
O	2.74097	-0.63288	-0.46380
F	2.19713	2.95871	-0.33665
F	2.88902	1.62305	1.29516
O	-1.33203	-2.71397	2.42485
H	-2.20256	-2.77712	2.00798
C	-4.18864	-0.93060	-1.55874
N	-3.61544	-0.18483	-0.43611
C	-2.76357	0.85490	-0.62560
C	-2.17978	1.38694	0.66704
N	-1.64838	2.61702	0.58964
N	-0.70166	3.25635	0.46697
O	-2.40762	1.27150	-1.73029
H	-3.39433	-1.19687	-2.26572
H	-4.65001	-1.83995	-1.16261
H	-3.96157	-0.38543	0.49362
H	-2.67842	1.18141	1.61362
H	-4.94622	-0.33229	-2.08428
HF: -1562.5133799			
Sum of electronic and zero-point Energies=			-1562.300283

Sum of electronic and thermal Energies=	-1562.278539
Sum of electronic and thermal Enthalpies=	-1562.277595
Sum of electronic and thermal Free Energies=	-1562.351825
Frequency: -324.38	

Coupling with D3

2 using B97D/6-311+G(d,p) and CPCM solvent model (water)

C	0.27406	0.17983	0.26550
C	-0.91772	0.52450	0.07398
C	-1.85596	1.60305	-0.29124
H	-2.33770	2.01822	0.60522
C	1.58258	0.60636	0.84204
C	-1.13535	2.70485	-1.08155
H	-1.86273	3.44912	-1.42250
H	-0.59775	2.29102	-1.94186
N	1.66035	2.06744	1.06421
S	1.41632	3.14825	-0.20222
O	1.98025	4.42552	0.22406
O	1.83669	2.48289	-1.43697
C	1.82436	-0.08217	2.21939
H	1.21070	0.41966	2.97873
H	2.39865	0.33937	0.16376
H	1.14429	2.38181	1.88659
O	-0.21186	3.47878	-0.24669
C	-1.98898	-1.39846	-0.16246
C	0.48813	-1.85488	-0.33796
N	-0.24496	-1.89803	-1.53261
N	-1.50106	-1.65442	-1.44704
N	-0.16732	-2.42362	0.76249
N	-1.42491	-2.17819	0.84712
H	-2.65909	1.22691	-0.93897
H	1.50518	-1.12747	2.14857
C	1.96394	-2.05558	-0.49638
C	4.68249	-2.35820	-0.74759
C	2.58603	-1.63782	-1.68704
N	2.64289	-2.59091	0.53753
C	3.97166	-2.74314	0.39803
C	3.96946	-1.79142	-1.81009
H	1.99465	-1.19888	-2.48585
H	4.49335	-3.18925	1.24611
H	4.47940	-1.46996	-2.71604
H	5.76044	-2.49519	-0.79576
C	-3.41800	-1.01469	0.01353
C	-6.03441	-0.23568	0.30115
C	-3.97598	-0.98105	1.30441
N	-4.10295	-0.66059	-1.09416
C	-5.38406	-0.28716	-0.93984
C	-5.30873	-0.58609	1.44584
H	-3.37476	-1.25846	2.16586
H	-5.91471	-0.00746	-1.85100

H	-5.76944	-0.54945	2.43116
H	-7.07395	0.07902	0.36283
O	3.18162	0.01297	2.63737
H	3.67352	-0.66759	2.15563

HF=-1777.7195987

Sum of electronic and zero-point Energies= -1777.381189

Sum of electronic and thermal Energies= -1777.355276

Sum of electronic and thermal Enthalpies= -1777.354332

Sum of electronic and thermal Free Energies= -1777.437525

Frequency: -358.69

3 using B97D/6-311+G(d,p) and CPCM solvent model (water)

C	0.53142	0.15824	0.36614
C	-0.66893	0.36262	0.04307
C	-1.50970	1.48209	-0.47765
C	1.79366	0.57346	1.04080
C	-0.71025	2.61787	-1.15132
H	-1.43678	3.32433	-1.56735
H	-0.09276	2.19510	-1.95094
N	1.86687	2.04048	1.24888
S	1.72027	3.09911	-0.03938
O	2.20503	4.39663	0.41019
O	2.23644	2.42606	-1.23066
C	1.90728	-0.06736	2.44015
H	2.85236	0.25172	2.89443
H	1.06622	0.25708	3.06642
H	2.65239	0.29365	0.42455
H	1.31503	2.37081	2.04147
O	0.07194	3.37496	-0.21185
C	-1.65080	-1.46408	-0.09245
C	0.82655	-1.96949	-0.15848
N	0.13316	-2.06025	-1.36831
N	-1.12748	-1.82606	-1.34494
N	0.13583	-2.44141	0.96161
N	-1.12076	-2.19585	0.99062
H	1.89592	-1.15665	2.35770
C	2.30528	-2.13936	-0.25355
C	5.03062	-2.39850	-0.39493
C	2.96934	-1.67487	-1.40391
N	2.94255	-2.70406	0.79051
C	4.27659	-2.82996	0.70646
C	4.35863	-1.80787	-1.47118
H	2.40568	-1.21676	-2.21243
H	4.76902	-3.29383	1.56213
H	4.90380	-1.45276	-2.34338
H	6.11152	-2.52068	-0.40011
C	-3.11960	-1.18967	0.04577
C	-5.80072	-0.71443	0.32435
C	-3.59227	-0.70383	1.27530
N	-3.91533	-1.44714	-1.00750
C	-5.22901	-1.21331	-0.85585
C	-4.96081	-0.45740	1.41335
H	-2.89933	-0.51884	2.09212

H	-5.85837	-1.43556	-1.71898
H	-5.36040	-0.07170	2.34927
H	-6.87270	-0.53741	0.38109
F	-2.37394	1.04269	-1.46459
F	-2.29612	2.00173	0.53570
HF=-1900.9537385			
Sum of electronic and zero-point Energies=			-1900.636707
Sum of electronic and thermal Energies=			-1900.610446
Sum of electronic and thermal Enthalpies=			-1900.609502
Sum of electronic and thermal Free Energies=			-1900.692583
Frequency: -392.96			

3a using B97D/6-311+G(d,p) and CPCM solvent model (water)

C	0.47460	0.20424	0.33516
C	-0.71853	0.42501	-0.00158
C	-1.59619	1.51293	-0.52807
H	-2.27112	1.88973	0.25003
C	1.73268	0.62055	1.02003
C	-0.78256	2.65273	-1.17286
H	-1.48356	3.36561	-1.61964
H	-0.11605	2.24846	-1.94260
N	1.77676	2.08509	1.26576
S	1.60309	3.18546	0.01549
O	2.03263	4.48056	0.52838
O	2.17424	2.58268	-1.18881
C	1.86958	-0.03964	2.40795
H	2.81055	0.29170	2.86238
H	1.02664	0.25853	3.04490
H	2.59573	0.37179	0.39559
H	1.21410	2.37794	2.06550
O	-0.04478	3.40776	-0.18233
C	-1.73000	-1.37973	-0.04729
C	0.72594	-1.94264	-0.13097
N	0.01439	-2.06331	-1.32787
N	-1.24122	-1.80122	-1.29403
N	0.04398	-2.37245	1.00979
N	-1.20719	-2.09588	1.04963
H	1.87803	-1.12754	2.31365
C	2.20142	-2.12972	-0.24659
C	4.92083	-2.42130	-0.43687
C	2.85341	-1.65287	-1.39871
N	2.84739	-2.72354	0.77550
C	4.17867	-2.86417	0.66768
C	4.23948	-1.80197	-1.49112
H	2.28248	-1.17211	-2.18899
H	4.67832	-3.35131	1.50613
H	4.77538	-1.43760	-2.36531
H	5.99984	-2.55721	-0.46175
C	-3.18482	-1.04434	0.10990
C	-5.83502	-0.43797	0.42711
C	-3.58816	-0.38429	1.28185
N	-4.03340	-1.41521	-0.86465
C	-5.33207	-1.11493	-0.69362

C	-4.94073	-0.06899	1.43843
H	-2.85434	-0.12371	2.04138
H	-6.00590	-1.43121	-1.49135
H	-5.28697	0.45229	2.32882
H	-6.89714	-0.21420	0.50080
F	-2.40314	1.03684	-1.58743

HF=-1801.7278708

Sum of electronic and zero-point Energies= -1801.402369

Sum of electronic and thermal Energies= -1801.376853

Sum of electronic and thermal Enthalpies= -1801.375909

Sum of electronic and thermal Free Energies= -1801.457555

Frequency: -388.62

4 using B97D/6-311+G(d,p) and CPCM solvent model (water)

C	0.39299	0.17854	0.35426
C	-0.78768	0.51076	0.08503
C	-1.72049	1.56384	-0.35821
H	-2.28724	1.96568	0.49350
C	1.65180	0.62668	1.03020
C	-0.97085	2.68506	-1.09006
H	-1.68801	3.41356	-1.48300
H	-0.36012	2.28770	-1.90830
N	1.67538	2.09489	1.25340
S	1.49584	3.17609	-0.02105
O	2.00025	4.46320	0.44951
O	2.01854	2.52837	-1.22608
C	1.80508	-0.02398	2.41814
H	2.75460	0.29581	2.86347
H	0.97243	0.28191	3.06543
H	2.51689	0.38756	0.40533
H	1.10178	2.39335	2.04296
O	-0.13128	3.47559	-0.18563
C	-1.84119	-1.42246	-0.14129
C	0.64291	-1.86211	-0.19212
N	-0.03497	-1.94190	-1.41911
N	-1.29551	-1.70501	-1.39602
N	-0.05680	-2.40990	0.89087
N	-1.31881	-2.17242	0.91201
H	-2.45682	1.16261	-1.06790
H	1.79873	-1.11285	2.32260
C	2.12413	-2.05835	-0.28888
C	4.84548	-2.36764	-0.44405
C	2.80050	-1.54809	-1.41211
N	2.74865	-2.69073	0.72242
C	4.08093	-2.83961	0.63214
C	4.18644	-1.70707	-1.48758
H	2.24741	-1.03462	-2.19428
H	4.56214	-3.35800	1.46276
H	4.73969	-1.31784	-2.34009
H	5.92362	-2.51238	-0.45582
C	-3.27783	-1.04129	-0.03581
C	-5.90556	-0.26193	0.12323

C	-3.88802	-0.97182	1.23000
N	-3.91876	-0.72296	-1.17989
C	-5.20576	-0.34883	-1.08838
C	-5.22595	-0.57674	1.30600
H	-3.32137	-1.22178	2.12274
H	-5.69989	-0.09839	-2.02819
H	-5.72605	-0.51238	2.27051
H	-6.94717	0.05182	0.13370

HF=-1702.5202887

Sum of electronic and zero-point Energies= -1702.186891

Sum of electronic and thermal Energies= -1702.162156

Sum of electronic and thermal Enthalpies= -1702.161212

Sum of electronic and thermal Free Energies= -1702.241230

Frequency: -357.15

9 using B97D/6-311+G(d,p) and CPCM solvent model (water)

C	0.41655	0.16608	0.26432
C	-0.79896	0.36681	0.00204
C	-1.65432	1.49696	-0.47549
C	1.71834	0.56905	0.84992
C	-0.87647	2.62039	-1.19585
H	-1.61526	3.33598	-1.57301
H	-0.31024	2.18715	-2.02720
N	1.83618	2.02891	1.04977
S	1.62206	3.08425	-0.23175
O	2.14131	4.37918	0.18441
O	2.06027	2.40202	-1.44843
C	1.92056	-0.09860	2.25201
H	1.27405	0.41240	2.97682
H	2.53484	0.26219	0.18992
H	1.34846	2.37597	1.87631
O	-0.03239	3.36816	-0.30349
C	-1.77889	-1.45314	-0.11514
C	0.69220	-1.96684	-0.29987
N	-0.05472	-2.03791	-1.47700
N	-1.31209	-1.80145	-1.39505
N	0.04939	-2.45160	0.84315
N	-1.20384	-2.20322	0.93214
H	1.61956	-1.14860	2.18848
C	2.16657	-2.13349	-0.45342
C	4.88919	-2.38732	-0.69631
C	2.77412	-1.77763	-1.67148
N	2.86114	-2.58333	0.61209
C	4.19147	-2.71395	0.47613
C	4.16082	-1.90592	-1.78949
H	2.17037	-1.40681	-2.49510
H	4.72697	-3.09213	1.34816
H	4.66065	-1.63160	-2.71617
H	5.96972	-2.50299	-0.74058
C	-3.24020	-1.18060	0.09319
C	-5.90474	-0.71077	0.50293
C	-3.65227	-0.69453	1.34408

N	-4.08577	-1.44134	-0.91952
C	-5.39094	-1.20999	-0.70353
C	-5.01288	-0.45082	1.54908
H	-2.92022	-0.50761	2.12570
H	-6.06160	-1.43476	-1.53425
H	-5.36681	-0.06509	2.50317
H	-6.97295	-0.53581	0.61228
O	3.25946	0.02875	2.70362
H	3.77466	-0.66272	2.26331
F	-2.57659	1.06772	-1.41180
F	-2.37533	2.02750	0.57887

HF=-1976.1525486

Sum of electronic and zero-point Energies=	-1975.830303
Sum of electronic and thermal Energies=	-1975.802952
Sum of electronic and thermal Enthalpies=	-1975.802008
Sum of electronic and thermal Free Energies=	-1975.887556

Frequency: -391.53

Coupling with D4 (*anti* TS)

2 using M06-2X/6-311++G(d,p) and IEFPCM solvent model (water)

C	-0.69874	0.38865	0.14177
C	-0.97158	-0.81287	0.09353
C	-0.58307	-2.23256	0.12545
H	-1.15490	-2.79209	0.87086
H	-0.76518	-2.69720	-0.84652
C	0.34193	1.43923	0.25223
C	0.89218	-2.31962	0.49249
H	1.26086	-3.34162	0.42396
H	1.07540	-1.92876	1.49276
N	1.53884	1.07780	-0.53471
S	2.44934	-0.20958	-0.07735
O	3.60549	-0.21673	-0.93707
O	2.57718	-0.15320	1.36020
C	-0.08846	2.84277	-0.19050
H	-0.49026	2.80398	-1.20928
H	0.78881	3.48973	-0.18203
H	0.66114	1.51442	1.29459
H	1.39032	1.07564	-1.54221
O	1.67253	-1.56039	-0.46851
O	-1.02108	3.39230	0.71118
H	-1.86024	2.93605	0.58602
H	-3.50692	-2.85029	0.09349
C	-3.93175	-1.85506	0.19901
H	-4.90400	-1.83754	-0.29311
H	-4.03954	-1.60748	1.25656
N	-3.00375	-0.93703	-0.47172
N	-3.22891	0.28228	-0.44055
N	-2.74631	1.31827	-0.36985

HF=-1191.7337607

Sum of electronic and zero-point Energies=	-1191.519521
Sum of electronic and thermal Energies=	-1191.503518

Sum of electronic and thermal Enthalpies= -1191.502574
 Sum of electronic and thermal Free Energies= -1191.563106
 Frequency: -440.17

2 using M06-2X/6-311++G(d,p) and IEFPCM solvent model (acetonitrile)

C	-0.69875	0.38851	0.14219
C	-0.97153	-0.81299	0.09396
C	-0.58284	-2.23262	0.12555
H	-1.15441	-2.79239	0.87102
H	-0.76513	-2.69691	-0.84657
C	0.34192	1.43920	0.25285
C	0.89269	-2.31942	0.49195
H	1.26141	-3.34145	0.42331
H	1.07612	-1.92870	1.49227
N	1.53865	1.07787	-0.53414
S	2.44975	-0.20940	-0.07726
O	3.60525	-0.21631	-0.93748
O	2.57701	-0.15387	1.36025
C	-0.08840	2.84276	-0.18987
H	-0.48929	2.80390	-1.20909
H	0.78890	3.48967	-0.18068
H	0.66107	1.51419	1.29523
H	1.39034	1.07611	-1.54160
O	1.67213	-1.56008	-0.46907
O	-1.02159	3.39225	0.71098
H	-1.86088	2.93667	0.58473
H	-3.50718	-2.84983	0.09606
C	-3.93199	-1.85439	0.19991
H	-4.90423	-1.83782	-0.29233
H	-4.04005	-1.60525	1.25712
N	-3.00387	-0.93757	-0.47212
N	-3.22888	0.28190	-0.44144
N	-2.74612	1.31780	-0.37086

HF=-1191.7332383

Sum of electronic and zero-point Energies= -1191.518979
 Sum of electronic and thermal Energies= -1191.502980
 Sum of electronic and thermal Enthalpies= -1191.502036
 Sum of electronic and thermal Free Energies= -1191.562558
 Frequency: -440.06

2 using B97D/6-311+G(d,p) and CPCM solvent model (water)

C	-0.70046	0.40593	0.14194
C	-0.97533	-0.80710	0.10264
C	-0.58453	-2.22555	0.14583
H	-1.17443	-2.79034	0.88316
H	-0.74493	-2.70350	-0.83075
C	0.35123	1.44419	0.24500
C	0.89300	-2.32947	0.55132
H	1.23047	-3.37167	0.53591

H	1.06524	-1.90111	1.54449
N	1.55343	1.08012	-0.56356
S	2.51592	-0.21626	-0.08542
O	3.65039	-0.23276	-1.00692
O	2.69041	-0.10745	1.36562
C	-0.06424	2.87261	-0.19307
H	-0.43982	2.84454	-1.22865
H	0.81952	3.51855	-0.14663
H	0.68414	1.51404	1.28877
H	1.34435	0.99101	-1.55940
O	1.74247	-1.64600	-0.43853
O	-1.03209	3.42086	0.69603
H	-1.84852	2.91380	0.55980
H	-3.55108	-2.88234	0.01642
C	-4.04778	-1.91100	0.09868
H	-4.95167	-1.92250	-0.52446
H	-4.31289	-1.71838	1.14760
N	-3.08794	-0.91586	-0.40170
N	-3.34386	0.30434	-0.38082
N	-2.83820	1.35899	-0.34009

HF=-1191.5900034

Sum of electronic and zero-point Energies=	-1191.385711
Sum of electronic and thermal Energies=	-1191.368824
Sum of electronic and thermal Enthalpies=	-1191.367880
Sum of electronic and thermal Free Energies=	-1191.430617

Frequency:-322.77

2 using B97D/6-311+G(d,p) and CPCM solvent model (acetonitrile)

C	-0.70040	0.40596	0.14223
C	-0.97557	-0.80702	0.10394
C	-0.58463	-2.22541	0.14694
H	-1.17423	-2.79040	0.88439
H	-0.74536	-2.70314	-0.82973
C	0.35151	1.44410	0.24529
C	0.89326	-2.32920	0.55149
H	1.23059	-3.37149	0.53626
H	1.06601	-1.90072	1.54455
N	1.55339	1.08001	-0.56353
S	2.51626	-0.21637	-0.08572
O	3.65001	-0.23313	-1.00780
O	2.69057	-0.10796	1.36528
C	-0.06394	2.87270	-0.19215
H	-0.43937	2.84503	-1.22785
H	0.81990	3.51850	-0.14538
H	0.68460	1.51353	1.28903
H	1.34428	0.99100	-1.55934
O	1.74164	-1.64600	-0.43889
O	-1.03169	3.42057	0.69705
H	-1.84828	2.91395	0.56035
H	-3.55225	-2.88166	0.01912
C	-4.04894	-1.91005	0.09875

H	-4.95155	-1.92252	-0.52627
H	-4.31643	-1.71592	1.14682
N	-3.08784	-0.91596	-0.40109
N	-3.34378	0.30445	-0.38214
N	-2.83750	1.35886	-0.34247

HF=-1191.5896413

Sum of electronic and zero-point Energies=	-1191.385340
Sum of electronic and thermal Energies=	-1191.368456
Sum of electronic and thermal Enthalpies=	-1191.367511
Sum of electronic and thermal Free Energies=	-1191.430235

Frequency: -322.61

3 using M06-2X/6-311++G(d,p) and IEFPCM solvent model (water)

C	-0.38568	1.02328	0.05050
C	-0.94879	-0.06578	-0.06683
C	-0.84392	-1.51830	-0.23610
C	0.80885	1.88967	0.17722
C	0.51924	-2.04860	0.18958
H	0.59389	-3.10033	-0.08589
H	0.62770	-1.92684	1.26704
N	2.02089	1.21712	-0.34533
S	2.48305	-0.24335	0.20970
O	3.79393	-0.50593	-0.32084
O	2.20914	-0.28274	1.62571
C	0.70122	3.23002	-0.54371
H	-0.10282	3.81781	-0.10773
H	1.64017	3.77374	-0.44140
H	0.48550	3.07693	-1.60318
H	0.97940	2.06115	1.24261
H	2.16298	1.30553	-1.34878
O	1.54949	-1.35841	-0.51593
F	-1.77252	-2.19185	0.50441
F	-1.08775	-1.86099	-1.53503
H	-4.08000	-1.44103	0.08150
C	-4.09039	-0.44114	0.50267
H	-5.05593	0.02279	0.30362
H	-3.90902	-0.48946	1.57756
N	-3.02735	0.31695	-0.17776
N	-2.89889	1.52369	0.08165
N	-2.13921	2.37516	0.19625

HF: -1315.0011383

Sum of electronic and zero-point Energies=	-1314.808642
Sum of electronic and thermal Energies=	-1314.792090
Sum of electronic and thermal Enthalpies=	-1314.791146
Sum of electronic and thermal Free Energies=	-1314.853668

Frequency: -413.64

3 using B97D/6-311+G(d,p) and CPCM solvent model (water)

C	-0.41424	1.03241	0.08277
C	-0.96674	-0.07788	-0.03470
C	-0.83286	-1.52998	-0.15315
C	0.78721	1.89267	0.20846
C	0.55239	-2.04904	0.27388
H	0.60217	-3.12412	0.06772
H	0.68272	-1.86330	1.34547
N	1.99536	1.24764	-0.39738
S	2.56591	-0.21996	0.15595
O	3.84513	-0.44789	-0.50761
O	2.41663	-0.23244	1.61207
C	0.67378	3.28243	-0.44215
H	-0.13540	3.84145	0.03488
H	1.61929	3.82118	-0.31147
H	0.45240	3.18616	-1.51322
H	1.00348	2.01158	1.27810
H	1.99115	1.26064	-1.41814
O	1.60317	-1.43903	-0.50381
F	-1.74988	-2.20884	0.65034
F	-1.10664	-1.93986	-1.45675
H	-4.09337	-1.49633	-0.10419
C	-4.23482	-0.48869	0.29185
H	-5.17153	-0.07246	-0.10049
H	-4.26416	-0.52209	1.38948
N	-3.09282	0.31282	-0.18422
N	-3.00753	1.52899	0.08037
N	-2.22935	2.39603	0.20514
HF: -1314.834029			
Sum of electronic and zero-point Energies=			-1314.650919
Sum of electronic and thermal Energies=			-1314.633512
Sum of electronic and thermal Enthalpies=			-1314.632568
Sum of electronic and thermal Free Energies=			-1314.696614
Frequency: -319.47			

3a using M06-2X/6-311++G(d,p) and IEFPCM solvent model (water)

C	-0.47233	0.90265	-0.10237
C	-0.98173	-0.19362	-0.34011
C	-0.81599	-1.60340	-0.71057
C	0.67060	1.81549	0.12000
C	0.48791	-2.13699	-0.11623
H	0.65090	-3.16774	-0.42694
H	0.45334	-2.07182	0.97144
N	1.95471	1.19404	-0.28365
S	2.38790	-0.28541	0.25112
O	3.76325	-0.48240	-0.12758
O	1.95545	-0.40286	1.62305
C	0.56220	3.13648	-0.63674
H	-0.31881	3.67854	-0.30022
H	1.44903	3.74235	-0.45004

H	0.46959	2.95268	-1.70936
H	0.74030	2.01368	1.19192
H	2.20728	1.32887	-1.25964
O	1.59163	-1.38113	-0.63543
F	-1.82687	-2.40757	-0.19310
H	-4.12270	-1.65700	-0.10964
C	-4.08654	-0.73353	0.45785
H	-5.07003	-0.26407	0.45026
H	-3.77876	-0.94326	1.48375
N	-3.11167	0.14153	-0.21477
N	-2.96770	1.29557	0.21714
N	-2.20133	2.13394	0.39021
H	-0.83016	-1.72449	-1.79534

HF=-1215.7512054

Sum of electronic and zero-point Energies= -1215.550249

Sum of electronic and thermal Energies= -1215.534425

Sum of electronic and thermal Enthalpies= -1215.533481

Sum of electronic and thermal Free Energies= -1215.593874

Frequency: -419.26

3a using B97D/6-311+G(d,p) and CPCM solvent model (water)

C	-0.52676	0.86828	0.05509
C	-1.01087	-0.26745	-0.10797
C	-0.79638	-1.69007	-0.40124
H	-0.90356	-1.89482	-1.47491
C	0.60402	1.81865	0.14727
C	0.58664	-2.14846	0.10774
H	0.73085	-3.21052	-0.11834
H	0.66412	-1.97804	1.18718
N	1.86113	1.25163	-0.44361
S	2.49934	-0.19538	0.10118
O	3.81193	-0.32867	-0.52588
O	2.31631	-0.24214	1.55323
C	0.36988	3.16393	-0.56283
H	-0.49552	3.66154	-0.11668
H	1.25709	3.79828	-0.45070
H	0.17071	3.00084	-1.63055
H	0.81887	2.00182	1.20775
H	1.86309	1.26528	-1.46452
O	1.64214	-1.45331	-0.60876
F	-1.73400	-2.53471	0.26284
H	-3.95648	-1.70824	-0.66398
C	-4.19798	-0.64501	-0.59339
H	-4.20776	-0.19381	-1.59547
H	-5.18126	-0.52906	-0.11855
N	-3.14924	-0.04637	0.25124
N	-3.11572	1.18736	0.44191
N	-2.37874	2.08154	0.61298

HF=-1215.6059007

Sum of electronic and zero-point Energies= -1215.414439

Sum of electronic and thermal Energies= -1215.397779

Sum of electronic and thermal Enthalpies= -1215.396834
Sum of electronic and thermal Free Energies= -1215.458970
Frequency: -325.81

4 using M06-2X/6-311++G(d,p) and IEFPCM solvent model (water)

C	-0.69941	0.63331	0.12925
C	-1.05317	-0.54109	0.00789
C	-0.76077	-1.97310	-0.17979
H	-1.40709	-2.60151	0.43754
H	-0.91970	-2.26004	-1.22279
C	0.33613	1.68915	0.15675
C	0.68403	-2.23689	0.22356
H	0.97883	-3.26072	-0.00097
H	0.83934	-2.03182	1.28212
N	1.60537	1.22651	-0.46154
S	2.34681	-0.13458	0.06069
O	3.63802	-0.17300	-0.58094
O	2.22472	-0.17126	1.49999
C	-0.05719	2.97421	-0.56594
H	-0.92483	3.41579	-0.08096
H	0.77095	3.68267	-0.53733
H	-0.31383	2.76159	-1.60637
H	0.56986	1.91858	1.19874
H	1.62140	1.28742	-1.47716
O	1.57615	-1.40380	-0.55869
H	-3.65513	-2.23894	-0.70897
C	-4.01185	-1.21311	-0.64809
H	-3.94391	-0.74072	-1.62998
H	-5.04761	-1.22496	-0.30793
N	-3.15462	-0.53740	0.33426
N	-3.25502	0.69992	0.44063
N	-2.66074	1.67320	0.55213

HF: -1116.514391

Sum of electronic and zero-point Energies= -1116.305936
Sum of electronic and thermal Energies= -1116.290824
Sum of electronic and thermal Enthalpies= -1116.289880
Sum of electronic and thermal Free Energies= -1116.348766
Frequency: -446.92

4 using M06-2X/6-311++G(d,p) and IEFPCM solvent model (acetonitrile)

C	-0.69992	0.63318	0.13061
C	-1.05364	-0.54127	0.00990
C	-0.76105	-1.97359	-0.17483
H	-1.40676	-2.60052	0.44466
H	-0.92073	-2.26310	-1.21703
C	0.33641	1.68833	0.15877
C	0.68435	-2.23563	0.22780
H	0.97937	-3.26004	0.00601
H	0.84039	-2.02747	1.28568
N	1.60429	1.22600	-0.46207

S	2.34788	-0.13461	0.05880
O	3.63656	-0.17330	-0.58737
O	2.22953	-0.17064	1.49828
C	-0.05678	2.97536	-0.56043
H	-0.92358	3.41652	-0.07355
H	0.77200	3.68304	-0.53114
H	-0.31488	2.76539	-1.60106
H	0.57169	1.91513	1.20100
H	1.61860	1.28707	-1.47765
O	1.57477	-1.40429	-0.55763
H	-3.65560	-2.24005	-0.70886
C	-4.01149	-1.21378	-0.65024
H	-3.94116	-0.74304	-1.63281
H	-5.04802	-1.22433	-0.31236
N	-3.15574	-0.53744	0.33282
N	-3.25636	0.70011	0.43757
N	-2.66243	1.67355	0.54891

HF: -1116.5139428

Sum of electronic and zero-point Energies= -1116.305467

Sum of electronic and thermal Energies= -1116.290359

Sum of electronic and thermal Enthalpies= -1116.289415

Sum of electronic and thermal Free Energies= -1116.348277

Frequency: -446.57

4 using B97D/6-311+G(d,p) and CPCM solvent model (water)

C	-0.70509	0.65437	0.08400
C	-1.05415	-0.52985	-0.06683
C	-0.75588	-1.96004	-0.25471
H	-1.44054	-2.60085	0.31852
H	-0.85762	-2.24242	-1.31281
C	0.34387	1.69577	0.14261
C	0.66932	-2.25703	0.23434
H	0.93218	-3.30589	0.05598
H	0.77698	-2.02487	1.29942
N	1.63162	1.22911	-0.47723
S	2.41320	-0.14513	0.08423
O	3.71172	-0.17352	-0.58953
O	2.29920	-0.14766	1.54579
C	-0.01542	3.01210	-0.56890
H	-0.90931	3.43883	-0.10513
H	0.81804	3.71960	-0.48287
H	-0.22679	2.82587	-1.63077
H	0.57500	1.90832	1.19423
H	1.58513	1.19691	-1.49692
O	1.66163	-1.49657	-0.53814
H	-3.82523	-2.28667	-0.57332
C	-4.20563	-1.26182	-0.51999
H	-4.30427	-0.85215	-1.53535
H	-5.18522	-1.27574	-0.02307
N	-3.22879	-0.50207	0.27553
N	-3.34526	0.73669	0.40960

N	-2.71358	1.71371	0.54872
HF: -1116.3898			
Sum of electronic and zero-point Energies=			-1116.190850
Sum of electronic and thermal Energies=			-1116.174908
Sum of electronic and thermal Enthalpies=			-1116.173964
Sum of electronic and thermal Free Energies=			-1116.234471
Frequency: -328.18			

4 using B97D/6-311+G(d,p) and CPCM solvent model (acetonitrile)

C	-0.70519	0.65405	0.08375
C	-1.05426	-0.53020	-0.06686
C	-0.75585	-1.96048	-0.25374
H	-1.44033	-2.60085	0.32022
H	-0.85775	-2.24370	-1.31163
C	0.34387	1.69541	0.14274
C	0.66973	-2.25664	0.23502
H	0.93277	-3.30564	0.05755
H	0.77748	-2.02362	1.29993
N	1.63146	1.22910	-0.47725
S	2.41370	-0.14505	0.08396
O	3.71147	-0.17348	-0.59080
O	2.29981	-0.14772	1.54543
C	-0.01550	3.01214	-0.56800
H	-0.90942	3.43864	-0.10409
H	0.81801	3.71955	-0.48159
H	-0.22685	2.82650	-1.62999
H	0.57494	1.90731	1.19451
H	1.58507	1.19708	-1.49692
O	1.66104	-1.49643	-0.53834
H	-3.82703	-2.28631	-0.57331
C	-4.20639	-1.26103	-0.52029
H	-4.30417	-0.85151	-1.53583
H	-5.18633	-1.27396	-0.02400
N	-3.22920	-0.50222	0.27561
N	-3.34527	0.73671	0.40962
N	-2.71309	1.71338	0.54854
HF: -1116.3894926			
Sum of electronic and zero-point Energies=			-1116.190536
Sum of electronic and thermal Energies=			-1116.174595
Sum of electronic and thermal Enthalpies=			-1116.173651
Sum of electronic and thermal Free Energies=			-1116.234154
Frequency: -327.98			

8 using M06-2X/6-311++G(d,p) and IEFPCM solvent model (water)

C	-0.66320	0.67239	-0.04233
C	-1.05620	-0.46321	-0.31195
C	-0.79159	-1.87013	-0.65680
H	-1.50937	-2.55351	-0.19818
H	-0.85031	-2.00802	-1.73899

C	0.39105	1.66852	0.16249
C	0.59210	-2.24680	-0.14227
H	0.89369	-3.23035	-0.49626
H	0.62974	-2.21476	0.94543
O	1.67559	1.14322	-0.35816
S	2.27842	-0.20658	0.20915
O	3.65858	-0.18782	-0.18337
O	1.90067	-0.37176	1.59072
C	0.20045	2.97274	-0.58586
H	-0.69254	3.46967	-0.20941
H	1.06435	3.61815	-0.42986
H	0.07710	2.77735	-1.65158
H	0.53769	1.84327	1.23022
O	1.59353	-1.33610	-0.67662
H	-3.82950	-2.27060	-0.15911
C	-3.98848	-1.34282	0.38443
H	-5.04659	-1.08767	0.32883
H	-3.68714	-1.46498	1.42701
N	-3.17961	-0.31743	-0.28698
N	-3.20818	0.84273	0.16140
N	-2.57985	1.77502	0.37968

HF: -1136.3789719

Sum of electronic and zero-point Energies= -1136.183015

Sum of electronic and thermal Energies= -1136.168151

Sum of electronic and thermal Enthalpies= -1136.167207

Sum of electronic and thermal Free Energies= -1136.225261

Frequency: -428.82

8 using B97D/6-311+G(d,p) and CPCM solvent model (water)

C	-0.67754	0.69194	-0.05457
C	-1.06084	-0.45921	-0.32520
C	-0.78311	-1.86645	-0.65584
H	-1.52102	-2.55265	-0.21759
H	-0.80563	-2.01782	-1.74452
C	0.37025	1.68810	0.14098
C	0.58832	-2.26502	-0.09008
H	0.85843	-3.27882	-0.40318
H	0.60203	-2.19406	1.00204
O	1.69422	1.15330	-0.40711
S	2.34459	-0.20203	0.21614
O	3.73028	-0.17217	-0.23400
O	2.00087	-0.33226	1.63388
C	0.18940	3.00216	-0.61317
H	-0.71266	3.49367	-0.23195
H	1.05587	3.65255	-0.44664
H	0.06612	2.81204	-1.68612
H	0.54211	1.86586	1.20969
O	1.66418	-1.42373	-0.64930
H	-3.82447	-2.30358	-0.22920
C	-4.10850	-1.38511	0.29321
H	-5.16215	-1.16923	0.07235
H	-3.96818	-1.51426	1.37571

N	-3.24120	-0.32151	-0.23766
N	-3.30328	0.83843	0.22543
N	-2.66525	1.79726	0.42959

HF: -1136.2515528

Sum of electronic and zero-point Energies= -1136.065246

Sum of electronic and thermal Energies= -1136.049451

Sum of electronic and thermal Enthalpies= -1136.048507

Sum of electronic and thermal Free Energies= -1136.108542

Frequency: -322.39

9 using M06-2X/6-311++G(d,p) and IEFPCM solvent model (water)

C	-0.32778	0.90352	0.16652
C	-1.11933	-0.03209	0.05450
C	-1.33872	-1.48126	-0.00410
C	1.05064	1.40942	0.32932
C	-0.07246	-2.26003	0.33246
H	-0.24236	-3.31943	0.14200
H	0.18207	-2.09655	1.37951
N	2.00950	0.57614	-0.42962
S	2.25171	-0.98509	0.01400
O	3.35354	-1.47887	-0.76433
O	2.24321	-1.03456	1.45464
C	1.26815	2.85780	-0.11126
H	1.02894	2.95953	-1.17705
H	1.32999	1.33025	1.38305
H	1.91511	0.65139	-1.44222
O	0.98753	-1.84272	-0.53059
F	-2.29849	-1.88327	0.88086
F	-1.79305	-1.84815	-1.23605
H	-4.36938	-0.74751	-0.01185
C	-4.25805	0.29712	0.26267
H	-5.10193	0.86263	-0.13116
H	-4.21016	0.39236	1.34848
N	-3.01133	0.76168	-0.36578
N	-2.65949	1.94087	-0.20699
N	-1.77383	2.65273	-0.07829
H	0.58860	3.49390	0.45210
O	2.57925	3.28558	0.17547
H	3.19876	2.69541	-0.26760

HF: -1390.220133

Sum of electronic and zero-point Energies= -1390.022135

Sum of electronic and thermal Energies= -1390.004546

Sum of electronic and thermal Enthalpies= -1390.003602

Sum of electronic and thermal Free Energies= -1390.068214

Frequency: -398.27

9 using B97D/6-311+G(d,p) and CPCM solvent model (water)

C	-0.36285	0.90213	0.16507
C	-1.13564	-0.06715	0.05890

C	-1.29446	-1.52147	0.03050
C	1.00443	1.43887	0.32111
C	0.00009	-2.27306	0.39615
H	-0.16906	-3.34817	0.27030
H	0.25927	-2.05075	1.43678
N	1.99104	0.63641	-0.46405
S	2.34292	-0.94024	-0.00447
O	3.43508	-1.38717	-0.85986
O	2.41432	-0.96608	1.45625
C	1.19394	2.91327	-0.10708
H	0.97123	3.01405	-1.18224
H	1.29809	1.35657	1.37589
H	1.81306	0.66412	-1.47015
O	1.07191	-1.92121	-0.50851
F	-2.25926	-1.95254	0.94243
F	-1.74383	-1.94572	-1.21615
H	-4.40332	-0.86737	-0.10157
C	-4.38905	0.19483	0.15176
H	-5.21802	0.70080	-0.35936
H	-4.47850	0.31965	1.23929
N	-3.10177	0.72079	-0.33874
N	-2.79561	1.91895	-0.18075
N	-1.89413	2.65353	-0.06519
H	0.48254	3.52331	0.45522
O	2.49804	3.39229	0.20968
H	3.13555	2.84089	-0.26701

HF: -1390.0339451

Sum of electronic and zero-point Energies=	-1389.845753
Sum of electronic and thermal Energies=	-1389.827273
Sum of electronic and thermal Enthalpies=	-1389.826329
Sum of electronic and thermal Free Energies=	-1389.892641

Frequency: -311.34

10 using M06-2X/6-311++G(d,p) and IEFPCM solvent model (water)

C	-0.27466	0.88367	0.06736
C	-1.09387	-0.01911	-0.10128
C	-1.32043	-1.44378	-0.37739
C	1.08153	1.42019	0.19413
C	-0.14336	-2.30363	0.07027
H	-0.28564	-3.32002	-0.29387
H	-0.08164	-2.28795	1.15768
O	2.05956	0.44910	-0.31220
S	2.15121	-0.99725	0.32291
O	3.42575	-1.50809	-0.07791
O	1.74557	-0.95781	1.70310
C	1.33490	2.67639	-0.63613
H	0.58675	3.42001	-0.35655
H	1.20778	2.42732	-1.69064
H	1.31162	1.59907	1.24782
O	1.06766	-1.82347	-0.52400

F	-2.41957	-1.92884	0.26454
F	-1.55030	-1.63120	-1.70788
O	2.64749	3.15641	-0.47080
H	2.70977	3.62374	0.36807
H	-4.45988	-0.59666	0.07843
C	-4.19145	0.32053	0.59133
H	-5.00853	1.03547	0.50451
H	-3.97955	0.11316	1.64117
N	-2.99732	0.85565	-0.08811
N	-2.57911	1.97499	0.24255
N	-1.65436	2.63333	0.38435
HF: -1410.0809259			
Sum of electronic and zero-point Energies=			-1409.895713
Sum of electronic and thermal Energies=			-1409.878214
Sum of electronic and thermal Enthalpies=			-1409.877270
Sum of electronic and thermal Free Energies=			-1409.942135
Frequency: -386.00			

10 using B97D/6-311+G(d,p) and CPCM solvent model (water)

C	0.31681	0.87920	-0.07840
C	1.11258	-0.06345	0.08927
C	1.27011	-1.50066	0.33600
C	-1.01690	1.46519	-0.18343
C	0.05661	-2.33052	-0.12899
H	0.20006	-3.36749	0.19178
H	-0.01472	-2.27298	-1.21962
O	-2.04761	0.51971	0.37105
S	-2.25944	-0.94332	-0.30887
O	-3.55302	-1.38993	0.17778
O	-1.92289	-0.90674	-1.73086
C	-1.22139	2.75285	0.64454
H	-0.42602	3.45163	0.35677
H	-1.11740	2.50946	1.70815
H	-1.27289	1.64258	-1.23645
O	-1.16715	-1.89034	0.50801
F	2.36096	-2.03966	-0.33736
F	1.50904	-1.73227	1.68687
O	-2.51485	3.31945	0.46630
H	-2.53705	3.74486	-0.40191
H	4.47668	-0.73132	0.09848
C	4.34488	0.21544	-0.42818
H	5.17622	0.88819	-0.18390
H	4.30273	0.03868	-1.51116
N	3.07893	0.79718	0.05985
N	2.71522	1.93277	-0.30108
N	1.77749	2.61455	-0.45149
HF: -1409.890866			
Sum of electronic and zero-point Energies=			-1409.715338
Sum of electronic and thermal Energies=			-1409.696942
Sum of electronic and thermal Enthalpies=			-1409.695998
Sum of electronic and thermal Free Energies=			-1409.762608
Frequency: -304.31			

Coupling with D4 (syn TS)

2 using M06-2X/6-311++G(d,p) and IEFPCM solvent model (water)

C	-0.81581	-0.19482	-0.25205
C	-0.66141	-1.38412	-0.53086
C	0.20629	-2.54006	-0.80786
H	-0.24147	-3.47637	-0.46790
H	0.37785	-2.62869	-1.88349
C	-0.32742	1.17888	-0.02168
C	1.53194	-2.34323	-0.08252
H	2.24398	-3.12734	-0.33447
H	1.38866	-2.30735	0.99680
N	1.12722	1.28890	-0.25345
S	2.18573	0.22168	0.37995
O	3.50103	0.76652	0.14878
O	1.73180	-0.10589	1.71182
C	-1.01155	2.18772	-0.95539
H	-2.08856	2.14351	-0.78333
H	-0.82222	1.89437	-1.99046
H	-0.51101	1.46727	1.01827
H	1.40226	1.60181	-1.18061
O	2.15935	-1.11114	-0.51999
O	-0.50251	3.49340	-0.80215
H	-0.77903	3.84113	0.05178
H	-4.49679	0.63861	1.42934
C	-3.40747	0.63027	1.38437
H	-3.05574	1.65976	1.36180
H	-2.99948	0.12178	2.26035
N	-2.94768	0.00101	0.13831
N	-3.15598	-1.21987	0.00087
N	-2.67997	-2.20236	-0.35273

HF: -1191.7321801

Sum of electronic and zero-point Energies= -1191.518585

Sum of electronic and thermal Energies= -1191.502266

Sum of electronic and thermal Enthalpies= -1191.501322

Sum of electronic and thermal Free Energies= -1191.562835

Frequency: -446.02

2 using M06-2X/6-311++G(d,p) and IEFPCM solvent model (acetonitrile)

C	-0.81659	-0.19344	-0.25207
C	-0.66364	-1.38317	-0.52973
C	0.20223	-2.54073	-0.80538
H	-0.24695	-3.47581	-0.46385
H	0.37304	-2.63123	-1.88098
C	-0.32570	1.17931	-0.02127
C	1.52852	-2.34464	-0.08087
H	2.23927	-3.13026	-0.33193
H	1.38555	-2.30722	0.99846

N	1.12864	1.28713	-0.25392
S	2.18664	0.21932	0.37925
O	3.50211	0.76231	0.14607
O	1.73288	-0.10728	1.71133
C	-1.00905	2.19037	-0.95303
H	-2.08579	2.14944	-0.77822
H	-0.82347	1.89681	-1.98870
H	-0.50800	1.46699	1.01915
H	1.40441	1.60275	-1.17985
O	2.15730	-1.11424	-0.52008
O	-0.49545	3.49432	-0.80123
H	-0.75770	3.83826	0.05871
H	-4.49726	0.64001	1.43099
C	-3.40799	0.63164	1.38458
H	-3.05626	1.66115	1.36348
H	-2.99895	0.12171	2.25927
N	-2.94943	0.00479	0.13689
N	-3.15855	-1.21599	-0.00161
N	-2.68289	-2.19862	-0.35514

HF: -1191.7316097

Sum of electronic and zero-point Energies= -1191.518103

Sum of electronic and thermal Energies= -1191.501729

Sum of electronic and thermal Enthalpies= -1191.500785

Sum of electronic and thermal Free Energies= -1191.562499

Frequency: -445.73

2 using B97D/6-311+G(d,p) and CPCM solvent model (water)

C	-0.79972	-0.21544	-0.27741
C	-0.63802	-1.42058	-0.53678
C	0.26199	-2.56614	-0.75808
H	-0.18692	-3.51089	-0.42058
H	0.48805	-2.67741	-1.82867
C	-0.31253	1.15880	-0.05766
C	1.56384	-2.35722	0.03006
H	2.25946	-3.18684	-0.13881
H	1.36586	-2.25192	1.10236
N	1.14465	1.28464	-0.36475
S	2.27144	0.27536	0.36383
O	3.58141	0.83781	0.03728
O	1.84077	0.06246	1.74822
C	-1.05380	2.20080	-0.93868
H	-2.13105	2.05943	-0.78659
H	-0.82620	2.00378	-1.99419
H	-0.43913	1.43597	0.99771
H	1.33737	1.34048	-1.36566
O	2.29353	-1.17493	-0.45276
O	-0.65464	3.54439	-0.67862
H	-0.98852	3.78846	0.19549
H	-4.77104	0.62118	1.13274
C	-3.67895	0.65240	1.24649
H	-3.34902	1.69267	1.16683
H	-3.39235	0.25018	2.22872

N	-3.02060	-0.08366	0.15366
N	-3.20698	-1.31575	0.03327
N	-2.66780	-2.29155	-0.33520

HF: -1191.5882326

Sum of electronic and zero-point Energies= -1191.384128

Sum of electronic and thermal Energies= -1191.367109

Sum of electronic and thermal Enthalpies= -1191.366165

Sum of electronic and thermal Free Energies= -1191.429007

Frequency: -334.64

2 using B97D/6-311+G(d,p) and CPCM solvent model (acetonitrile)

C	-0.79953	-0.21501	-0.27737
C	-0.63853	-1.42012	-0.53724
C	0.26093	-2.56602	-0.75899
H	-0.18834	-3.51058	-0.42141
H	0.48644	-2.67723	-1.82971
C	-0.31218	1.15912	-0.05717
C	1.56326	-2.35737	0.02857
H	2.25878	-3.18699	-0.14102
H	1.36570	-2.25274	1.10103
N	1.14502	1.28508	-0.36312
S	2.27144	0.27465	0.36459
O	3.58147	0.83673	0.03852
O	1.83993	0.06011	1.74841
C	-1.05329	2.20092	-0.93859
H	-2.13055	2.06066	-0.78522
H	-0.82703	2.00228	-1.99409
H	-0.43942	1.43600	0.99824
H	1.33887	1.34373	-1.36358
O	2.29227	-1.17494	-0.45402
O	-0.65252	3.54444	-0.68114
H	-0.98194	3.78930	0.19441
H	-4.77048	0.62235	1.13433
C	-3.67830	0.65257	1.24775
H	-3.34768	1.69273	1.16916
H	-3.39183	0.24920	2.22959
N	-3.02068	-0.08258	0.15398
N	-3.20730	-1.31474	0.03327
N	-2.66830	-2.29039	-0.33571

HF: -1191.5878365

Sum of electronic and zero-point Energies= -1191.383744

Sum of electronic and thermal Energies= -1191.366717

Sum of electronic and thermal Enthalpies= -1191.365773

Sum of electronic and thermal Free Energies= -1191.428652

Frequency: -334.35

3 using M06-2X/6-311++G(d,p) and IEFPCM solvent model (water)

C	0.83358	-0.38586	-0.28730
C	0.80058	0.84508	-0.24914
C	-0.02231	2.05484	-0.21700

C	0.22808	-1.73393	-0.38852
C	-1.36061	1.82071	0.47475
H	-1.96350	2.72568	0.40400
H	-1.18714	1.55592	1.51761
N	-1.23314	-1.64999	-0.59684
S	-2.17840	-0.72264	0.35611
O	-3.54267	-1.09198	0.09005
O	-1.62542	-0.75058	1.68818
C	0.79770	-2.56571	-1.53532
H	1.86895	-2.70252	-1.40144
H	0.30986	-3.53999	-1.55901
H	0.63559	-2.05531	-2.48694
H	0.38140	-2.25334	0.56075
H	-1.53338	-1.62872	-1.56833
O	-2.08284	0.79614	-0.20826
F	0.58272	3.08494	0.44224
F	-0.24319	2.50806	-1.48807
H	2.76994	-2.78342	0.78482
C	3.20869	-1.83467	1.08506
H	2.80418	-1.52665	2.05122
H	4.28937	-1.95763	1.15064
N	2.87129	-0.86153	0.03286
N	3.23003	0.31848	0.20805
N	2.91991	1.41588	0.12826

HF: -1315.0015915

Sum of electronic and zero-point Energies= -1314.809193

Sum of electronic and thermal Energies= -1314.792660

Sum of electronic and thermal Enthalpies= -1314.791716

Sum of electronic and thermal Free Energies= -1314.853262

Frequency: -414.71

3 using B97D/6-311+G(d,p) and CPCM solvent model (water)

C	-0.83950	-0.37958	0.26331
C	-0.80859	0.86537	0.23790
C	0.03302	2.05983	0.20366
C	-0.23467	-1.72805	0.35593
C	1.38537	1.82983	-0.49953
H	1.96747	2.75712	-0.45707
H	1.20003	1.54411	-1.54071
N	1.23457	-1.65966	0.62260
S	2.25239	-0.75484	-0.35039
O	3.61496	-1.13412	0.00732
O	1.74686	-0.82940	-1.72158
C	-0.83485	-2.60376	1.47230
H	-1.90973	-2.72308	1.31179
H	-0.35131	-3.58714	1.46426
H	-0.68173	-2.12772	2.44955
H	-0.35315	-2.23238	-0.61142
H	1.46024	-1.49466	1.60460
O	2.17696	0.83906	0.19018
F	-0.56371	3.12106	-0.47470
F	0.25650	2.52855	1.50024

H	-2.93968	-2.79493	-0.71141
C	-3.42237	-1.85939	-1.00686
H	-3.14683	-1.60768	-2.04014
H	-4.50983	-1.98164	-0.92330
N	-2.95127	-0.82785	-0.06270
N	-3.31738	0.35928	-0.20848
N	-2.96443	1.46667	-0.08532
HF: -1314.8343449			
Sum of electronic and zero-point Energies=			-1314.651411
Sum of electronic and thermal Energies=			-1314.633930
Sum of electronic and thermal Enthalpies=			-1314.632986
Sum of electronic and thermal Free Energies=			-1314.696790
Frequency: -324.07			

3a using M06-2X/6-311++G(d,p) and IEFPCM solvent model (water)

C	0.81632	-0.29874	-0.35109
C	0.80487	0.92951	-0.45747
C	0.02808	2.16220	-0.59917
C	0.16500	-1.62851	-0.29276
C	-1.27930	2.04127	0.18432
H	-1.87107	2.94932	0.08027
H	-1.07235	1.84334	1.23627
N	-1.29013	-1.51766	-0.53653
S	-2.21746	-0.46784	0.30604
O	-3.58908	-0.82017	0.04588
O	-1.69448	-0.39958	1.64928
C	0.71278	-2.62264	-1.31325
H	1.77843	-2.77361	-1.15117
H	0.19411	-3.57636	-1.21610
H	0.57498	-2.23708	-2.32563
H	0.28145	-2.03159	0.71632
H	-1.56434	-1.55923	-1.51519
O	-2.06997	0.98603	-0.38480
F	0.68815	3.27157	-0.07557
H	2.66759	-2.60597	1.02751
C	3.13570	-1.64218	1.21468
H	2.73740	-1.20915	2.13455
H	4.21157	-1.79101	1.30432
N	2.83256	-0.79299	0.05172
N	3.22880	0.38869	0.08949
N	2.95017	1.47674	-0.12627
H	-0.17408	2.37363	-1.65110
HF=-1215.7518409			
Sum of electronic and zero-point Energies=			-1215.551026
Sum of electronic and thermal Energies=			-1215.535204
Sum of electronic and thermal Enthalpies=			-1215.534260
Sum of electronic and thermal Free Energies=			-1215.594232
Frequency: -425.93			

3a using B97D/6-311+G(d,p) and CPCM solvent model (water)

C	0.82625	-0.28290	-0.33474
C	0.80722	0.95803	-0.44502
C	-0.00226	2.16777	-0.58718
H	-0.22696	2.37340	-1.64252
C	0.18213	-1.61655	-0.28513
C	-1.30810	2.04924	0.22824
H	-1.87940	2.98077	0.15307
H	-1.08445	1.82522	1.27713
N	-1.28345	-1.52864	-0.57031
S	-2.28271	-0.50810	0.30726
O	-3.65208	-0.88269	-0.03577
O	-1.79836	-0.48966	1.68870
C	0.75591	-2.62509	-1.29748
H	1.82735	-2.75522	-1.12049
H	0.24637	-3.58944	-1.18809
H	0.61793	-2.25161	-2.32084
H	0.27592	-2.02164	0.73023
H	-1.49229	-1.43985	-1.56560
O	-2.16898	1.03011	-0.35085
F	0.64902	3.33445	-0.08280
H	2.80245	-2.63155	0.94336
C	3.32359	-1.69064	1.14079
H	3.05075	-1.31687	2.13745
H	4.40537	-1.86880	1.08653
N	2.90427	-0.75053	0.08419
N	3.31431	0.43229	0.11115
N	3.00575	1.53172	-0.13856

HF=-1215.6064093

Sum of electronic and zero-point Energies= -1215.415033
Sum of electronic and thermal Energies= -1215.398340
Sum of electronic and thermal Enthalpies= -1215.397396
Sum of electronic and thermal Free Energies= -1215.459411
Frequency: -329.13

4 using M06-2X/6-311++G(d,p) and IEFPCM solvent model (water)

C	0.84979	-0.03800	-0.33014
C	0.75097	1.18288	-0.45764
C	-0.06315	2.40385	-0.57028
H	0.43631	3.26962	-0.12989
H	-0.25324	2.63370	-1.62166
C	0.29613	-1.40671	-0.24354
C	-1.38179	2.18132	0.15993
H	-2.05558	3.02722	0.03386
H	-1.21883	1.99393	1.22080
N	-1.16418	-1.40855	-0.50170
S	-2.16860	-0.38697	0.29148
O	-3.51107	-0.83066	0.00696
O	-1.69037	-0.27200	1.64981
C	0.91745	-2.38400	-1.23794

H	1.98836	-2.46412	-1.06176
H	0.45897	-3.36709	-1.12923
H	0.76821	-2.02648	-2.25913
H	0.43119	-1.78193	0.77404
H	-1.41730	-1.48354	-1.48417
O	-2.08565	1.05289	-0.41928
H	4.46175	-1.26673	1.22832
C	3.37553	-1.18115	1.18743
H	2.95584	-2.17496	1.04630
H	2.99810	-0.75205	2.11803
N	2.96330	-0.38260	0.02451
N	3.23720	0.83337	0.04102
N	2.81666	1.87678	-0.18469

HF: -1116.5140827

Sum of electronic and zero-point Energies= -1116.305602

Sum of electronic and thermal Energies= -1116.290567

Sum of electronic and thermal Enthalpies= -1116.289623

Sum of electronic and thermal Free Energies= -1116.347605

Frequency: -450.71

4 using B97D/6-311+G(d,p) and CPCM solvent model (water)

C	0.84257	-0.03492	-0.31894
C	0.74734	1.19654	-0.46011
C	-0.08398	2.40846	-0.56518
H	0.41760	3.28855	-0.13835
H	-0.30102	2.63789	-1.61881
C	0.28811	-1.40044	-0.22124
C	-1.39745	2.19976	0.20318
H	-2.04632	3.07846	0.11502
H	-1.20827	1.98365	1.26036
N	-1.18073	-1.41429	-0.53070
S	-2.24890	-0.40993	0.29261
O	-3.58906	-0.86523	-0.07726
O	-1.80990	-0.35017	1.68965
C	0.93497	-2.41483	-1.18170
H	2.00844	-2.47480	-0.98063
H	0.47950	-3.40236	-1.04224
H	0.79594	-2.09165	-2.22212
H	0.38687	-1.76102	0.81044
H	-1.36951	-1.35120	-1.53237
O	-2.18995	1.10965	-0.38591
H	4.74844	-1.27667	0.92816
C	3.66106	-1.21636	1.07288
H	3.23225	-2.21145	0.92106
H	3.43693	-0.87202	2.09269
N	3.04809	-0.33736	0.06268
N	3.31526	0.88591	0.06052
N	2.83982	1.92691	-0.20111

HF: -1116.3898282

Sum of electronic and zero-point Energies= -1116.190701

Sum of electronic and thermal Energies= -1116.174849

Sum of electronic and thermal Enthalpies= -1116.173905

Sum of electronic and thermal Free Energies= -1116.233783
 Frequency: -335.82

8 using M06-2X/6-311++G(d,p) and IEFPCM solvent model (water)

C	0.84053	-0.03026	-0.30146
C	0.74657	1.19108	-0.41824
C	-0.06447	2.41199	-0.54195
H	0.42021	3.27408	-0.07885
H	-0.22240	2.64974	-1.59665
C	0.26837	-1.38249	-0.25742
C	-1.40218	2.18282	0.15026
H	-2.08766	3.01116	-0.01581
H	-1.27275	2.01399	1.21828
O	-1.16974	-1.30003	-0.57455
S	-2.13752	-0.38466	0.28932
O	-3.45223	-0.89565	0.02621
O	-1.63687	-0.27467	1.63637
C	0.82177	-2.34225	-1.29234
H	1.88573	-2.49388	-1.11487
H	0.30433	-3.29852	-1.22266
H	0.68913	-1.92527	-2.29102
H	0.34187	-1.79587	0.75126
O	-2.07439	1.02915	-0.43229
H	2.91720	-2.20525	1.02903
C	3.35699	-1.22005	1.16918
H	2.99585	-0.78433	2.10282
H	4.44163	-1.32537	1.19841
N	2.95031	-0.41194	0.00960
N	3.23113	0.80095	0.03259
N	2.82537	1.85364	-0.17122

HF: -1136.3784769

Sum of electronic and zero-point Energies= -1136.182424
 Sum of electronic and thermal Energies= -1136.167654
 Sum of electronic and thermal Enthalpies= -1136.166710
 Sum of electronic and thermal Free Energies= -1136.224188
 Frequency: -436.83

8 using B97D/6-311+G(d,p) and CPCM solvent model (water)

C	0.83953	-0.02843	-0.28460
C	0.74483	1.20361	-0.41577
C	-0.08513	2.41277	-0.54558
H	0.39628	3.29296	-0.09677
H	-0.26060	2.64357	-1.60632
C	0.27868	-1.37876	-0.22988
C	-1.42477	2.20136	0.17459
H	-2.08956	3.05870	0.02712
H	-1.27876	2.01921	1.24403
O	-1.19125	-1.31457	-0.59711
S	-2.21862	-0.40706	0.29268
O	-3.53394	-0.93153	-0.04938

O	-1.75934	-0.32488	1.68038
C	0.85137	-2.37142	-1.23852
H	1.91593	-2.51491	-1.02432
H	0.33194	-3.33265	-1.15237
H	0.74599	-1.97908	-2.25685
H	0.31858	-1.78041	0.79027
O	-2.17684	1.07354	-0.41450
H	3.20446	-2.24335	0.89409
C	3.63409	-1.25112	1.06039
H	3.39410	-0.90991	2.07725
H	4.72292	-1.31260	0.93078
N	3.04181	-0.36349	0.04384
N	3.30805	0.85812	0.05434
N	2.84385	1.90863	-0.18227

HF: -1136.2507745

Sum of electronic and zero-point Energies= -1136.064226

Sum of electronic and thermal Energies= -1136.048545

Sum of electronic and thermal Enthalpies= -1136.047600

Sum of electronic and thermal Free Energies= -1136.107098

Frequency: -333.32

9 using M06-2X/6-311++G(d,p) and IEFPCM solvent model (water)

C	-0.85182	0.12299	-0.19796
C	-0.72292	-1.09885	-0.28668
C	0.19296	-2.23971	-0.34486
C	-0.31508	1.49865	-0.13891
C	1.49807	-1.96429	0.39552
H	2.15989	-2.82279	0.28491
H	1.28698	-1.77589	1.44815
N	1.12934	1.52637	-0.44572
S	2.17393	0.62563	0.44741
O	3.49824	1.10902	0.17103
O	1.65254	0.54708	1.78890
C	-0.98731	2.47284	-1.11423
H	-0.77124	2.16243	-2.14330
H	-0.43510	1.88782	0.87573
H	1.34373	1.43791	-1.43860
O	2.16938	-0.85616	-0.20691
F	-0.33985	-3.36566	0.21018
F	0.46837	-2.55948	-1.64407
H	-2.06511	2.43058	-0.97272
O	-0.58372	3.79941	-0.87147
H	0.36117	3.87801	-1.04090
H	-2.92671	2.22091	1.15679
C	-3.31741	1.21881	1.31952
H	-2.90608	0.80443	2.24167
H	-4.40365	1.27607	1.38242
N	-2.91984	0.41410	0.15073
N	-3.18853	-0.80219	0.18210
N	-2.80011	-1.85838	-0.01490

HF: -1390.2193579

Sum of electronic and zero-point Energies= -1390.021503

Sum of electronic and thermal Energies=	-1390.003917
Sum of electronic and thermal Enthalpies=	-1390.002973
Sum of electronic and thermal Free Energies=	-1390.067273
Frequency: -409.50	

9 using B97D/6-311+G(d,p) and CPCM solvent model (water)

C	-0.85225	0.11609	-0.17294
C	-0.73059	-1.11914	-0.27461
C	0.19879	-2.24624	-0.33480
C	-0.31605	1.49048	-0.12239
C	1.52227	-1.98095	0.41241
H	2.16251	-2.86492	0.31859
H	1.30305	-1.77953	1.46658
N	1.13604	1.53271	-0.45986
S	2.24371	0.65320	0.45166
O	3.56650	1.15130	0.09581
O	1.75911	0.61210	1.83081
C	-1.00642	2.47288	-1.10672
H	-0.78839	2.15489	-2.13982
H	-0.42348	1.88935	0.89406
H	1.31360	1.36022	-1.45152
O	2.26458	-0.89867	-0.19250
F	-0.32450	-3.40402	0.23597
F	0.47181	-2.57636	-1.66258
H	-2.08670	2.42302	-0.95306
O	-0.61304	3.82064	-0.87502
H	0.33666	3.88730	-1.05039
H	-3.08298	2.25559	1.07728
C	-3.51012	1.26454	1.25388
H	-3.21177	0.90124	2.24655
H	-4.60328	1.33417	1.18682
N	-2.98998	0.38644	0.18636
N	-3.26991	-0.83259	0.19970
N	-2.84692	-1.89486	-0.03819

HF: -1390.0332557

Sum of electronic and zero-point Energies=	-1389.844817
Sum of electronic and thermal Energies=	-1389.826438
Sum of electronic and thermal Enthalpies=	-1389.825494
Sum of electronic and thermal Free Energies=	-1389.891364
Frequency: -321.02	

10 using M06-2X/6-311++G(d,p) and IEFPCM solvent model (water)

C	-0.82835	0.12966	-0.16005
C	-0.71201	-1.09065	-0.26274
C	0.19611	-2.23334	-0.38476
C	-0.29393	1.49842	-0.13447
C	1.53032	-1.97562	0.30866
H	2.20905	-2.80205	0.10334
H	1.36826	-1.86423	1.38009

O	1.13918	1.46555	-0.41218
S	2.11853	0.60987	0.49892
O	3.41498	1.17654	0.29084
O	1.55584	0.45095	1.81337
C	-0.87677	2.39373	-1.22719
H	-1.96582	2.37141	-1.14480
H	-0.59448	1.97722	-2.19514
H	-0.42756	1.94521	0.85484
O	2.14535	-0.80652	-0.24768
F	-0.31507	-3.37037	0.16270
F	0.41703	-2.51580	-1.70154
O	-0.36136	3.70062	-1.16122
H	-0.81716	4.18821	-0.46808
H	-4.36957	1.31248	1.43562
C	-3.28388	1.27259	1.35508
H	-2.91395	2.27730	1.16337
H	-2.84908	0.88280	2.27706
N	-2.89441	0.45158	0.19508
N	-3.16643	-0.76177	0.23148
N	-2.79555	-1.82362	0.03465

HF: -1410.0805688

Sum of electronic and zero-point Energies= -1409.895403

Sum of electronic and thermal Energies= -1409.877947

Sum of electronic and thermal Enthalpies= -1409.877003

Sum of electronic and thermal Free Energies= -1409.941242

Frequency: -390.33

10 using B97D/6-311+G(d,p) and CPCM solvent model (water)

C	0.82899	-0.09818	-0.13759
C	0.68263	1.13277	-0.24201
C	-0.27127	2.23504	-0.36671
C	0.34355	-1.48024	-0.12107
C	-1.62046	1.94661	0.32286
H	-2.30385	2.77886	0.12589
H	-1.45591	1.82885	1.39854
O	-1.11246	-1.50877	-0.44909
S	-2.17887	-0.70081	0.49129
O	-3.45884	-1.32080	0.19849
O	-1.66306	-0.55740	1.85084
C	0.99060	-2.37886	-1.19956
H	2.07993	-2.28689	-1.09524
H	0.69903	-2.00290	-2.18683
H	0.46273	-1.92472	0.87572
O	-2.26762	0.78002	-0.24637
F	0.19223	3.41519	0.20205
F	-0.48991	2.52534	-1.71209
O	0.55856	-3.73074	-1.11783
H	0.99929	-4.14257	-0.36194
H	4.62258	-1.21423	1.22650
C	3.52632	-1.20916	1.27118
H	3.16055	-2.21624	1.05295
H	3.18613	-0.89253	2.26624

N	2.98174	-0.32874	0.21813
N	3.21614	0.89736	0.24633
N	2.76720	1.95055	0.01800

HF: -1409.8905771

Sum of electronic and zero-point Energies=	-1409.715154
Sum of electronic and thermal Energies=	-1409.696759
Sum of electronic and thermal Enthalpies=	-1409.695814
Sum of electronic and thermal Free Energies=	-1409.761971

Frequency: -310.93

Triple, Mutually Orthogonal Cycloadditions Through the De... (1.09 MiB) [view on ChemRxiv](#) • [download file](#)

Supplementary Materials Part 2 for

Triple, Mutually Orthogonal Cycloadditions Through the Design of Electronically Activated SNO-OCTs

Yun Hu,^{†,‡} Jessica M. Roberts,^{†,‡} Henry R. Kilgore,^{§,‡} Amirah S. Mat Lani,[†]
Ronald T. Raines,^{*,§} and Jennifer M. Schomaker^{*,†}

[†]Department of Chemistry, University of Wisconsin, Madison, Wisconsin 53706, United States

[§]Department of Chemistry, Massachusetts Institute of Technology, Cambridge, Massachusetts 02139, United States

[‡]These authors contributed equally to this work.

*Corresponding authors: schomakerj@chem.wisc.edu, rtraines@mit.edu

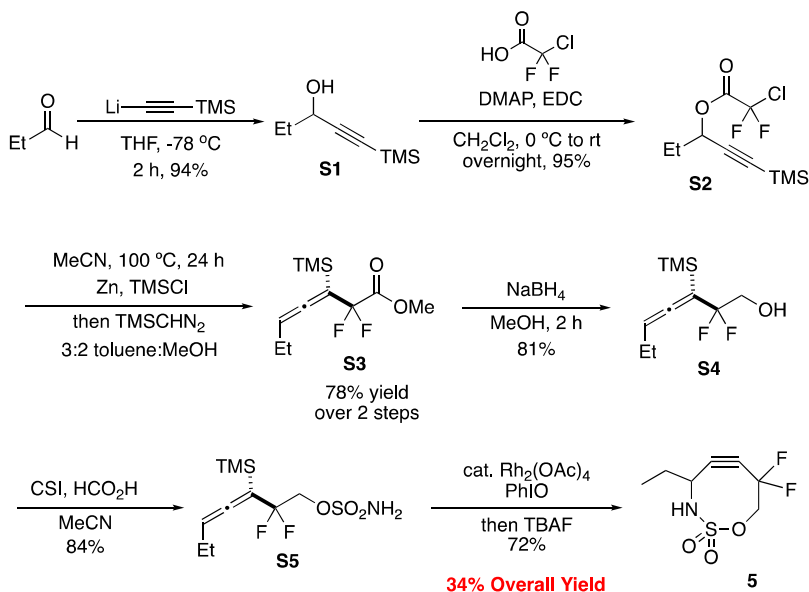
Table of Contents	S2-1
I. General information	S2-2
II. Additional reaction schemes and figures	S2-3
III. Preparation of DF-SNO-OCT	S2-5
IV. Reactions of alkyne with dipoles	S2-8
V. Preparation of chromophore-conjugated SNO-OCT derivatives	S2-11
VI. NMR kinetics for SNO-OCT/dipole cyclization	S2-17
VII. Plate reader kinetics SNO-OCT/dipole cyclization	S2-22
VIII. Reactions of one SNO-OCT with two competing dipoles	S2-25
IX. Reactions of two SNO-OCTs with one dipole	S2-27
X. Reactions of two SNO-OCTs with two competing dipoles	S2-28
XI. Triple ligation results	S2-32
XII. UPLC-MS methods and calibration curves	S2-34
XIII. <i>In cellulo</i> assays	S2-39
XIV. References	S2-48
XV. NMR spectra	S2-50

I. General information

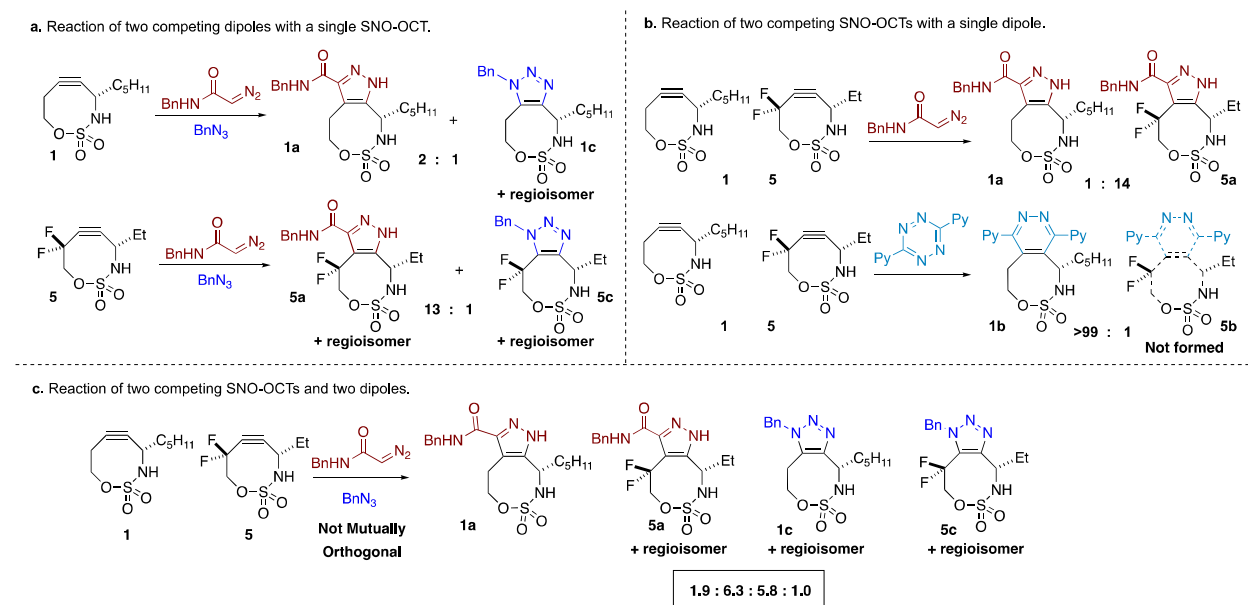
All glassware was either oven-dried overnight at 130 °C or flame dried under a stream of dry nitrogen prior to use. Reagents were used as obtained from the vendor without further purification unless otherwise specified. Dichloromethane, acetonitrile, dimethylformamide were dried over CaH_2 and freshly distilled prior to use. All other solvents and reagents were purified in accordance with "Purification of Laboratory Chemicals".^{1a} Air- and moisture sensitive reactions were performed under an atmosphere of nitrogen. Analytical thin layer chromatography (TLC) was performed utilizing pre-coated silica gel 60 F254 plates containing a fluorescent indicator, while preparative chromatography was performed using SilicaFlash P60 silica gel (230-400 mesh) via Still's method.^{1b} The mobile phases for column chromatography varied depending on substrate as hexanes/ether, pentane/ether, hexanes/ethyl acetate, or benzene/ethyl acetate were used. Columns were typically run using a gradient method, beginning with 100% of the less polar eluent and gradually increasing the polarity with the other solvent. For reactions producing products without a UV signature, potassium permanganate was employed to visualize the reaction progress.

^1H NMR and ^{13}C NMR spectra were obtained using Bruker Avance III 500, Bruker Avance III 400, Bruker Avance III 600, and Varian Mercury-300 NMR spectrometers. For ^1H NMR, chemical shifts are reported relative to residual protiated solvent peaks (δ 7.26, 2.49, 7.15 and 4.80 ppm for CDCl_3 , $(\text{CD}_3)_2\text{SO}$, C_6D_6 and CD_3OD respectively). ^{13}C NMR spectra were measured at either 125 MHz or 150 MHz on the same instruments noted above for recording ^1H NMR spectra. Chemical shifts were again reported in accordance with residual protiated solvent peaks (δ 77.1, 39.5, 128.0 and 49.0 ppm for CDCl_3 , $(\text{CD}_3)_2\text{SO}$, C_6D_6 , and CD_3OD , respectively). UPLC/LC-MS data were collected on an Acquity UPLC I-Class PLUS with an Acquity QDA MS detector (Waters) using an ACQUITY UPLC BEH C18 1.7 μm 2.1 X 50 mm column (Waters). Plate reader kinetics were performed on a Perkin-Elmer Envision plate reader with a 531 nm filter. Accurate mass measurements were acquired at the University of Wisconsin, Madison using a Thermo Q ExactiveTM Plus (electrospray ionization or atmospheric solids analysis probe (ASAP-MS) methods). The NMR facilities are funded by the NSF (CHE-1048642, CHE-0342998), the University of Wisconsin, the NIH (S10 OD012245), and a generous gift from Paul J. and Margaret M. Bender. The purchase of the Thermo Q ExactiveTM Plus in 2015 was funded by NIH Award 1S10 OD020022-1 to the University of Wisconsin-Madison Department of Chemistry.

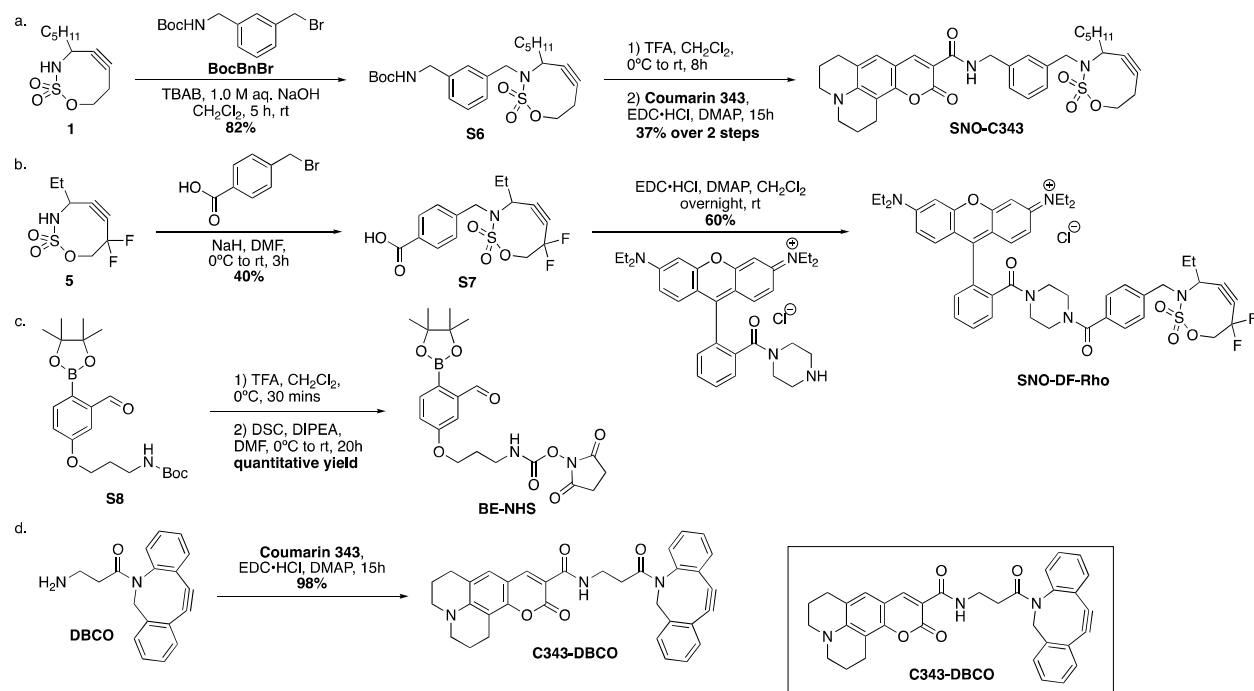
II. Additional reaction schemes and figures



Scheme S2-1. Synthesis of difluorinated SNO-OCT 5 (DF-SNO-OCT).

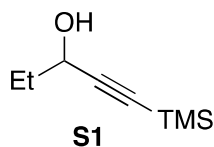


Scheme S2-2. Competition experiments and extrapolation of chemoselectivity. (a) The competition between benzyl diazoacetamide and benzyl azide showed slight chemoselectivity favoring **1a**, while formation of **5c** is more favorable. Overall, the selectivity between the two dipoles for **1** and **5** do not reach the ideal >20:1 selectivity. (b) The competition between two competing SNO-OCTs and a Type I or Type III dipole. Benzyl diazoacetamide prefers reaction with **5**, with excellent chemoselectivity of dipyrindyl tetrazine for **1**. (c) Competition between two SNO-OCTs and two dipoles amplifies the poor selectivity when all four are combined in one pot, showing the non-orthogonality of Type I and Types II dipoles (for more details, see Figure S2-10B).

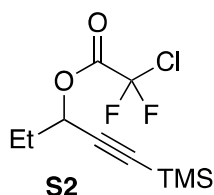


Scheme S2-3. The synthesis of bioorthogonal labeling agents: (a) C343-SNO (b) Rho-DF-SNO (c) BE-NHS (d) C343-DBCO.

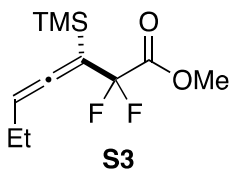
III. Preparation of DF-SNO-OCT



Propargylic alcohol precursor to 5. This compound was prepared based on a previously reported procedure with a comparable yield of 94%.²

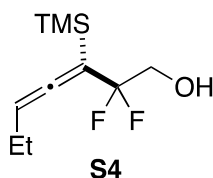


Chlorodifluoro ester precursor to 5. The ester was prepared from the corresponding propargylic alcohol (3.6 mL, 19.85 mmol) in a dry 50 mL round bottom flask. The alcohol was dissolved in 20 mL dichloromethane under a nitrogen atmosphere. Chlorodifluoroacetic acid (3.4 mL, 40.1 mmol) was added to the mixture, followed by the addition of DMAP (0.13 g, 1.10 mmol). The mixture was cooled to 0 °C. EDC·HCl (8.30 g, 43.30 mmol) was added in small portions at 0 °C and the reaction mixture was stirred for an additional 5 min at 0 °C. The mixture was stirred at room temperature overnight, then quenched with saturated NaHCO₃. The aqueous phase was extracted with three portions of dichloromethane, the combined organics washed with brine, dried over Na₂SO₄, filtered through cotton and concentrated *in vacuo*. The crude material was purified using Kugelrohr distillation resulting a clear colorless liquid (5.06 g, 18.81 mmol) with a yield of 95%. ¹H NMR (500 MHz, CDCl₃) δ 5.43 (t, *J* = 7.1, 6.4 Hz, 1H), 1.915 (p, *J* = 7.3 Hz, 2H), 1.05 (t, *J* = 7.4 Hz, 3H), 0.18 (s, 9H). ¹³C NMR (126 MHz, CDCl₃) δ 158.28 (t, *J* = 34.6 Hz), 116.77 (t, *J* = 300.8 Hz), 99.44, 93.24, 70.11, 27.82, 9.08, -0.40. ¹⁹F NMR (377 MHz, CDCl₃) δ -64.07. HRMS (ESI) *m/z* calculated for C₁₀H₁₅ClF₂O₂Si [M + H]⁺ 269.0571, found 269.0566.

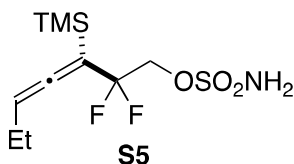


Homoallenic methyl ester precursor to 5. The following reactions were adapted from a previously reported procedure.^{3,4} The corresponding chlorodifluoro ester (2.00 g, 7.44 mmol) was added to a 50 mL round bottom containing ~5 g activated zinc. Trimethylsilylchloride (1.7 mL, 13.39 mmol) was added, followed by the addition of 20 mL acetonitrile. The reaction was refluxed overnight at 100 °C. All volatiles were *in vacuo* and the residue was diluted with EtOAc. The organic phase was washed with brine, dried over Na₂SO₄, and filtered through cotton. The crude material was re-concentrated under

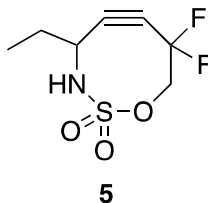
reduced pressure and was used directly in the methylation. The crude material was dissolved in 28 mL methanol and 42 mL toluene in a 250 mL round bottom flask. Trimethylsilyldiazomethane (4.5 mL, 2.0 M in diethyl ether) was added to the reaction mixture at room temperature in a slow and steady stream with vigorous stirring. The mixture was stirred at room temperature for 30 min, then quenched with acetic acid (0.04 mL, 0.702 mmol). The crude mixture was concentrated under reduced pressure and was purified via column chromatography (0% EtOAc/hexanes to 5% EtOAc/hexanes, gradient) resulting a clear yellow oil (1.45 g, 5.84 mmol) in a yield of 78%. ^1H NMR (500 MHz, CDCl_3) δ 5.32 (p, J = 6.2 Hz, 1H), 3.84 (s, 3H), 2.03 – 1.98 (m, 2H), 1.00 (t, J = 7.4 Hz, 3H), 0.21 (s, 9H). ^{13}C NMR (126 MHz, CDCl_3) δ 208.58 (t, J = 13.3 Hz), 164.26 (t, J = 43.9 Hz), 116.18 (t, J = 248.0 Hz), 96.34 (t, J = 36.1 Hz), 92.29, 52.68, 20.20, 12.84, -0.99. ^{19}F NMR (377 MHz, CDCl_3) δ -93.59 (d, J = 256.5 Hz), -93.75 (d, J = 257.2 Hz). HRMS (ESI) m/z calculated for $\text{C}_{11}\text{H}_{18}\text{F}_2\text{O}_2\text{Si}$ [$\text{M} + \text{NH}_4$] $^+$ 266.1382, found 266.1378.



Homoallenic alcohol precursor to 5. The homoallenic alcohol precursor was prepared from the corresponding methyl ester. In a 50 mL round bottom flask, the homoallenic methyl ester (1.45 g, 5.82 mmol) was dissolved in 12 mL methanol. The mixture was cooled to 0 °C before the addition of NaBH_4 (0.35 g, 9.25 mmol). The reaction was stirred at 0 °C for 30 min, warmed to room temperature and reaction progression monitored by TLC. The mixture was quenched with 1.0 M HCl and diluted with diethyl ether. The organic layer was washed with 10% Na_2CO_3 , then washed with brine, dried over Na_2SO_4 , and filtered through cotton. The volatiles were removed *in vacuo*, and the residue purified via column chromatography (0% EtOAc/hexanes to 20% EtOAc/hexanes, gradient) resulting a clear, champagne-color liquid (1.04 g, 4.72 mmol) with a yield of 81%. ^1H NMR (400 MHz, CDCl_3) δ 5.26 (p, J = 6.1 Hz, 1H), 3.85 (td, J = 13.3, 7.2 Hz, 2H), 2.05 (p, J = 7.3 Hz, 2H), 1.81 (t, J = 7.0 Hz 1H), 1.02 (t, J = 7.5 Hz, 3H), 0.19 (s, 9H). ^{13}C NMR (126 MHz, CDCl_3) δ 207.70 (t, J = 13.7 Hz), 122.09 (t, J = 240.0 Hz), 96.86 (t, J = 36.7 Hz), 91.40, 65.13 (t, J = 30.9 Hz), 20.61, 13.25, -0.74. ^{19}F NMR (376 MHz, CDCl_3) δ -95.89 (d, J = 254.5 Hz), -97.35 (d, J = 254.4 Hz). HRMS (ESI) m/z calculated for $\text{C}_{10}\text{H}_{18}\text{F}_2\text{OSi}$ [$\text{M} - \text{F}$] $^-$ 201.1106, found 201.1105.



Homoallenic sulfamate precursor to 5. The following procedure was adapted from our previously reported synthesis of SNO-OCT analogues.⁵ In a 250 mL three-neck round bottom flask, chlorosulfonyl isocyanate (4.5 mL, 51.70 mmol) in 38 mL acetonitrile was cooled to 0 °C. Formic acid (2.0 mL, 53.15 mmol) was added dropwise at 0 °C under a nitrogen atmosphere. The mixture was then allowed to warm up to room temperature and stirred overnight. The reaction was cooled to 0 °C, and the homoallenic alcohol (4.69 g, 21.26 mmol) was added as a solution in N,N-dimethylacetamide (35.0 mL, 0.6 M) in a dropwise fashion. The reaction was stirred for 1 h at room temperature and quenched by the addition of an equal volume of H₂O. The aqueous phase was extracted with three portions of EtOAc and the combined organic phases were washed with five portions of H₂O. The combined organics were dried over Na₂SO₄, filtered through cotton, and concentrated *in vacuo*. The crude material was purified via column chromatography (0% EtOAc/hexanes to 20% EtOAc/hexanes, gradient) resulting a waxy white solid (5.34 g, 17.83 mmol) with a yield of 84%. ¹H NMR (500 MHz, CDCl₃) δ 5.33 (p, *J* = 6.1 Hz, 1H), 4.99 (s, 1H), 4.46 – 4.37 (m, 2H), 2.07 (dtd, *J* = 13.7, 7.4, 3.3 Hz, 2H), 1.03 (t, *J* = 7.4 Hz, 3H), 0.19 (s, 9H). ¹³C NMR (126 MHz, CDCl₃) δ 208.07 (t, *J* = 13.6 Hz), 120.01 (t, *J* = 241.17 Hz), 96.28 (t, *J* = 36.27 Hz), 92.44, 69.97 (t, *J* = 31.44 Hz), 20.51, 13.18, -0.79. ¹⁹F NMR (377 MHz, CDCl₃) δ -93.24 (d, *J* = 257.8 Hz), -93.68 (d, *J* = 257.2 Hz). HRMS (ESI) *m/z* calculated for C₁₀H₁₉F₂NO₃SSi [M – H][–] 298.0750, found 298.0748.

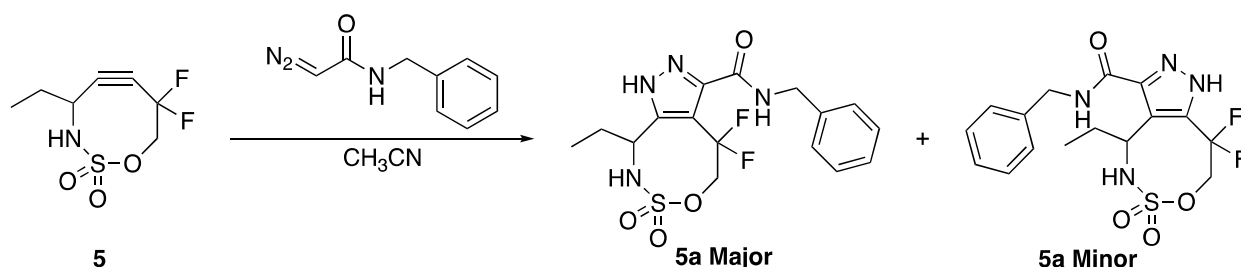


Compound 5. The following procedure was adapted from our previously reported synthesis of SNO-OCT analogues.⁵ In a 100 mL round bottom flask, the homoallenic sulfamate (2.67 g, 7.04 mmol) was dissolved in 36 mL of dichloromethane. Rh₂(OAc)₄ (156.0 mg, 0.35 mmol) was added to the mixture and then stirred for 5 min at room temperature. PhIO (3.19 mg, 14.50 mmol) was added in one portion and the reaction mixture was stirred for 30 min with monitoring by TLC. When the TLC indicated the complete consumption of starting material, the crude mixture was filtered through a layer of Celite, diluted with dichloromethane, and concentrated under reduced pressure. The resulting residue was quickly purified via column chromatography (0% EtOAc/hexanes to 10% EtOAc/hexanes, gradient) to yield an oil as the endocyclic methyleneaziridine intermediate. Due to concerns with decomposition, the purified product was quickly transferred to a round bottom flask and diluted with 36 mL of dichloromethane, followed by the addition of a steady stream of TBAF (35.2 mL, 1.0 M in THF). After stirring at room temperature for 30 min, an equal volume of water was added. The phases were extracted with three portions of

dichloromethane. The combined organics were dried with Na₂SO₄, filtered through cotton, and concentrated under reduced pressure. The resulting crude was quickly purified via column chromatography (0% EtOAc/hexanes to 20% EtOAc/hexanes, gradient) resulting a white solid (1.14 g, 5.06 mmol) with a yield of 72% over two steps. ¹H NMR (500 MHz, CDCl₃) δ 5.62 (d, *J* = 7.0 Hz, 1H), 4.92 (m, 1H), 4.67 (dt, *J* = 12.2, 6.0 Hz, 1H), 4.24 (tt, *J* = 7.2, 3.3 Hz, 1H), 1.91 – 1.72 (m, 2H), 1.04 (t, *J* = 7.5 Hz, 3H). ¹³C NMR (126 MHz, CDCl₃) δ 112.55 (d, *J* = 241.4 Hz), 111.15 (t, *J* = 10.8 Hz), 88.37 (t, *J* = 42.9 Hz), 79.04 (m), 50.08 (t, *J* = 1.7 Hz), 25.03, 10.11. ¹⁹F NMR (376 MHz, CDCl₃) δ -96.48 (d, *J* = 277.8 Hz), -101.07 (d, *J* = 277.2 Hz). HRMS (ESI) *m/z* calculated for C₇H₉F₂NO₃S [M – H][–] 224.0198, found 224.0200.

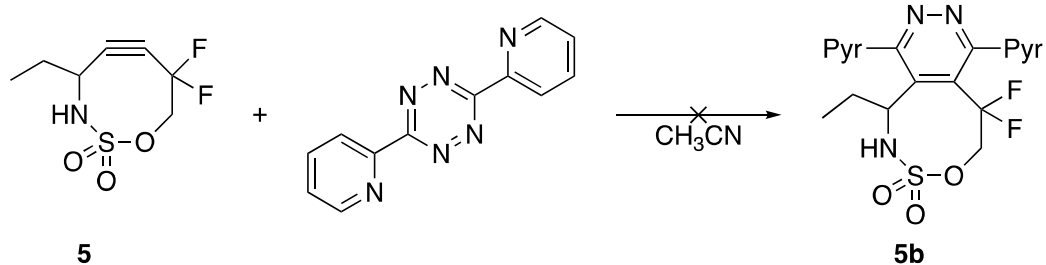
IV. Reactions of SNO-OCTs with dipoles

General procedure. The cyclic alkyne (1.0 equiv) was dissolved in CH₃CN (0.1 M). The corresponding dipole (1.0 equiv) was added to the alkyne solution and the mixture was stirred for 1 h to ensure full conversion. The solvent was then removed under reduced pressure and transferred using dichloromethane.

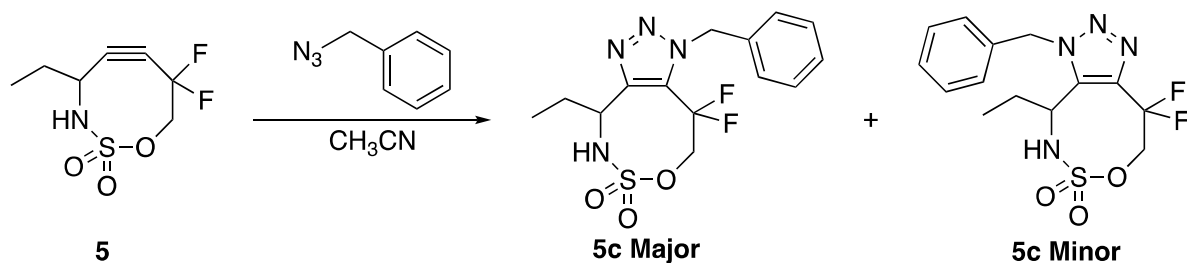


Diazoles 5a major and 5a minor from reaction of 5 with benzyl diazo acetamide. The diazoles **5a major** and **5a minor** were prepared from alkyne **5** (50.0 mg, 0.222 mmol) according to the general procedure. The crude material was purified via column chromatography (0% EtOAc/hexanes to 60% EtOAc/hexanes, gradient) to yield two regioisomers as white solids (**major** 70.3 mg, 0.176 mmol; **minor** 13.0 mg, 0.032 mmol; ratio = 5.4:1) with a total yield of 94%. ¹H NMR (**major**, 500 MHz, CDCl₃) δ 12.42 (s, 1H), 7.42 – 7.23 (m, 5H), 7.06 (p, *J* = 5.2 Hz, 1H), 5.76 (s, 1H), 4.90 – 4.73 (m, 1H), 4.68 – 4.45 (m, 4H), 2.12 – 2.00 (m, 1H), 1.97 – 1.86 (m, 1H), 1.04 (t, *J* = 7.3 Hz, 3H). ¹³C NMR (**major**, 126 MHz, CDCl₃) δ 159.35, 148.54, 139.65, 136.72, 128.88, 127.92, 127.67, 118.81 (t, *J* = 238.4 Hz), 110.43 (t, *J* = 29.9 Hz), 70.69 (t, *J* = 40.4 Hz), 52.34, 44.26, 26.83, 10.66. ¹⁹F NMR (**major**, 376 MHz, CDCl₃) δ -77.28 (d, *J* = 274.7 Hz), -84.20. ¹H NMR (**minor**, 500 MHz, CDCl₃) δ 10.36 (s, 1H), 7.40 – 7.27 (m, 8H), 5.31 – 5.21 (m, 1H), 4.95 – 4.81 (m, 2H), 4.65 (dd, *J* = 14.8, 6.1 Hz, 1H), 4.56 (dd, *J* = 14.8, 5.8 Hz, 1H), 4.30 (ddd, *J* = 23.7, 14.2, 12.4 Hz, 1H), 2.22 (ddq, *J* = 14.9, 7.5, 3.3 Hz, 1H), 1.69 (ddq, *J* = 14.5, 8.7, 7.3 Hz,

1H), 1.07 (t, $J = 7.4$ Hz, 3H). ^{13}C NMR (**minor**, 126 MHz, CDCl_3) δ 160.85, 144.26, 137.80, 131.62, 128.78, 127.79, 127.63, 124.80 (d, $J = 6.1$ Hz), 118.83 (dd, $J = 249.6, 239.0$ Hz), 71.30 (dd, $J = 46.4, 36.2$ Hz), 51.89 (d, $J = 1.2$ Hz), 43.09, 30.11, 10.18. ^{19}F NMR (**minor**, 376 MHz, CDCl_3) δ -70.51 (d, $J = 268.5$ Hz), -101.71 (d, $J = 269.5$ Hz). HRMS (ESI) m/z calculated for $\text{C}_{16}\text{H}_{18}\text{F}_2\text{N}_4\text{O}_4\text{S}$ (**major**) $[\text{M} + \text{H}]^+$ 401.1090, found 401.1088. HRMS (ESI) m/z calculated for $\text{C}_{16}\text{H}_{18}\text{F}_2\text{N}_4\text{O}_4\text{S}$ (**minor**) $[\text{M} + \text{H}]^+$ 401.1090, found 401.1090.

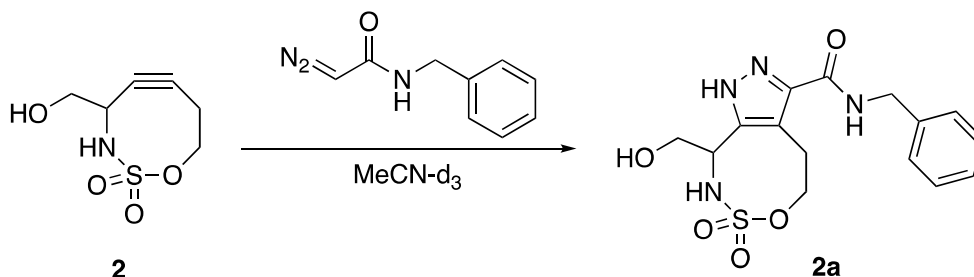


Pyridazine 5b from reaction of 5 with 3,6-di-2-pyridyl-1,2,4,5-tetrazine. The reaction was performed under the general procedure. No reaction of these two components to yield **5b** was observed.

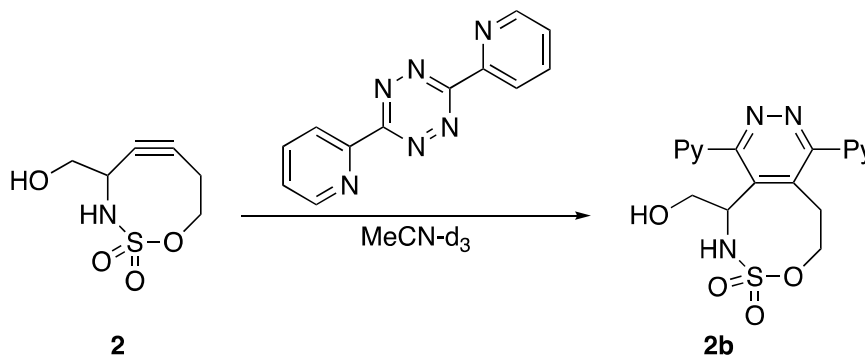


Triazoles 5c major and 5c minor from reaction of 5 with benzyl azide. The triazoles **5c major** and **5c minor** were prepared from alkyne **5** (40.0 mg, 0.178 mmol) according to the general procedure. The crude was purified via column chromatography (0% EtOAc/hexanes to 45% EtOAc/hexanes, gradient) to yield a clear viscous oil (61.0 mg, 0.171 mmol) as a mixture of regioisomers (**5c major**:**5c minor** 1.8:1) in 96% yield. ^1H NMR (**major**, 500 MHz, CDCl_3) δ 7.42 – 7.30 (m, 3H), 7.19 (dd, $J = 7.0, 2.6$ Hz, 2H), 5.78 (d, $J = 15.1$ Hz, 1H), 5.68 (d, $J = 15.1$ Hz, 1H), 4.94 (d, $J = 9.9$ Hz, 1H), 4.62 (q, $J = 8.7$ Hz, 1H), 4.48 – 4.38 (m, 1H), 4.39 – 4.26 (m, 1H), 2.33 (dq, $J = 14.7, 7.4, 5.0$ Hz, 1H), 2.07 (dq, $J = 15.9, 7.3, 5.8$ Hz, 1H), 1.12 (t, $J = 7.4$ Hz, 3H). ^{13}C NMR (**major**, 126 MHz, CDCl_3) δ 147.19 (t, $J = 3.8$ Hz), 134.22, 128.93, 128.80, 127.55, 125.96 (t, $J = 29.5$ Hz), 116.39 (t, $J = 242.6$ Hz), 69.96 – 69.10 (m), 54.74 (t, $J = 3.9$ Hz), 52.23, 27.07, 10.23. ^{19}F NMR (**major**, 376 MHz, CDCl_3) δ -83.51 (d, $J = 288.1$ Hz), -93.18 (d, $J = 286.4$ Hz). ^1H NMR (**minor**, 500 MHz, CDCl_3) δ 7.43 – 7.35 (m, 3H), 7.17 (dd, $J = 8.0, 1.9$ Hz, 2H), 5.61 (d, $J = 15.8$ Hz, 1H), 5.57 (d, $J = 15.9$ Hz, 1H), 5.05 (s, 1H), 4.84 (dd, $J = 13.9, 12.1$ Hz, 1H), 4.47 (m, 3H), 4.33 (ddd, $J = 26.5, 13.9, 9.9$ Hz, 1H), 1.63 (dq, $J = 15.0, 7.5, 3.3$ Hz, 1H), 1.52 (ddq,

$J = 14.7, 9.1, 7.4$ Hz, 1H), 0.92 (t, $J = 7.4$ Hz, 3H). ^{13}C NMR (**minor**, 126 MHz, CDCl_3) δ 137.47 (d, $J = 7.4$ Hz), 136.69 (dd, $J = 34.4, 25.5$ Hz), 132.99, 129.49, 129.21, 126.94, 118.76 (dd, $J = 248.3, 239.3$ Hz), 71.87 (dd, $J = 47.1, 35.8$ Hz), 53.21, 50.84 (d, $J = 1.4$ Hz), 28.05, 9.69. ^{19}F NMR (**minor**, 376 MHz, CDCl_3) δ -71.62 (d, $J = 270.2$ Hz), -104.51 (d, $J = 269.7$ Hz). HRMS (ESI) m/z calculated for $\text{C}_{14}\text{H}_{16}\text{F}_2\text{N}_4\text{O}_3\text{S}$ (**major**) $[\text{M} + \text{H}]^+$ 359.0984, found 359.0982. HRMS (ESI) m/z calculated for $\text{C}_{14}\text{H}_{16}\text{F}_2\text{N}_4\text{O}_3\text{S}$ (**minor**) $[\text{M} + \text{H}]^+$ 359.0984, found 359.0984.



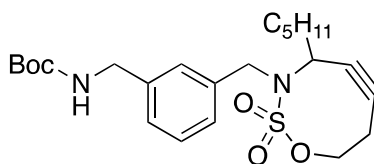
Diazoles 2a from reaction of 2 with benzyl diazo acetamide. The diazoles **2a** were prepared from alkyne **2** (9.6 mg, 0.05 mmol) according to the general procedure, with the exception that deuterated acetonitrile was used and the reaction mixture was stirred at room temperature overnight. Product **2a** was obtained as a single regioisomer in 80% yield in the form of a white solid (13.6 mg, 0.04 mmol) without further purification. Due to the product's low solubility in acetonitrile, dichloromethane, and chloroform, the NMR spectra were taken in $\text{DMSO}-d_6$. ^1H NMR (600 MHz, $\text{DMSO}-d_6$) δ 13.06 (s, 1H), 8.67 (t, $J = 6.4$ Hz, 1H), 8.40 (d, $J = 9.0$ Hz, 1H), 7.31 – 7.27 (m, 4H), 7.24 – 7.20 (d, $J = 6.7$ Hz, 1H), 5.18 (t, $J = 5.8$ Hz, 1H), 4.48 (q, $J = 7.1$ Hz, 1H), 4.41 (d, $J = 6.0$ Hz, 2H), 4.40 (d, $J = 6.0$ Hz, 2H), 4.35 (ddd, $J = 11.2, 5.1, 3.4$ Hz, 1H), 4.02 (td, $J = 10.9, 5.6$ Hz, 1H), 3.79 (dt, $J = 10.9, 5.3$ Hz, 1H), 3.69 (dt, $J = 11.8, 6.1$ Hz, 1H), 3.59 – 3.46 (m, 2H). ^{13}C NMR (151 MHz, $\text{DMSO}-d_6$) δ 162.77, 142.54, 141.08, 139.90, 128.13, 127.10, 126.52, 113.71, 70.10, 62.54, 52.44, 41.59, 20.47. HRMS (ESI) m/z calculated for $\text{C}_{15}\text{H}_{18}\text{N}_4\text{O}_5\text{S}$ $[\text{M} + \text{Na}]^+$ 389.0890, found 389.0086.



Pyridazine 2b from reaction of 2 with 3,6-di-2-pyridyl-1,2,4,5-tetrazine. The pyridazine **2b** was prepared from alkyne **2** (9.6 mg, 0.05 mmol) and dipyridyl tetrazine (11.8 mg, 0.05 mmol) according to

the general procedure, except deuterated acetonitrile was used and the reaction was stirred at room temperature overnight. The products were obtained without further purification as white solids with pinkish tints (19.2 mg). Due to the products' low solubility in acetonitrile and chloroform, the NMR spectra were taken in DMSO- d_6 . The yield was calculated based on the ^1H NMR peak ratio between the cycloaddition product and the tetrazine starting material ($\delta_{\text{product}} = 8.78\text{--}8.72$ ppm, int. = 2.00, 2H; $\delta_{\text{tetrazine}} = 8.95$ ppm, int. = 0.43, 1H). ^1H NMR (600 MHz, DMSO- d_6) δ 9.14 (dd, $J = 6.2, 1.4$ Hz, 1H), 9.11 (dd, $J = 8.1, 1.4$ Hz, 1H), 8.78 – 8.72 (m, 2H), 8.23 (ddd, $J = 7.7, 6.0, 1.5$ Hz, 1H), 8.09 (td, $J = 7.7, 1.8$ Hz, 1H), 7.94 (dt, $J = 7.8, 1.2$ Hz, 1H), 7.61 (ddd, $J = 7.7, 4.9, 1.2$ Hz, 1H), 5.12 (d, $J = 6.1$ Hz, 1H), 5.00 (s, 1H), 4.95 (ddd, $J = 12.6, 6.9, 5.1$ Hz, 1H), 4.87 (ddd, $J = 13.9, 9.9, 4.6$ Hz, 1H), 4.68 (td, $J = 6.9, 3.3$ Hz, 1H), 4.06 – 3.96 (m, 1H), 3.88 – 3.81 (m, 1H), 3.72 – 3.66 (m, 1H), 3.60 (s, 1H). ^{13}C NMR (151 MHz, DMSO- d_6) δ 160.82, 155.77, 148.39, 147.52, 146.22, 145.77, 145.70, 138.72, 137.78, 137.40, 127.83, 125.35, 124.65, 124.15, 62.50, 55.39, 52.80, 23.13. HRMS (ESI) m/z calculated for $\text{C}_{18}\text{H}_{17}\text{N}_5\text{O}_4\text{S}$ $[\text{M} + \text{Na}]^+$ 422.0894, found 422.0892.

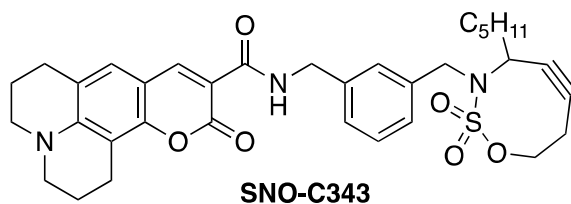
V. Preparation of bioorthogonal conjugates



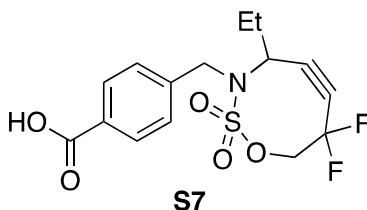
S6

Boc-protected aryl precursor to SNO-C343 (S6). A 50 mL round bottom flask equipped with a stir bar was charged with SNO-OCT **1** (148.0 mg, 0.64 mmol) dissolved in dichloromethane (9.0 mL, 0.07 M). BocBnBr (212.7 mg, 0.70 mmol) was added, followed by tetrabutylammonium bromide (20.6 mg, 0.06 mmol). A solution of 4.5 mL 1.0 M aqueous NaOH was added and the mixture stirred at room temperature for 5 h. Upon completion of the reaction as indicated by an NMR aliquot, an equal amount of water was added and the layers extracted with three portions of dichloromethane. The combined organics were dried with sodium sulfate, filtered through cotton, and concentrated under reduced pressure. The crude product was purified by silica gel chromatography using a 0 to 30% gradient of ethyl acetate in hexane with 5% increments. The product was obtained 82% yield (237.2 mg, 0.53 mmol) as a white foam. ^1H NMR (500 MHz, CDCl_3) δ 7.33 – 7.25 (d, 3H), 7.25 – 7.20 (d, $J = 7.4$ Hz, 1H), 5.01 – 4.92 (m, 1H), 4.81 – 4.71 (d, $J = 14.8$ Hz, 1H), 4.67 – 4.57 (m, 1H), 4.35 – 4.25 (t, $J = 5.4$ Hz, 2H), 4.23 – 4.17 (d, $J = 14.7$ Hz, 1H), 3.69 – 3.55 (t, $J = 7.8$ Hz, 1H), 2.87 – 2.72 (dddd, $J = 16.9, 11.4, 5.6, 2.5$ Hz, 1H), 2.36 – 2.23 (dd, $J = 17.1, 3.8$ Hz, 1H), 1.87 – 1.69 (td, $J = 8.4, 3.9$ Hz, 2H), 1.49 – 1.41 (s, 9H), 1.19 – 0.95 (m, 4H), 0.82 – 0.72 (t, $J = 7.2$ Hz, 3H). ^{13}C NMR (126 MHz, CDCl_3) δ 155.90, 139.60, 136.35, 128.92,

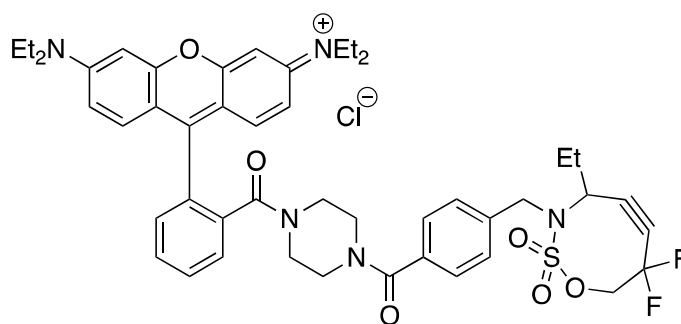
127.54, 127.22, 96.45, 93.75, 79.51, 75.96, 54.92, 54.53, 44.43, 33.82, 30.83, 28.39, 25.79, 22.35, 21.73, 13.86. HRMS (ESI) m/z calculated for $C_{23}H_{34}N_2O_5S$ $[M + NH_4]^+$ 468.2527, found 468.2522.



Compound SNO-C343. A 25 mL round bottom flask equipped with a stir bar was charged with Boc-protected aryl precursor (118.9 mg, 0.26 mmol) dissolved in dichloromethane (2.6 mL, 0.1 M). The solution was cooled to 0 °C and trifluoroacetic acid added dropwise at 0 °C. The mixture was stirred for 5 min before warming it to room temperature. After 8 h, the reaction mixture was quenched with an equal amount of saturated $NaHCO_3$. The layers were extracted with three portions of dichloromethane, filtered through cotton, and concentrated under reduced pressure. The crude product was directly carried forward into the next reaction. A 10 mL round bottom flask was charged with the crude product in dichloromethane (2.2 mL, 0.1 M). Coumarin 343 (61.7 mg, 0.22 mmol, 1.0 equiv) and 4-dimethylaminopyridine (DMAP; 8.0 mg, 0.07 mmol, 0.2 equiv) were added, followed by EDC•HCl (91.3 mg, 0.48 mmol, 2.2 equiv). The reaction mixture was stirred at room temperature for 15 h, stopped by addition of an equal volume of water and diluted with dichloromethane. The layers were extracted with three portions of dichloromethane, the combined organics were dried with sodium sulfate, filtered through cotton, and concentrated under reduced pressure. The crude product was purified by silica gel chromatography using a 40 to 80% gradient of ethylacetate in hexane with 10% increments. The product was obtained 37% yield (60.7 mg, 0.098 mmol) over two steps as a dark yellow solid. 1H NMR (500 MHz, $CDCl_3$) δ 9.25 (t, J = 6.0 Hz, 1H), 8.63 (s, 1H), 7.41 – 7.28 (m, 4H), 7.01 (s, 1H), 4.97 (td, J = 11.2, 4.0 Hz, 1H), 4.76 (d, J = 14.7 Hz, 1H), 4.71 – 4.57 (m, 3H), 4.22 (d, J = 14.8 Hz, 1H), 3.65 (t, J = 8.2 Hz, 1H), 3.33 (q, J = 5.7 Hz, 4H), 2.93 – 2.71 (m, 5H), 2.29 (dd, J = 17.0, 3.9 Hz, 1H), 1.97 (h, J = 6.3, 5.5 Hz, 4H), 1.80 (dh, J = 20.4, 7.7, 7.3 Hz, 2H), 1.20 – 0.94 (m, 6H), 0.76 (t, J = 7.2 Hz, 3H). HRMS (ESI) m/z calculated for $C_{34}H_{39}N_3O_6S$ $[M + H]^+$ 618.2632, found 618.2639.



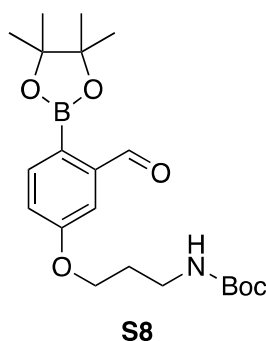
Benzoic acid precursor to SNO-DF-Rho (S7). A 10 mL round bottom flask equipped with a stir bar was charged with SNO-OCT 5 (128.5 mg, 0.57 mmol) dissolved in 2.2 mL dimethylformamide. The solution was cooled to 0 °C, followed by the addition of NaH 60% in mineral oil (43.3 mg, 1.08 mmol). The mixture was stirred at 0 °C for 5 min, removed from the ice bath and a solution of 4-(bromomethyl)benzoic acid (97.7 mg, 0.45 mmol) in 2.2 mL dimethylformamide (DMF) was added dropwise over 10 min. Solid formation was observed during the course of the addition. The reaction mixture was stirred at room temperature for 3 h. Upon the full consumption of the 4-(bromomethyl)benzoic acid, the reaction mixture was cooled to 0 °C, and 4 mL 1.0 M HCl was added dropwise at 0 °C under an inert atmosphere. The crude mixture was quickly transferred to a separatory funnel and diluted with ethyl acetate. The mixture was extracted with three portions of ethyl acetate and the combined organics dried with sodium sulfate, filtered through cotton, and concentrated under reduced pressure. The crude product was purified by silica gel chromatography using a 0 to 30% gradient of ethyl acetate in hexane with 10% increments containing a consistent 1% acetic acid. After two rounds of purification, the product was obtained in 40% yield (64.7mg, 0.18 mmol) as a white solid. ¹H NMR (400 MHz, CDCl₃) δ 8.24 – 8.06 (d, *J* = 8.2 Hz, 2H), 7.61 – 7.45 (d, *J* = 8.0 Hz, 2H), 5.11 – 4.97 (dd, *J* = 26.4, 12.4 Hz, 1H), 4.95 – 4.83 (d, *J* = 15.3 Hz, 1H), 4.73 – 4.60 (dd, *J* = 12.4, 8.6 Hz, 1H), 4.48 – 4.34 (d, *J* = 15.3 Hz, 1H), 3.80 – 3.61 (s, 1H), 2.02 – 1.90 (dt, *J* = 15.0, 7.7 Hz, 1H), 1.90 – 1.78 (dt, *J* = 14.0, 7.3 Hz, 1H). ¹³C NMR (126 MHz, CDCl₃) δ 170.89, 140.92, 130.82, 129.52, 128.64, 112.50 (t, *J* = 241.3 Hz), 111.06 (t, *J* = 10.9 Hz), 85.79 (t, *J* = 43.4 Hz), 78.77 (m), 56.03, 54.81, 26.19, 10.66. ¹⁹F NMR (376 MHz, CDCl₃) δ -94.47 (d, *J* = 277.0 Hz), -103.11 (d, *J* = 276.9 Hz). HRMS (ESI) *m/z* calculated for C₁₅H₁₅F₂NO₅S [M – H][–] 358.0566, found 358.0569.



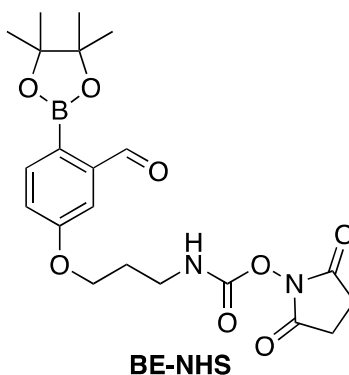
SNO-DF-Rho

Compound SNO-DF-Rho. The following reaction work-up was adopted from a previously reported procedure.⁶ A 25 ml round bottom flask was charged with ArCOOH-DF-SNO-OCT (5.2 mg, 0.0145 mmol) and dissolved in 4.0 mL dichloromethane. Rhodamine-piperazine (13.2 mg, 0.0258 mmol) and 4-dimethylaminopyridine (0.8 mg, 0.0065 mmol) were added, followed by EDC•HCl (15.3 mg, 0.0798

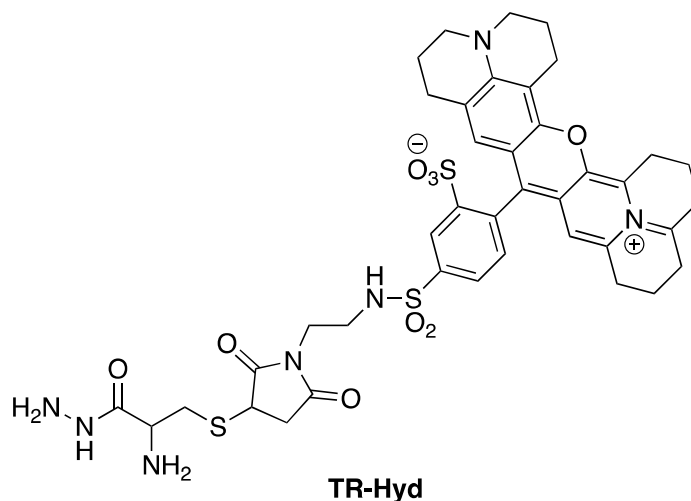
mmol). The reaction mixture was stirred at room temperature overnight and quenched by the addition of saturated NaHCO_3 . The aqueous phase was saturated with NaCl and extracted with three portions of dichloromethane. The combined organic layers were dried with sodium sulfate, filtered through cotton, and concentrated under reduced pressure. The crude product was purified by silica gel chromatography using a 0 to 10% gradient of MeOH in dichloromethane with 5% increments containing a consistent 1% NH_4OH . After two rounds of purification, the product was obtained 60 % yield (7.7 mg, 0.0087 mmol) as a purple solid. ^1H NMR (400 MHz, CDCl_3) δ 7.75 – 7.31 (m, 10H), 7.27 – 7.15 (m, 2H), 6.91 – 6.74 (m, 2H), 5.02 (ddd, J = 23.7, 12.5, 3.1 Hz, 1H), 4.79 (d, J = 15.2 Hz, 1H), 4.61 (dd, J = 11.4, 7.4 Hz, 1H), 4.41 (d, J = 15.2 Hz, 1H), 3.85 – 3.77 (m, 1H), 3.76 – 3.63 (q, J = 7.2 Hz, 8H), 3.62 – 3.41 (m, 8H), 1.95 (dq, J = 15.4, 7.5 Hz, 1H), 1.84 (dq, J = 13.8, 7.3 Hz, 1H), 1.35 (t, J = 7.1 Hz, 13H), 0.77 (t, J = 7.4 Hz, 3H). ^{13}C NMR (126 MHz, CDCl_3) δ 170.21, 167.72, 159.10, 157.74, 155.70, 137.09, 134.97, 134.97, 132.05 (broad singlet), 130.44 (broad singlet), 130.34, 130.20, 128.96, 128.89, 128.67, 128.44, 128.11 (broad singlet), 127.87, 127.63, 113.80, 112.58 (t, J = 239.6 Hz, 1C), 96.31(m, 1C), 78.65 (dd, J = 46.3, 34.5 Hz, 1C), 55.88, 54.94, 46.24, 26.20, 12.72, 10.67. ^{19}F NMR (376 MHz, CDCl_3) δ -94.16 (d, J = 275.8 Hz), -103.08 (d, J = 275.8 Hz). HRMS (ESI) m/z calculated for $\text{C}_{47}\text{H}_{52}\text{F}_2\text{N}_5\text{O}_6\text{S}^+ [\text{M}]^+$ 852.3601, found 852.3602.



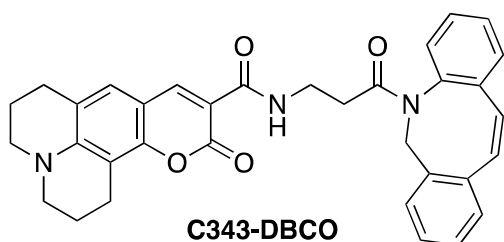
Compound S8. This compound was prepared based on a previously published procedure.⁷



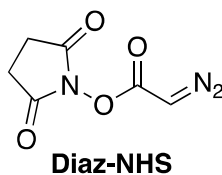
Compound BE-NHS (Boronic ester-NHS). The following reactions were based on previously published procedures.^{7,8} In a glass vial equipped with a stir bar, Compound **S6** (118.1 mg, 0.29 mmol) was dissolved in dichloromethane (3.0 mL). The solution homogeneous solution was cooled to 0 °C and trifluoroacetic acid (0.4 mL, 5.80 mmol) was added dropwise. The mixture was stirred at 0 °C under a nitrogen atmosphere for 30 min. All volatiles were removed under reduced pressure to give a viscous yellow oil. The crude material was carried forward without any purification. In a vial equipped with a stir bar, the crude material was diluted with DMF (0.64 mL). The mixture was cooled to 0 °C in an ice bath and followed by the dropwise addition of disuccinimidyl carbonate (DSC; 148.6 mg, 0.58 mmol) in DMF (0.58 mL). Diisopropylethylamine (DIPEA; 0.1 mL, 0.58 mmol) was then added at 0 °C. The mixture was warmed to room temperature and stirred under a nitrogen atmosphere for 20 h. The mixture was diluted with 50 mL ethyl acetate and washed with 50 mL of 1M HCl. The organic phase was then washed with 3 x 50 mL of water. The combined organics were dried with Na₂SO₄, filtered through cotton, and concentrated under reduced pressure. A brown viscous oil (152.7 mg) was obtained without further purification. Due to the presence of DMF as the only impurity, we determined a nearly quantitative yield based on ¹H-NMR integration between the desired product and DMF (ratio = 1 : 0.8; DMF = 0.24 mmol; Product = 0.30 mmol). ¹H NMR (400 MHz, CDCl₃) δ 10.64 (s, 1H), 7.86 (d, *J* = 8.2 Hz, 1H), 7.47 (d, *J* = 2.6 Hz, 1H), 7.13 (dd, *J* = 8.2, 2.6 Hz, 1H), 6.03 (s, 1H), 4.13 (t, *J* = 6.0 Hz, 2H), 3.49 (td, *J* = 6.7, 6.0 Hz, 2H), 2.81 (s, 4H), 2.09 (m, 3H), 1.37 (s, 12H). ¹³C NMR (101 MHz, CDCl₃) δ 195.03, 170.18, 160.98, 151.63, 143.53, 138.08, 120.36, 111.23, 84.32, 65.75, 39.58, 37.46, 25.55, 24.95. ¹¹B NMR (128 MHz, CDCl₃) δ 30.97. HRMS (ESI) *m/z* calculated for C₂₁H₂₇BN₂O₈ [M + Na]⁺ 469.1753, found 469.1757. (Note: ¹³C signal of the ¹³C_{Aryl}-B at 124.53 ppm was missing from the ¹³C- NMR spectra, due to the quadrupolar effect of ¹¹B, thus the shift of ¹³C_{Aryl}-B was determined by HSQC and HMBC correlations; see NMR spectra section for more details).



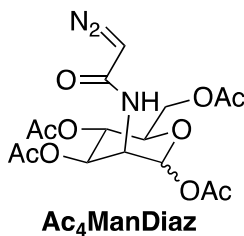
Compound TR-Hyd. This compound was prepared from a series of previously published procedures.⁷



Compound C343-DBCO. In a dried vial equipped with a stir bar, dibenzocyclooctyne-amine (DBCO; 10.0 mg, 0.036 mmol) and coumarin 343 (13.0 mg, 0.045 mmol) were dissolved in dichloromethane. EDC•HCl (9.3 mg, 0.049 mmol) was added to the mixture, followed by DMAP (0.6 mg, 0.005 mmol). The reaction was stirred at room temperature overnight, diluted with dichloromethane, then washed with brine. The organics were then dried over Na₂SO₄, filtered through cotton, and concentrated under reduced pressure. The crude product was purified by silica gel chromatography using a 0 to 100% gradient of ethyl acetate in hexane with 20% increments. The product was obtained 98% yield (19.2 mg, 0.035 mmol) as a brown solid. ¹H NMR (500 MHz, CDCl₃) δ 8.86 (t, *J* = 6.1 Hz, 1H), 8.50 (s, 1H), 7.71 (d, *J* = 7.5 Hz, 1H), 7.39 – 7.31 (m, 5H), 7.29 (dd, *J* = 7.5, 1.3 Hz, 1H), 7.19 (dd, *J* = 7.5, 1.4 Hz, 1H), 6.97 (s, 1H), 5.18 (d, *J* = 13.8 Hz, 1H), 3.64 (d, *J* = 13.8 Hz, 1H), 3.53 (qd, *J* = 6.7, 3.5 Hz, 2H), 3.32 (q, *J* = 5.4 Hz, 4H), 2.87 (t, *J* = 6.5 Hz, 2H), 2.76 (t, *J* = 6.3 Hz, 2H), 2.62 (dt, *J* = 16.2, 7.1 Hz, 1H), 2.11 (dt, *J* = 16.2, 6.4 Hz, 1H), 1.97 (h, *J* = 6.0 Hz, 4H). ¹³C NMR (126 MHz, CDCl₃) δ 171.52, 163.44, 162.63, 152.62, 151.40, 148.01, 147.99, 147.79, 132.27, 129.12, 128.47, 128.27, 128.03, 127.67, 127.05, 126.92, 125.46, 123.11, 122.58, 119.47, 115.00, 109.22, 108.18, 107.73, 105.67, 55.30, 50.20, 49.79, 35.77, 34.74, 27.45, 21.16, 20.23, 20.12. HRMS (ESI) *m/z* calculated for C₃₄H₂₉N₃O₄ [*M* + *H*]⁺ 544.2231, found 544.2231.



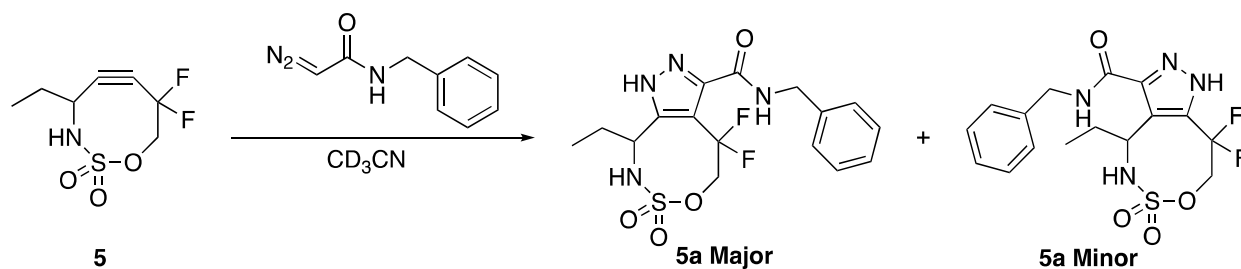
Compound Diaz-NHS. The compound was prepared from a series of previously published procedures.⁹



Compound Ac₄ManDiaz. The compound was prepared from previously published procedures.¹⁰

VI. NMR kinetics for SNO-OCT/dipole cyclization

General procedure for NMR kinetics. We employed previous published procedures for studying the NMR kinetics of SNO-OCT analogues.⁵



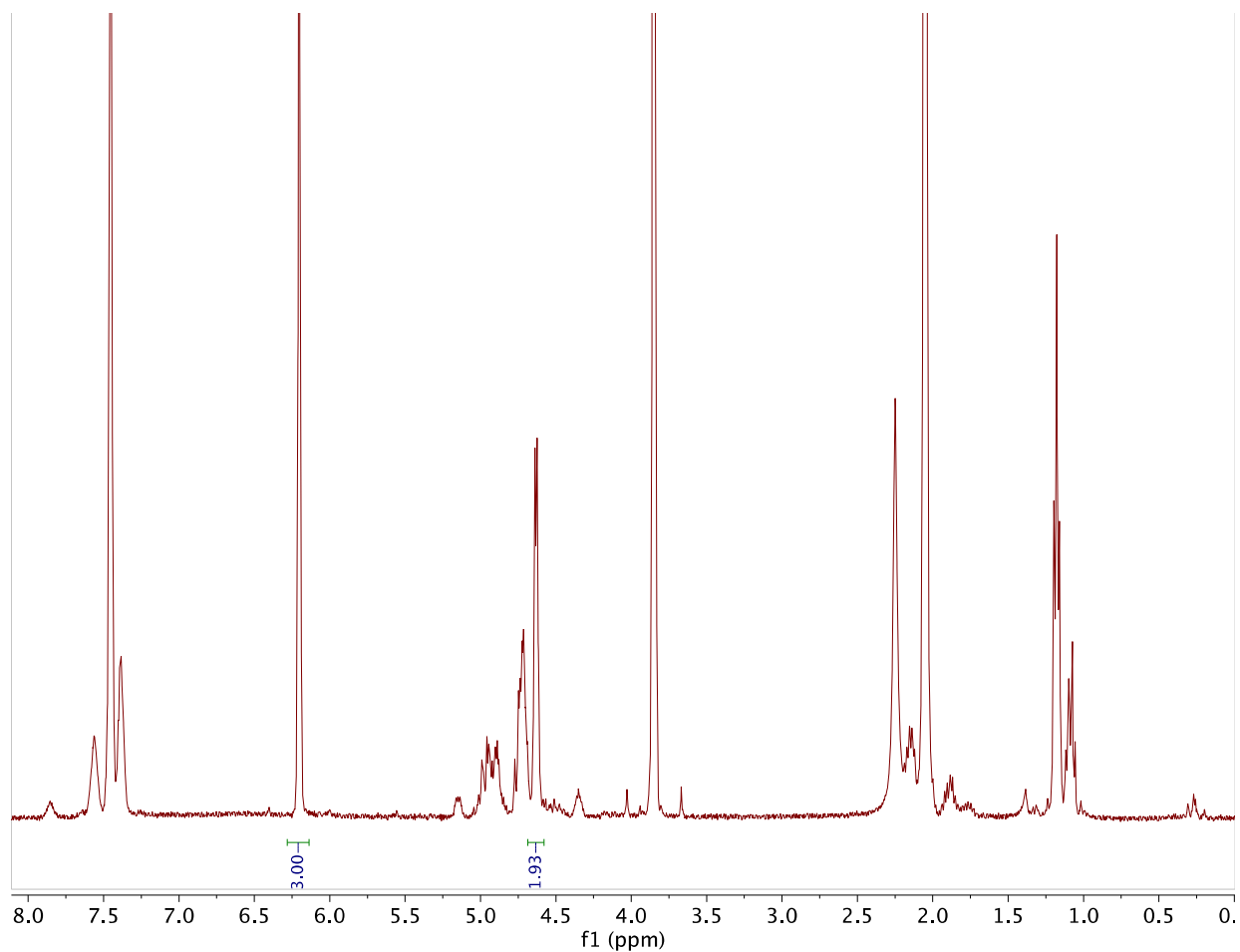


Figure S2-7. Reaction of **5** and benzyl diazoacetamide after 1 min and 45 s at 24 °C gave ~93% conversion.

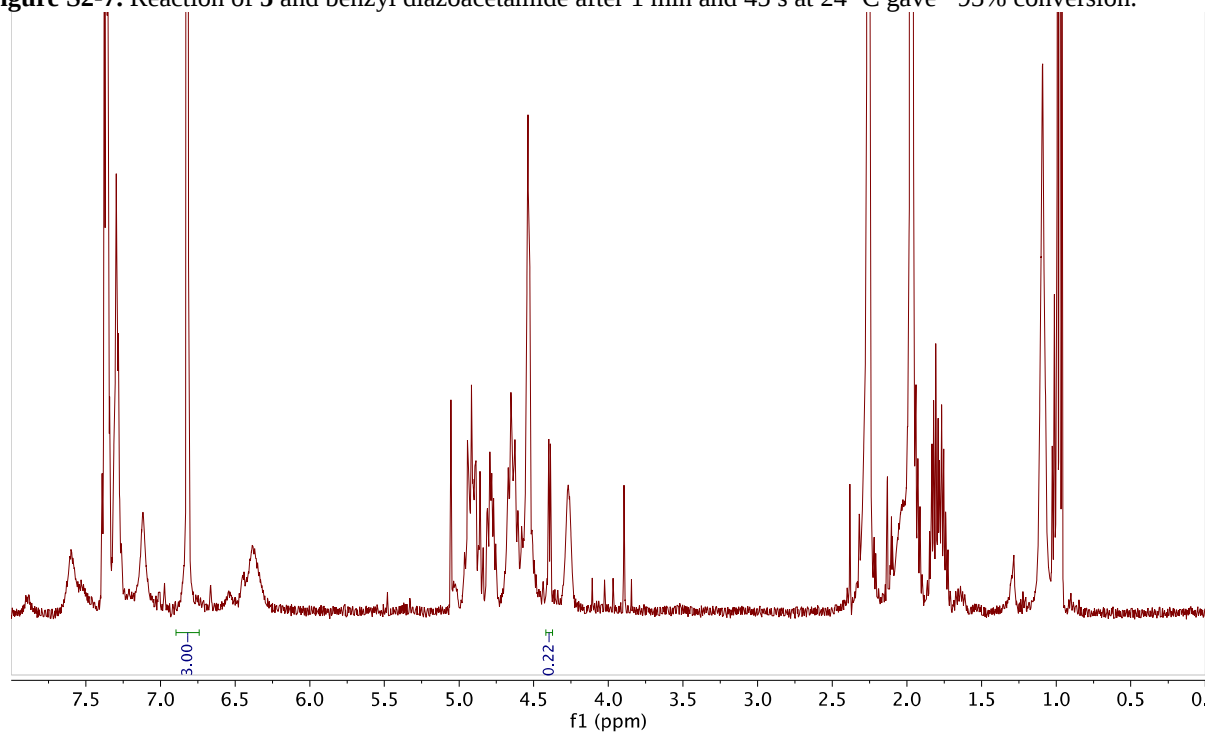


Figure S2-8. Reaction of **5** and benzyl diazoacetamide after 2 min and 15 s at 0 °C gave ~89% conversion.

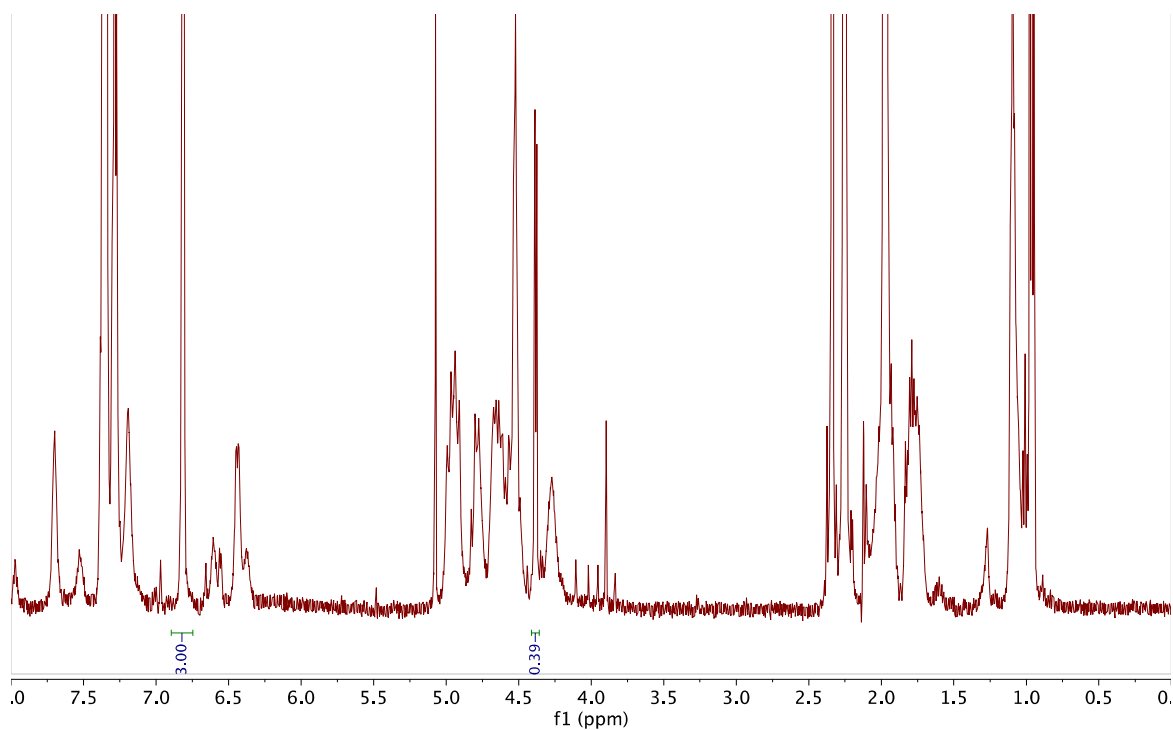


Figure S2-9. Reaction of **5** and benzyl diazoacetamide after 2 min and 13 s at -25 °C gave ~81% conversion.

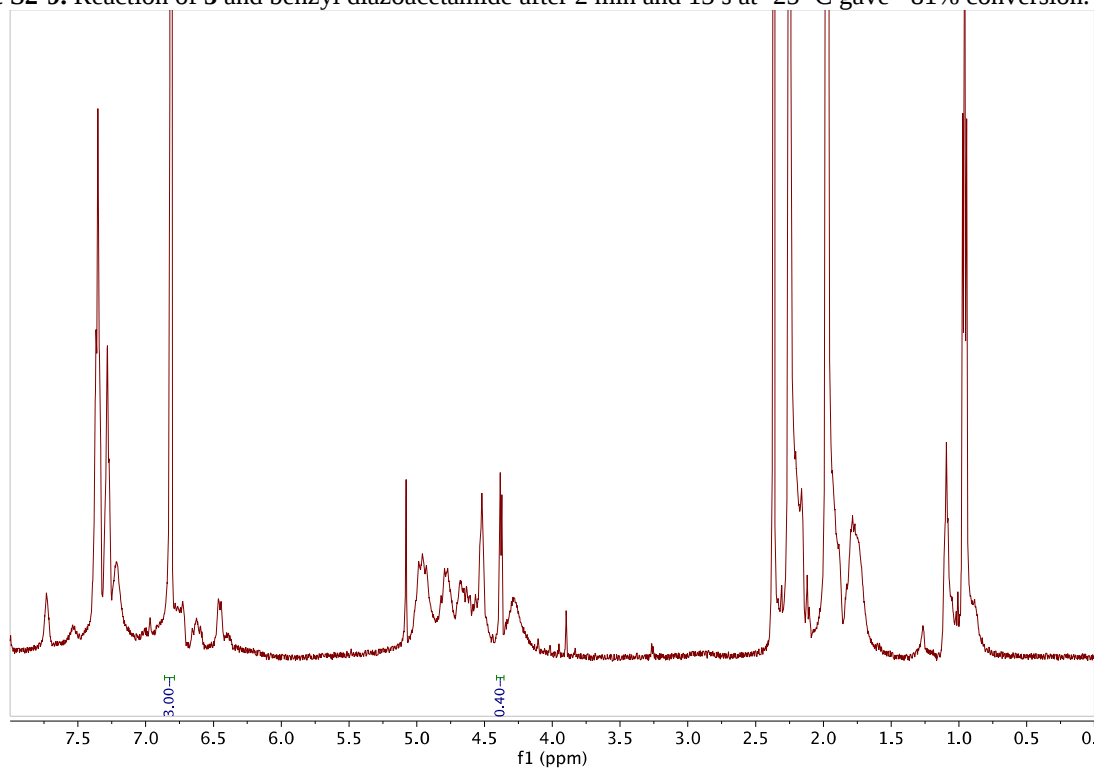
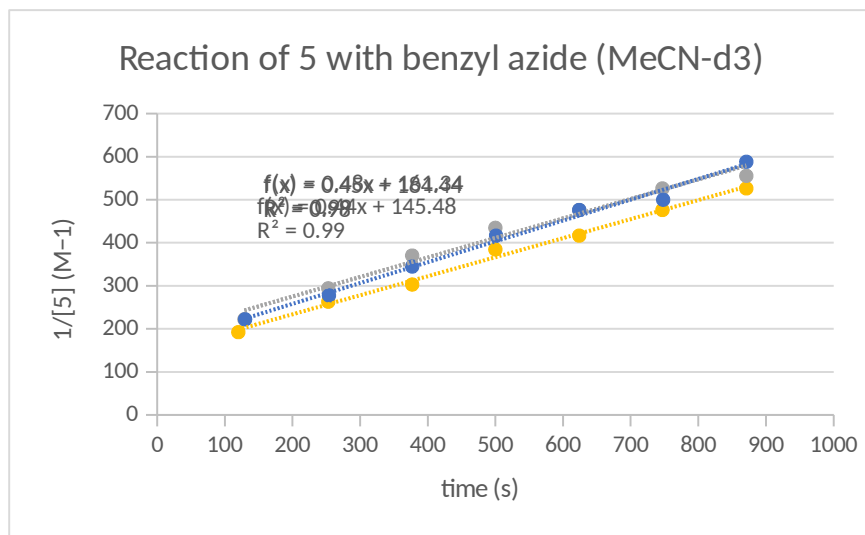
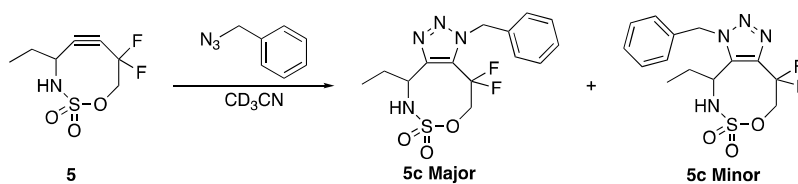
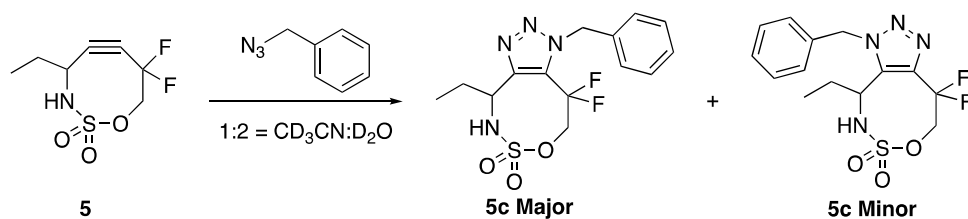


Figure S2-10. Reaction of **5** and benzyl diazoacetamide after 2 min and 4 s at -32 °C gave ~80% conversion.



$$k_2 = 0.459 \pm 0.02 \text{ M}^{-1}\text{s}^{-1}$$



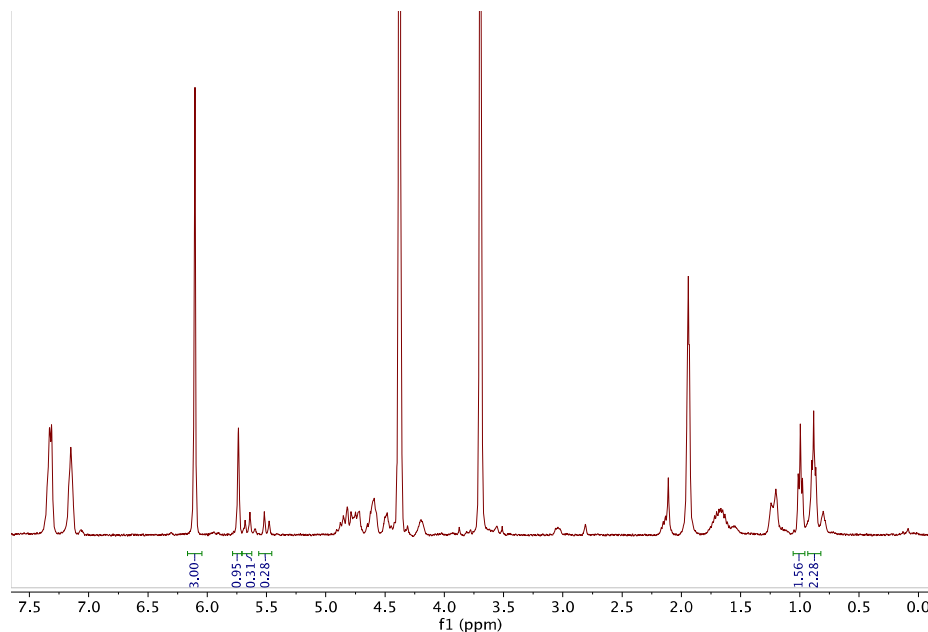
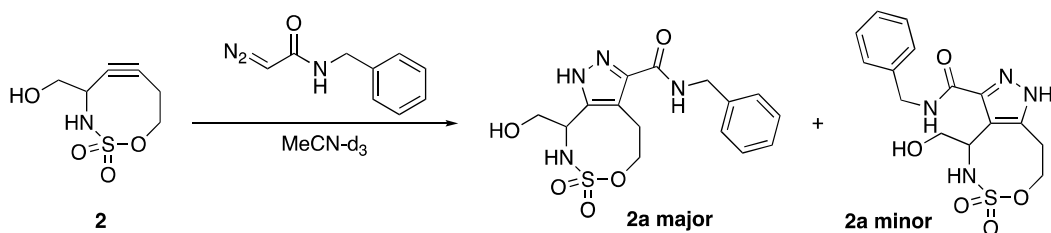
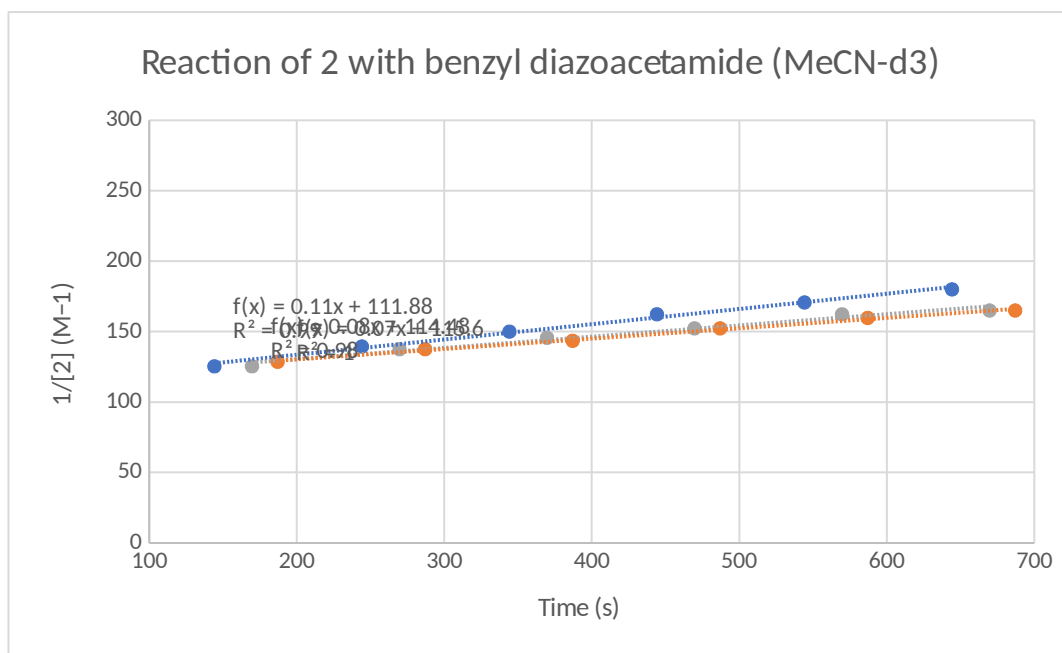


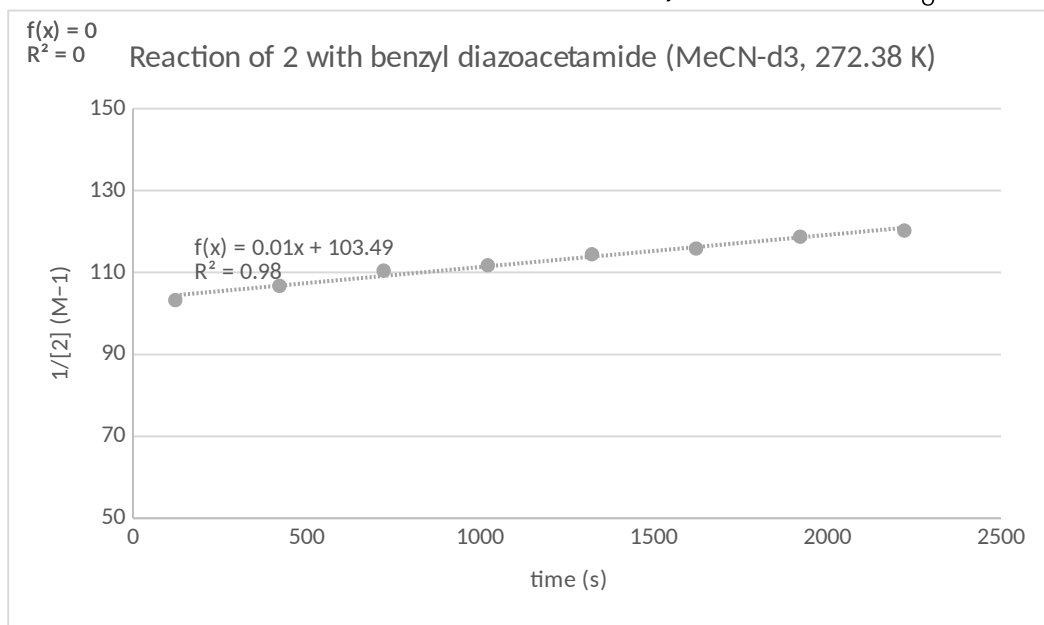
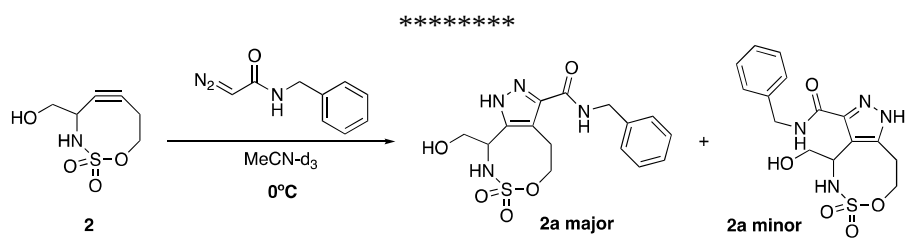
Figure S2-11. Reaction of **5** and benzyl azide in $\text{CD}_3\text{CN} : \text{D}_2\text{O}$ (1 : 2 ratio) for 1 min and 37 s gave ~77% conversion. Kinetics were too fast to measure by NMR at 23°C in this more aqueous environment. The rate increase is likely due to the stabilization effect of a more polar transition state previously observed in other cycloaddition reactions.¹¹

Note: VT-NMR kinetics on the OH-SNO-OCT **2** were performed using the same method as **5** + benzyl diazoacetamide. This information was not described in the manuscript, but is included for completeness.





$$k_2 = 0.087 \pm 0.011 \text{ M}^{-1}\text{s}^{-1}$$

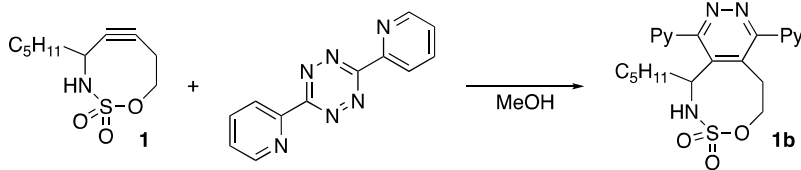


$$k_2 = 0.0081 \pm 0.0002 \text{ M}^{-1}\text{s}^{-1}$$

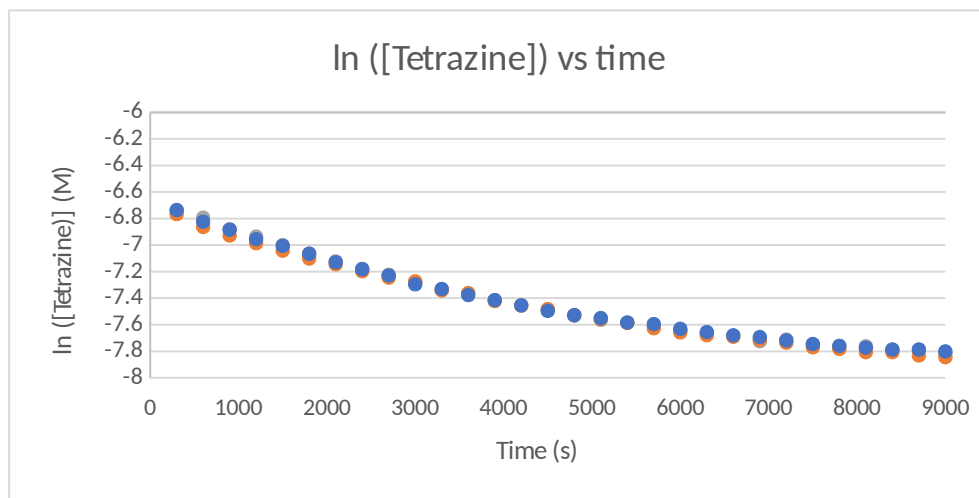
VII. Plate reader kinetics for SNO-OCT/tetrazine cyclization

General procedure. Individual stock solutions of SNO-OCT (0.02 M) and 3,6-di-2-pyridyl-1,2,4,5-tetrazine (0.002 M) in methanol were prepared. The kinetics between SNO-OCTs and tetrazine was monitored using a Perkin-Elmer Envision plate reader in clear flat-bottomed 96-well plates. A 100 μ L aliquot of the tetrazine solution was first added to a well and the initial absorption was measured (A_{int}). After the addition of SNO-OCT solution to the tetrazine-containing well, the decrease of tetrazine absorbance was measured at 531 nm over a period of 9,000 s at intervals of 300 s. All experiments were performed in triplicate. The second-order kinetic rate (k_2) was derived from the equations below:

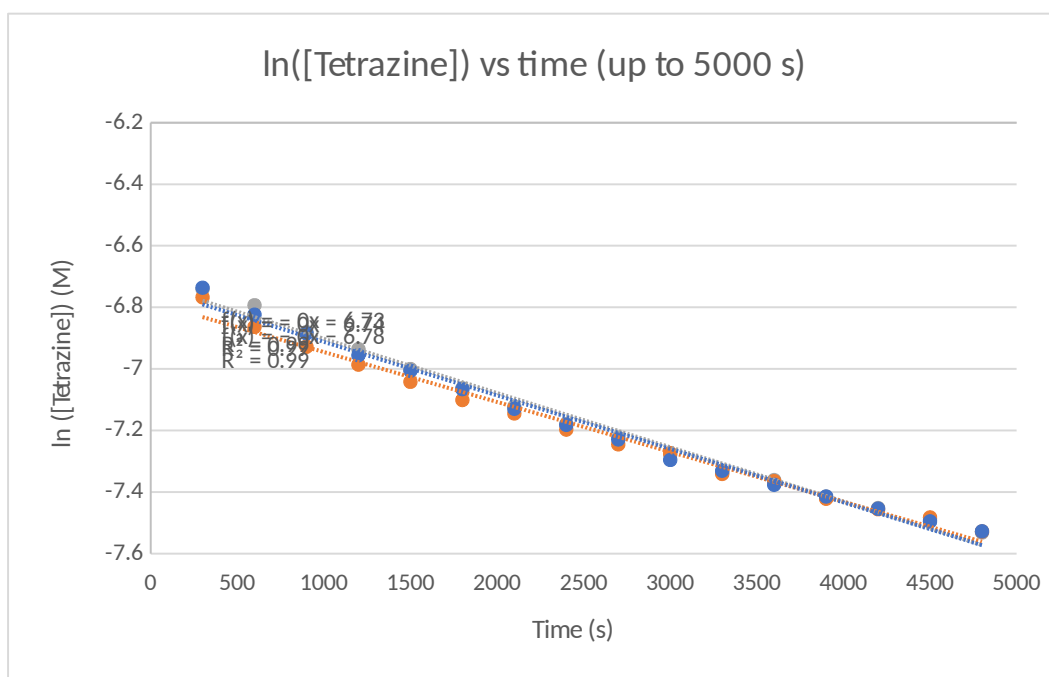
$$\begin{array}{ll}
 (1) & \epsilon \cdot l = A_{\text{int}} / 0.002 \text{ M} \\
 (2) & \ln[\text{tetrazine}] = \ln(A_{1-300} / (\epsilon \cdot l \times 2)) \\
 (3) & k_{\text{obs}} = \text{slope of } \ln[\text{tetrazine}] \text{ vs time} \\
 (4) & k_2 = k_{\text{obs}} / 0.01 \text{ M}
 \end{array}$$



Well No.	Abs 1	Abs 2	Abs 3	Average
A int	0.171	0.199	0.181	0.184
ϵ l	85.5	99.5	90.5	91.83

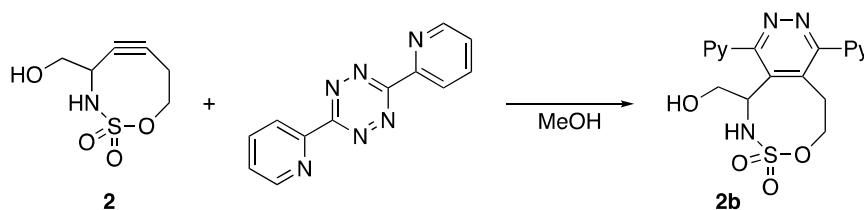


Note: Due to the change of the slope pass 5000 s, data points before 5000 s were used to achieve more accurate initial kinetic values. A version of data points up to 5000 s is below.

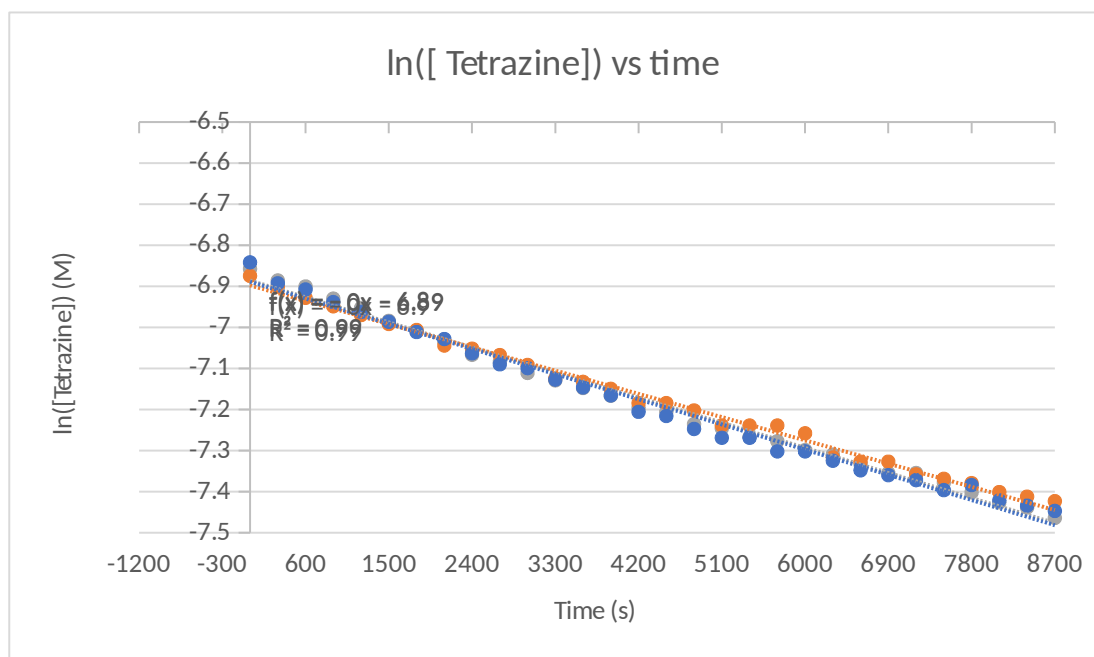


Well No.	Abs 1	Abs 2	Abs 3	Average
k_{obs}	1.7621E-04	1.6219E-04	1.7387E-04	1.7076E-04
k_2	1.7621E-02	1.6219E-02	1.7387E-02	1.7076E-02

$$k_2 = 0.0171 \pm 0.0004 \text{ M}^{-1}\text{s}^{-1}$$



Well No.	Abs 1	Abs 2	Abs 3	Average
A_{int}	0.132	0.149	0.136	0.139
$\epsilon \cdot l$	66.0	74.5	68.0	69.5



Well No.	Abs 1	Abs 2	Abs 3	Average
k_{obs}	6.8066E-05	6.2859E-05	6.7843E-05	6.6256E-05
k_2	6.8066E-03	6.2859E-03	6.7843E-03	6.6256E-03

$$k_2 = 0.0066 \pm 0.0002 \text{ M}^{-1}\text{s}^{-1}$$

VIII. Reactions of one SNO-OCT with two competing dipoles

General procedure. This procedure was adopted from a previously published SNO-OCT competition experiment.¹¹ Stock solutions (0.02 M in acetonitrile-*d*₃) of the SNO-OCTs and the dipoles were prepared. One equivalent of each of the two SNO-OCTs were combined in a vial equipped with a stir bar, followed by the addition of one equivalent of the dipole solution. The reaction was stirred at room temperature for 1 h to ensure full conversion. All volatiles were removed under reduced pressure and the selectivity was determined based on NMR integrations of the product peaks.

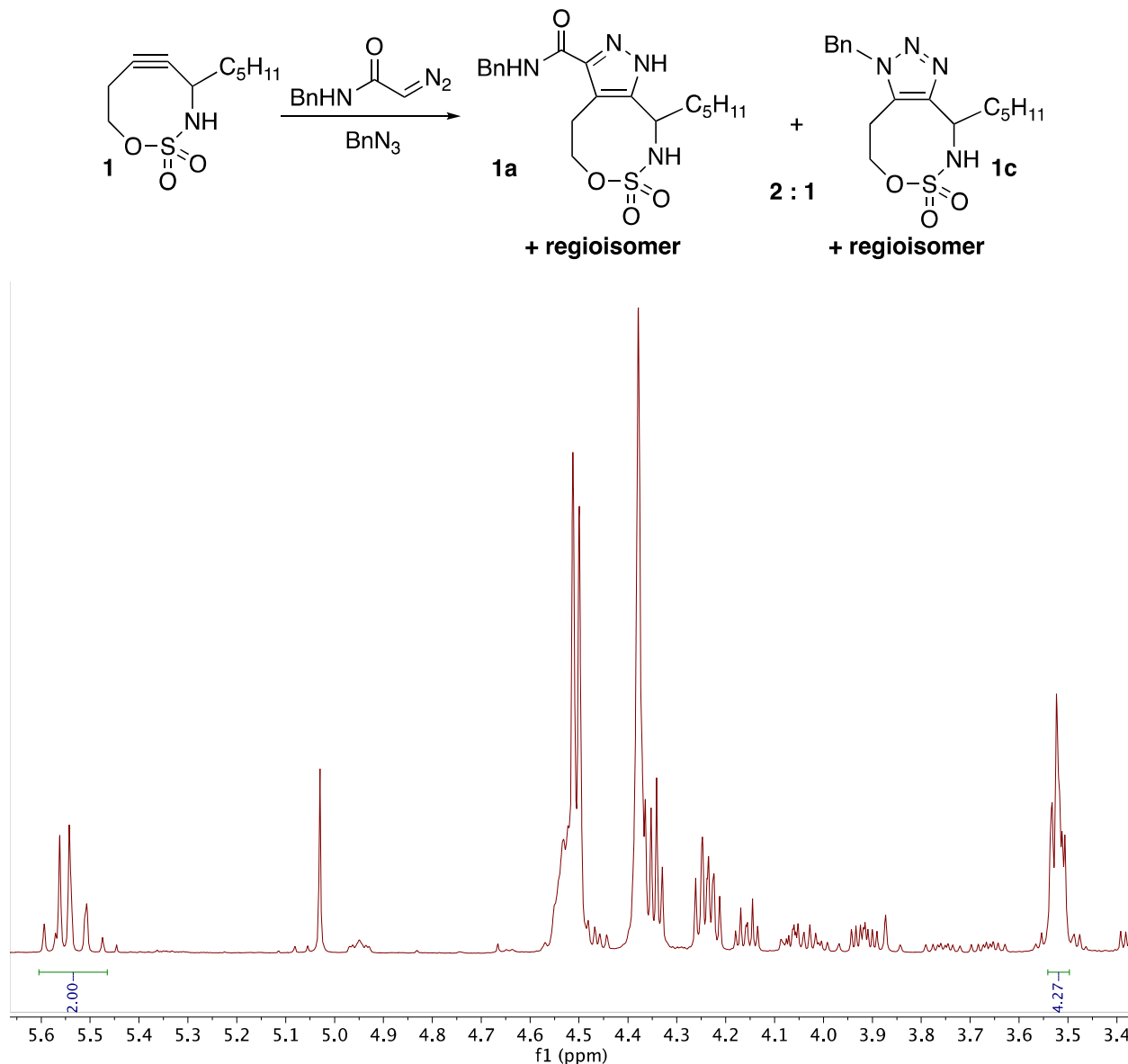


Figure S2-12. Competition between benzyl diazoacetamide and benzyl azide for **1**. Ratio of cycloaddition products was calculated based on the product formation ratio between **1** and diazoacetamide. Calculations indicate 4.27 equiv of **1a** vs. 2.00 equiv of **1c** to give a ratio of 2 : 1.

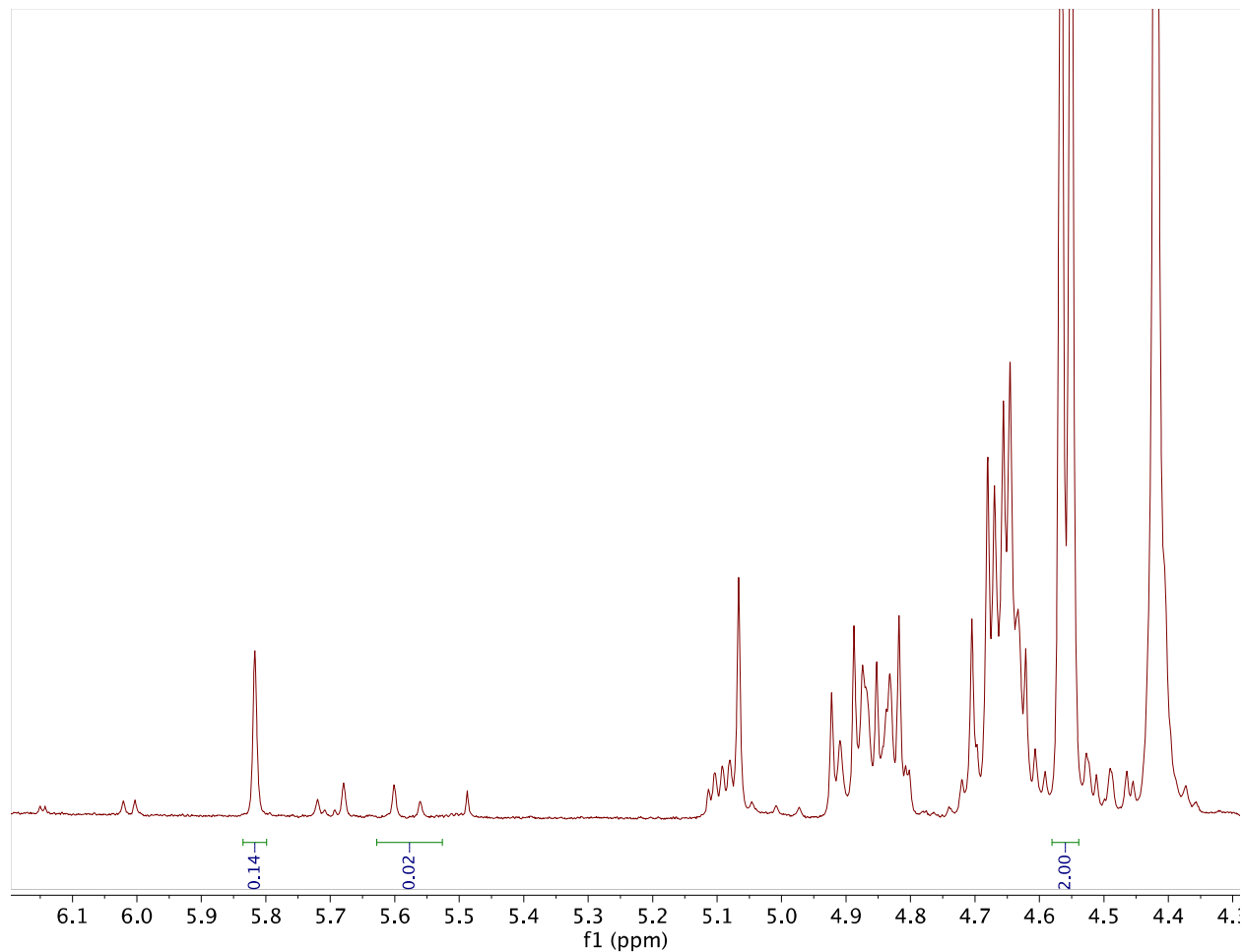
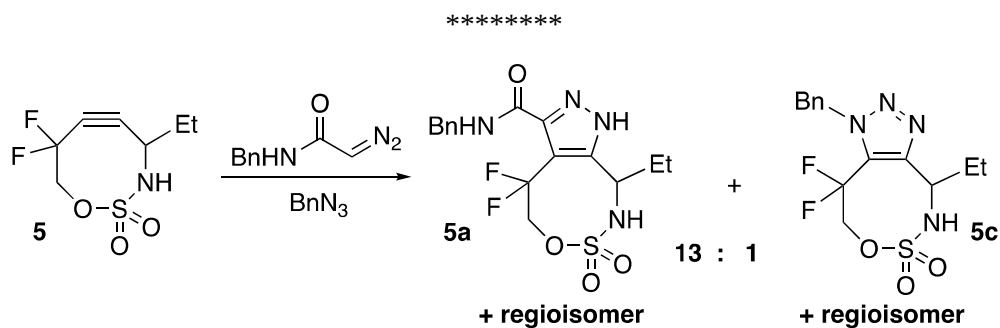


Figure S2-13. Competition between benzyl diazoacetamide and benzyl azide for **5**. Ratio of cycloaddition products calculated from the product formation ratio between **5** and diazoacetamide. Calculations indicate 1.16 equiv of **5a** vs. 0.09 equiv of **5c**, resulting in a 13 : 1 ratio.

IX. Reactions of two SNO-OCTs for one dipole

General procedure. This procedure was adopted from a previously published SNO-OCT competition study.¹² Stock solutions (0.02 M in acetonitrile-*d*₃) of the SNO-OCTs and the dipoles were prepared. One equivalent of the dipole solution was added to a vial equipped with a stir bar, followed by the addition of one equivalent of each of the SNO-OCT solutions. The reaction was stirred at room temperature for 1 h to ensure full conversion. All volatiles were removed under reduced pressure and the selectivity determined based on NMR integrations of the product peaks.

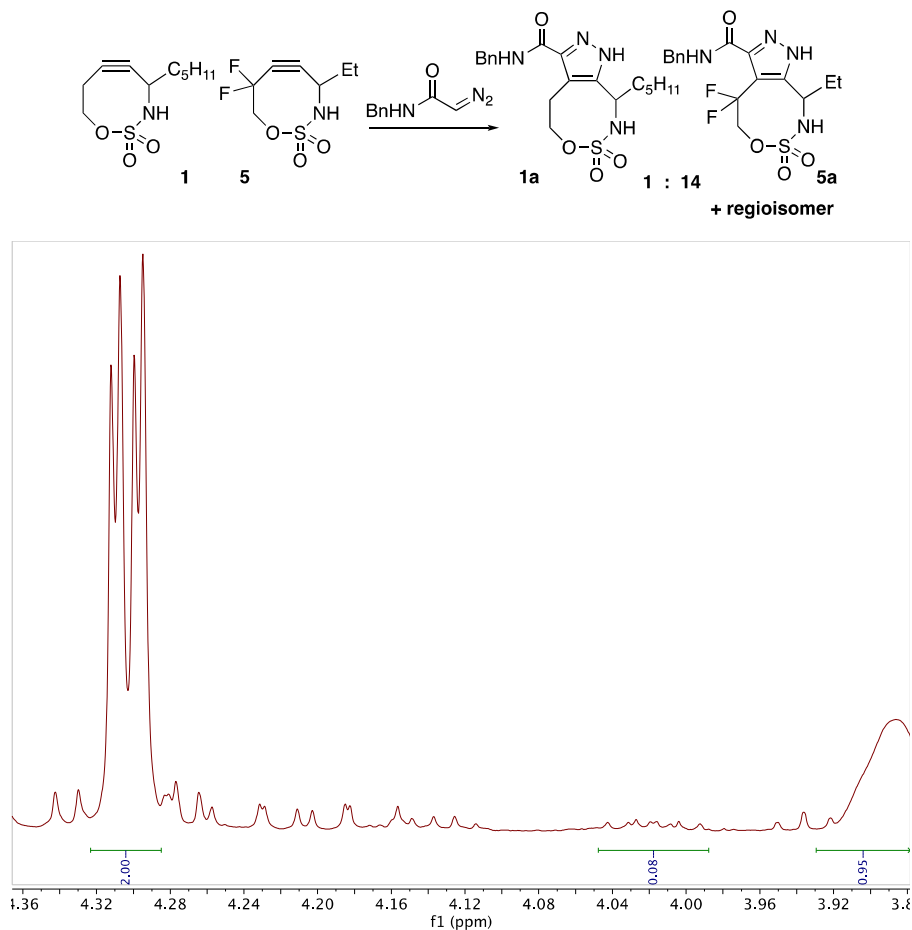


Figure S2-14. Competition between **1** and **5** for benzyl diazoacetamide. The amount of cycloaddition product was calculated based on integration of **1a** major's 2Hs at the benzylic position. Calculations indicate 1.16 equiv of **5a** vs. 0.08 equiv of **1a** to give a ratio of 14 : 1.

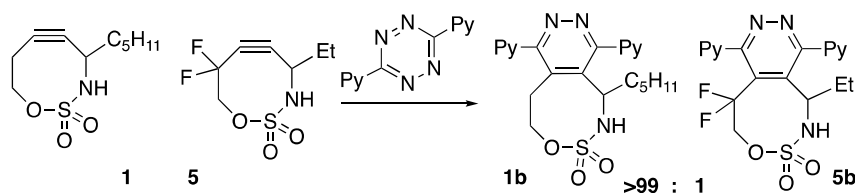


Figure S2-15. Competition between **1** and **5** for dipyrityl tetrazine showed only product resulting from the reaction of **1** and dipyrityl tetrazine **1b**. The NMR spectra match previously reported values.¹²

X. Reactions of two SNO-OCTs competing for two dipoles

General procedure. This procedure was adopted from a previously published SNO-OCT competition study.¹² Stock solutions (0.1 M in methanol) of the SNO-OCTs and the dipoles were prepared. One equivalent of each of the dipole solutions were combined in a vial equipped with a stir bar, followed by the addition of one equivalent of each of the SNO-OCT solutions. The reaction was stirred at room temperature for 1 h to ensure full conversion. All volatiles were removed under reduced pressure and the orthogonality analyzed using either an NMR or UPLC/LC-SM calibration curve.

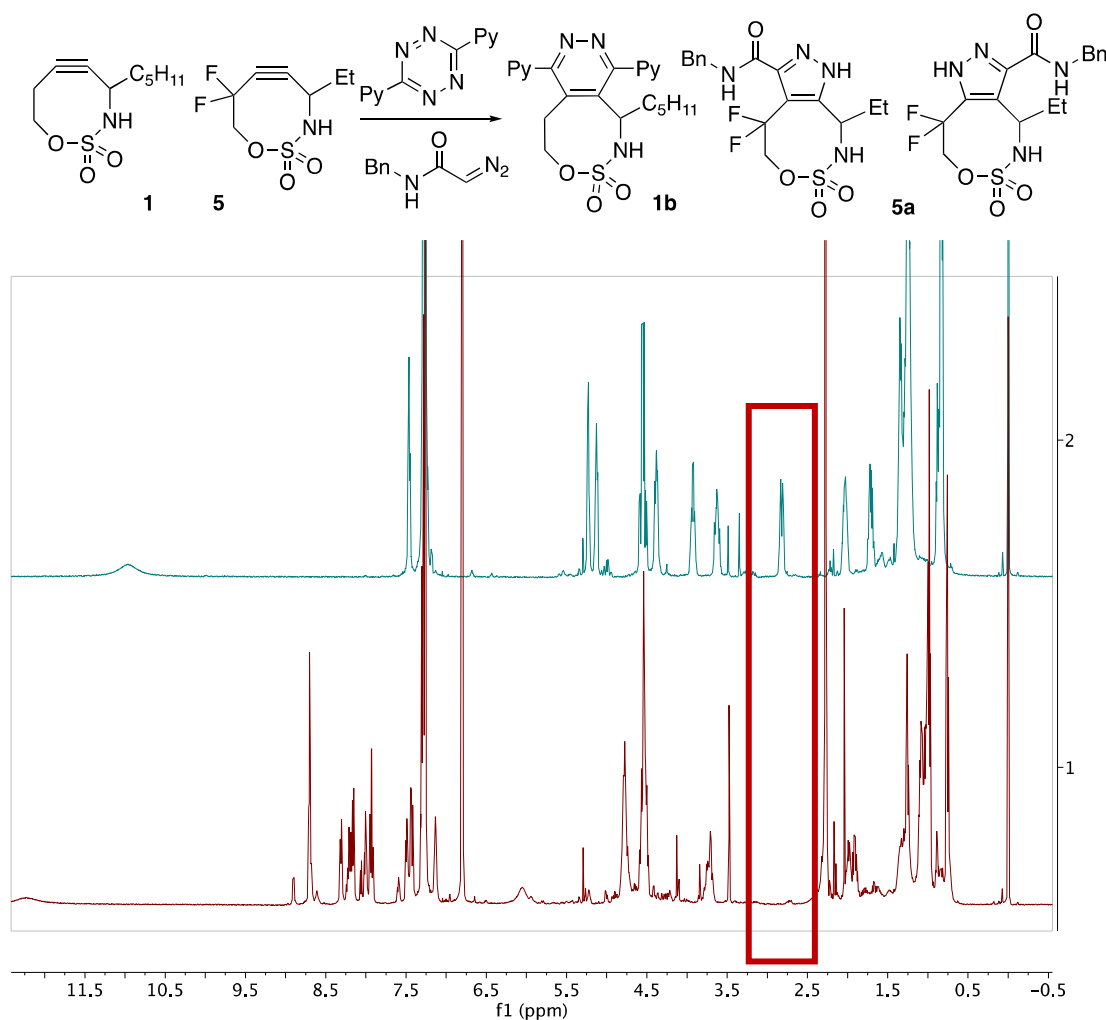
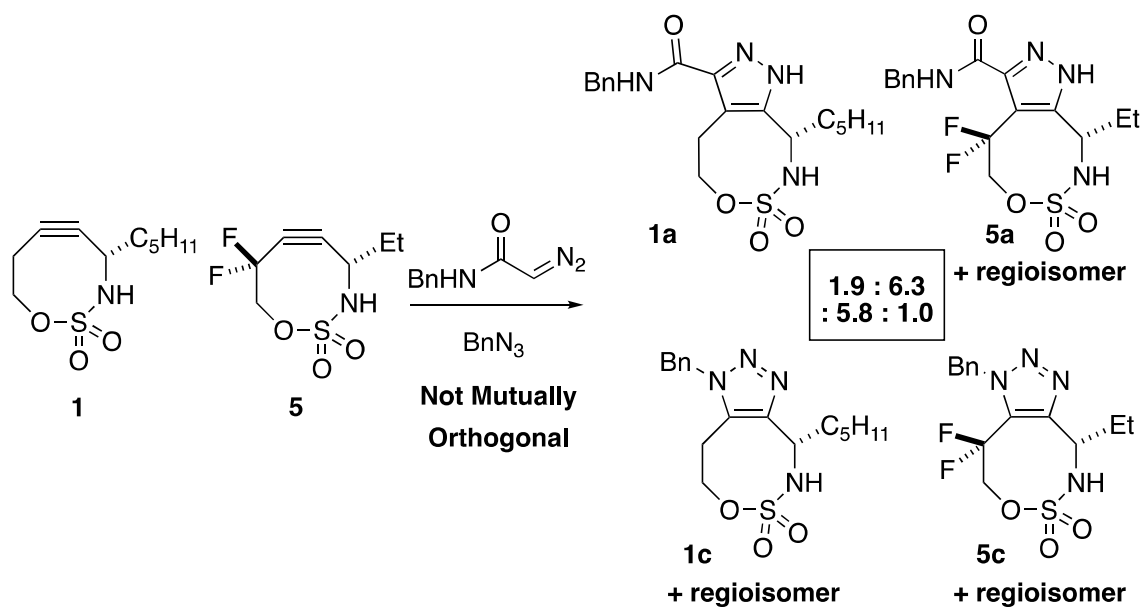
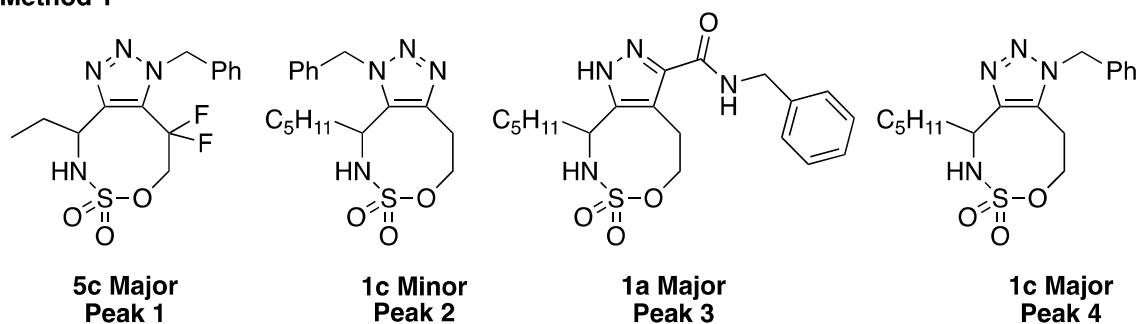


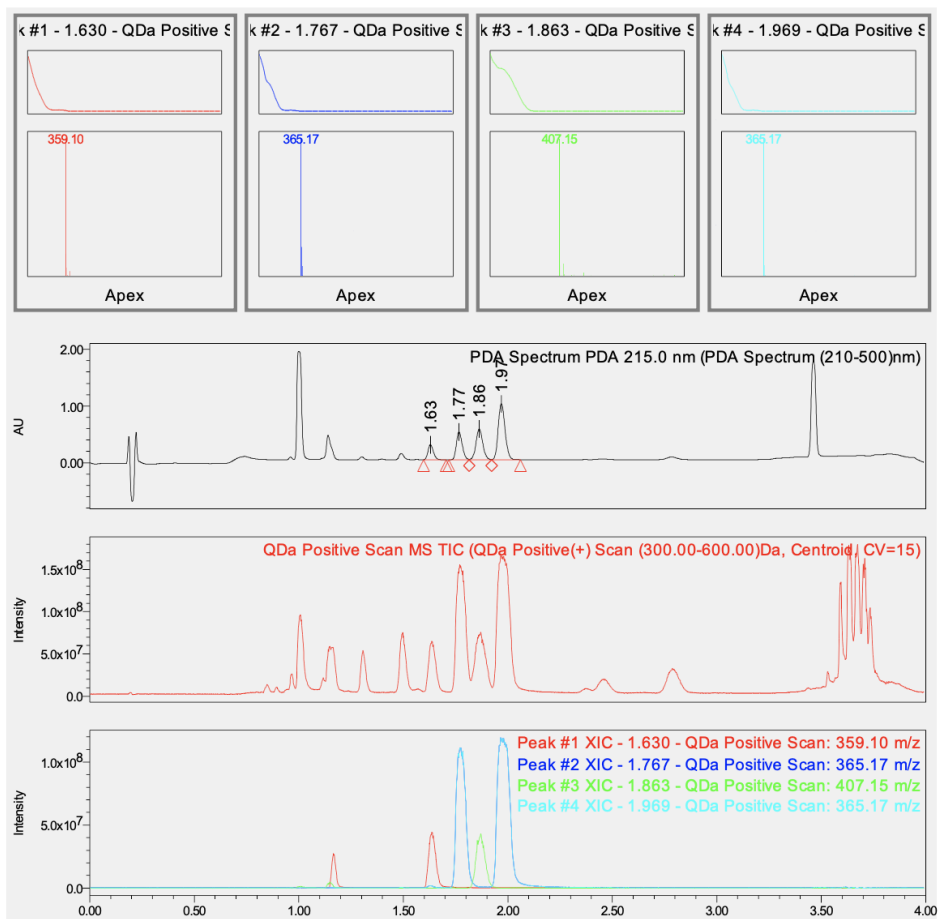
Figure S2-16A. Competition between **1** and **5** for dipyrindyl tetrazine and benzyl diazoacetamide; only products **1b** and **5a** (two regioisomers) were observed. The NMR spectra match previously reported values.^{5,13}



Method 1	RT (min)	Area (V·s)*
Peak 1 5c maj	1.6306667	0.48869333
Peak 2 1c min	1.7676667	0.969846
Peak 3 1a maj	1.8636667	1.25377233
Peak 4 1c maj	1.9696667	2.307522

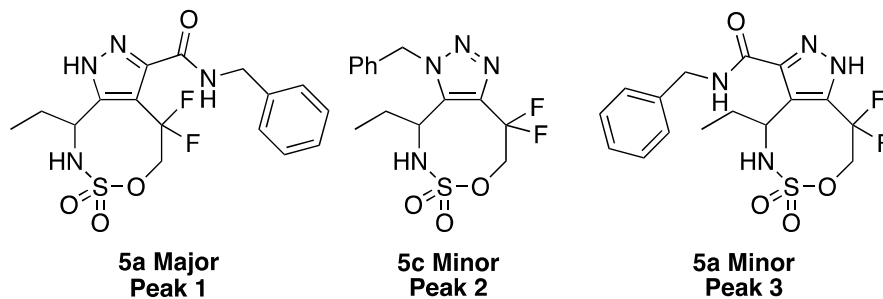
Method 1

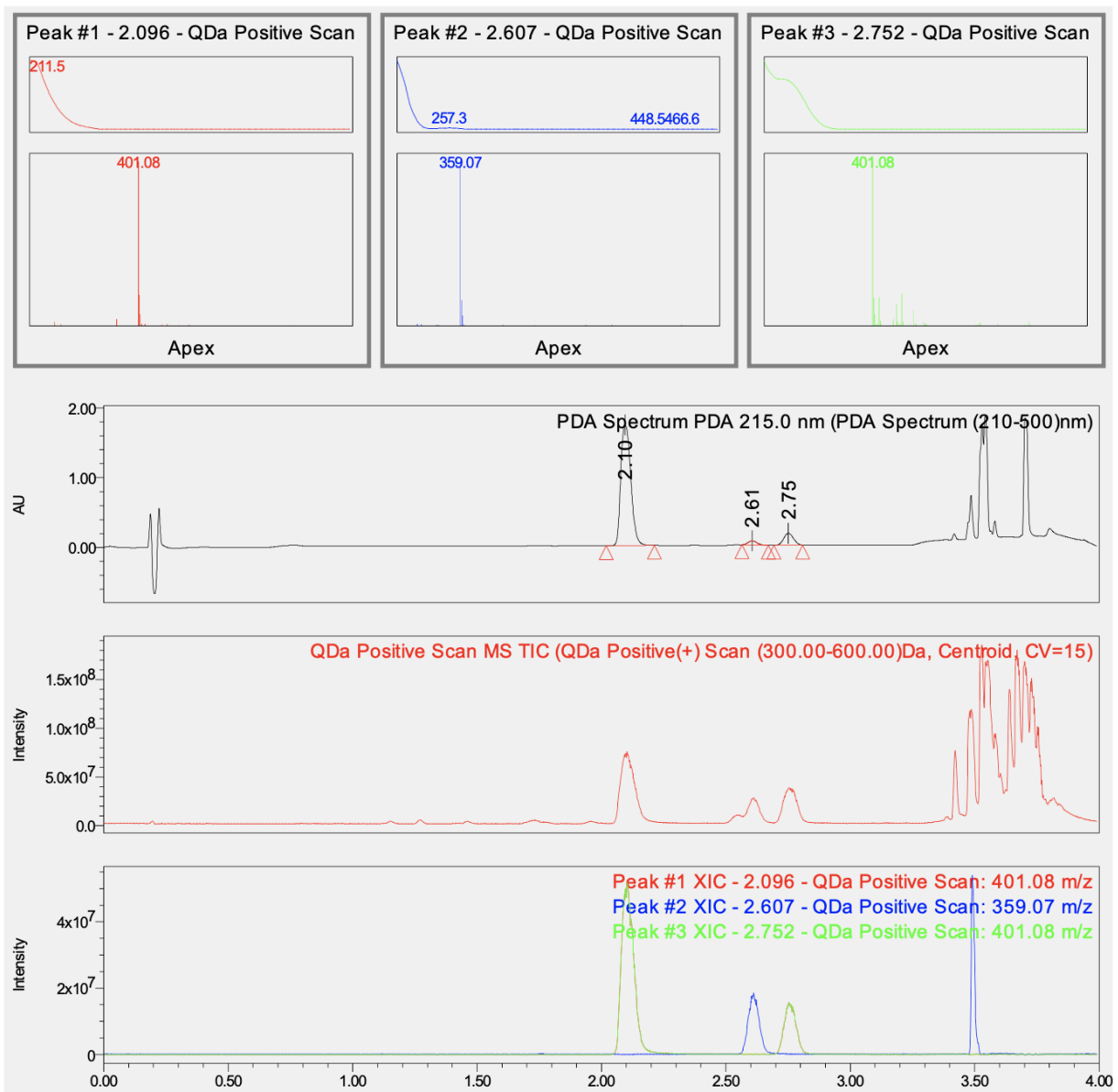




Method 2	RT (min)	Area (V·s)*
Peak 1 5a maj	2.086	4.89384233
Peak 2 5c min	2.607	0.15620833
Peak 3 5a min	2.751	0.48344133

Method 2



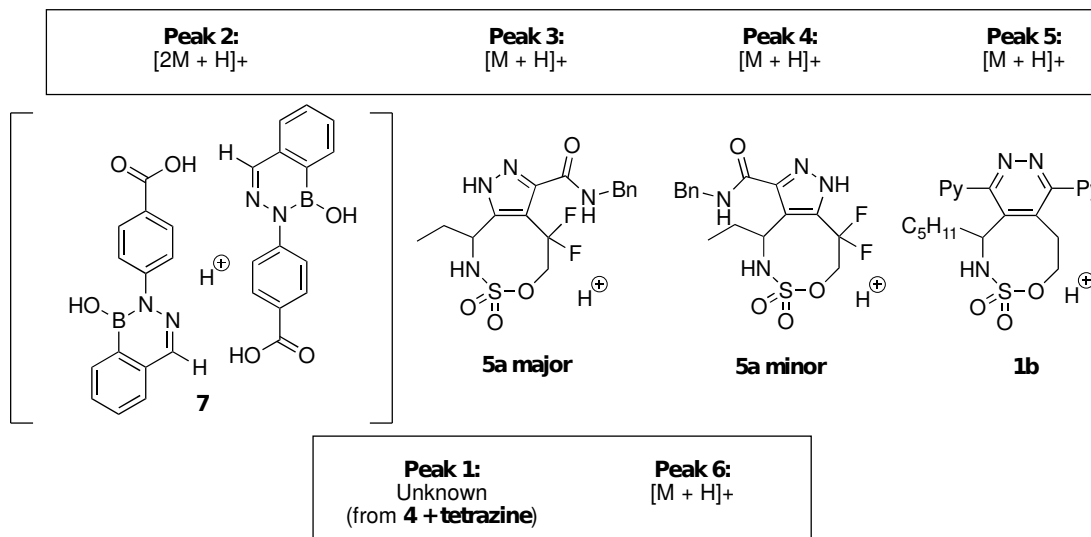
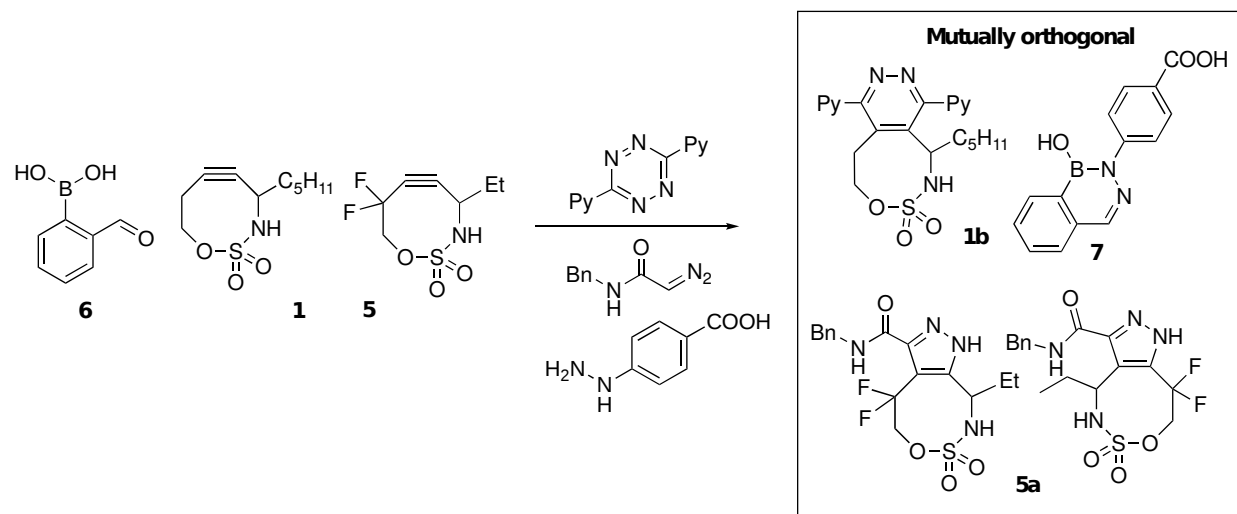


Ratio Calculation		
	[Conc.]	Ratio
1a	1.3955488 1	1.9
1c	4.2957829 5	5.8
5a	4.6092965 9	6.3
5c	0.7372923 6	1.0

Figure S2-16B. In the competition between **1** and **5** for benzyl diazoacetamide and benzyl azide, all possible products were observed. Due to the difficulties of analyzing the mixture by NMR, LC-MS was used to assess ratios. Two LC-MS method were used to analyze these mixtures, with concentrations based on the calibration curves in Section XII.

XI. Triple ligation results

General procedure. Stock solutions (0.1 M in methanol) of the SNO-OCTs and the dipoles were prepared. One equivalent of each dipole was combined in a vial equipped with a stir bar, followed by the addition of one equivalent of each of the SNO-OCT solutions. The reaction was stirred at room temperature for 1 h to ensure full conversion. All volatiles were removed under reduced pressure, and the selectivity determined based on UPLC/LC-MS analysis using Method 1.



Note: Peak 1 is an unknown that has been observed from the cycloaddition between **1** and dipyridyl tetrazine. We suspect this is a by-product from loss of one of the pyridine moieties, based on HRMS. Peak 6 is an undesired cross product. The cross-product:desired product ratio was not calculated, as the amount of cross product is below the limits of the calibration curve, while the desired products exceed the limits at the other end of the calibration curve. Similar minor cross reactivity products are observed in dual ligation systems when the mixture was injected into UPLC/LC-MS; however, the cross product is not observable by NMR, indicating a selectivity of > 20:1.

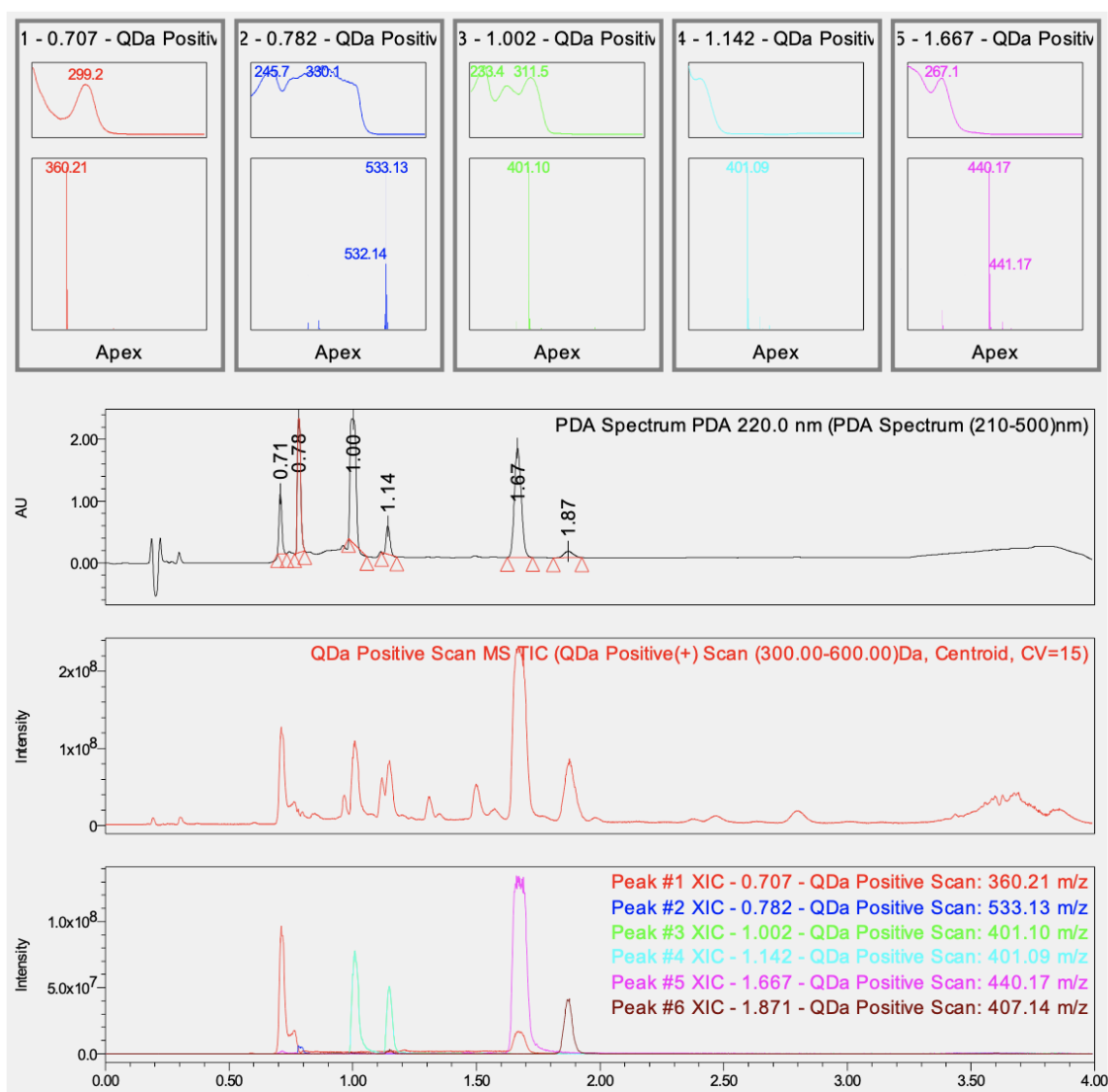


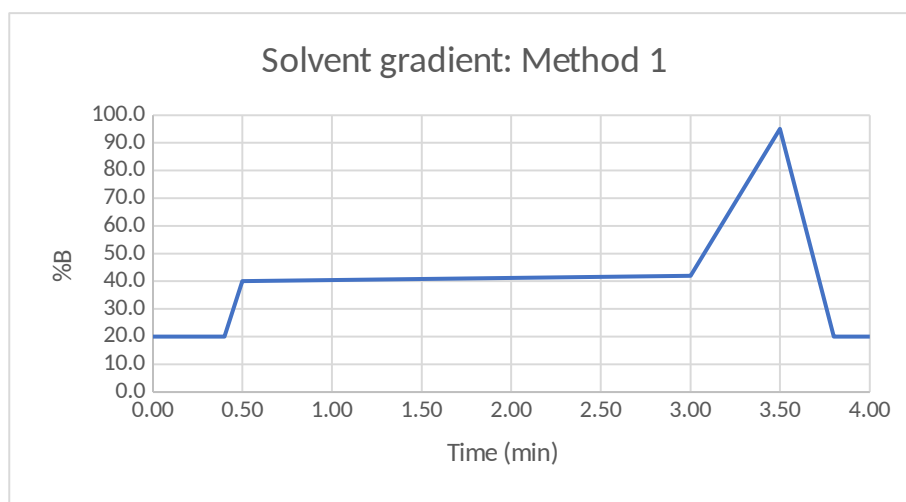
Figure S2-17. The triple ligation of three pairs of bioorthogonal reagents. Mutual orthogonality was observed, based on UPLC/LC-MS analysis.

XII. UPLC-MS methods and calibration curves

General procedure for calibration. Response factor curves were created for each compound, which were synthesized and purified based on the method reported above or on previously reported methods.⁵ Serial dilutions were performed in a 96-well plates to create a series of concentrations (5.0 mM – 0.4 mM). The UV absorption at 215 nm was measured, based on 1 μ L injections of samples at various concentrations. The calibration curves were generated based on the peak area of the corresponding compound vs. concentration. Each curve was generated in triplicate to furnish the following calibration curves. Error bars were also incorporated into each averaged point. Note: Due to the difficulties in separating all components in the competition mixture using a single method, two methods were developed to achieve optimal separation and efficiency.

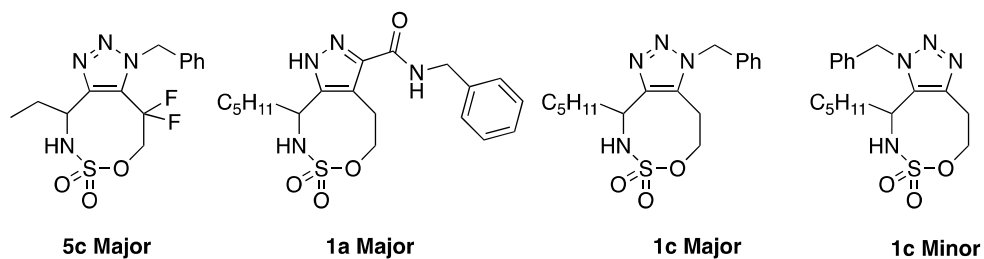
UPLC-MS methods:

Method 1

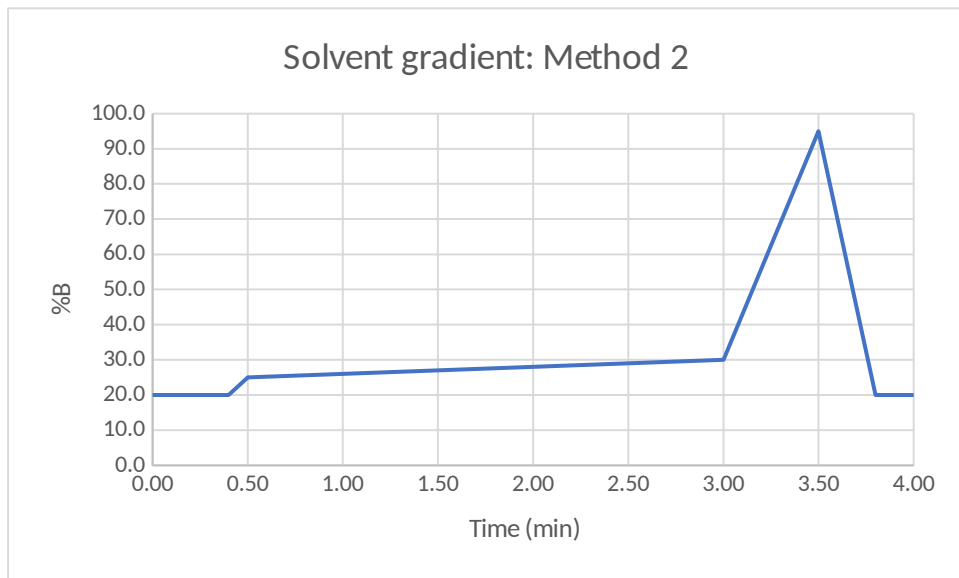


Solvents	A2	H ₂ O + 0.1% formic acid	B2	MeCN + 0.1% formic acid
1 μ L per injection	Time (min)	Flow speed (mL/min)	%A	%B
1	0.00	0.700	80.0	20.0
2	0.40	0.700	80.0	20.0
3	0.50	0.700	60.0	40.0
4	3.00	0.700	58.0	42.0
5	3.50	0.700	5.0	95.0
6	3.80	0.700	80.0	20.0
7	4.00	0.700	80.0	20.0

The following compounds were calibrated using **Method 1**:

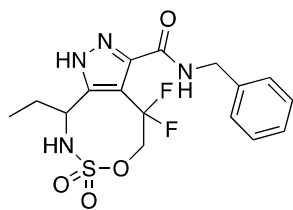


Method 2

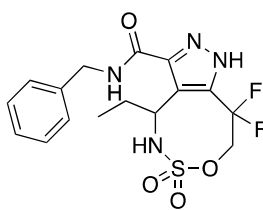


Solvents	A2	H ₂ O + 0.1% formic acid	B2	MeCN + 0.1% formic acid
1 µL per injection	Time (min)	Flow speed (mL/min)	%A	%B
1	0.00	0.700	80.0	20.0
2	0.40	0.700	80.0	20.0
3	0.50	0.700	75.0	25.0
4	3.00	0.700	70.0	30.0
5	3.50	0.700	5.0	95.0
6	3.80	0.700	80.0	20.0
7	4.00	0.700	80.0	20.0

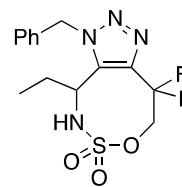
The following compounds were calibrated using **Method 2**:



5a Major

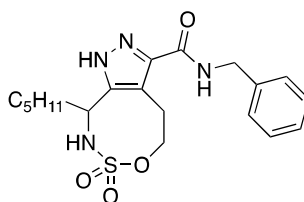


5a Minor

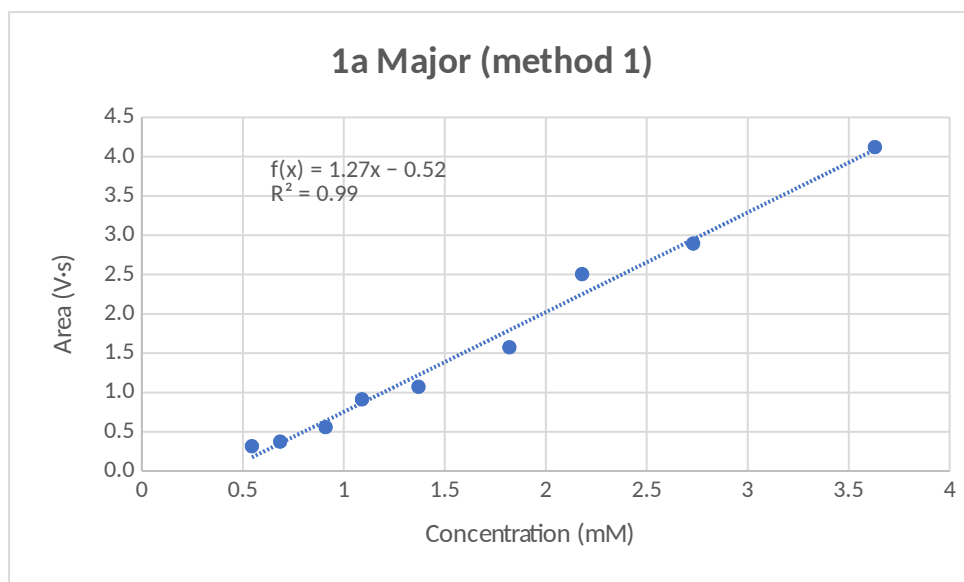


5c Minor

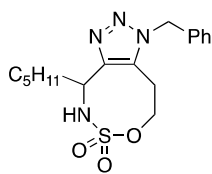
Compound 4a major calibration curve.



1a Major

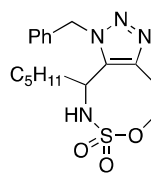


Compound 1c major and 1c minor calibration curve.



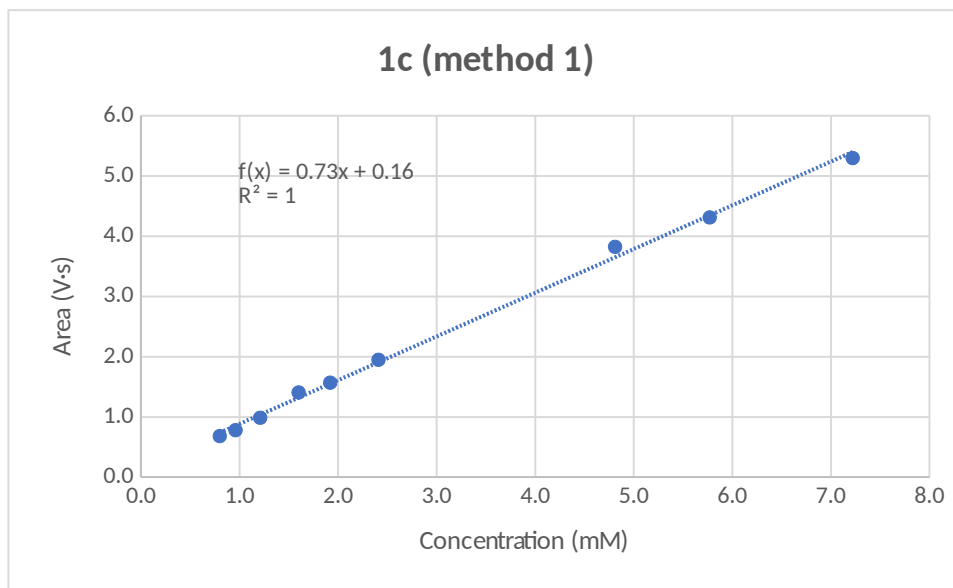
1c Major

+

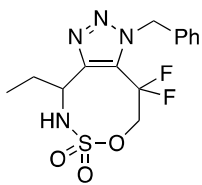


1c Minor

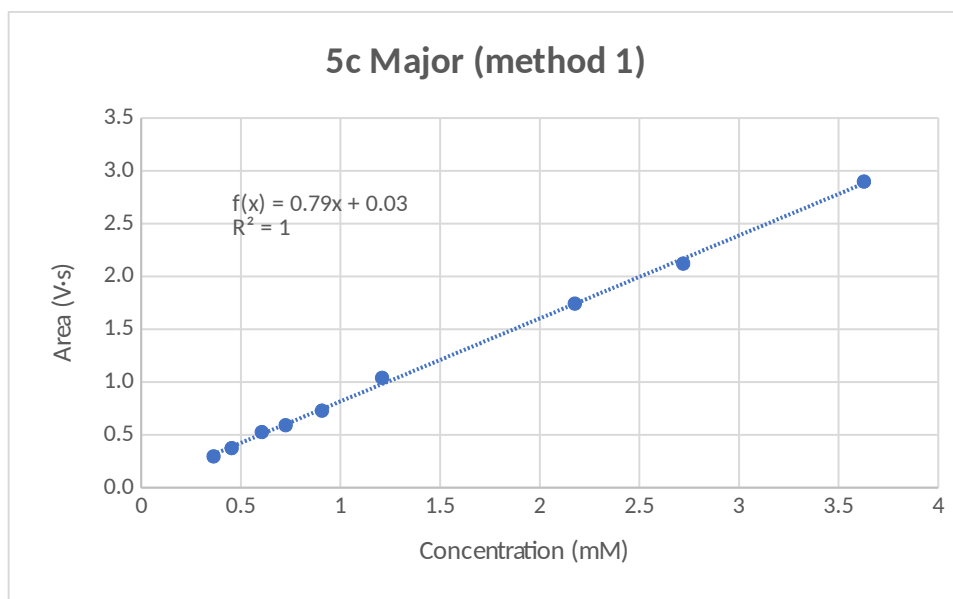
Note: Due to the difficulties in purification, the compound was calibrated as a mixture. The area was determined by the total combined integrated value.



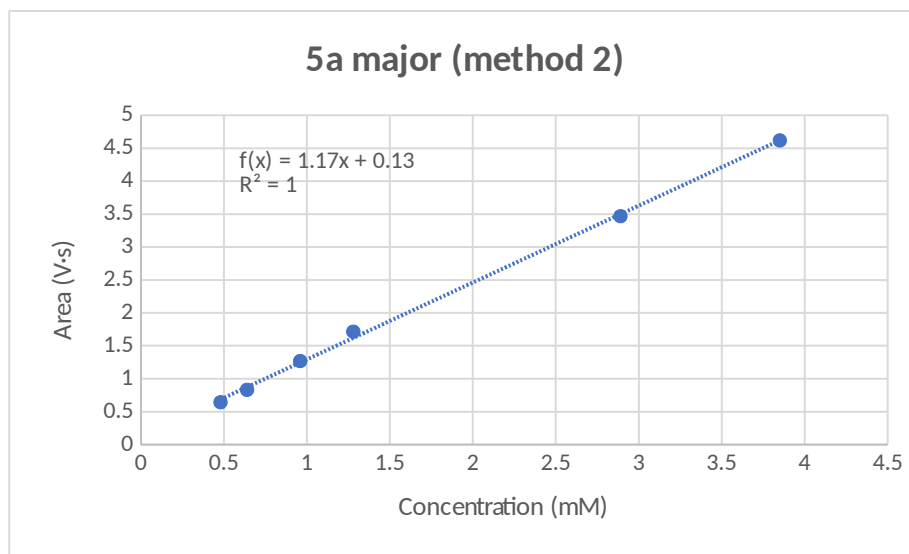
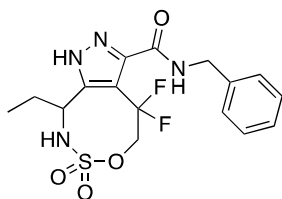
Compound 5c major calibration curve.



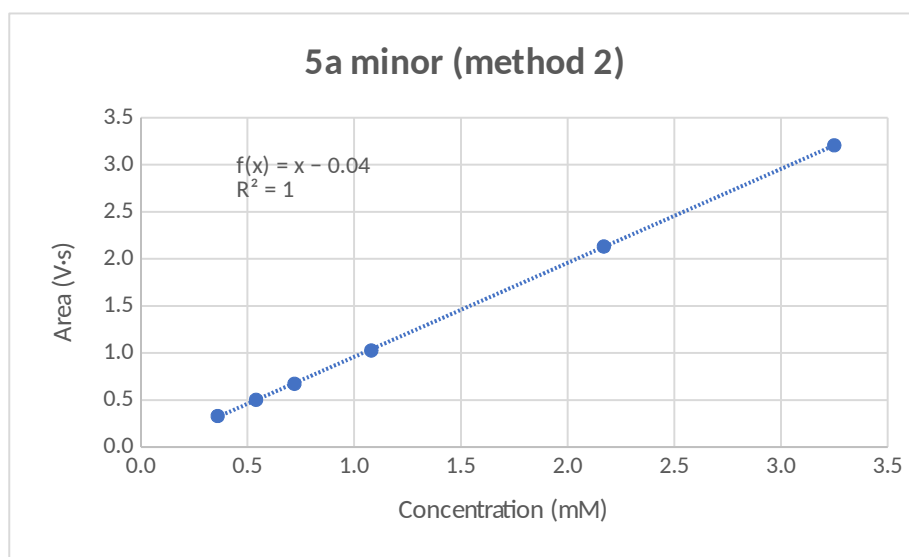
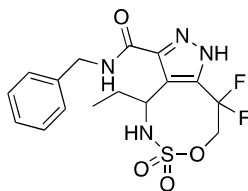
5c Major



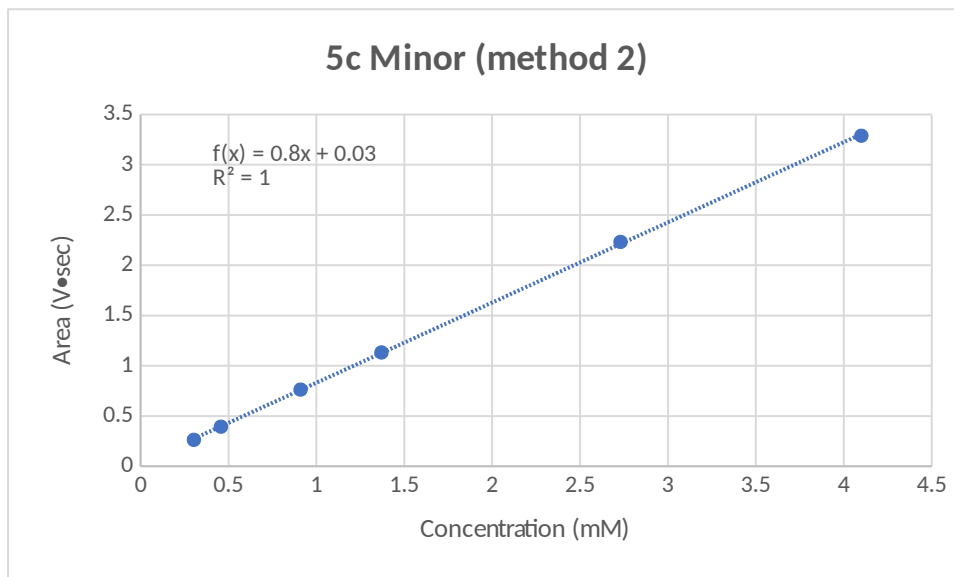
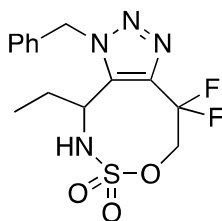
Compound 5a major calibration curve.



Compound 5a minor calibration curve.



Compound 5c minor calibration curve.



XIII. *In cellulo* assays

Mammalian cell culture

Chinese Hamster Ovary cells (CHO-K1, American Tissue Culture Catalog CCL-61™) were cultured in sterile T-75 flasks containing 20 mL of F12-K medium supplemented with 10% v/v fetal bovine serum (FBS), 100 units/mL penicillin, 100 µg/mL streptomycin, and 2 mM glutamine. Unless otherwise stated, supplemented F12-K medium contains 10% FBS 100 units/mL penicillin, 100 µg/mL streptomycin, and 2 mM glutamine. Cells were cultured at 37 °C with 5% v/v CO₂ in an incubator. Cells were counted to determine seeding density using a Countess™ II Automated Cell Counter, employing trypan blue and disposable countess chamber slides according to manufacturer recommendation.

Microscopy

Chinese hamster ovary cells (CHO-K1) were plated at 50,000–75,000 cells/well in an 8-well glass bottom microscopy dish (µ-Slide 8 well) in supplemented F-12K medium. These cells were incubated overnight at 37 °C. Prior to treatment, the cells were washed twice with 200 µL of Dulbecco's phosphate-buffered

saline (DPBS) supplemented with calcium and magnesium (DPBS, 0.9 mM CaCl_2 , 0.49 mM $\text{MgCl}_2 \cdot 6\text{H}_2\text{O}$, 2.67 mM KCl, 1.467 mM KH_2PO_4 , 138 mM NaCl, and 8.059 mM $\text{Na}_2\text{HPO}_4 \cdot 7\text{H}_2\text{O}$), followed by the addition of 200 μL of supplemented F-12K medium. Probe solutions prepared in supplemented F-12K were added to achieve the appropriate concentration of the molecule and allowed to incubate for 2 h at 37 °C. CHO-K1 cells were then washed twice with 200 μL of DPBS, and 160-200 μL DPBS was added to each well prior to counterstaining or addition of 200 μL of Invitrogen Live-Cell Imaging solution (140 mM NaCl, 2.5 mM KCl, 1.8 mM CaCl_2 , and 1.0 mM MgCl_2 in 20 mM HEPES, pH 7.4). Counterstaining involved treatment of cells with Hoechst 33342 at 2 $\mu\text{g}/\text{mL}$ or Invitrogen Wheat-Germ Agglutinin-AlexaFluor-647™ at 5 $\mu\text{g}/\text{mL}$ for 15 min on ice, then washing twice with 200 μL of Invitrogen Live-Cell Imaging Solution before addition to a final 200 μL of Invitrogen Live-Cell Imaging solution to each well.

Images were recorded with an Andor Spinning Disk Confocal Microscope using a 1.4 NA, 60x Plan Apo objective. Sample excitation was performed with a 50 mW, 405 nm; 50 mW, 488 nm; 50 mW, 561 nm; or 100 mW, 640 nm laser. Images were recorded with an Andor Zyla sCMOS or Andor iXion+ EMCCD camera and MetaMorph acquisition software. Further background subtraction and analysis was performed using Fiji software. Inspection of these images abated concerns of bleed-over from **SNO-C343** into the 488 nm channel used to observe **DCF**, as bright, high-intensity objects found in **SNO-C343** micrographs are not observed in the 488 nm channel.

Metabolic labeling

A sterile-stock solution of $\text{Ac}_4\text{ManDiaz}$ was prepared in absolute ethanol at a concentration of 10 mM. One hour prior to seeding CHO-K1 cells, 0–15 μL of the 10 mM $\text{Ac}_4\text{ManDiaz}$ stock solution was added to either a sterile 8-well Ibidi glass bottom slide or a sterile 12-well plate and allowed to evaporate prior to seeding. CHO-K1 cells were seeded at 50,000 cells/well at a volume of 200 or 500 μL in supplemented F-12K medium and allowed to incubate at 37 °C with 5% v/v CO_2 in a tissue culture cabinet for 24 h. Prior to labeling, cells were washed twice with DPBS, followed by the addition of 200 or 500 μL of fresh supplemented F-12K medium to each well. Cells were then treated with DIFO-SNO-Rho at 1 μM for 2 h, before being washed twice with DPBS and analyzed with flow cytometry or confocal microscopy.

Flow cytometry

Cells were released from 12-well culture dishes by incubation with 200 μL of 0.25% v/v trypsin–EDTA mix for 5 min at 37 °C with 5% v/v CO_2 in a tissue culture cabinet, and trypsinolysis was quenched with 500 μL of supplemented F-12K medium. Cells were then subjected to centrifugation at 200g for 5 min

and resuspended in 1 mL of DPBS supplemented with 1% w/v bovine serum albumin (BSA). To these cells was added 1 μ L of 30 μ M of SYTOX[®] Green solution to obtain a stain concentration of 30 nM; cells were then lightly vortexed and allowed to incubate for 20 min. Cells were centrifuged again at 200g for 5 min and resuspended in 1 mL of DPBS supplemented with 1% w/v BSA, and the process was repeated to remove excess dye before final resuspension in 1 mL of DPBS supplemented with 1% w/v BSA. Cells were then analyzed with an Attune NxT Flow Cytometer, and fluorescence intensity was quantified on 20,000 live, single cell events at the experimental conditions. Data were analyzed with FlowJo version 10.7.

Protein labeling

Preparation of RNase A–BA, RNase A–Tet, and Cytoc–AcDz.

Bovine pancreatic ribonuclease A (RNase A) and horse heart cytochrome c (Cytoc) were obtained from Sigma–Aldrich. Solutions of 10 mg/mL of RNase A and Cytoc were prepared in DPBS. Solutions of 10 mM tetrazine-NHS, diaz-NHS, and BE-NHS in DMSO were prepared immediately before use and stored at –20 °C. In a typical reaction, 1 equiv of tetrazine-NHS, or BE-NHS was added to a 1-mg (100 μ L) solution of RNase A on ice, and the resulting solution was mixed gently for 2 h. In an equivalent transformation, 1 mg of Cytoc was functionalized with 1 equiv of Diaz-NHS. Protein conjugates were then diluted to a volume of 250 μ L with DPBS, eluted from a PD-25 column equilibrated with DPBS elution that was monitored by absorption measurements at A_{280} . Functionalized proteins were concentrated with a 3.5-kDa molecular weight cut-off spin concentrator at 10,000g for 10 min. The mass of protein conjugates was measured with matrix-assisted laser-desorption ionization (MALDI) mass spectrometry.

Assessing mutual orthogonality

Protein-conjugates and small molecule mixtures were prepared to assay the extent of orthogonality among reactive species. The corresponding lane number presented in Figure 4a and Figure S2-12a–d imaged with *in situ* gel fluorescence is indicated in parentheses. To demonstrate the mutual orthogonality of reactive pairs, an aliquot of Cytoc–AcDz (7), RNase A–BA (6), or RNase A–Tet (5) was mixed with 5 equiv of SNO-DF–Rho, SNO–C343, and TR–Hyd and allowed to react shielded from light at room temperature overnight with gentle mixing. In a similar experiment, 1 equiv of Cytoc–AcDz, RNase A–BA, and RNase A–Tet were mixed with 5 equiv of SNO-DF–Rho (4), SNO–C343 (2), and TR–Hyd (3) allowed to react shielded from light at room temperature overnight with gentle mixing. Finally, the mutual orthogonality of all three pairs was tested by mixing 0.34 equiv (each) of Cytoc–AcDz, RNase A–BA, and RNase A–Tet and with 1.5 equiv (each) of SNO-DF–Rho, SNO–C343, and TR–Hyd (8). The

compounds were allowed to react while shielded from light at room temperature overnight with gentle mixing. A 20- μ L aliquot was then drawn from each reaction mixture and diluted 10-fold to 200 μ L. From the diluted stock, a 10- μ L portion was added to 10 μ L of 5% v/v β -mercaptoethanol in Laemmli sample buffer, and the resulting solution was heated to 95 °C for 20 min. Samples were then cooled and separated by gel electrophoresis. Fluorescent imaging of the gel was recorded with an Amersham Imager 680 blot and gel imager. Some bleed-through between blue and green channels was apparent. Excitation at 460 nm, 520 nm, and 630 nm with corresponding filter sets of 525/20 nm, 605/40 nm and 705/40 nm intrinsically lead to bleed-through between SNO-DF-Rho and Hyd-TR conjugates, which show excitation maxima at 570 nm and 600 nm, respectively.

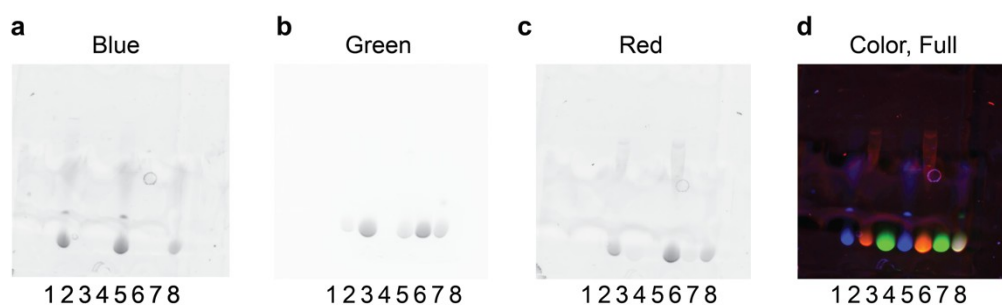


Figure S2-18. *In situ* gel fluorescence validation of tripartite biorthogonal set with protein labeling with a GE Amersham Imager 680. (a) 460 excitation 525/20 nm filter set (b) 520 nm excitation, 605/40 nm filter set. (c) 630 nm excitation and 705/40 nm filter set. (d) Combination of images in Figure S12a–c with false-color.

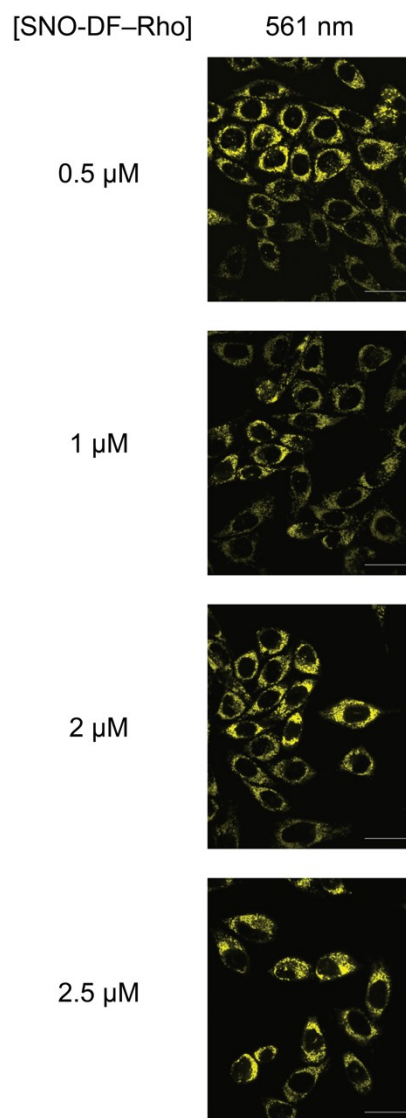


Figure S2-19. Uptake of SNO-DF-Rho by CHO-K1 cells. Images: 60% laser power, 200 ms exposure time with an sCMOS camera. Scale bar: 10 μm .

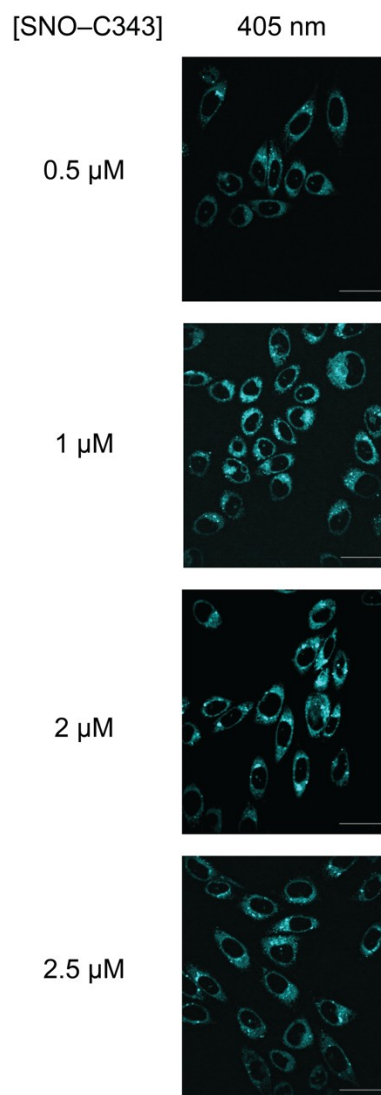


Figure S2-20. Uptake of SNO-C343 by CHO-K1 cells. Images: 45% laser power, 150 ms exposure time with an sCMOS camera. Scale bar: 10 μm .

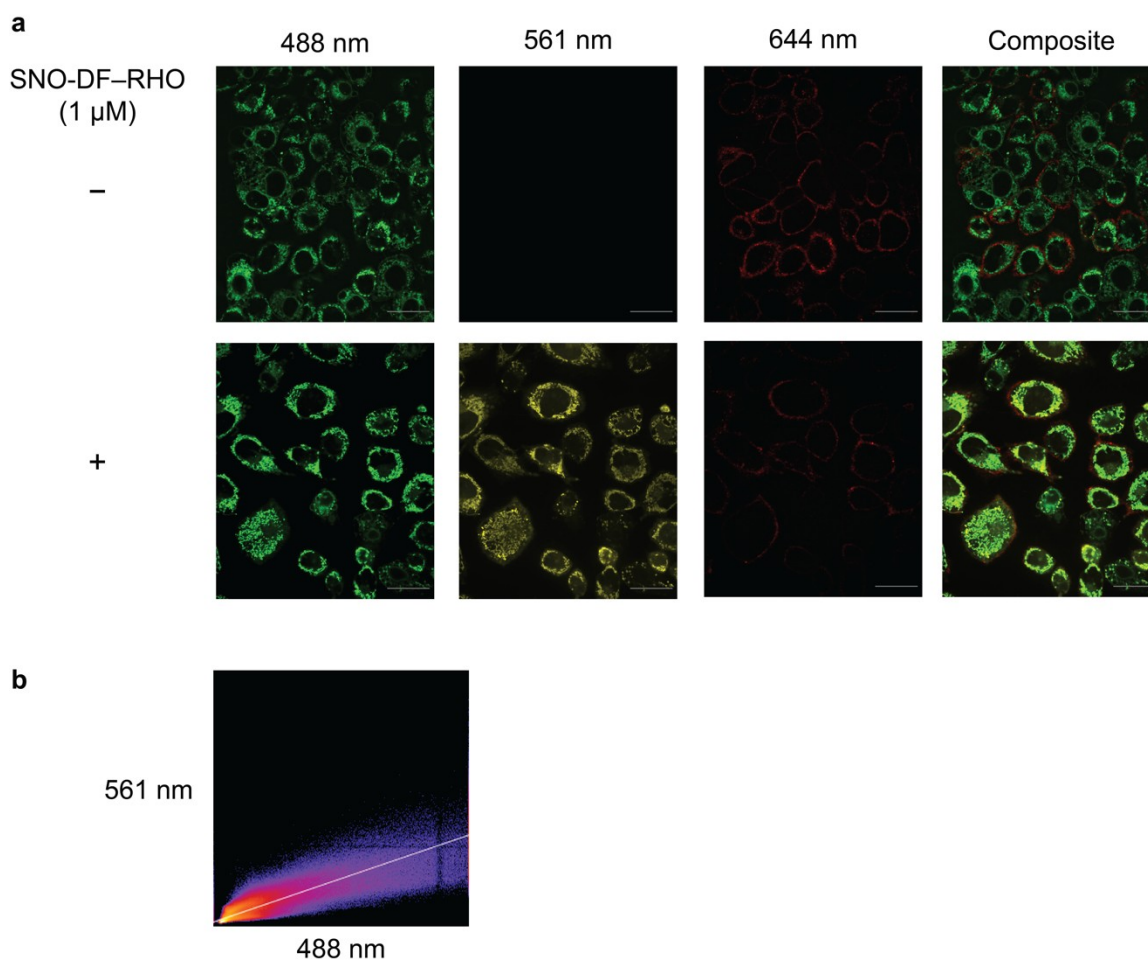


Figure S2-21. Mitochondrial labeling colocalization experiments of SNO-DF-Rho. (a) Comparison of CHO-K1 cells treated with MitoTracker® Green (500 nM) and with and without SNO-DF-Rho (1 μ M). (b) Two-dimensional intensity histogram of SNO-DF-Rho (561 nm channel) and MitoTracker® Green (488 nm channel). Pearson's coefficient for colocalization of MitoTracker® Green and SNO-DF-Rho was $R = 0.90 \pm 0.01$ ($n = 3$). Images were recorded with an sCMOS camera. Scale: 10 μ m.

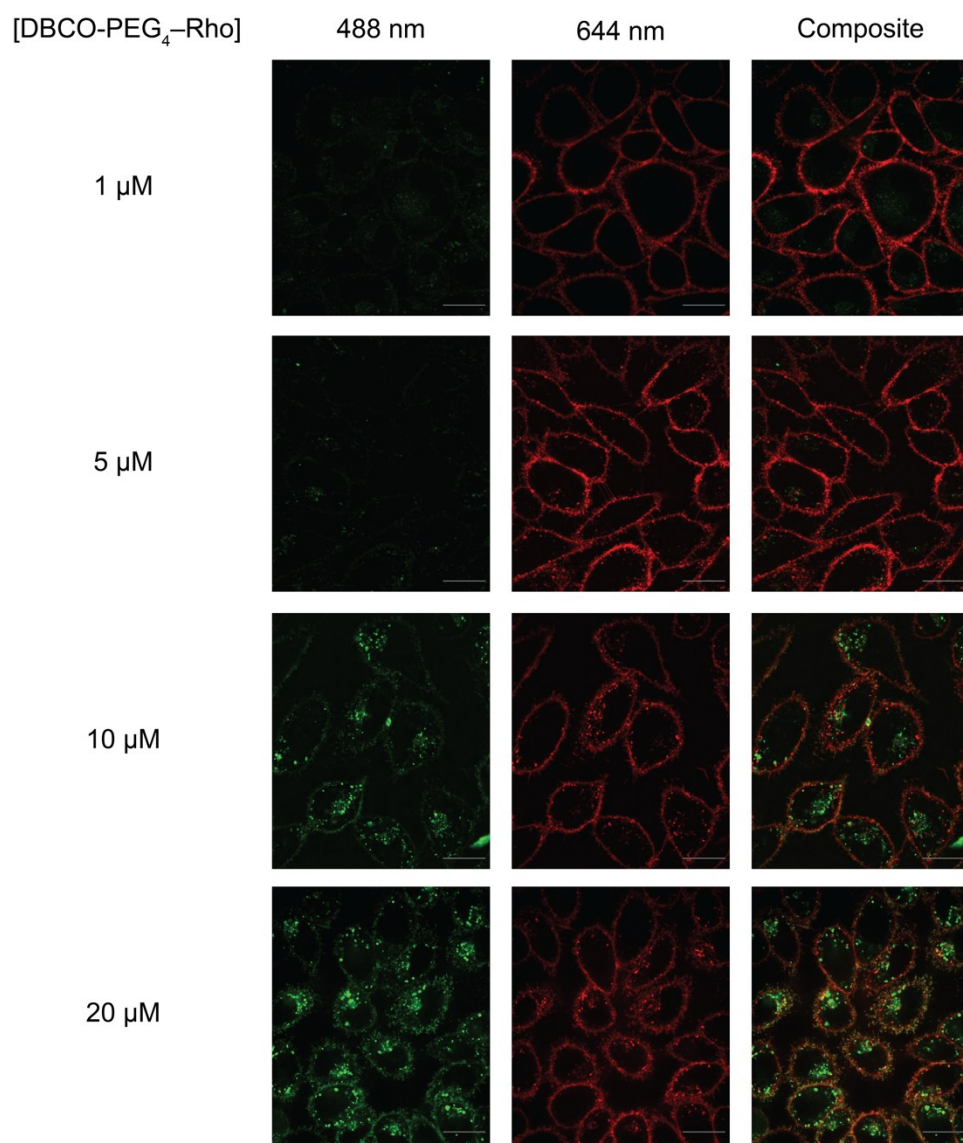


Figure S2-22. Uptake of DBCO-PEG₄-Rho into CHO K-1 cells. Images: 60% laser power, 200 ms exposure time with an sCMOS camera. Scale bar: 7.5 μ m.

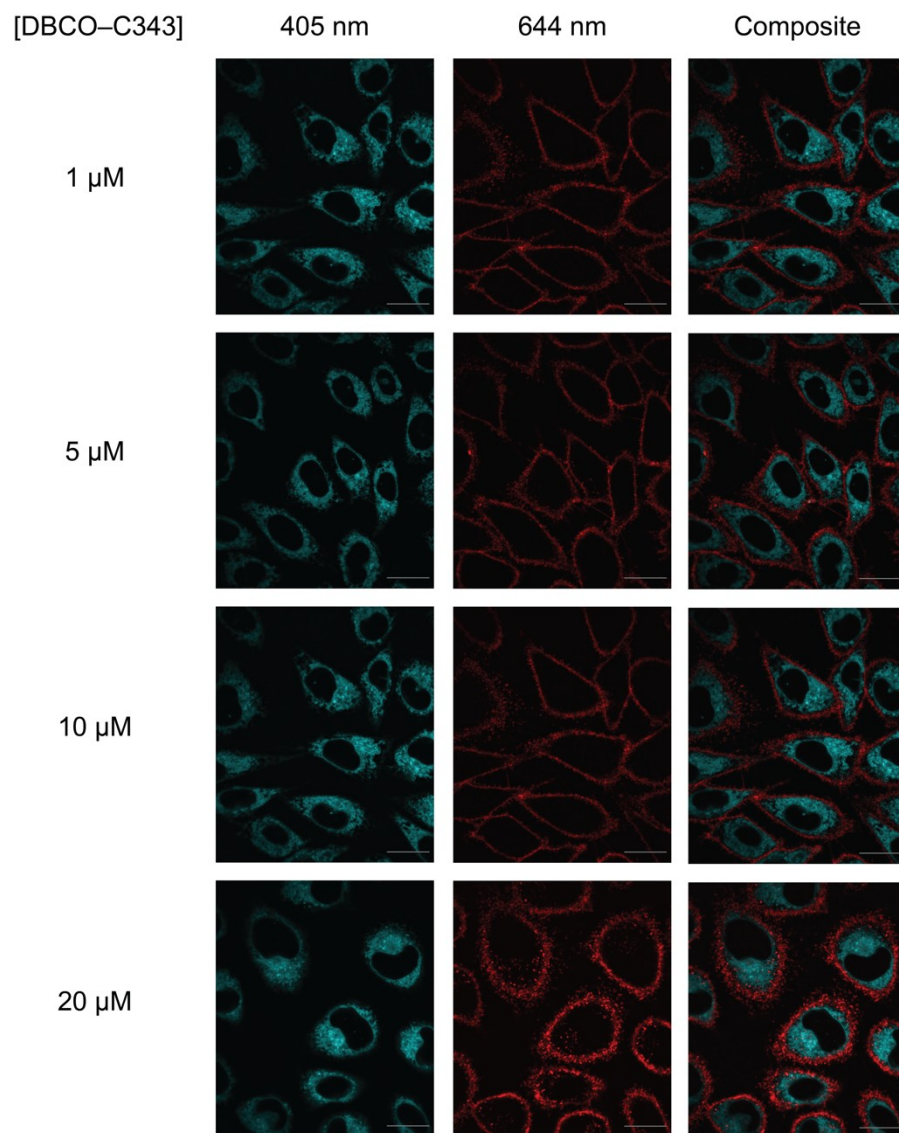


Figure S2-23. Uptake of DBCO-C343 into CHO-K1 cells. Images: 45% laser power, 200 ms exposure time with an sCMOS camera. Scale bar: 7.5 μ m.

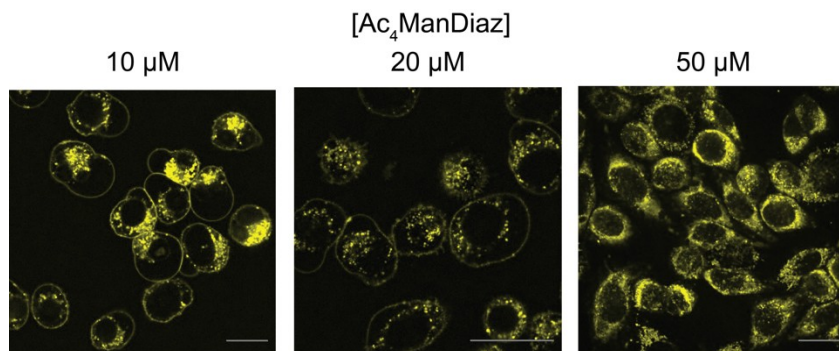


Figure S2-24. Titration of CHO-K1 cells with Ac₄ManDiaz after labeling with SNO-DF-Rho (1 μ M). Images: 561 nm, gain 10, exposure time 100 ms with an EMCCD camera. Scale Bar: 10 μ m.

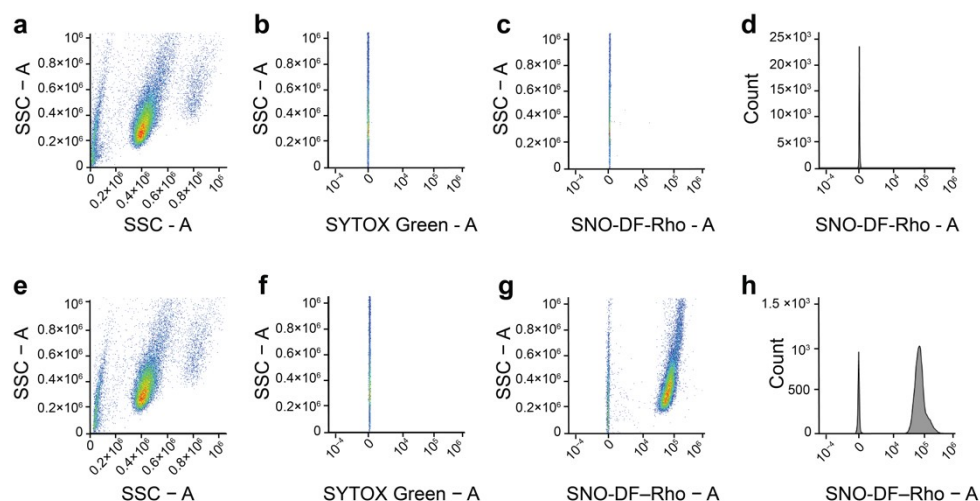


Figure S2-25. Analysis of CHO-K1 cells metabolically labeled with Ac₄ManDiaz (20 μ M) after incubation with SNO-DF-Rho (1 μ M) for 1 h, cells were the incubated with SYTOX green for 15 min (see *in vitro methods* for more information). (a) Scatter plot of metabolically labeled CHO-K1 cells, (b) Scatter plot of SYTOX Green-treated CHO-K1 cells with 488 nm excitation. (c) Scatter plot of metabolically labeled CHO-K1 cells with 561 nm excitation. (d) Fluorescence intensity histogram of metabolically labeled CHO-K1 cells with 561 nm excitation. (e) Scatter plot of metabolically labeled CHO-K1 cells incubated with 1 μ M SNO-DF-Rho. (f) Scatter plot of CHO-K1 cells incubated with 1 μ M SNO-DF-Rho with excitation 488 nm. (g) Scatter plot of CHO-K1 cells incubated with 1 μ M SNO-DF-Rho with excitation 561 nm. (h) Fluorescence intensity histogram of metabolically labeled cells treated with 1 μ M SNO-DF-Rho.

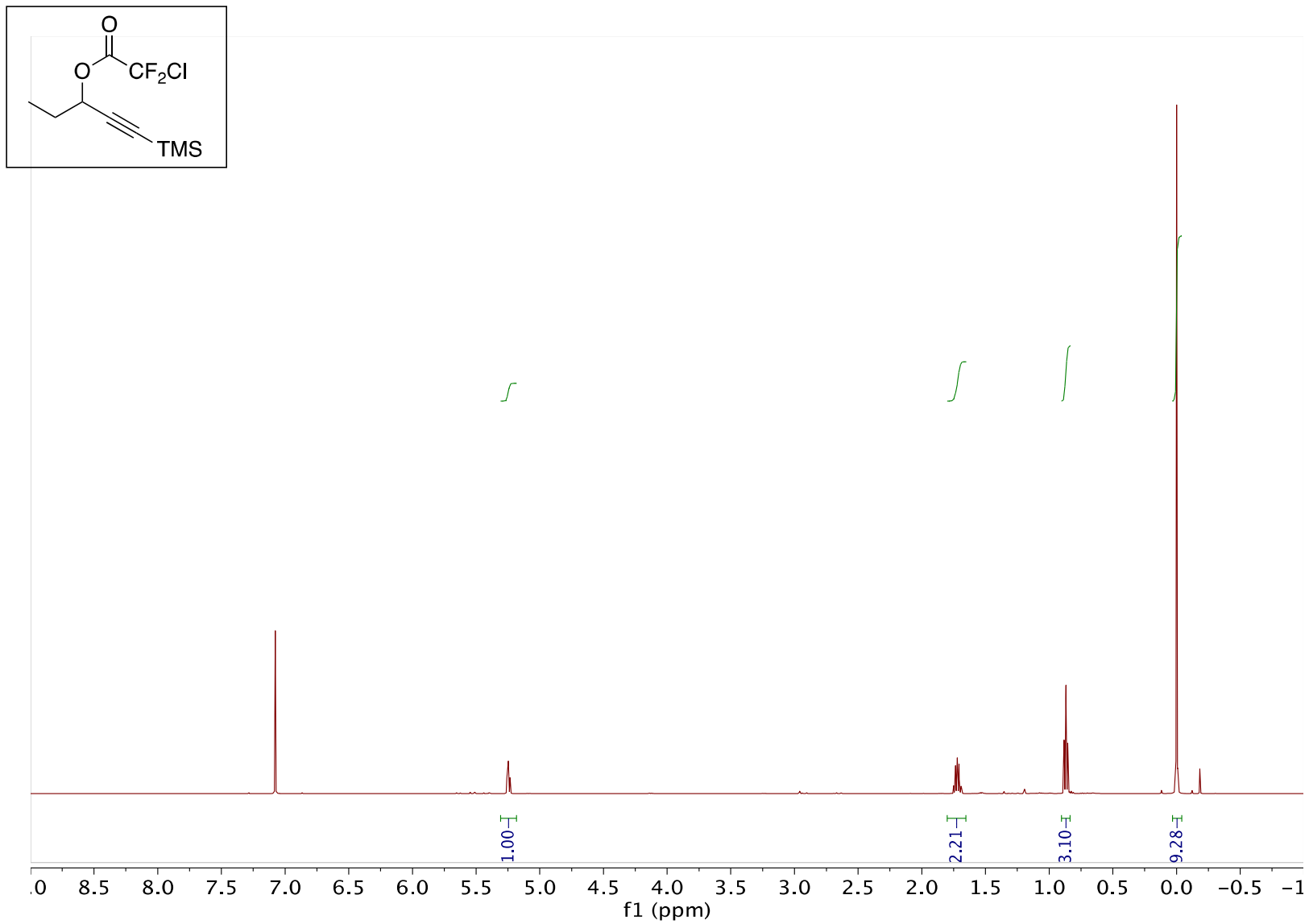
XIV. References

1. (a) Armarego, W. L. F.; Chai, C. L. L. *Purification of Laboratory Chemicals*, 6th ed., Elsevier: Burlington, MA, 2009. (b) Still, W. C.; Kahn, M.; Mitra, A. *J. Org. Chem.* **1978**, 43, 2923–2925.
2. Denmark, S. E.; Yang, S. *J. Am. Chem. Soc.* **2004**, 126, 12432–12440.
3. Yang, Y.; Meng, W.; Qing, F. *Org. Lett.* **2004**, 6, 4257–4359.
4. Hashimoto, N.; Aoyama, T.; Shioiri, T. *Chem. Pharm. Bull.* **1981**, 29, 1475–1478.
5. Burke, E. G.; Gold, B.; Hoang, T. T.; Raines, R. T.; Schomaker, J. M. *J. Am. Chem. Soc.* **2017**, 139, 8029–8037.
6. Nguyen, T.; Francis, M. B. *Org. Lett.* **2003**, 5, 3245–3248.
7. Chio, T. I.; Gu, H.; Mukherjee, K.; Tumey, L. N.; Bane, S. L. *Bioconjugate Chem.* **2019**, 30, 1554–1564.
8. Zhang, L.; Wu, Y.; Brunsveld, L. *Angew. Chem., Int. Ed.* **2007**, 46, 1798–1802.
9. Andersen, K. A.; Aronoff, M. R.; McGrath, N. A.; Raines, R. T. *J. Am. Chem. Soc.* **2015**, 137, 2412–2415.
10. Josa-Culler , L. Wainman, Y. A., Brindle, K. M., Leeper, F. J. *RSC Adv.* **2014**, 4, 52241–52244.

11. Aronoff, M. R.; Gold, B.; Raines, R. T. *Org. Lett.* **2016**, *18*, 1538–1541.
12. Burke, E. G.; Schomaker, J. M. *J. Org. Chem.* **2017**, *82*, 9038–9046.

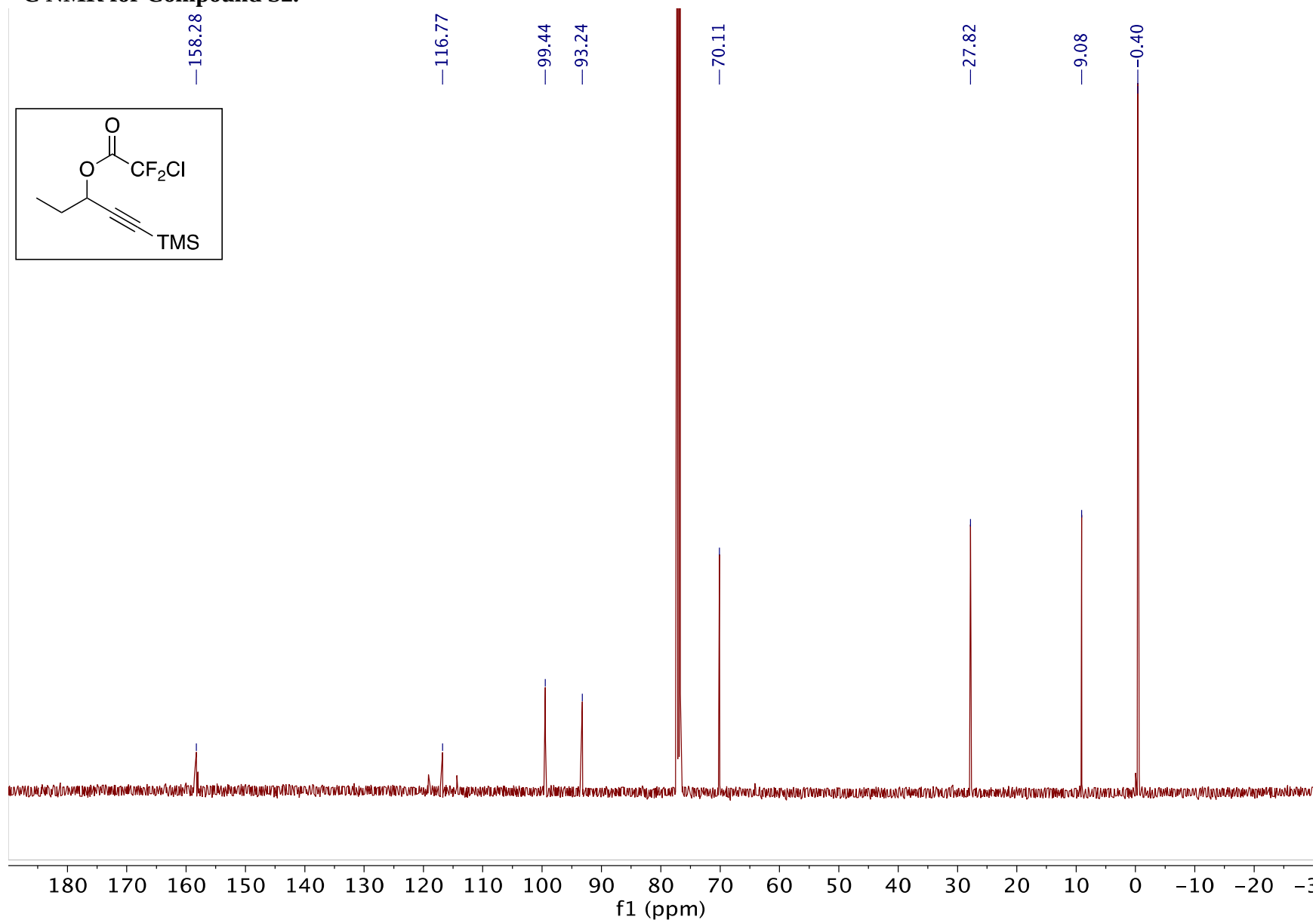
XV. NMR spectra

^1H NMR for Compound S2.



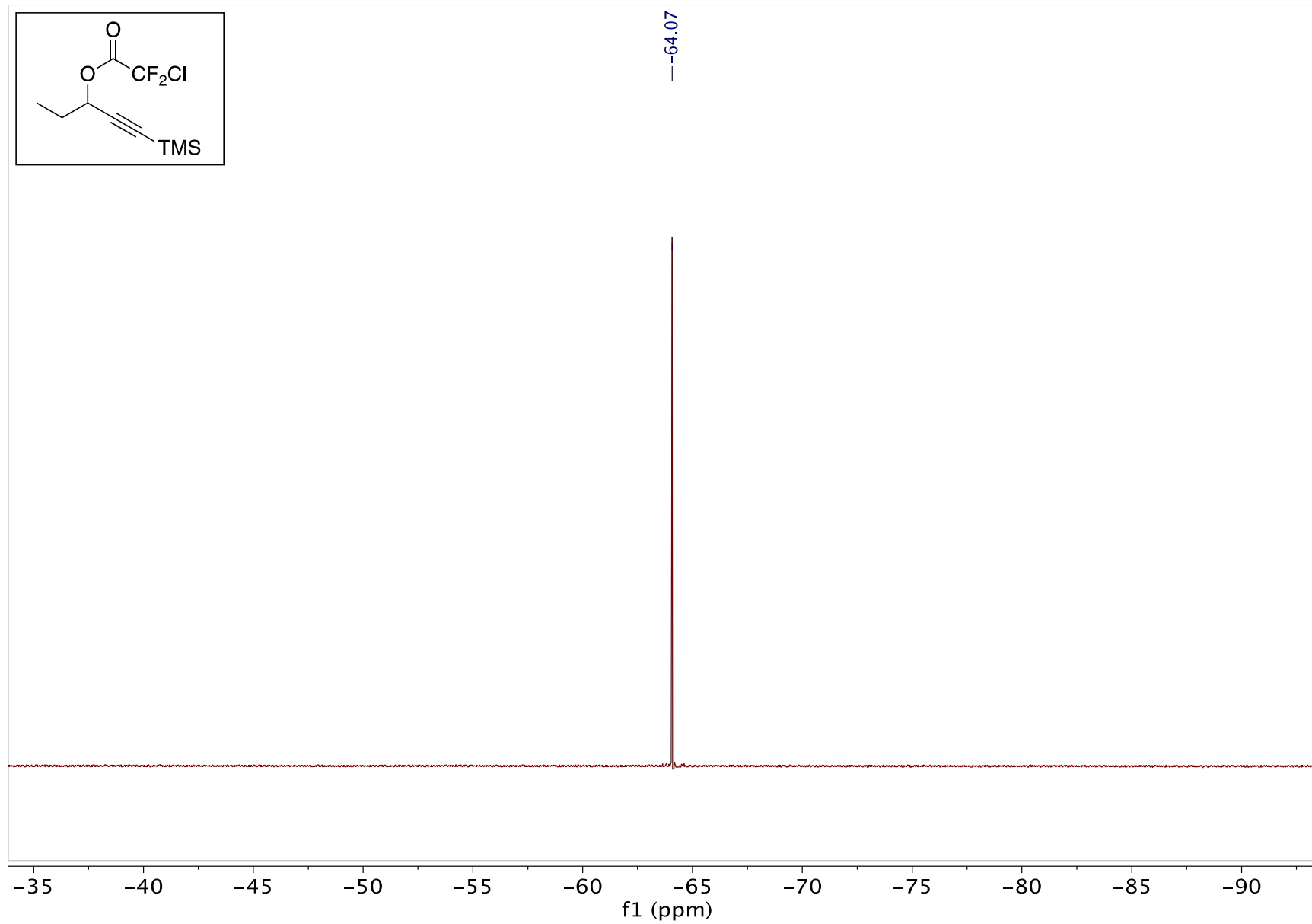
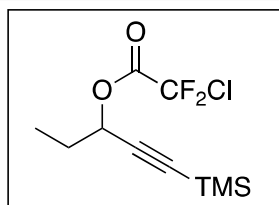
S2-52

¹³C NMR for Compound S2.



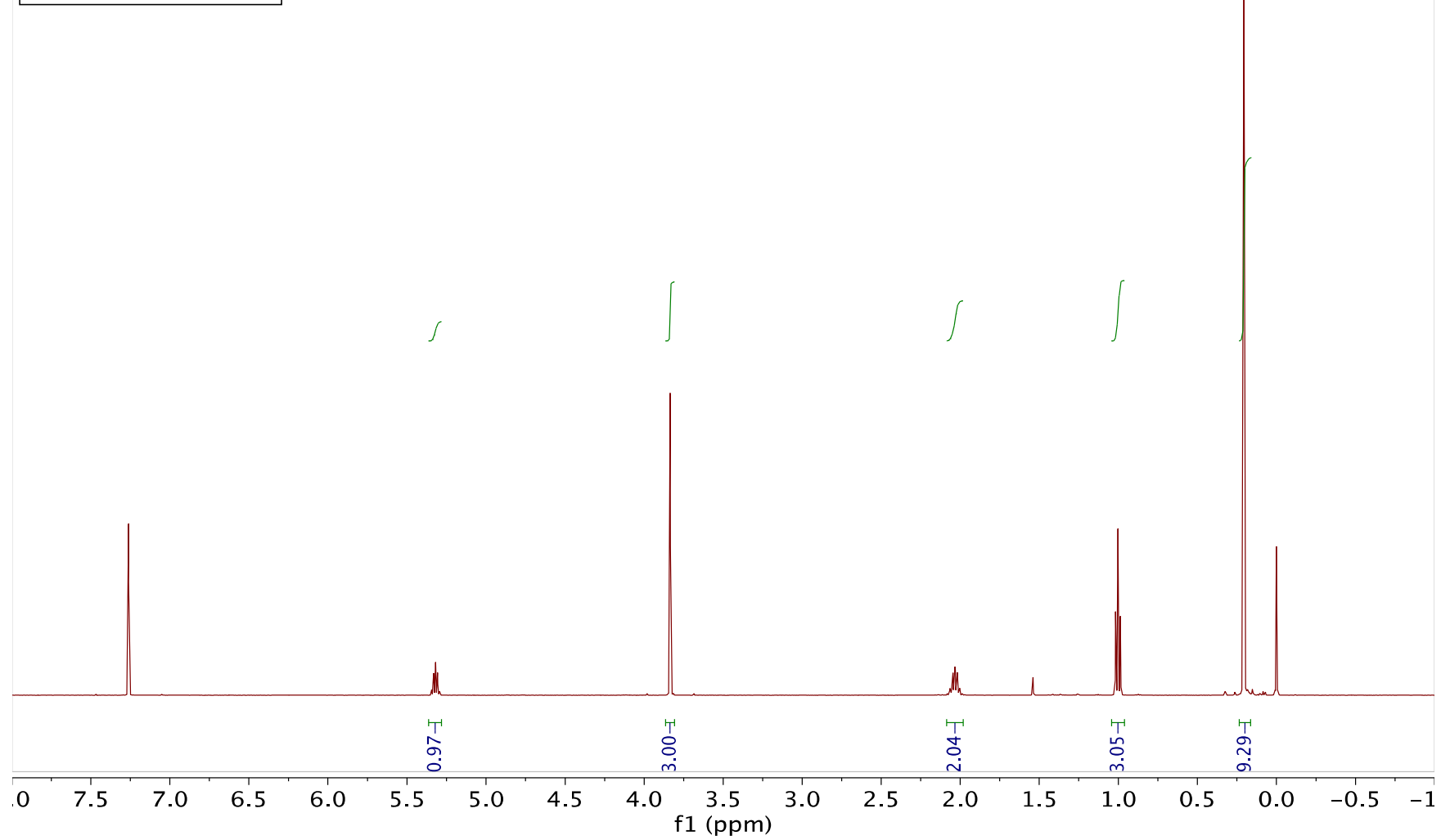
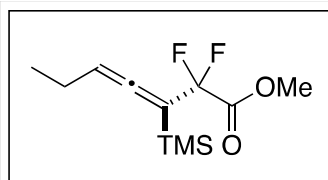
S2-53

^{19}F NMR for Compound S2.

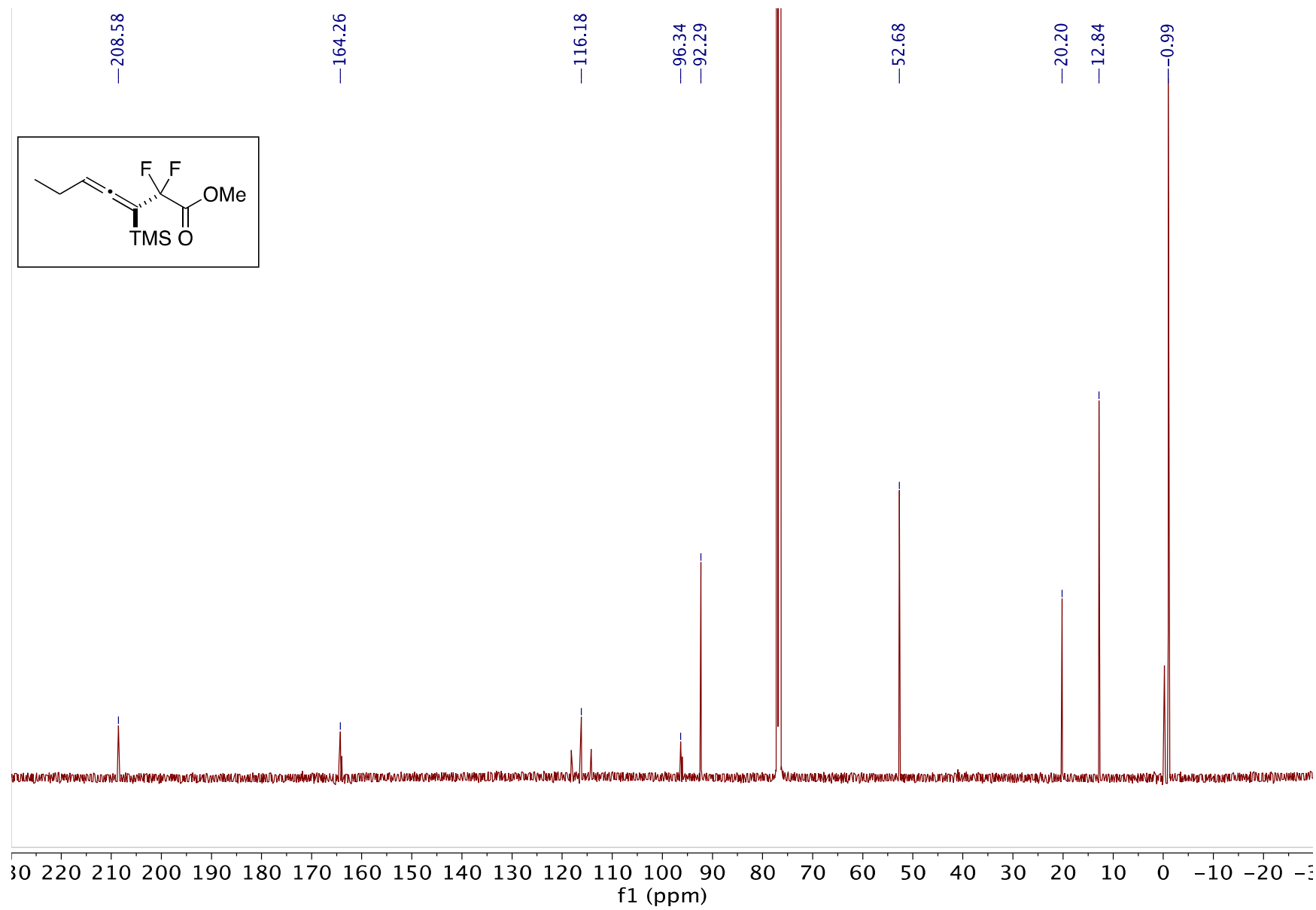


S2-54

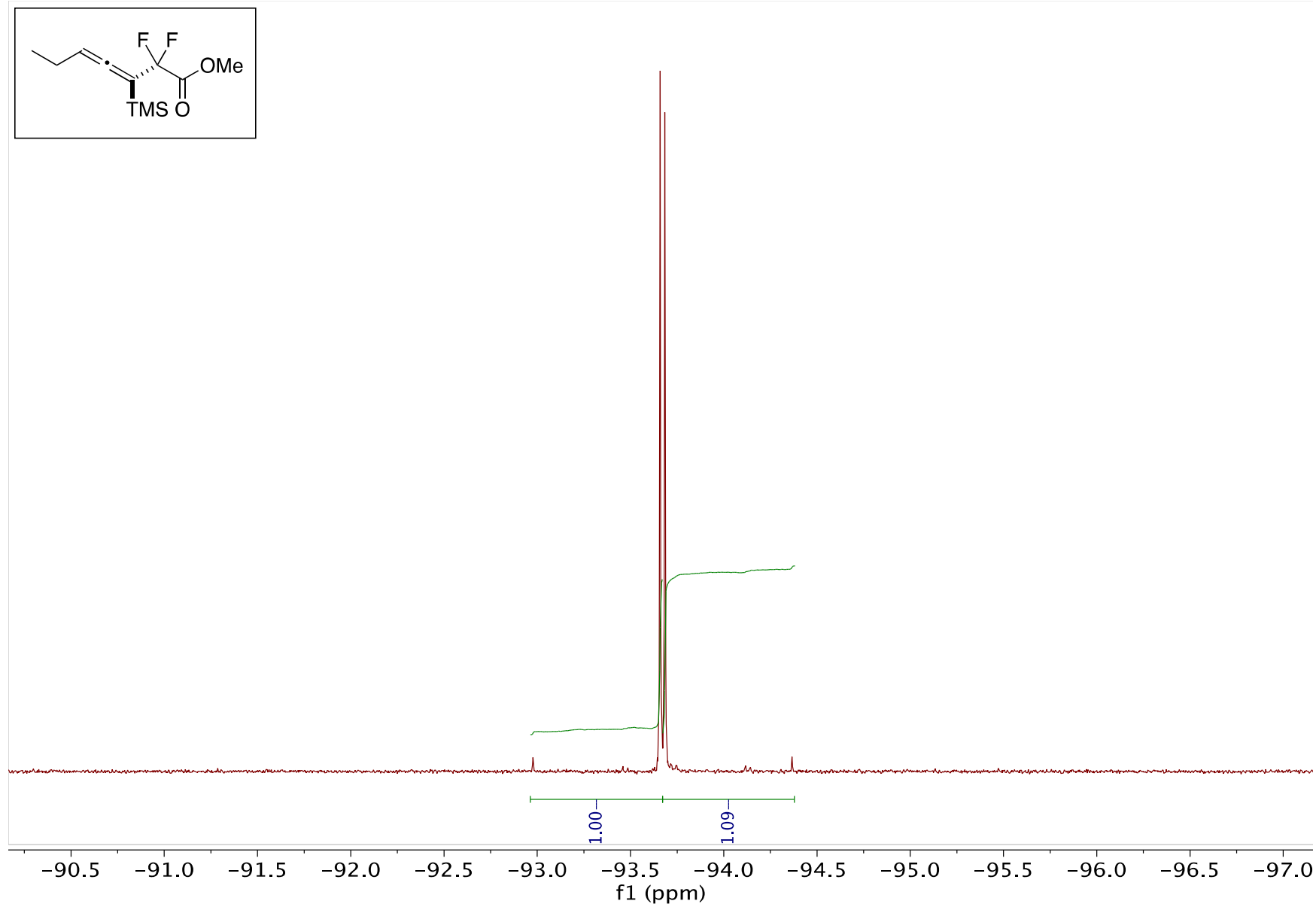
¹H NMR for Compound S3.



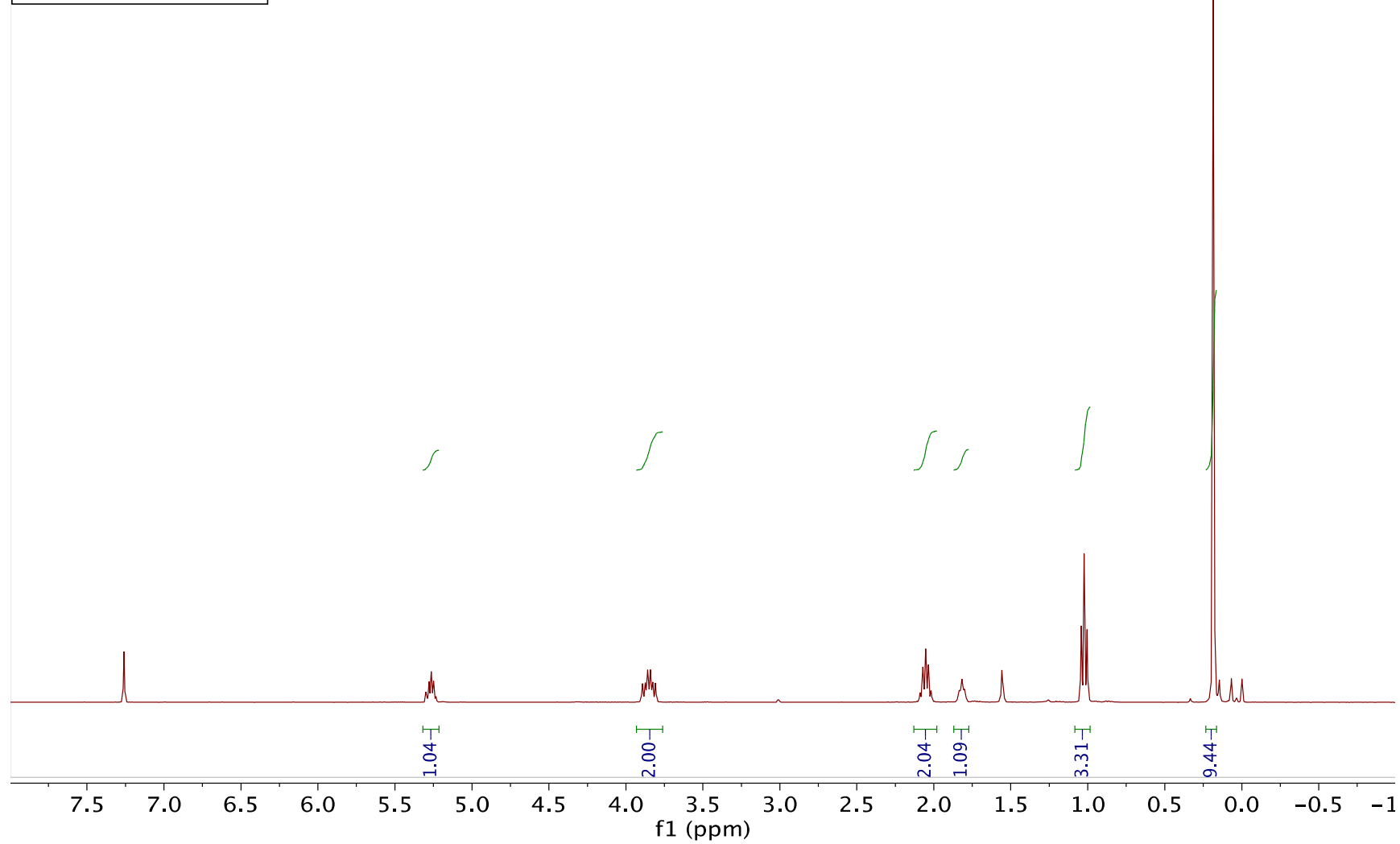
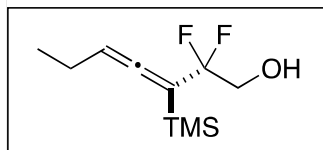
¹³C NMR for Compound S3.



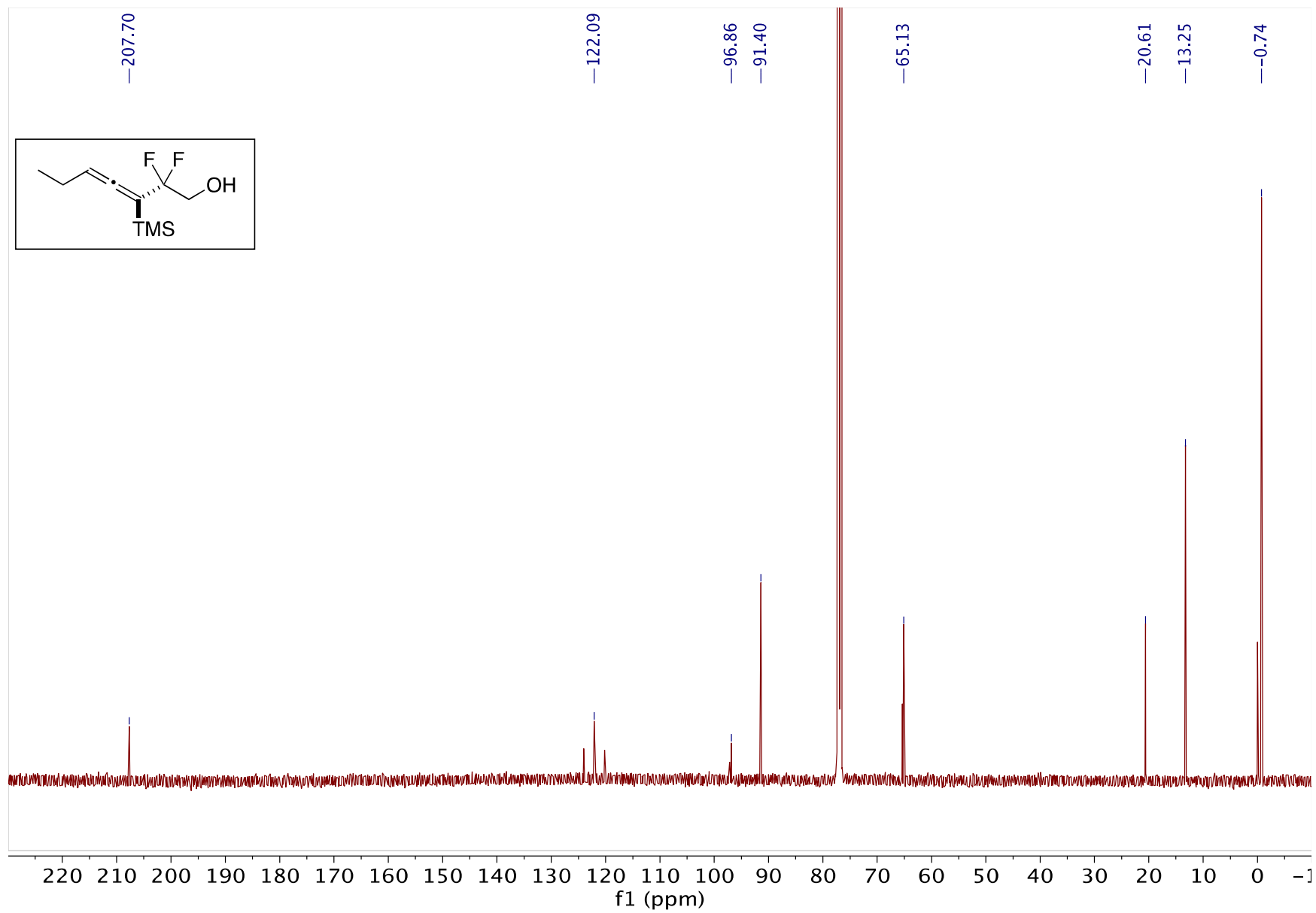
^{19}F NMR for Compound S3.



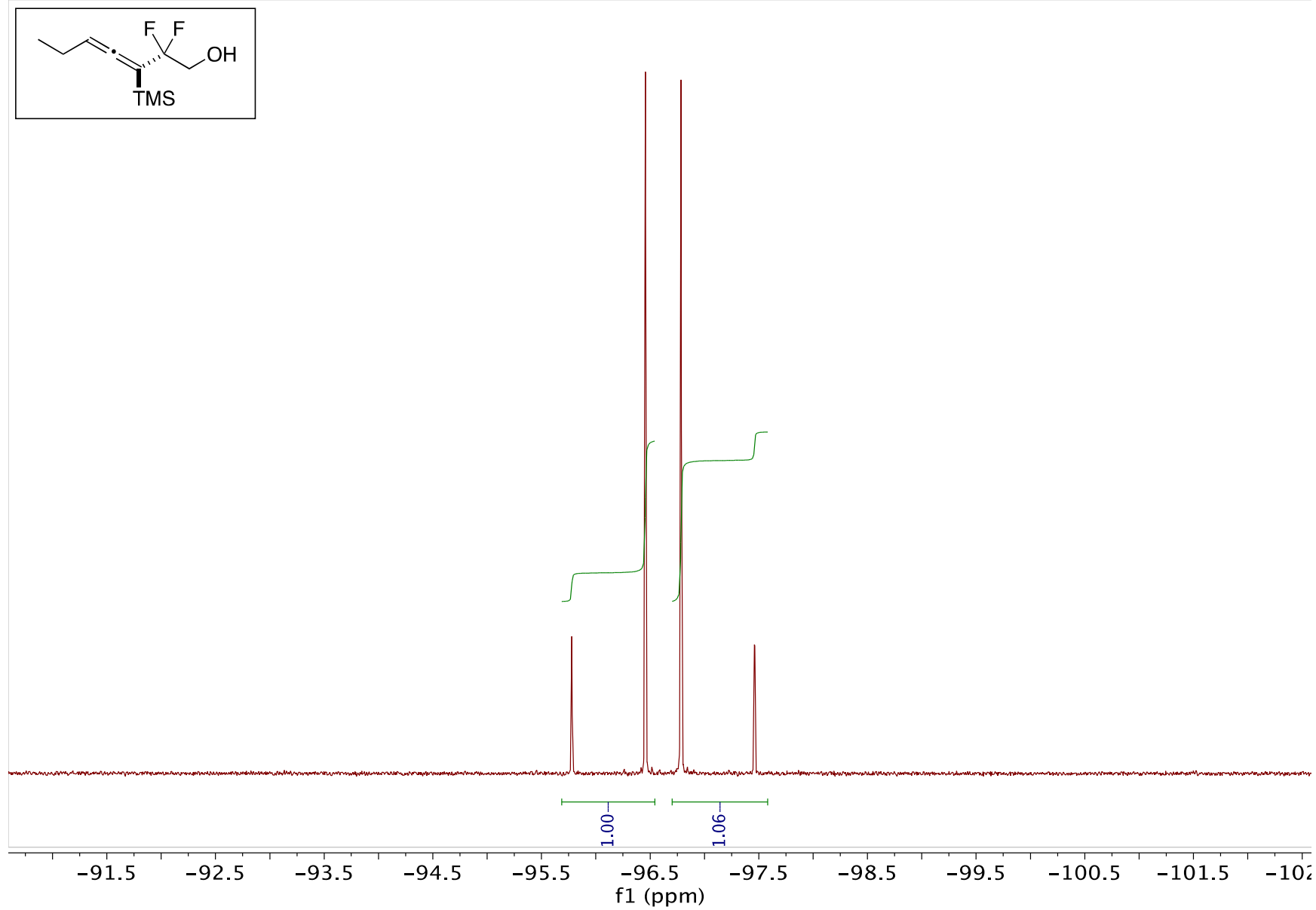
¹H NMR for Compound S4.



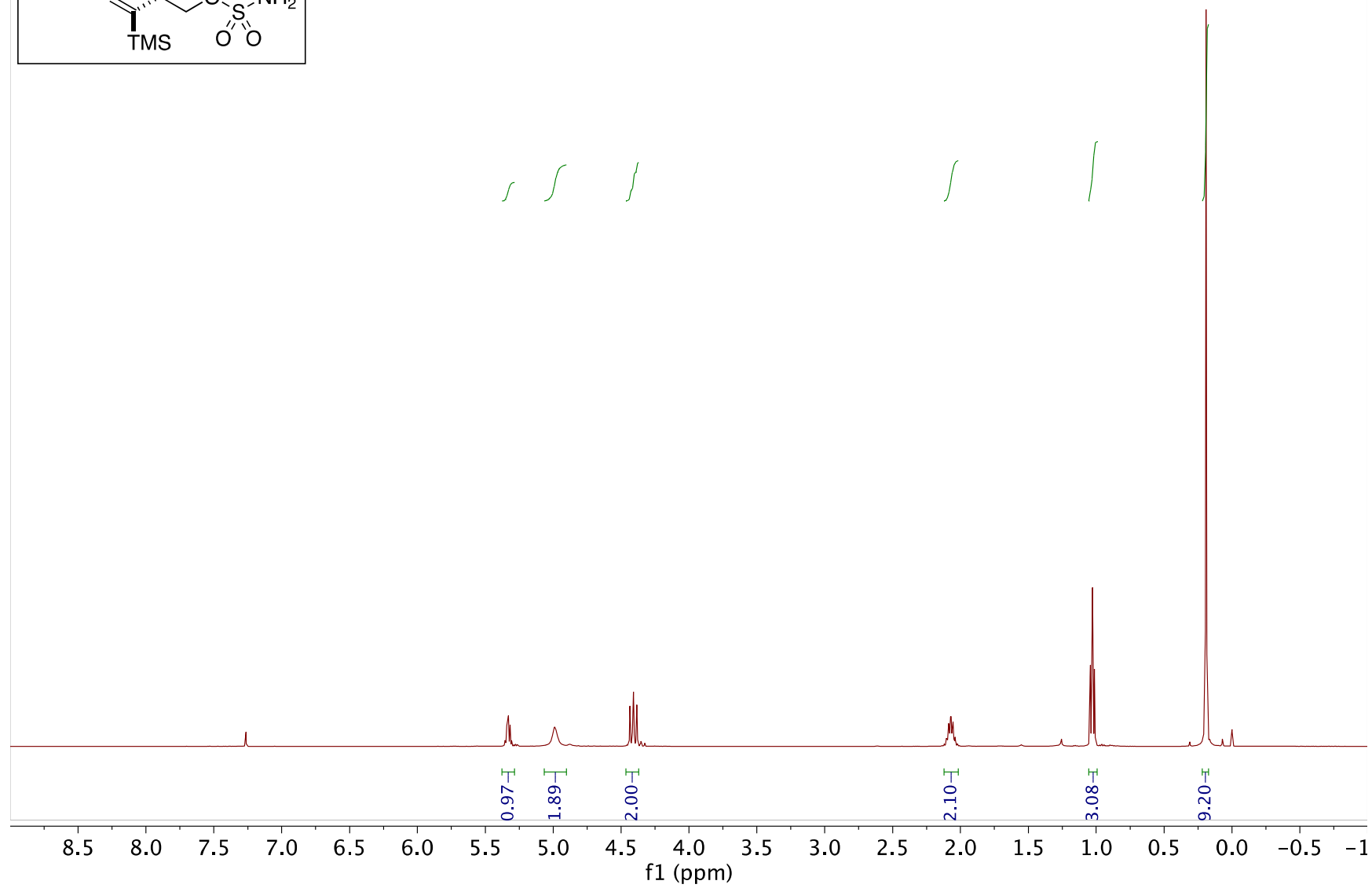
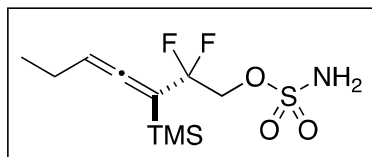
¹³C NMR for Compound S4.



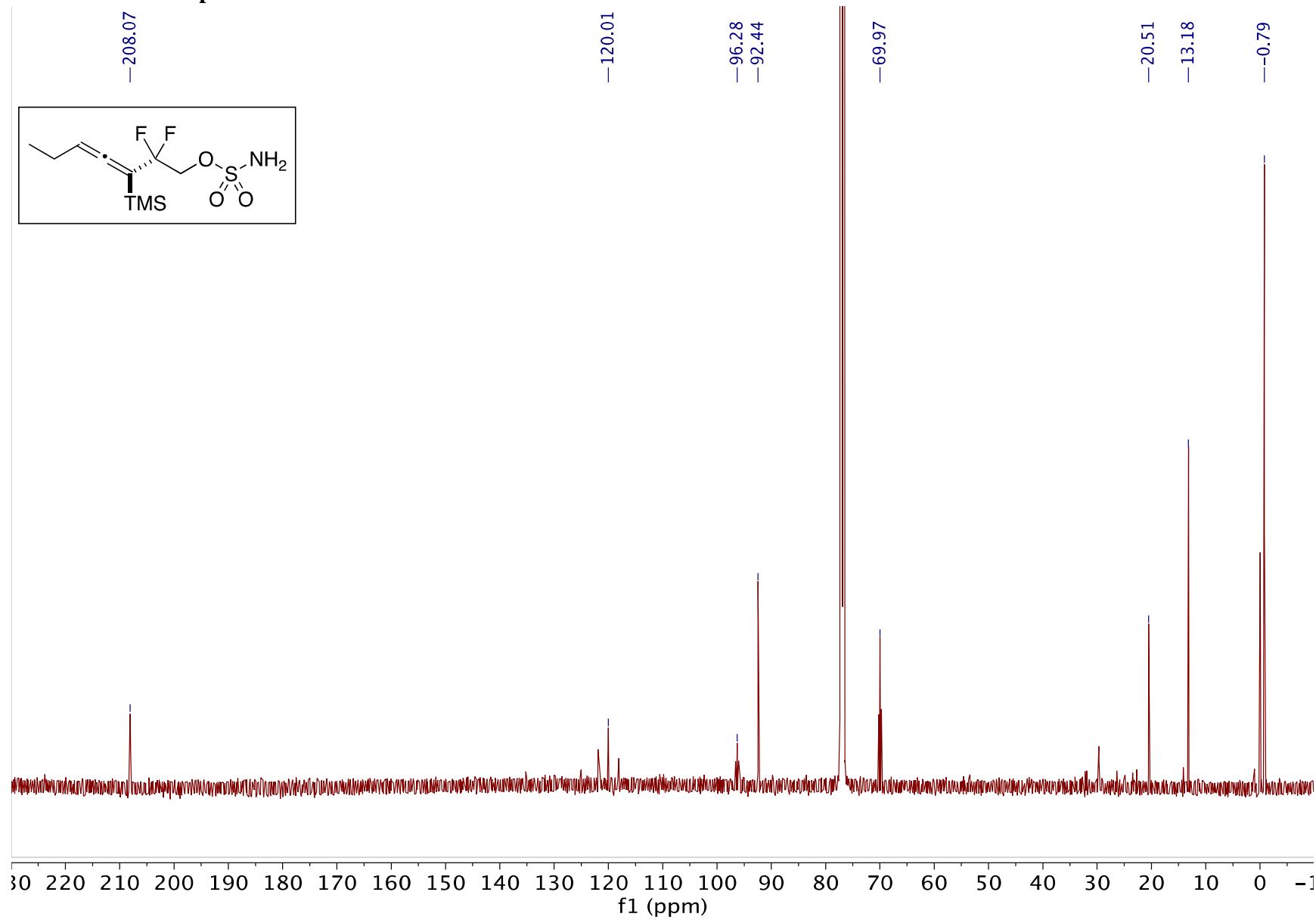
^{19}F NMR for Compound S4.



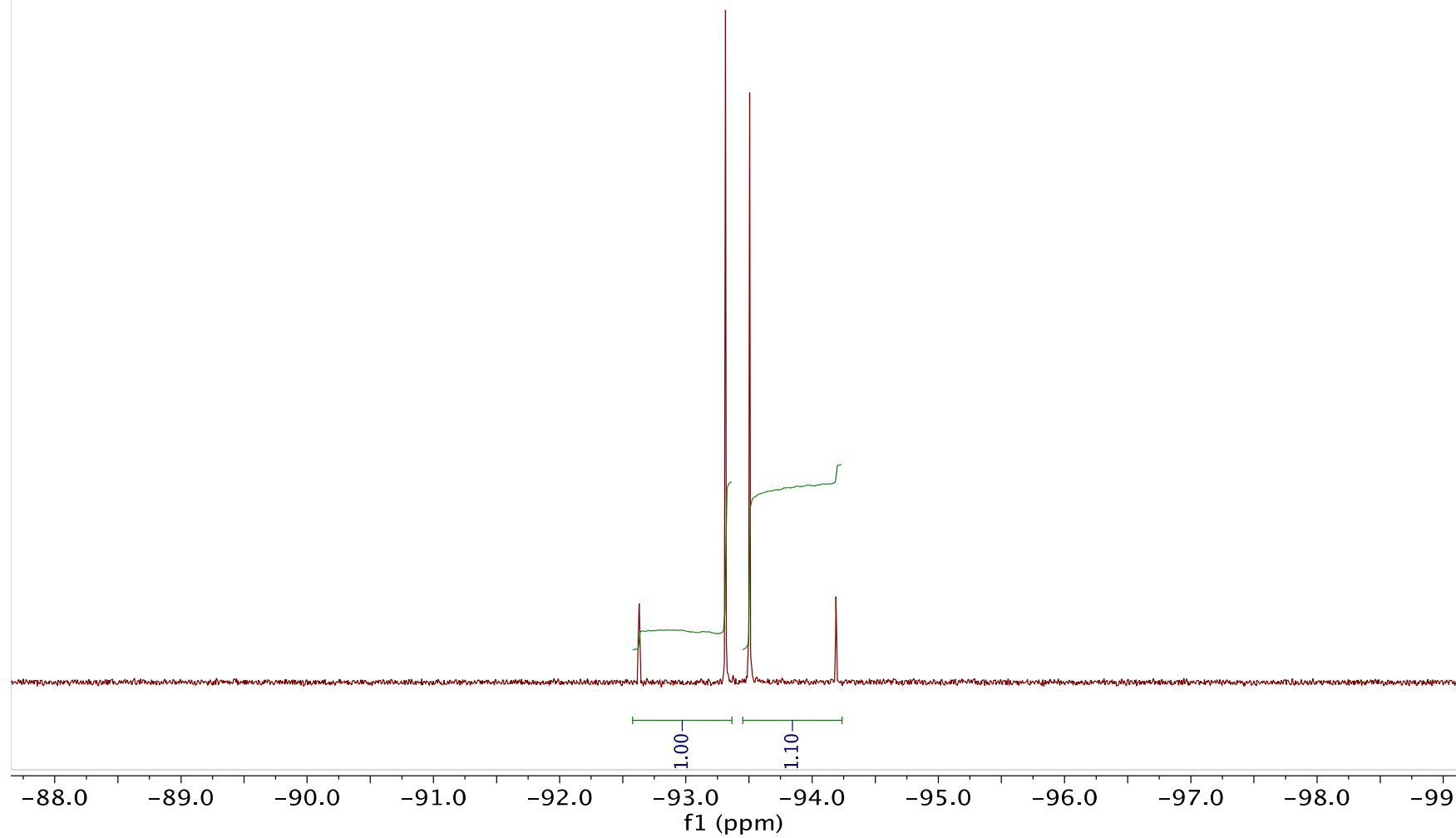
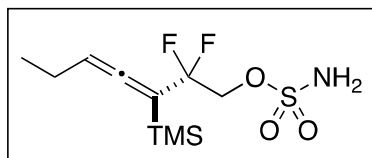
¹H NMR for Compound S5.



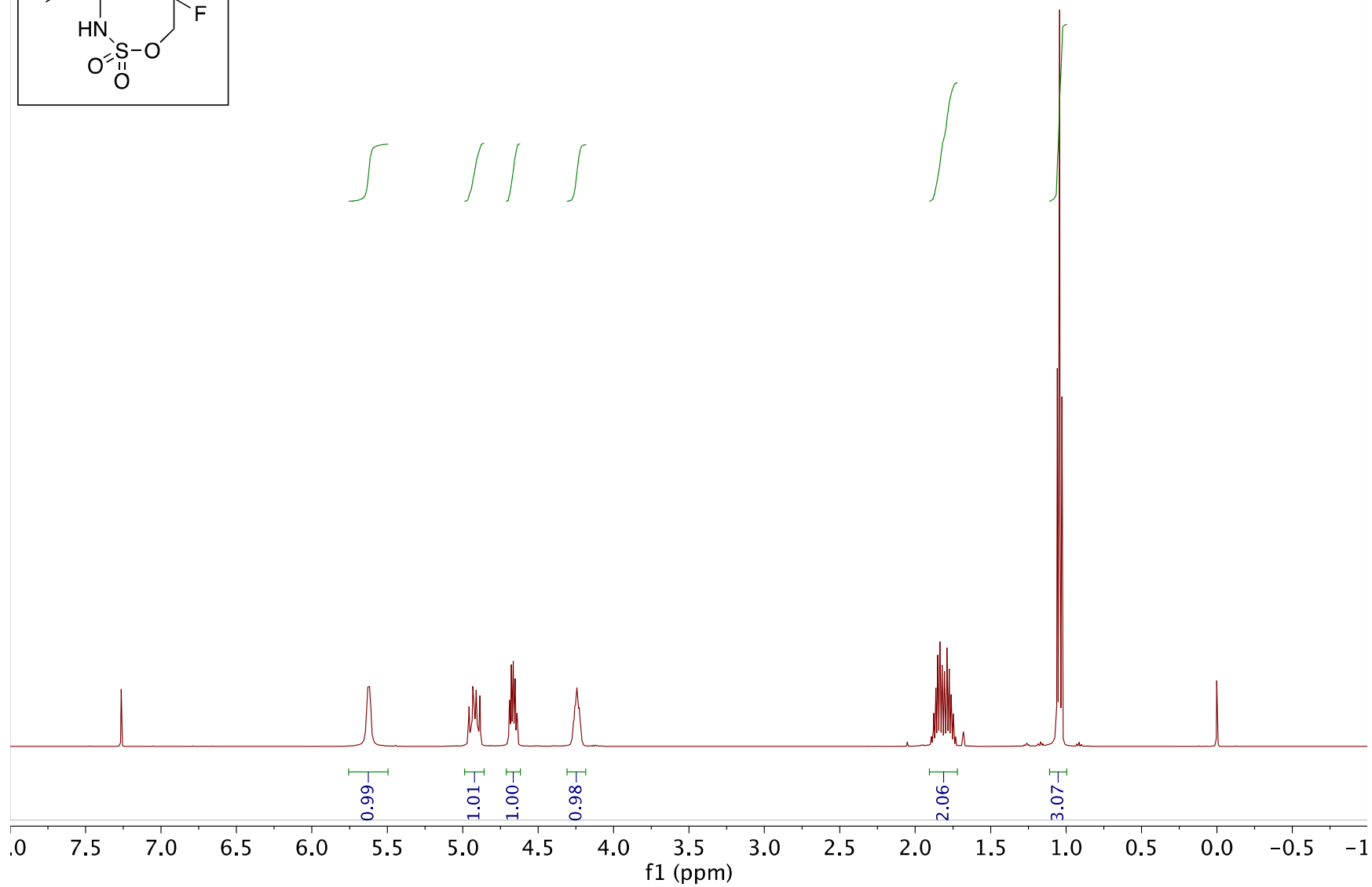
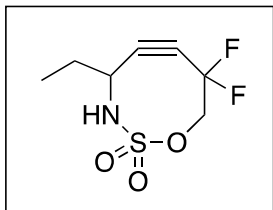
¹³C NMR for Compound S5.



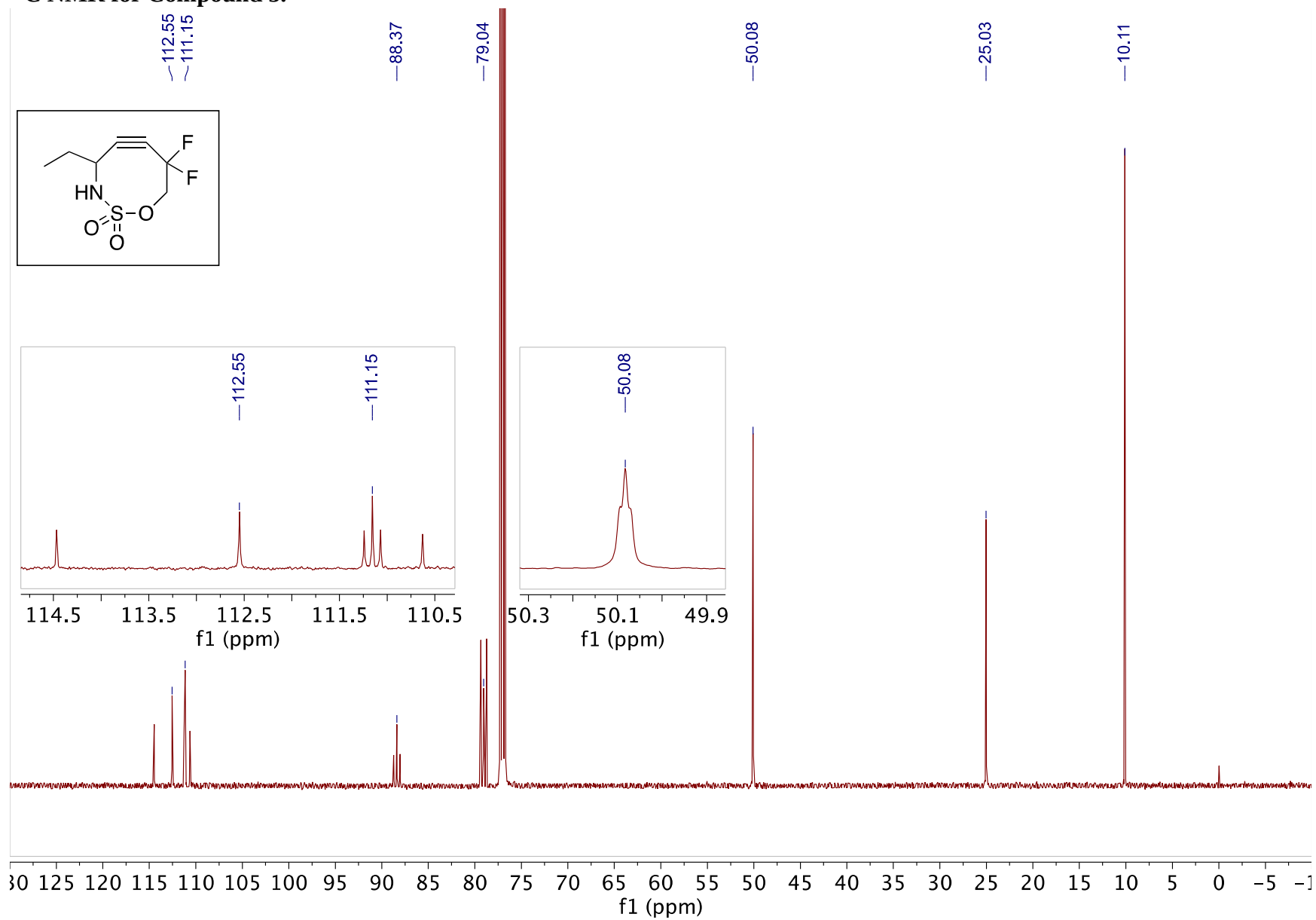
^{19}F NMR for Compound S5.



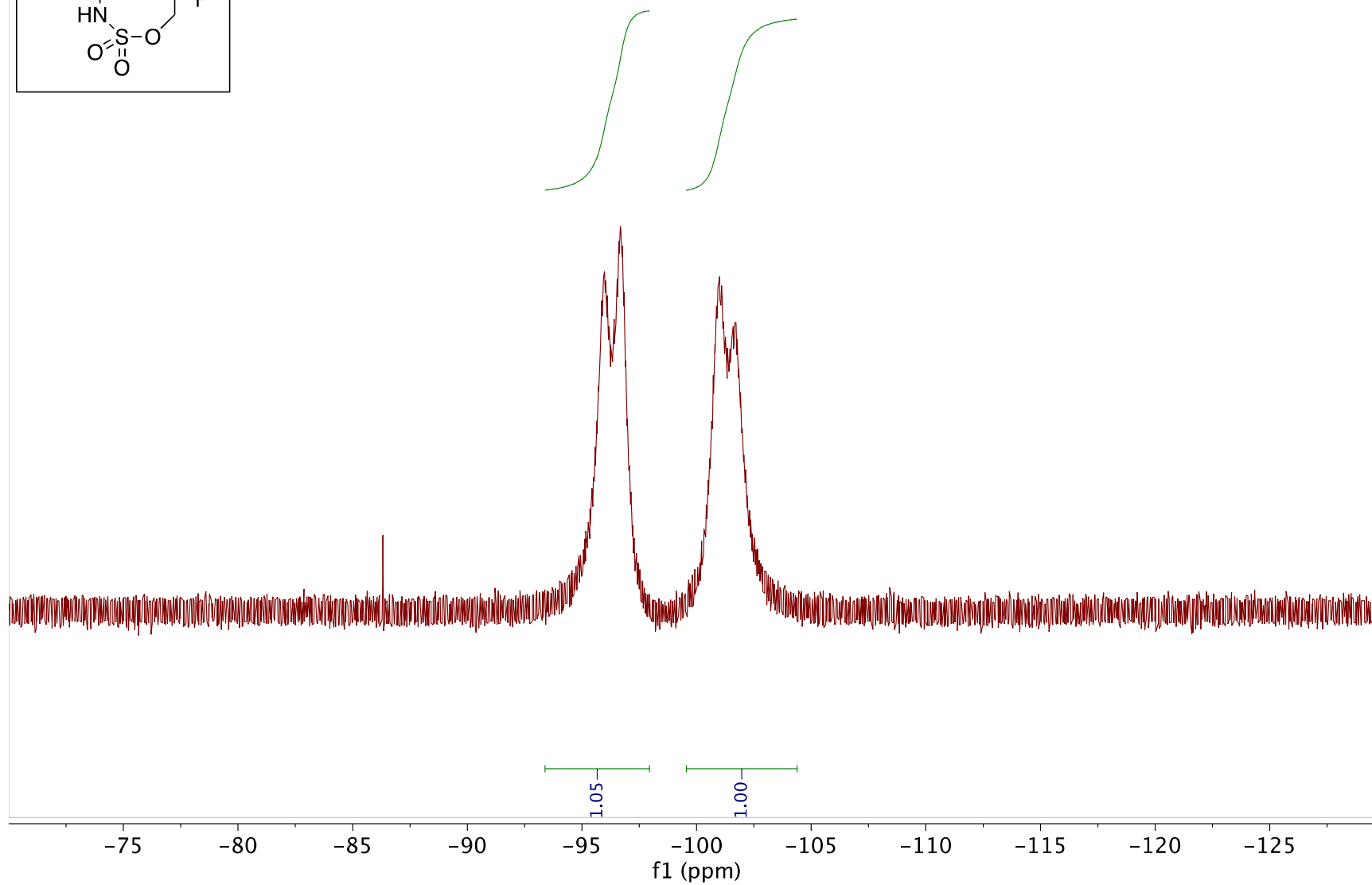
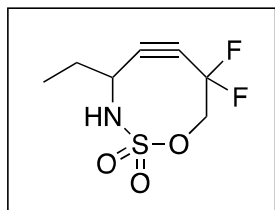
¹H NMR for Compound 5.



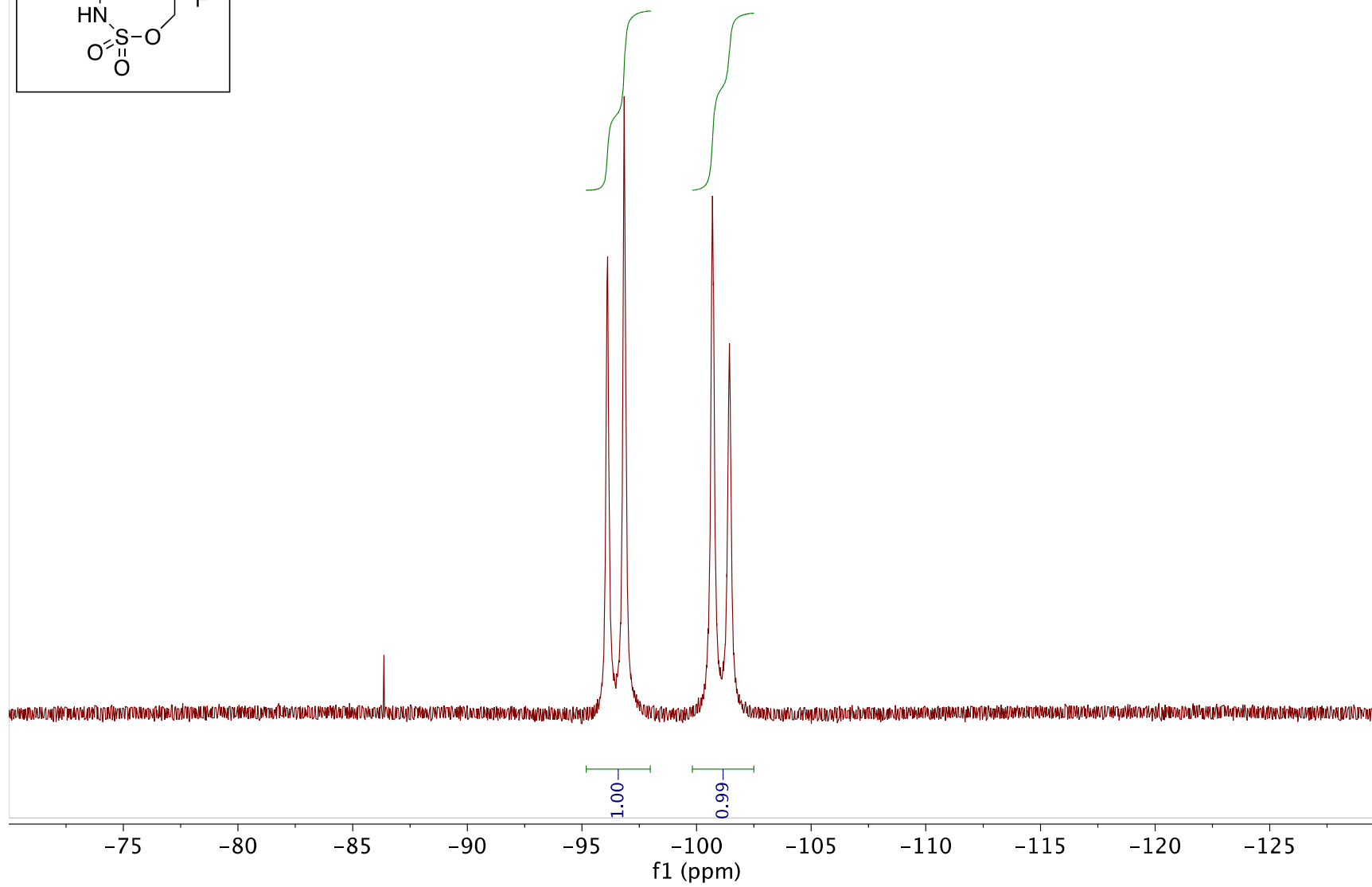
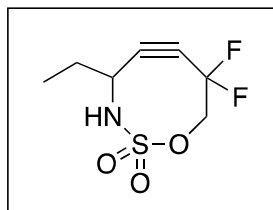
¹³C NMR for Compound 5.



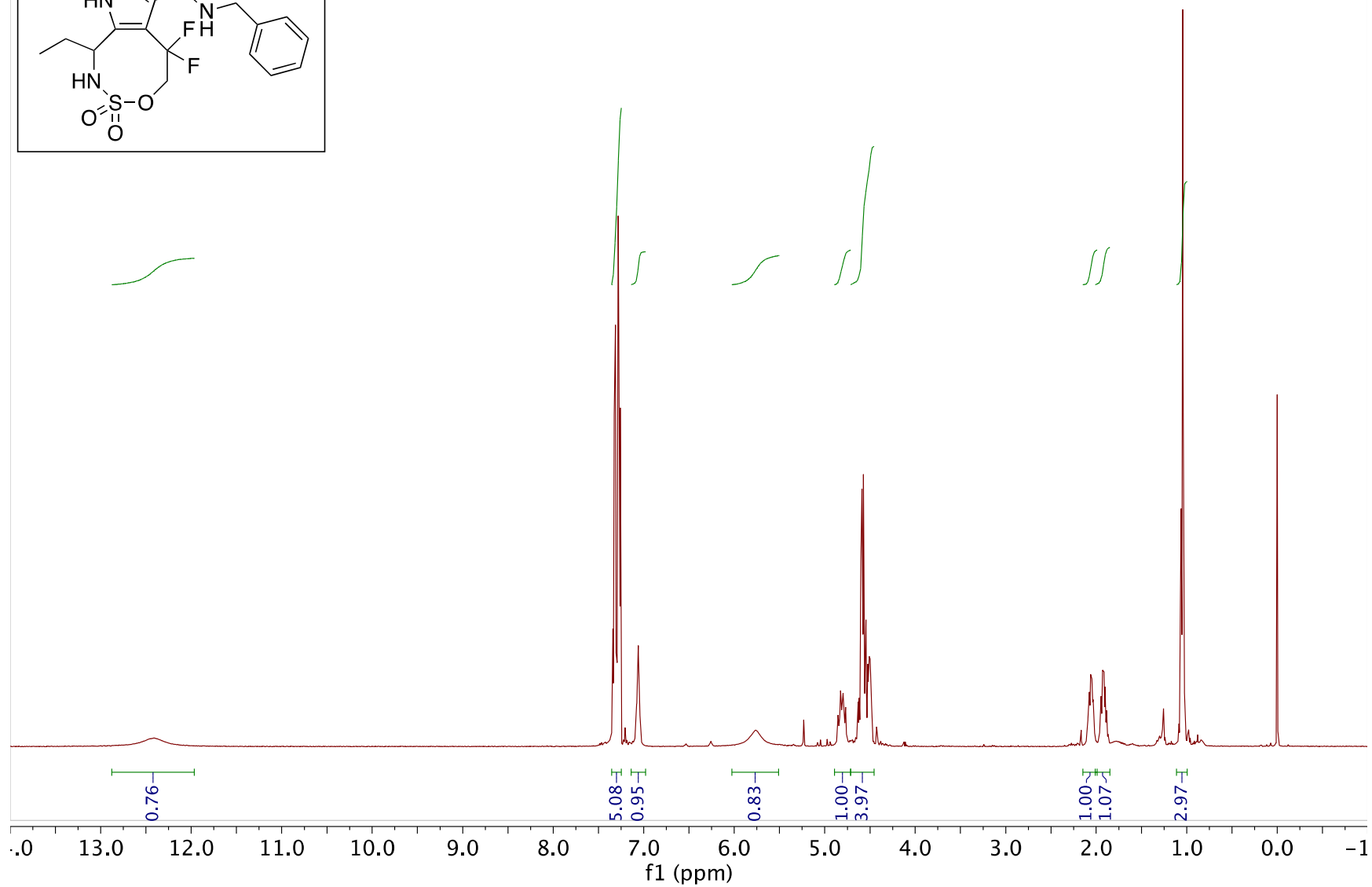
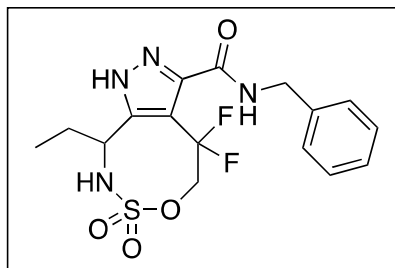
^{19}F NMR for Compound 5 (24°C, setpoint).



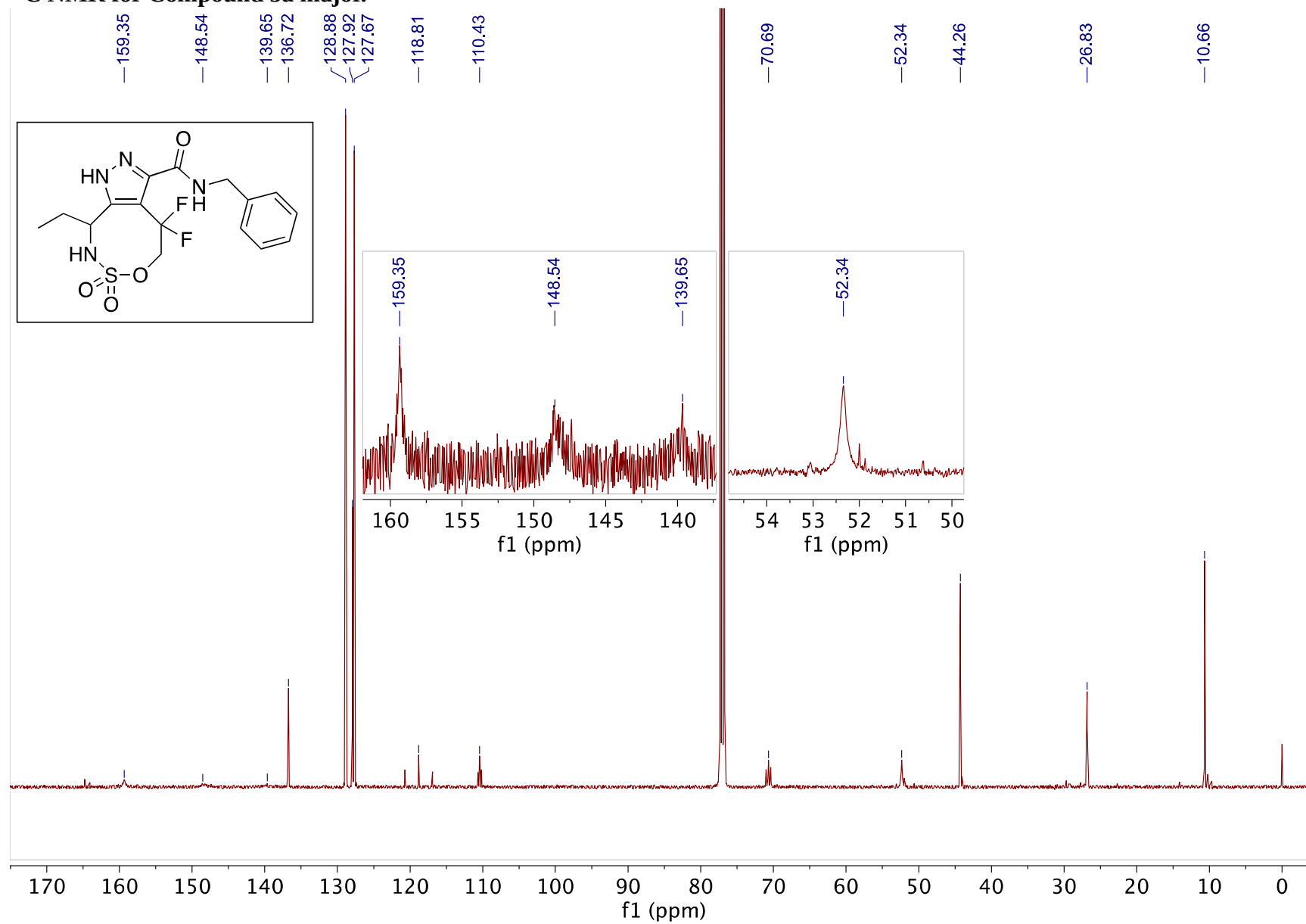
^{19}F NMR for Compound 5 (55°C, setpoint).



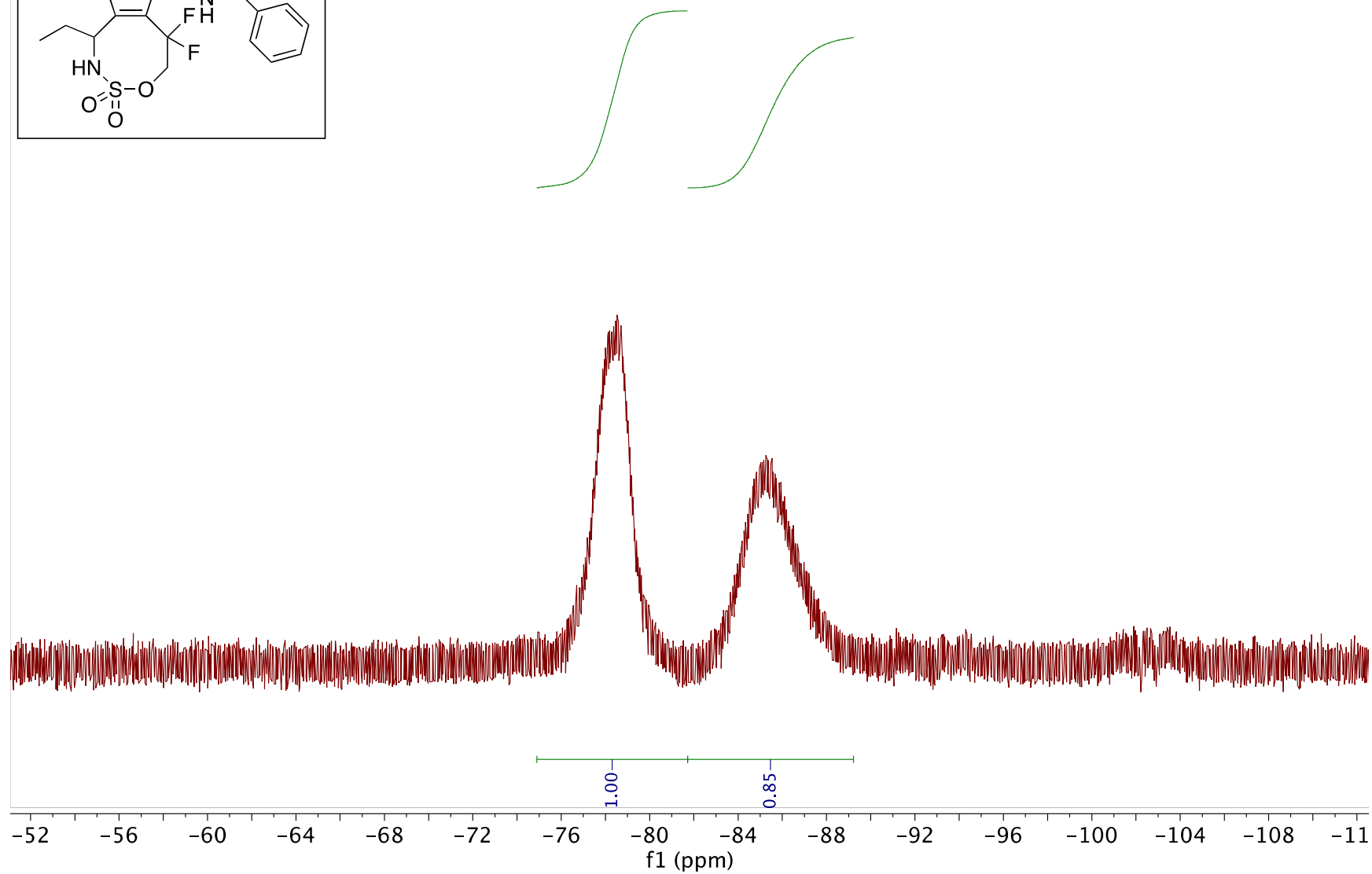
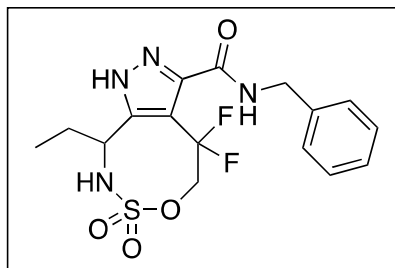
¹H NMR for Compound 5a major.



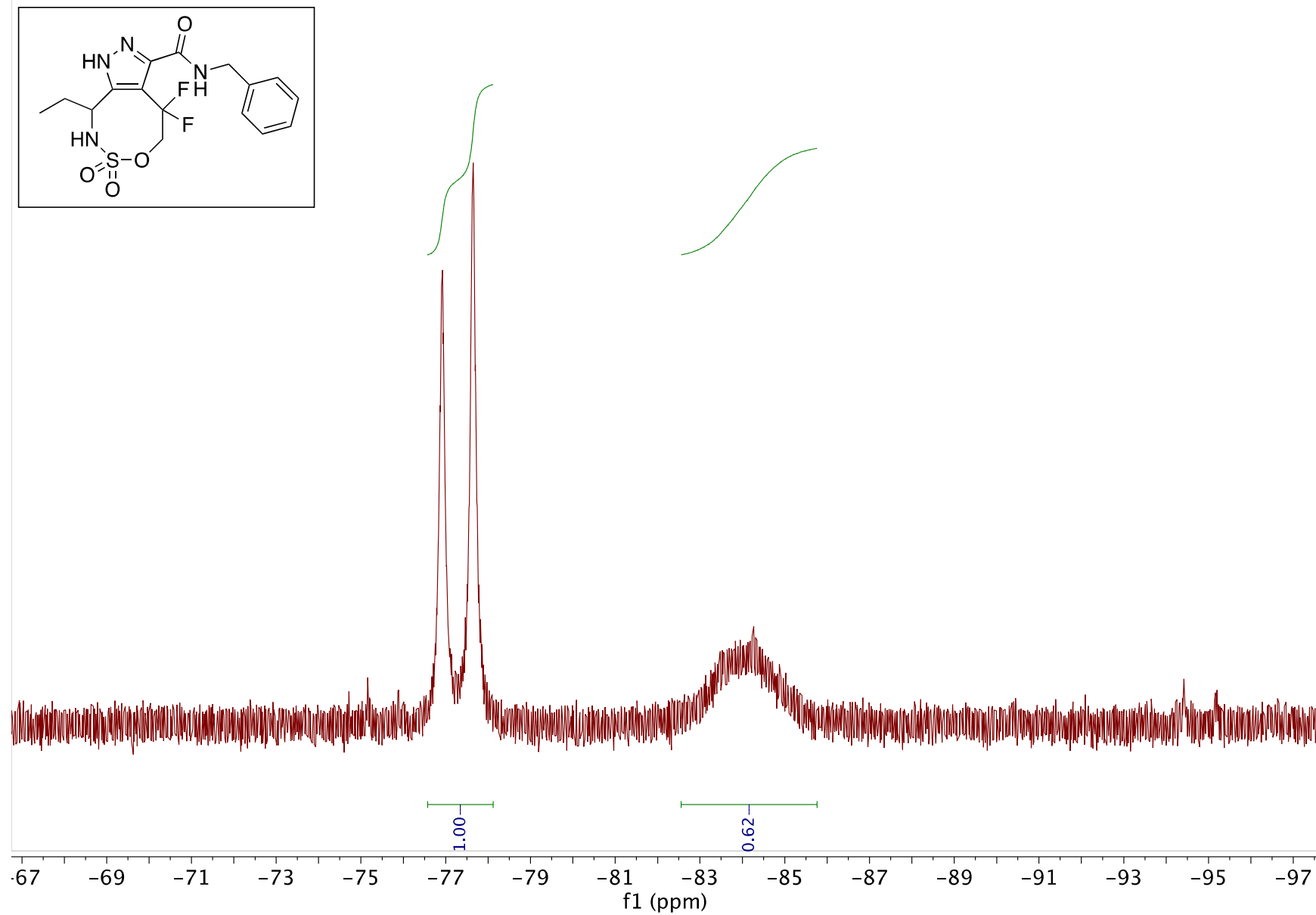
^{13}C NMR for Compound 5a major.



^{19}F NMR for Compound 5a major (at 24°C).

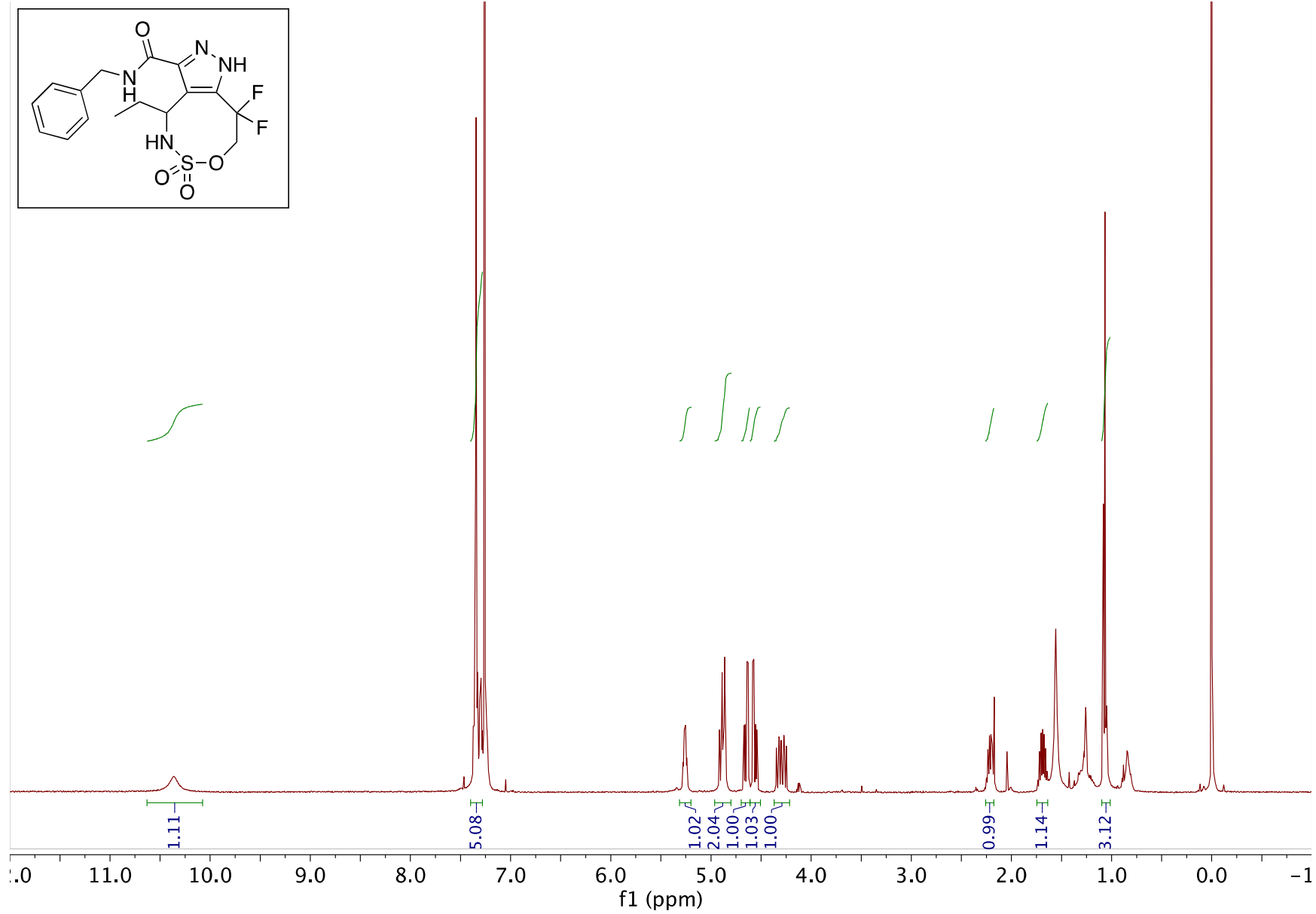


^{19}F NMR for Compound 5a major (at 55°C, setpoint).

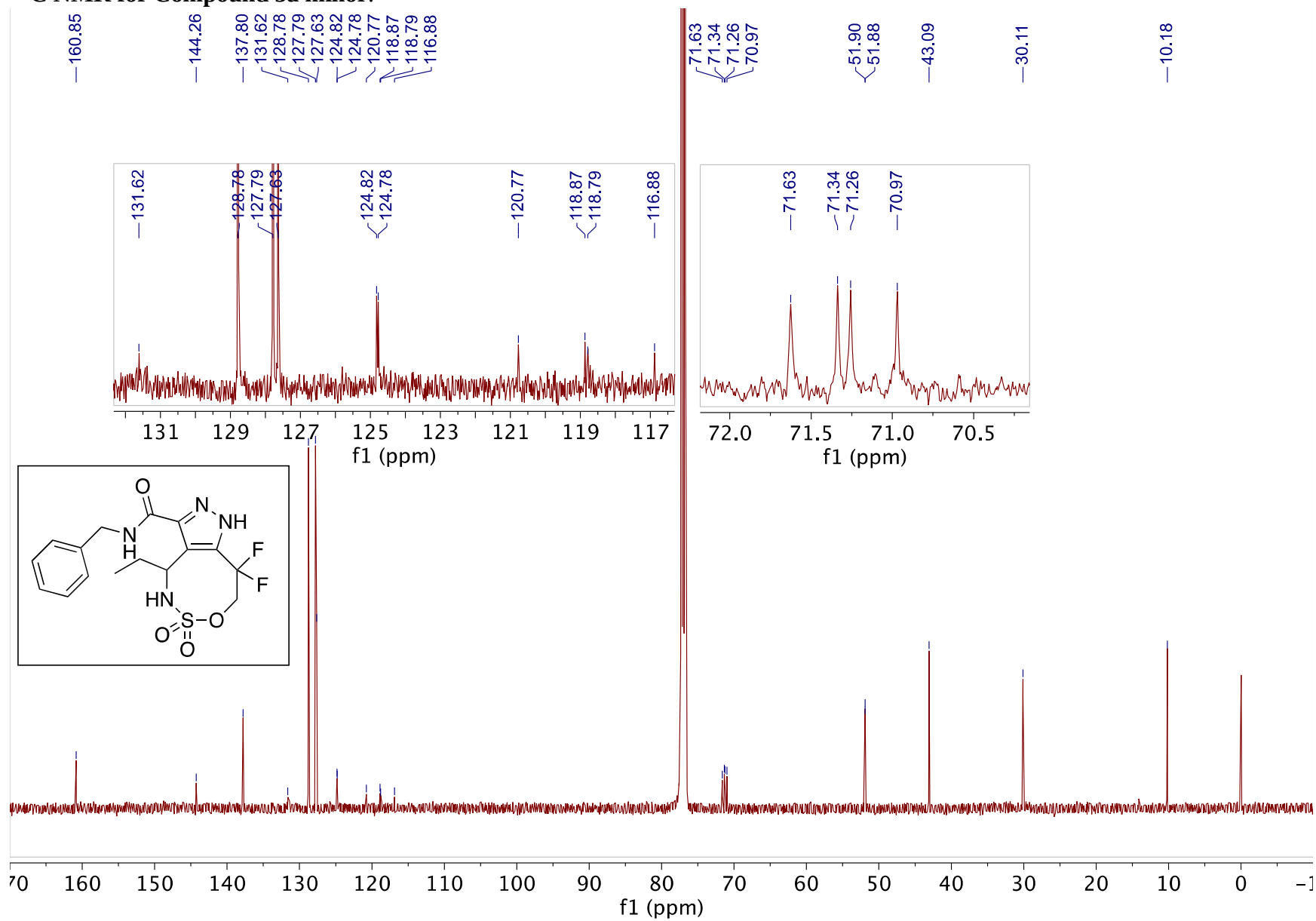


S2-71

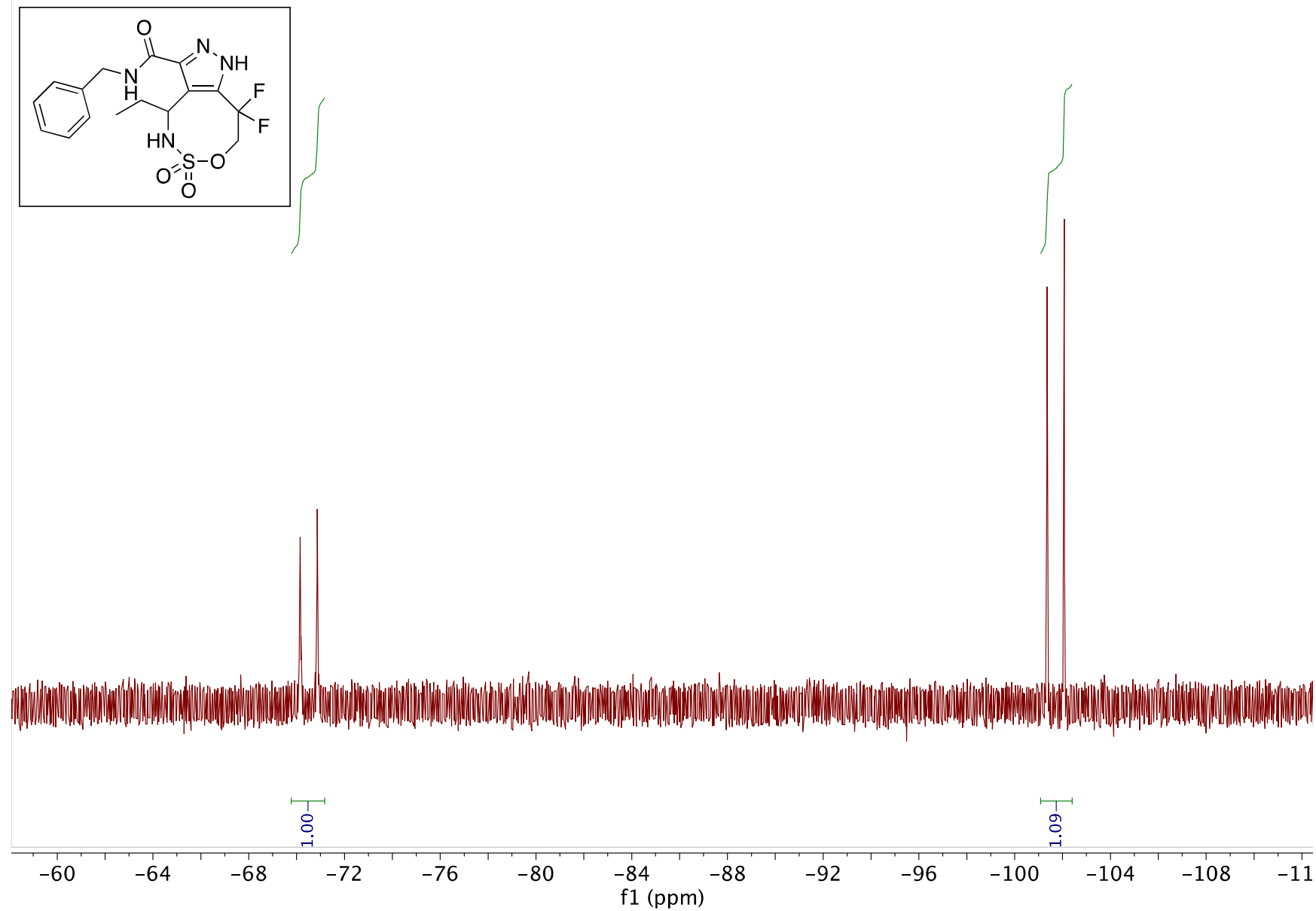
¹H NMR for Compound 5a minor.



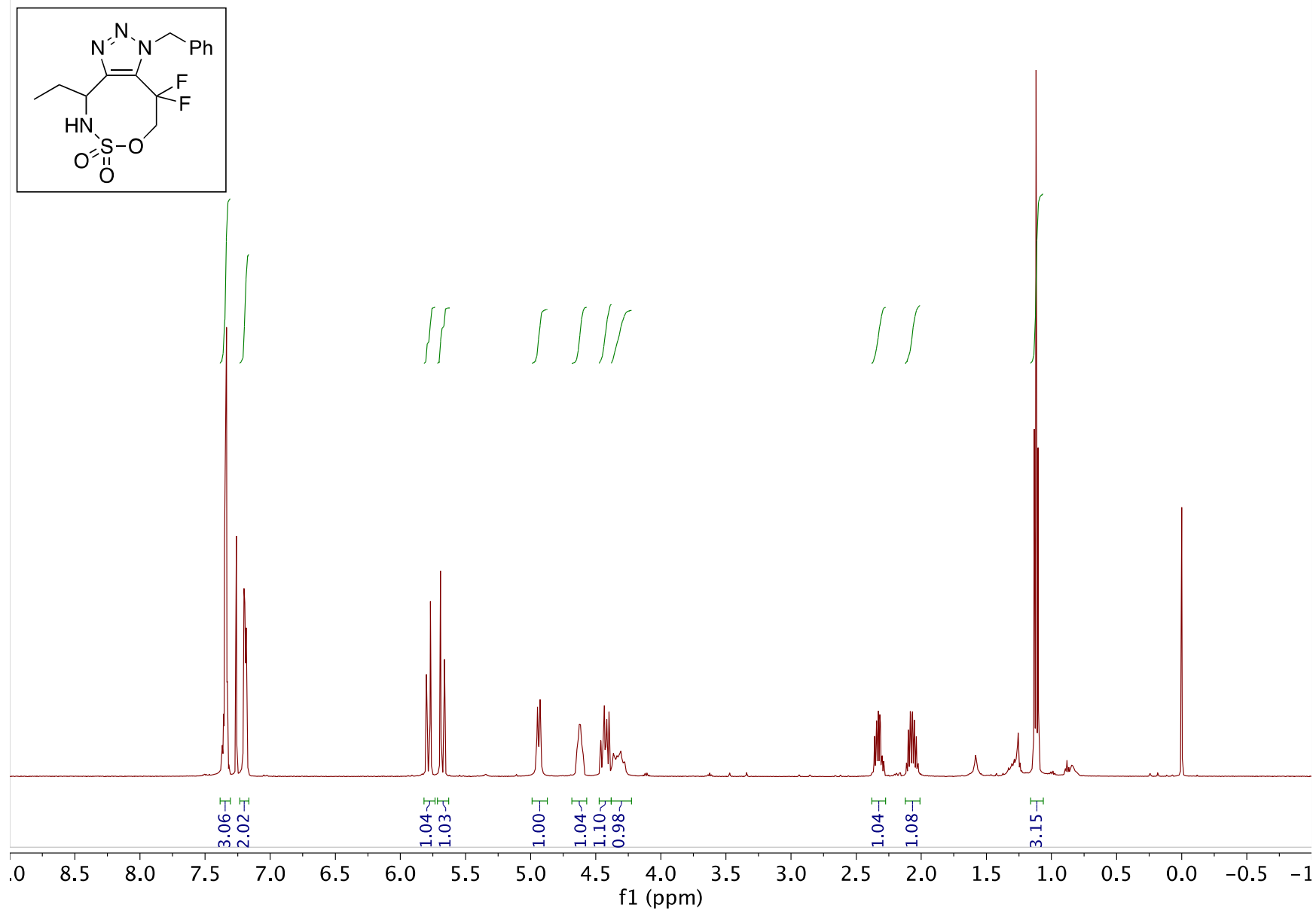
¹³C NMR for Compound 5a minor.



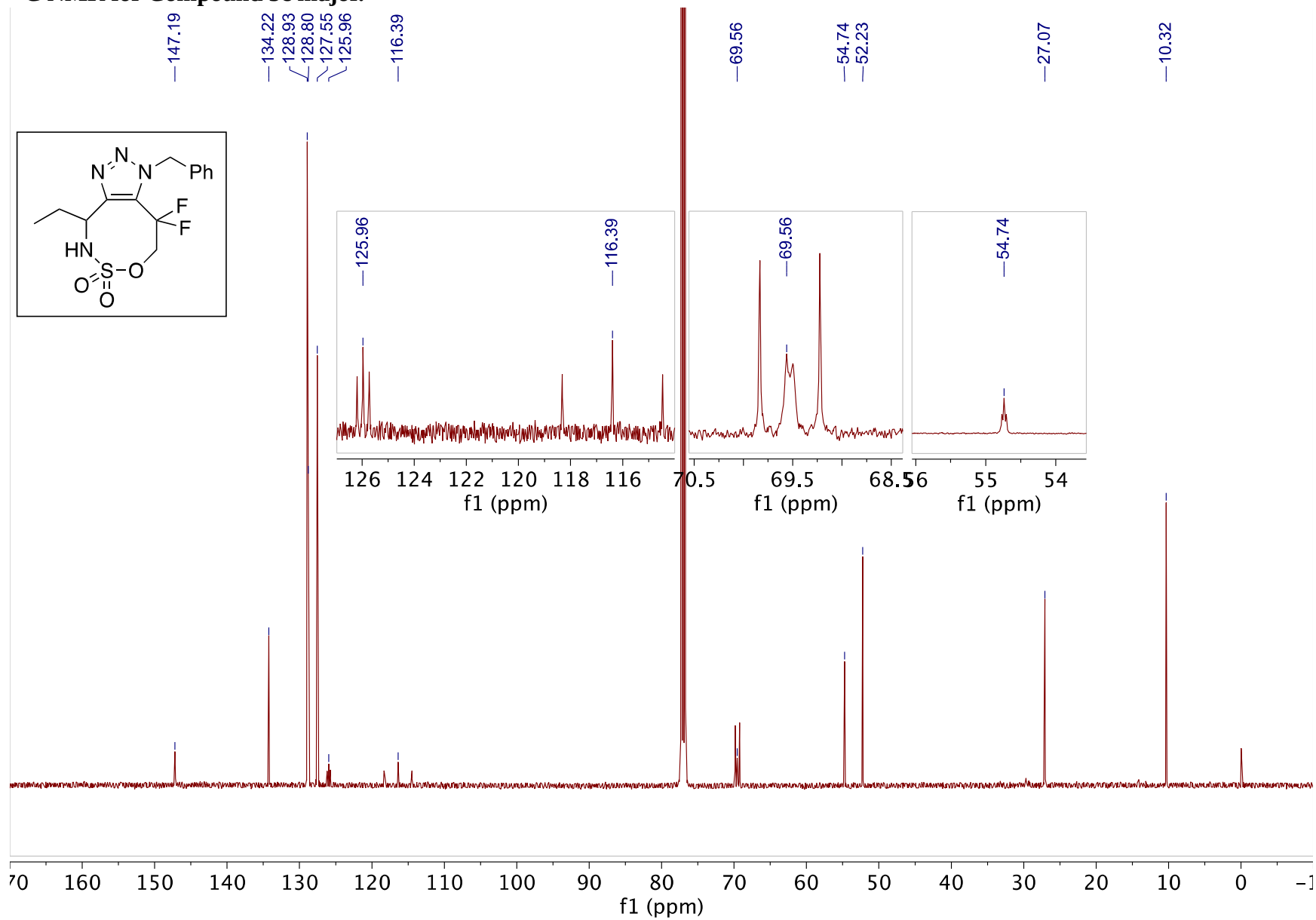
¹⁹F NMR for Compound 5a minor.



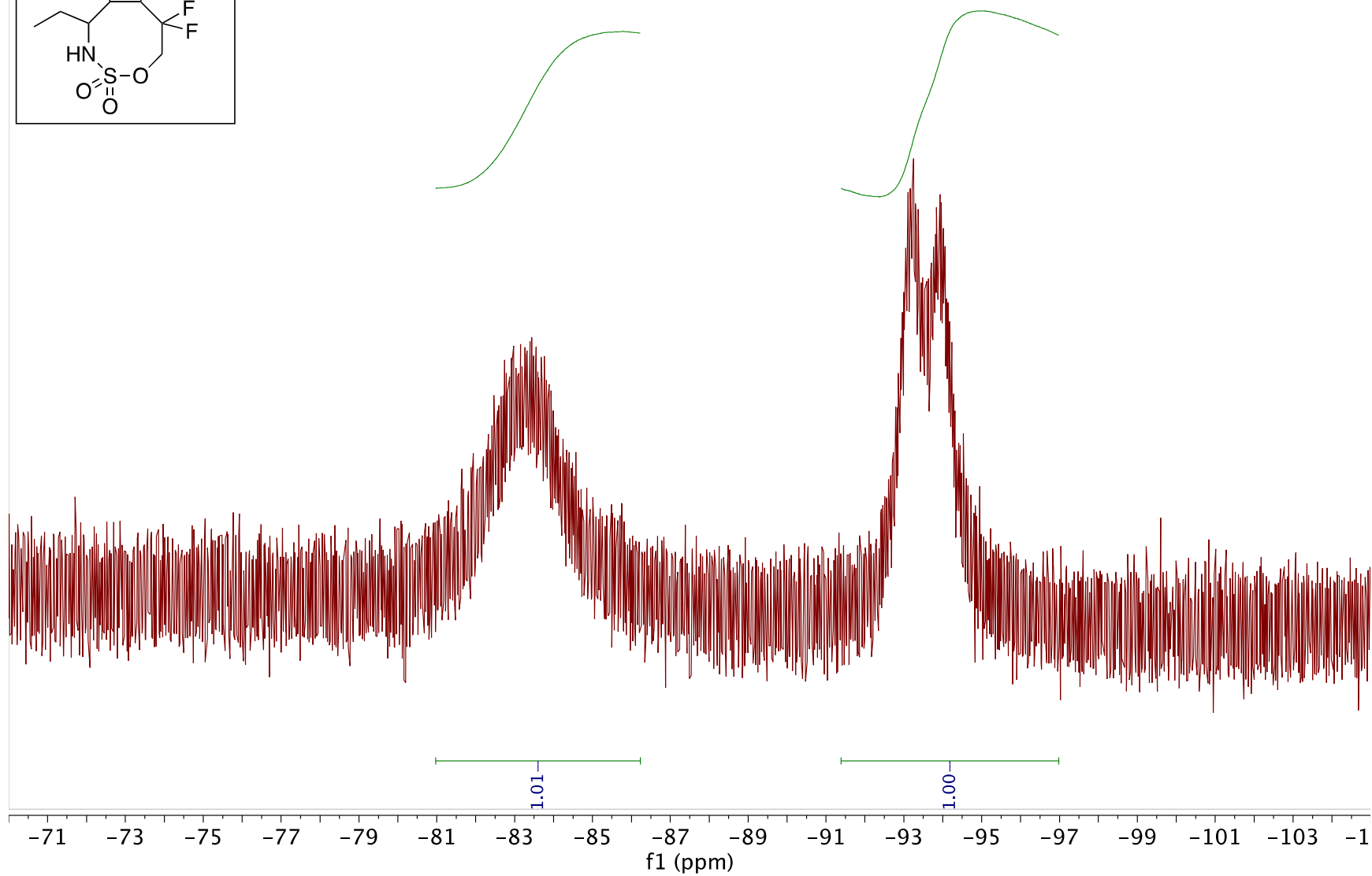
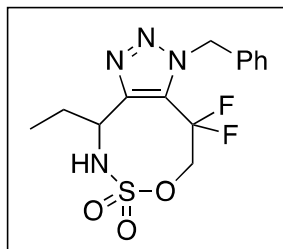
¹H NMR for Compound 5c major.



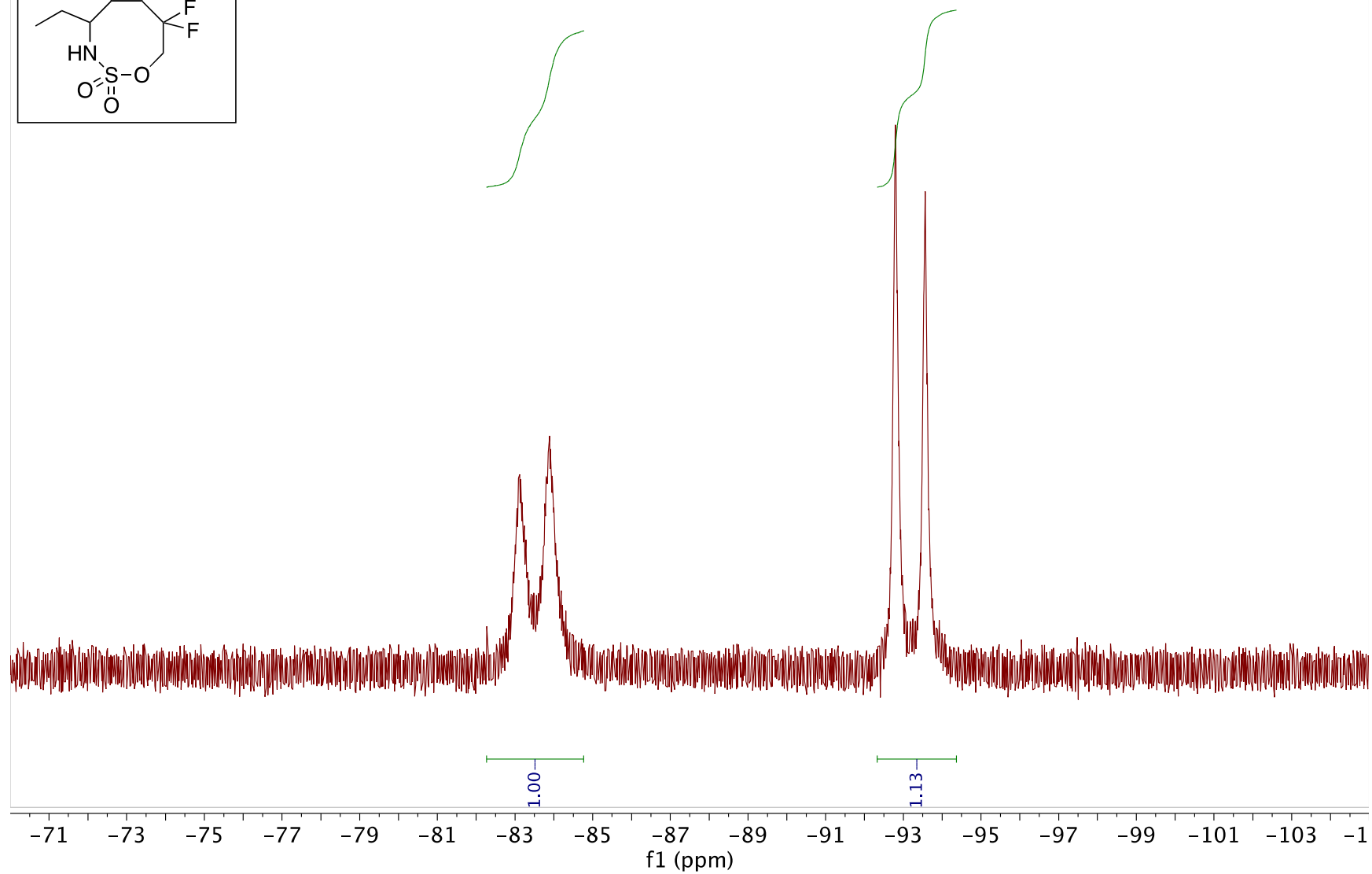
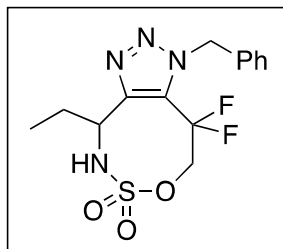
¹³C NMR for Compound 5c major.



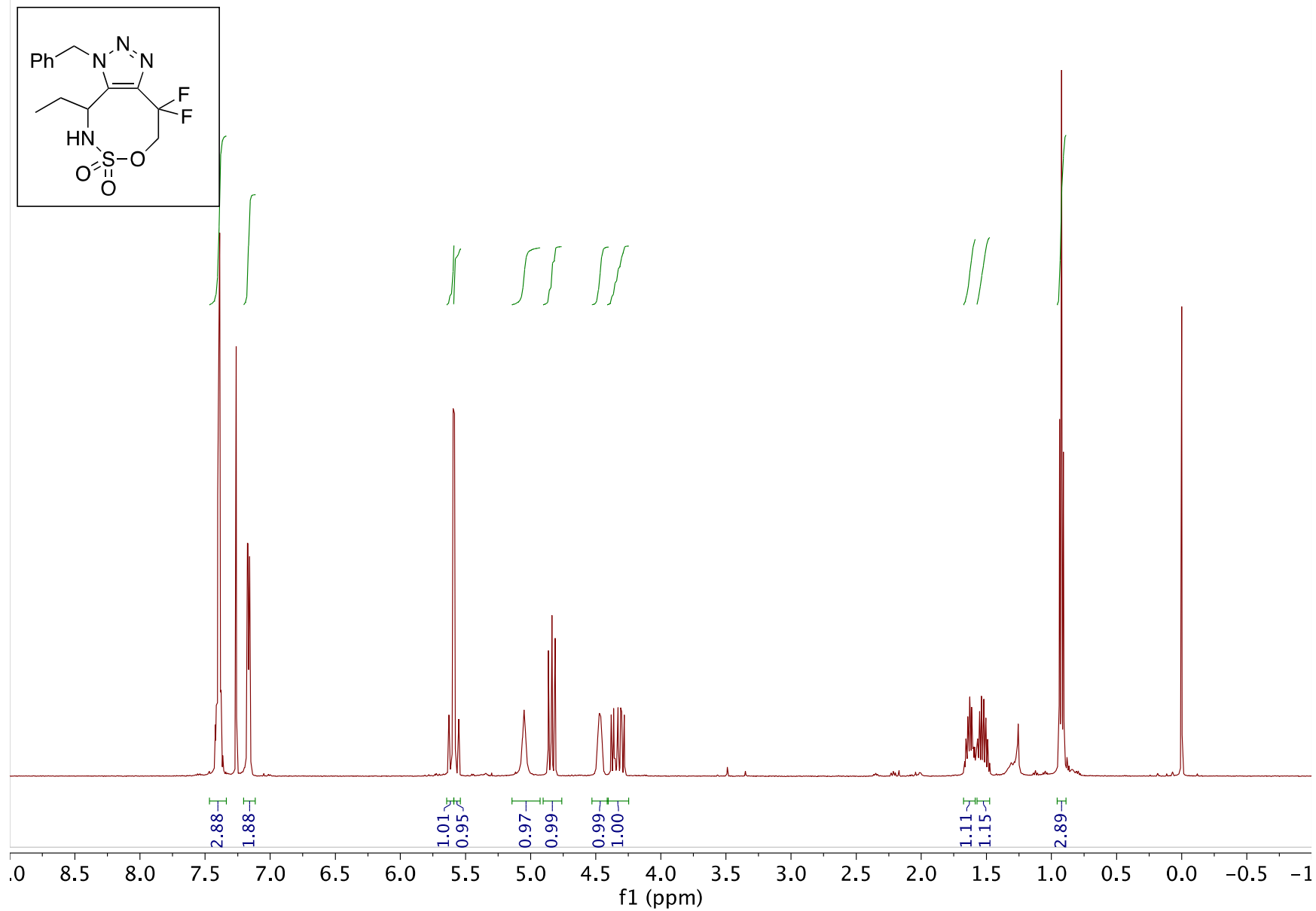
^{19}F NMR for Compound 5c major (at 24°C).



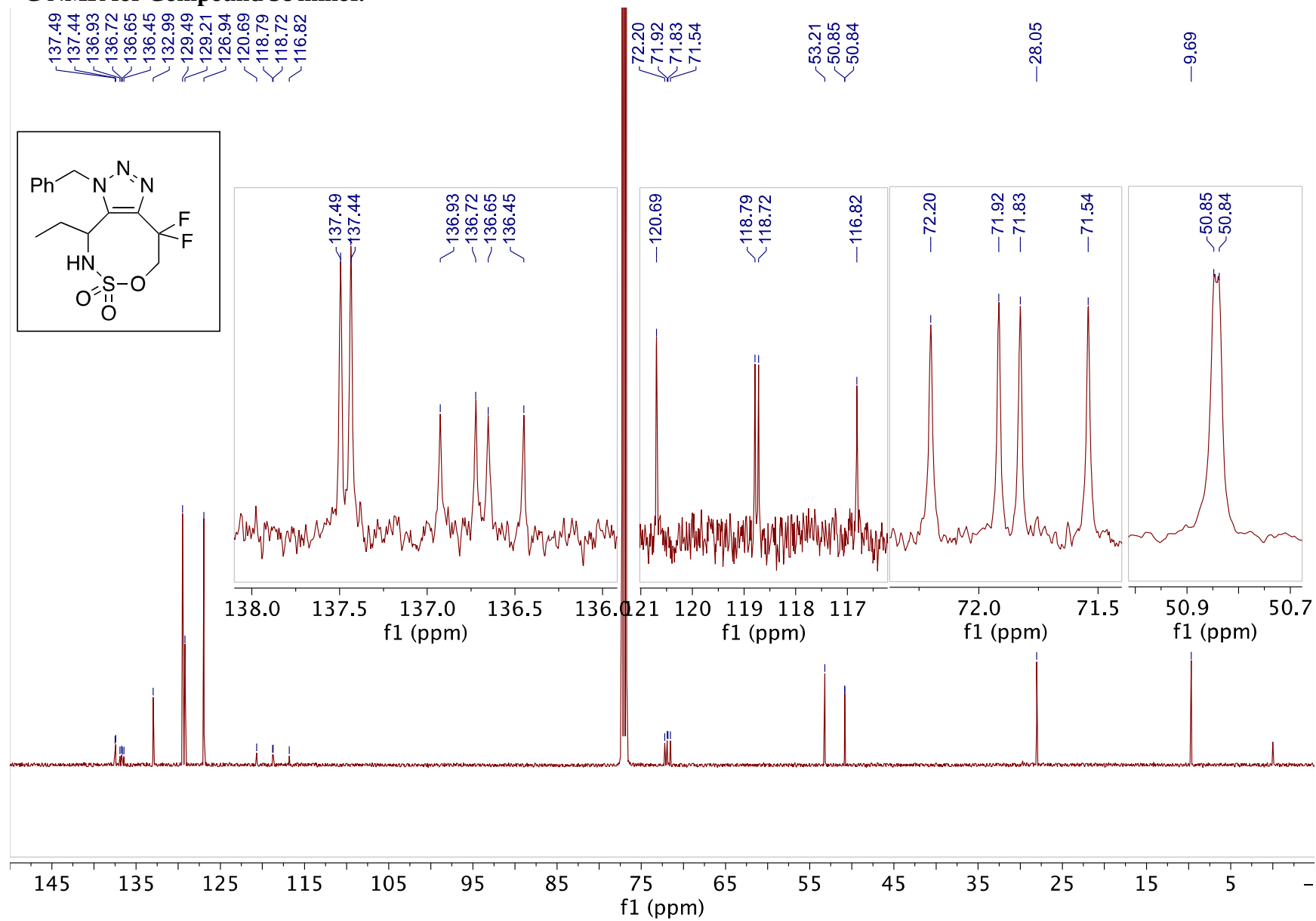
^{19}F NMR for Compound 5c major (at 55°C, setpoint).



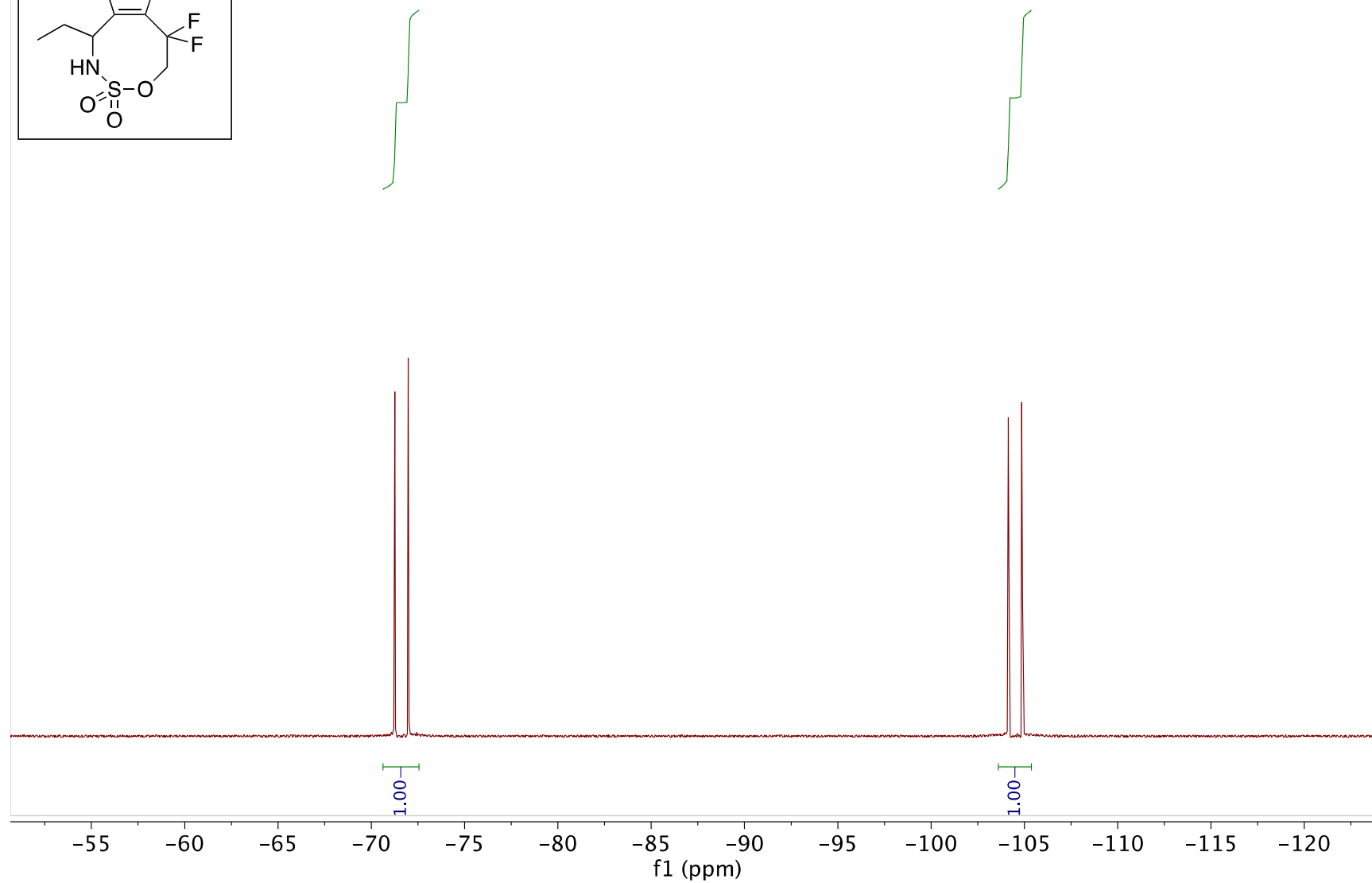
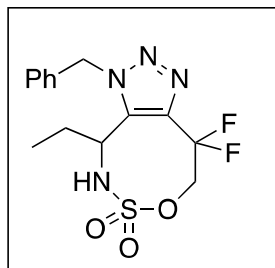
¹H NMR for Compound 5c minor.



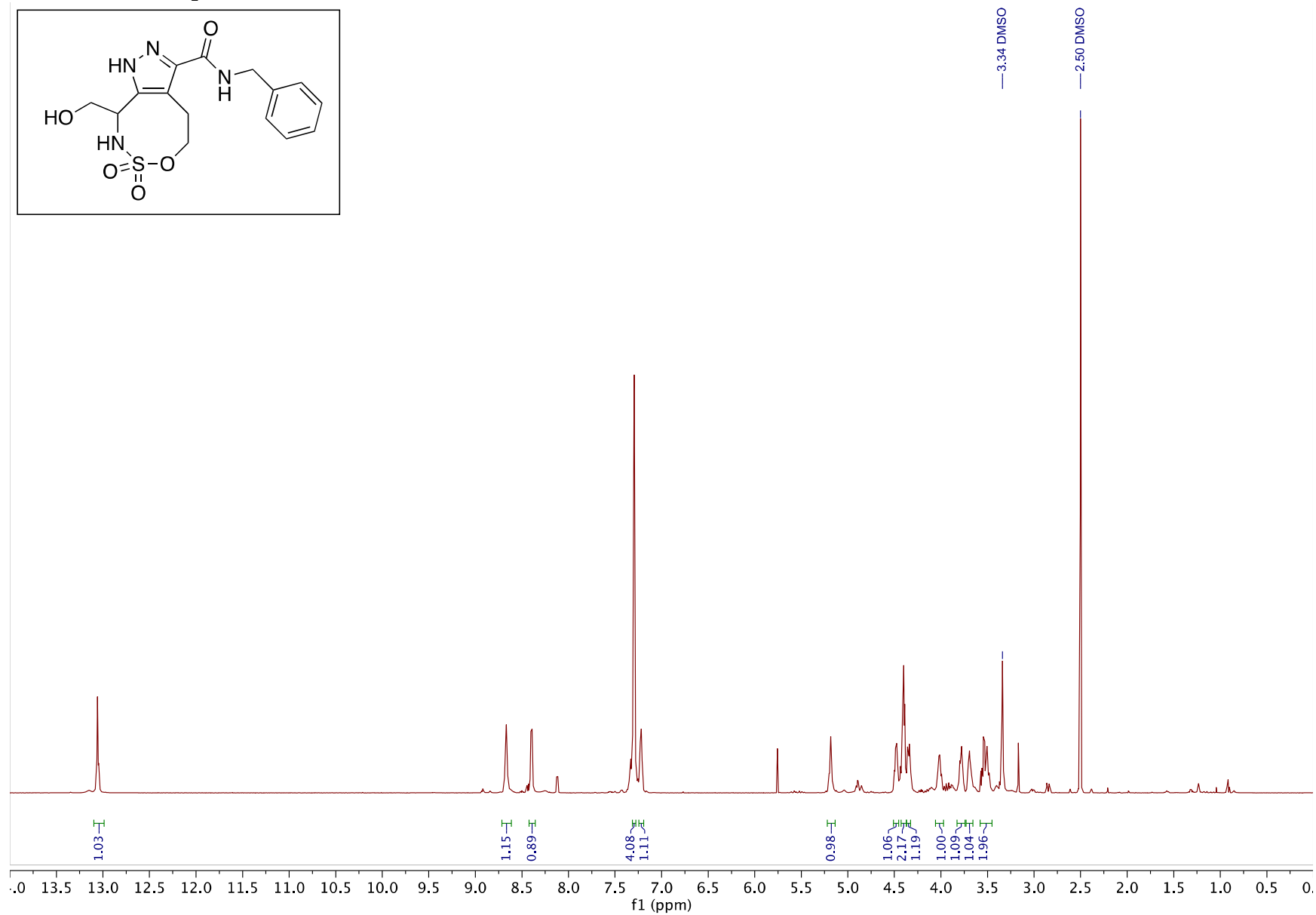
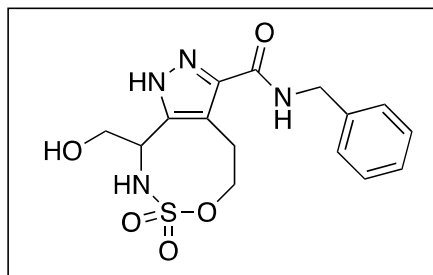
¹³C NMR for Compound 5c minor.



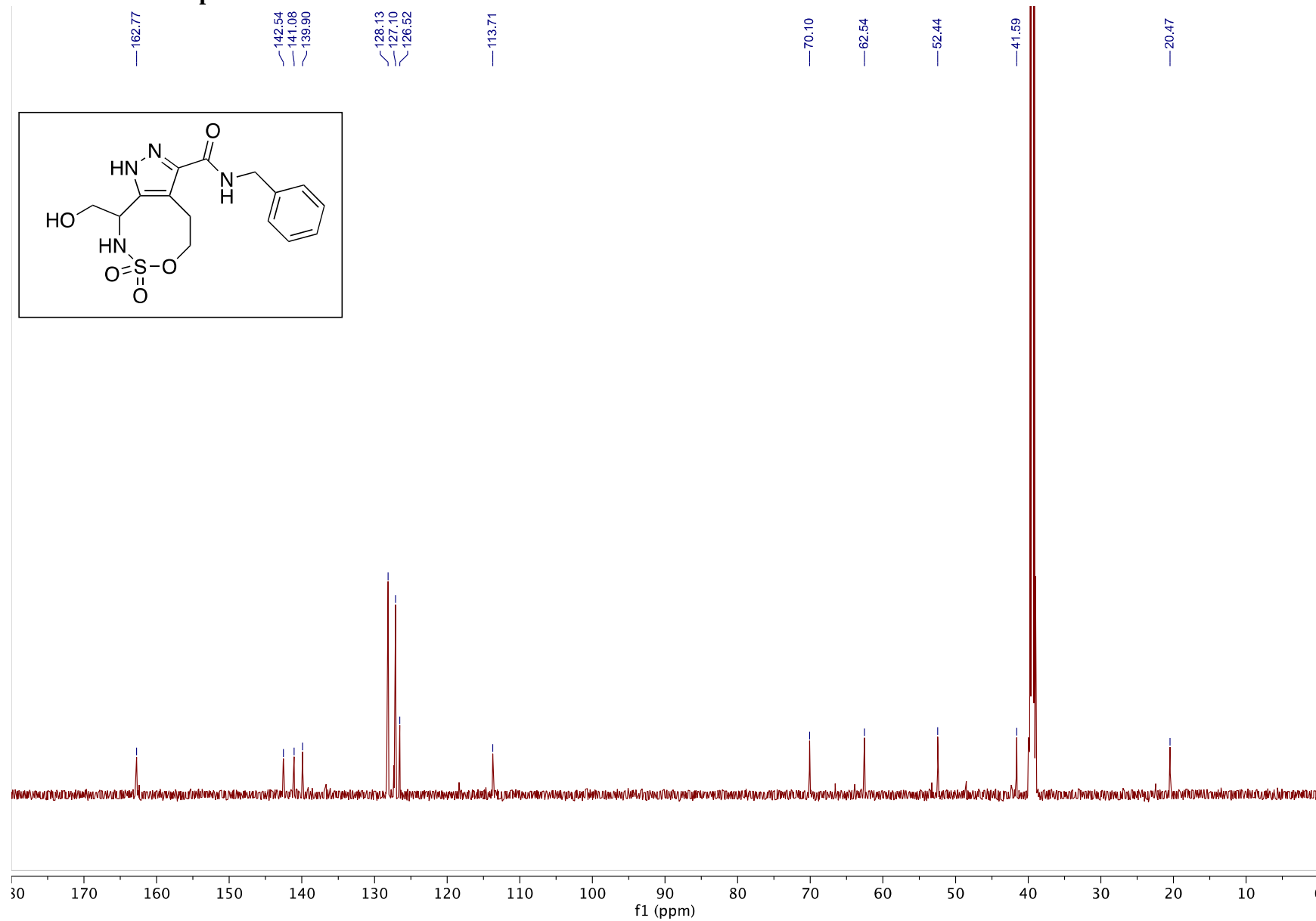
¹⁹F NMR for Compound 5c minor.



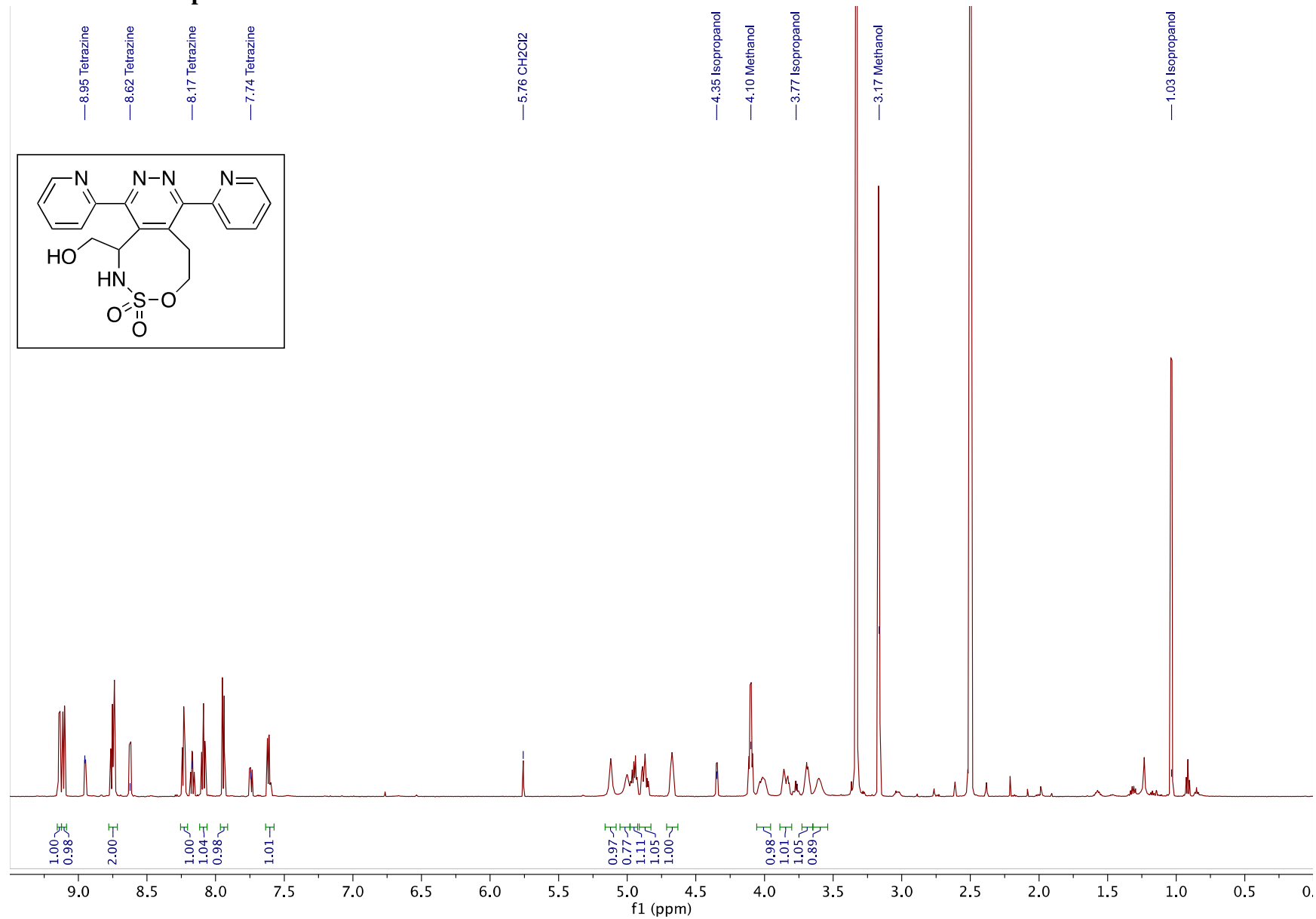
¹H NMR for Compound 2a.



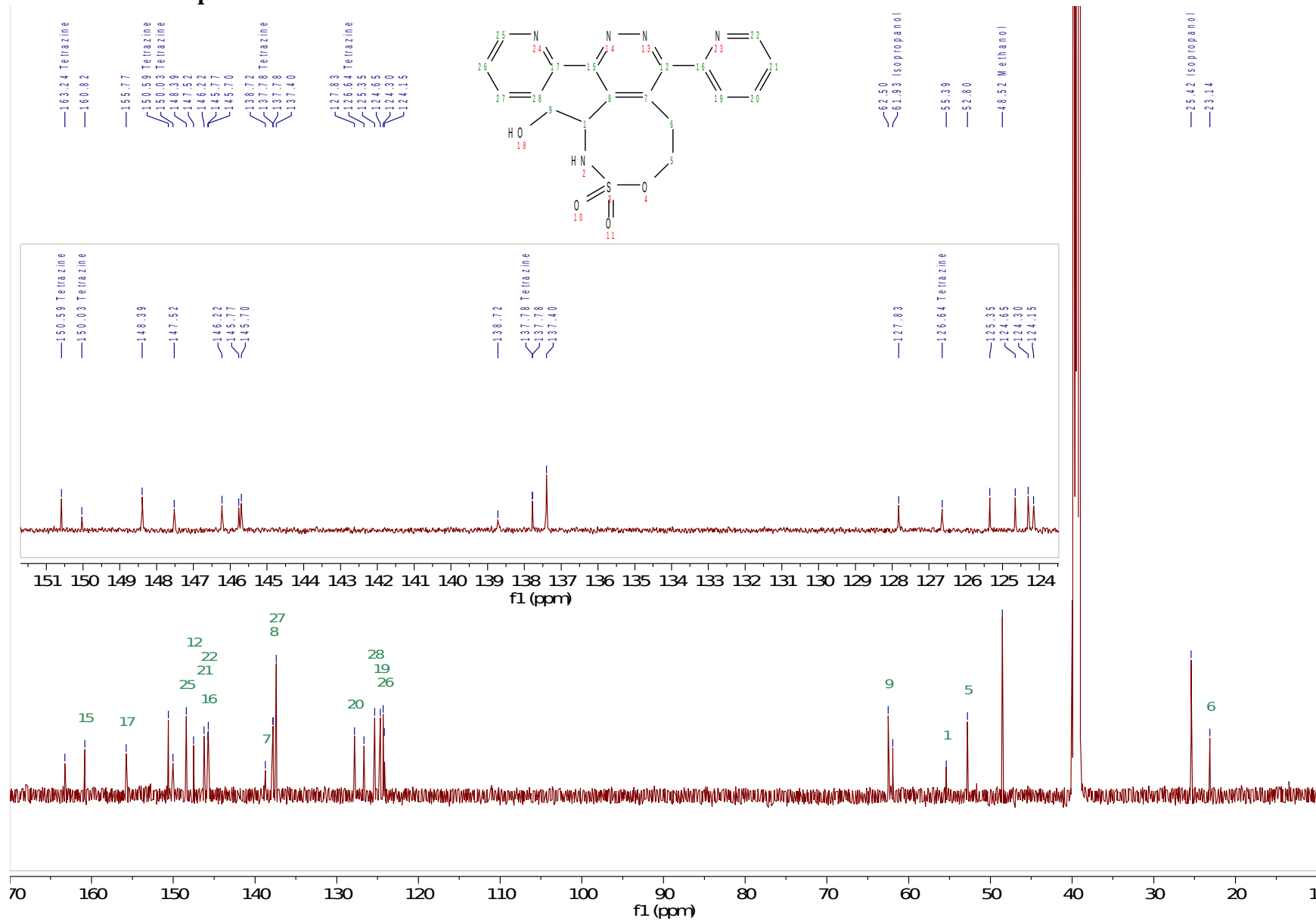
¹³C NMR for Compound 2a.



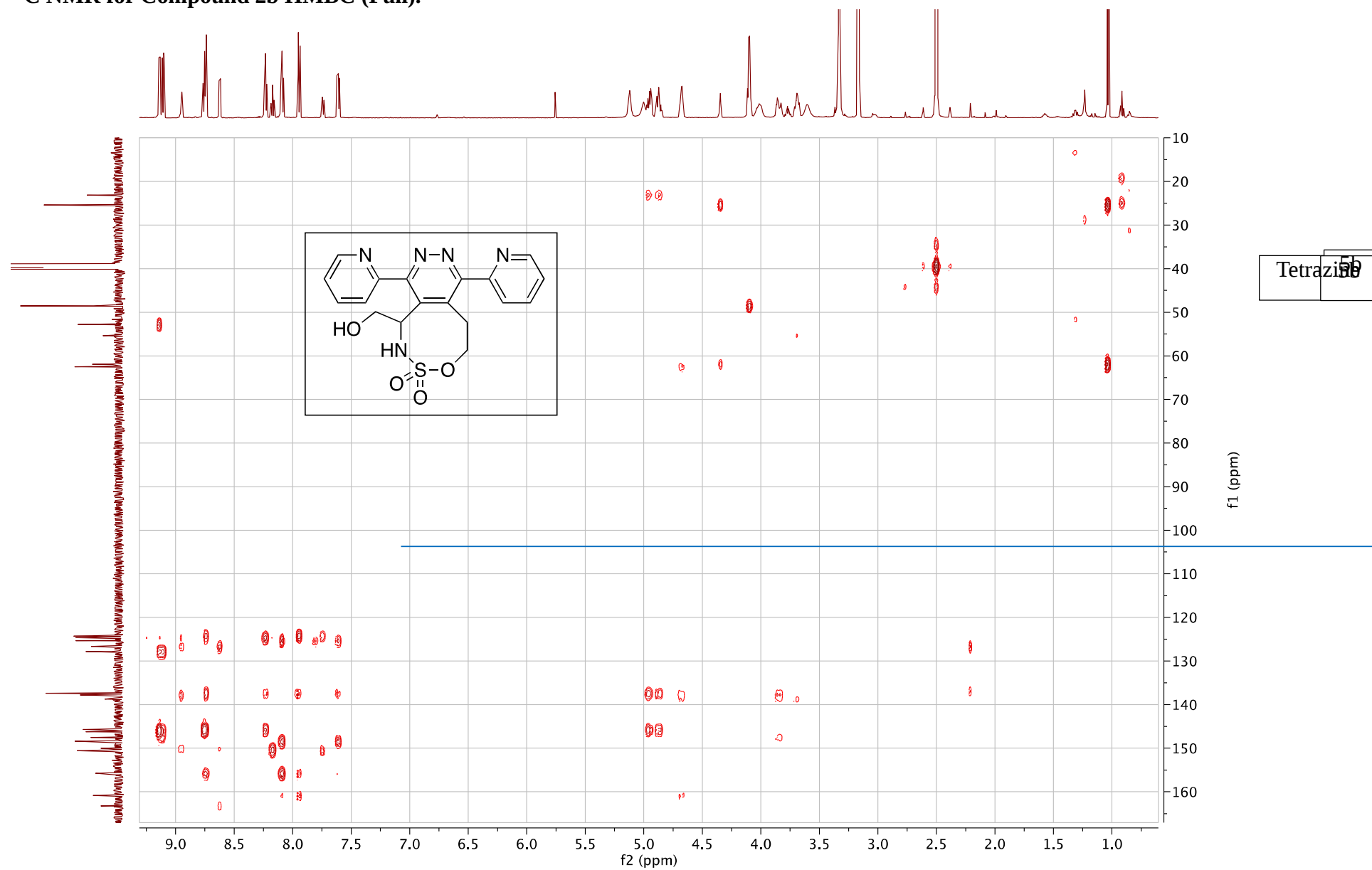
¹H NMR for Compound 2b.



¹³C NMR for Compound 2b.



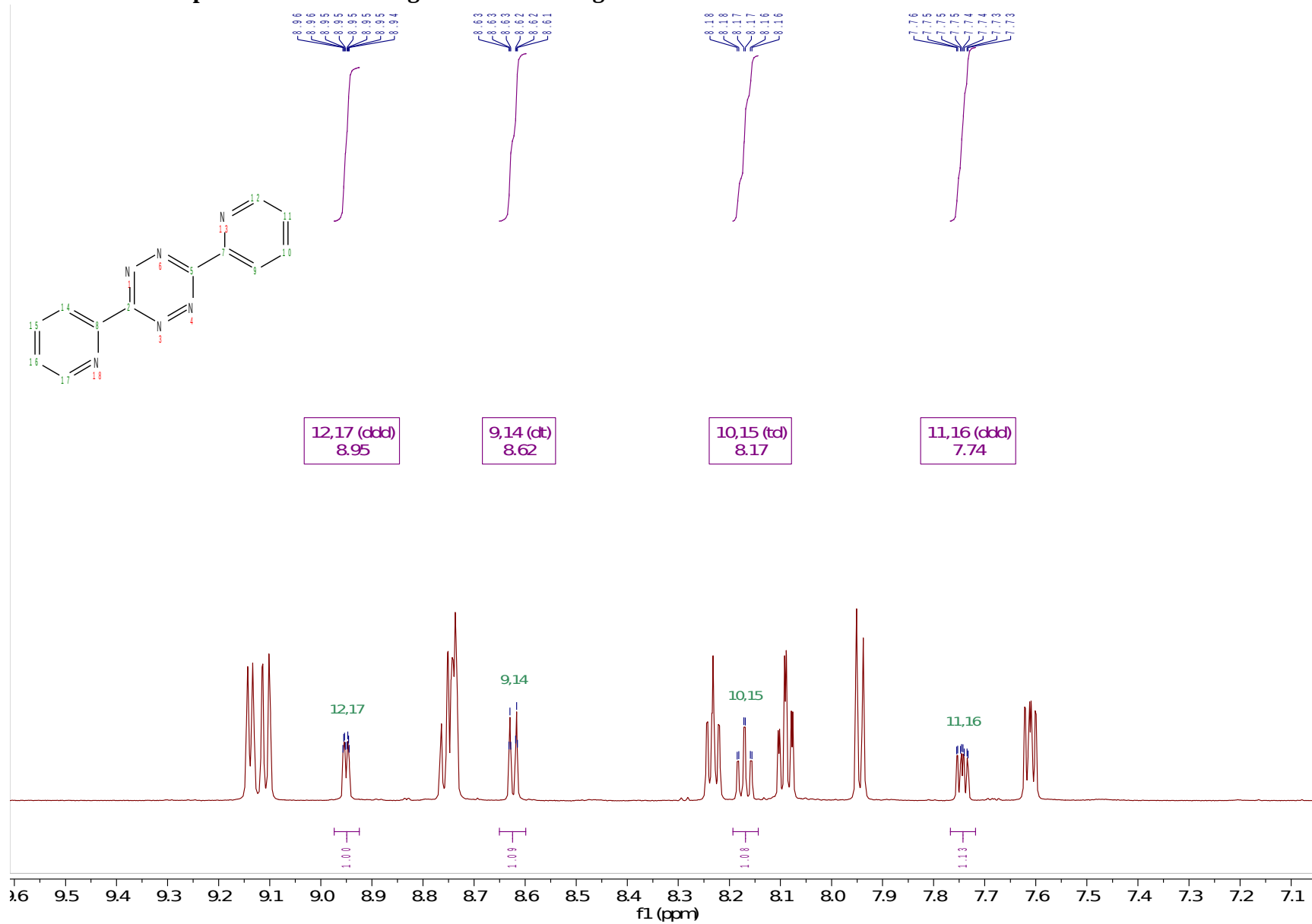
^{13}C NMR for Compound 2b HMBC (Full).



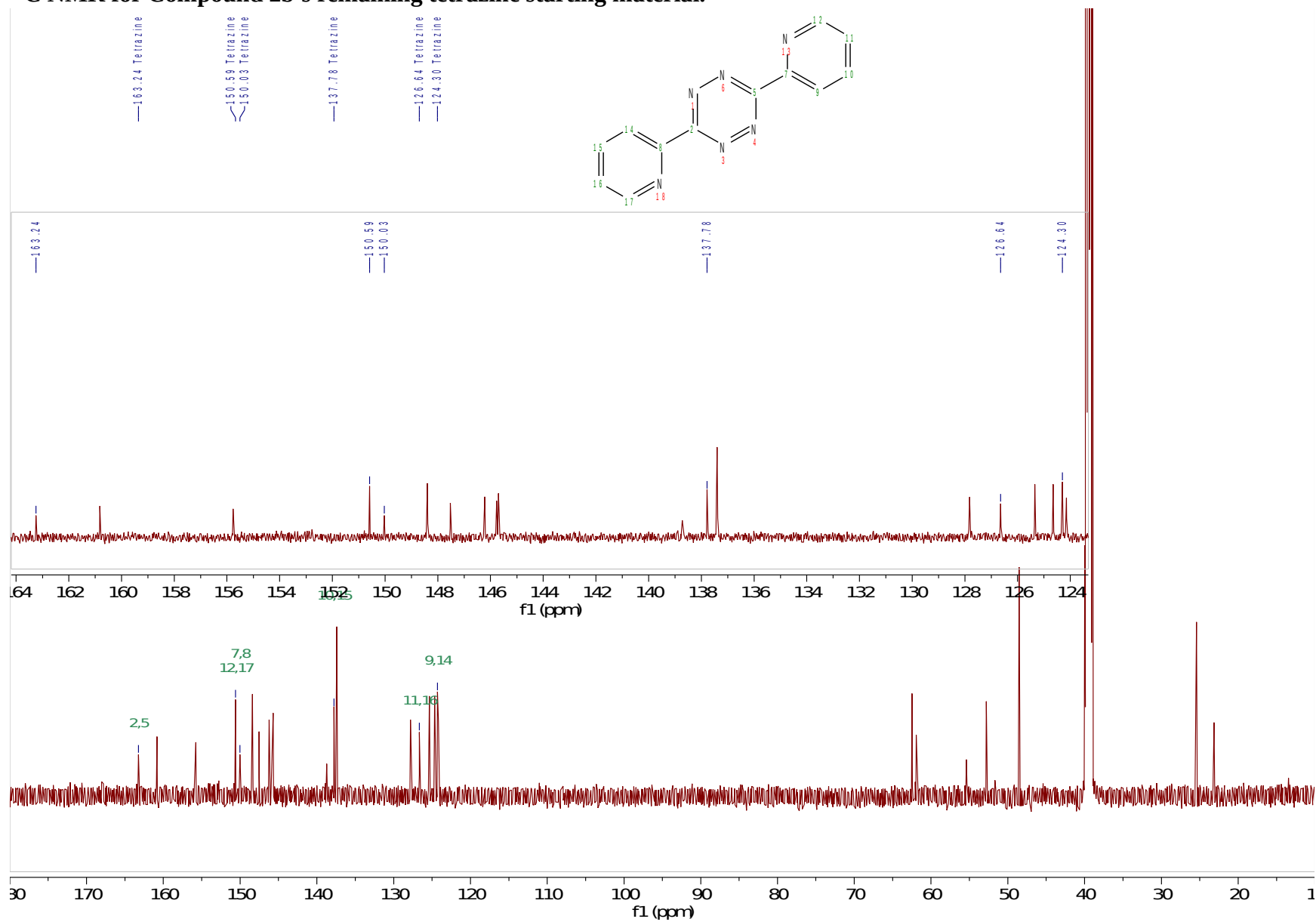
^{13}C NMR for Compound 2b HMBC (Zoom: Tetrazine and 2b overlap).



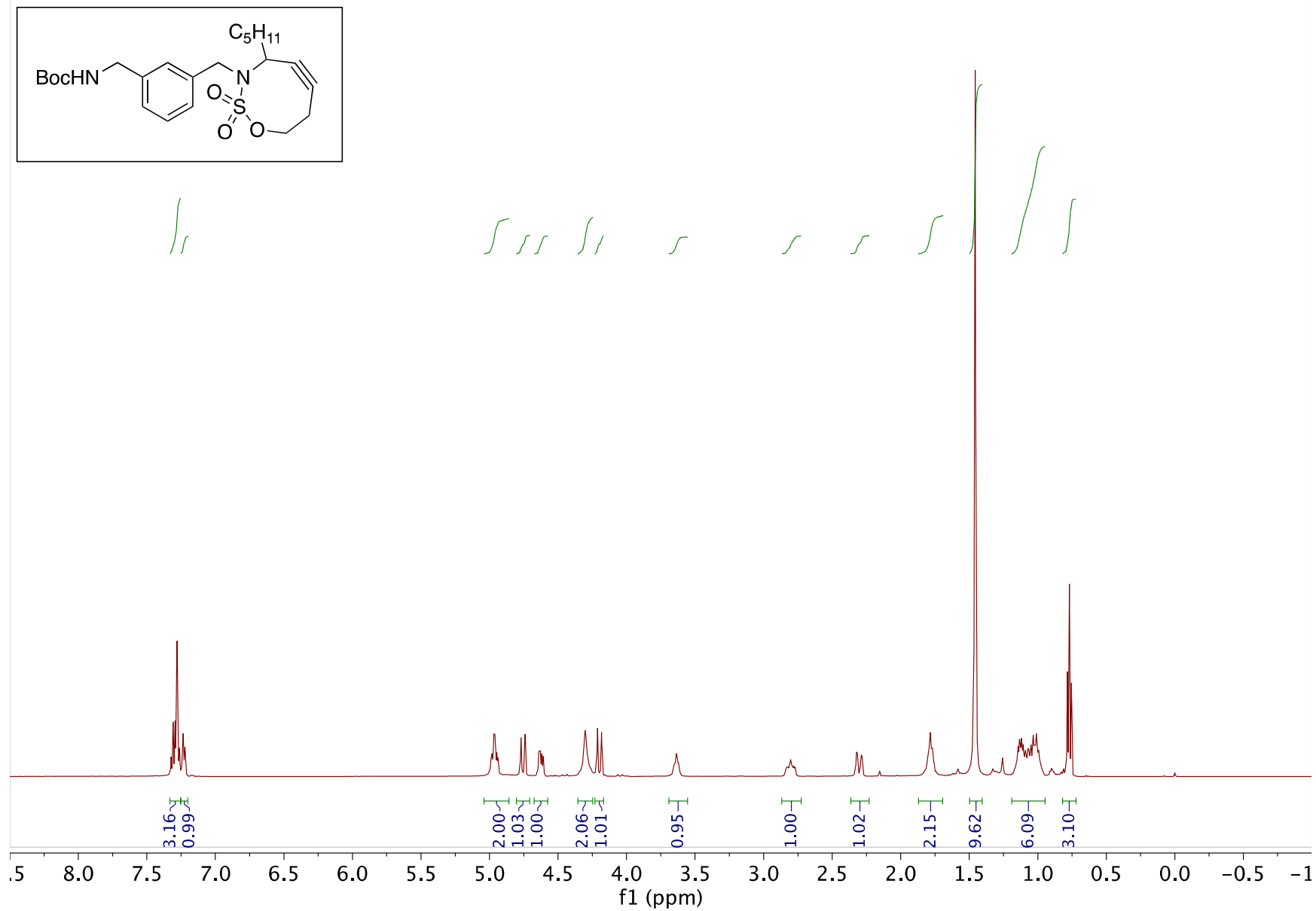
¹H NMR for Compound 2b's remaining tetrazine starting material.



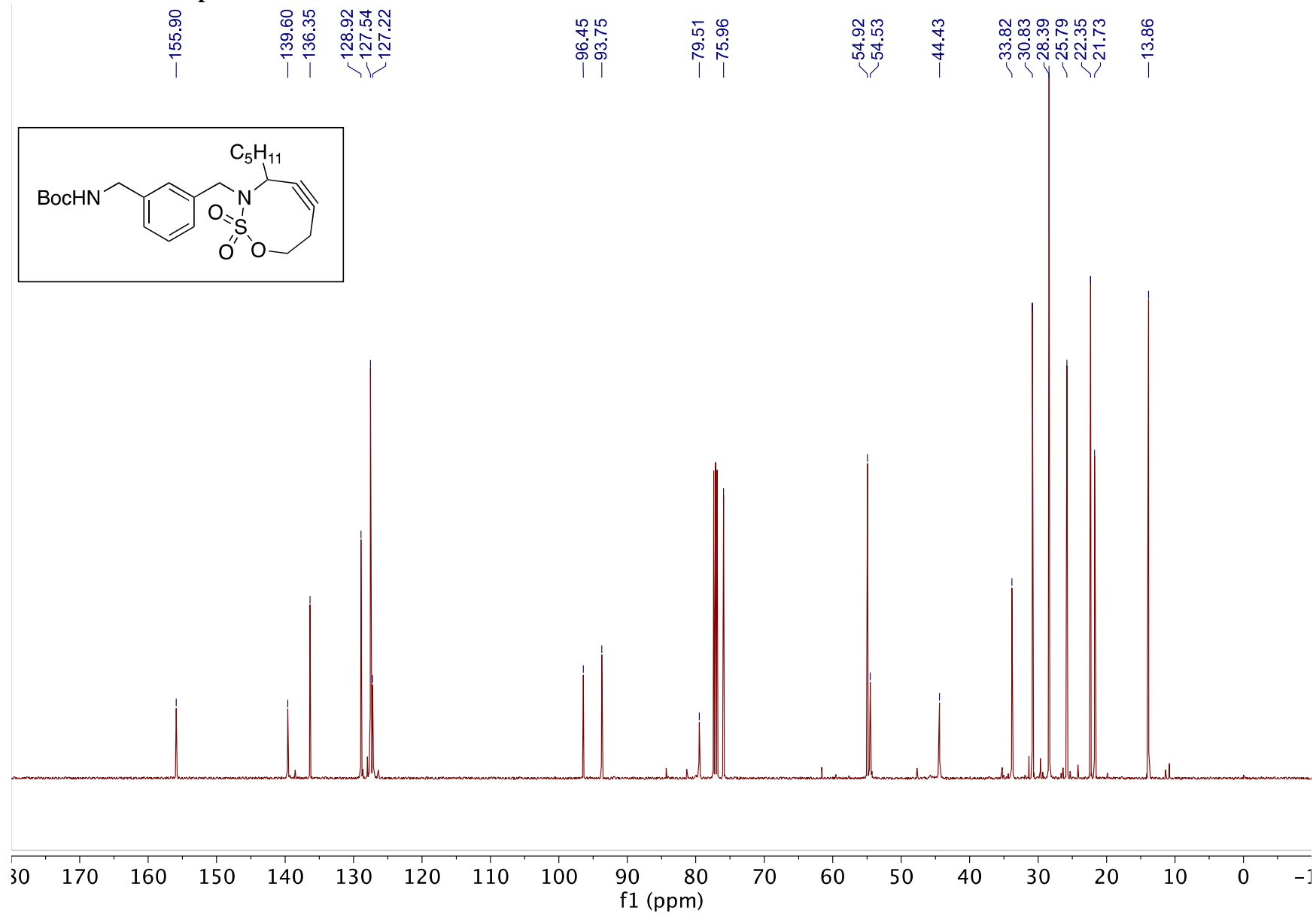
¹³C NMR for Compound 2b's remaining tetrazine starting material.



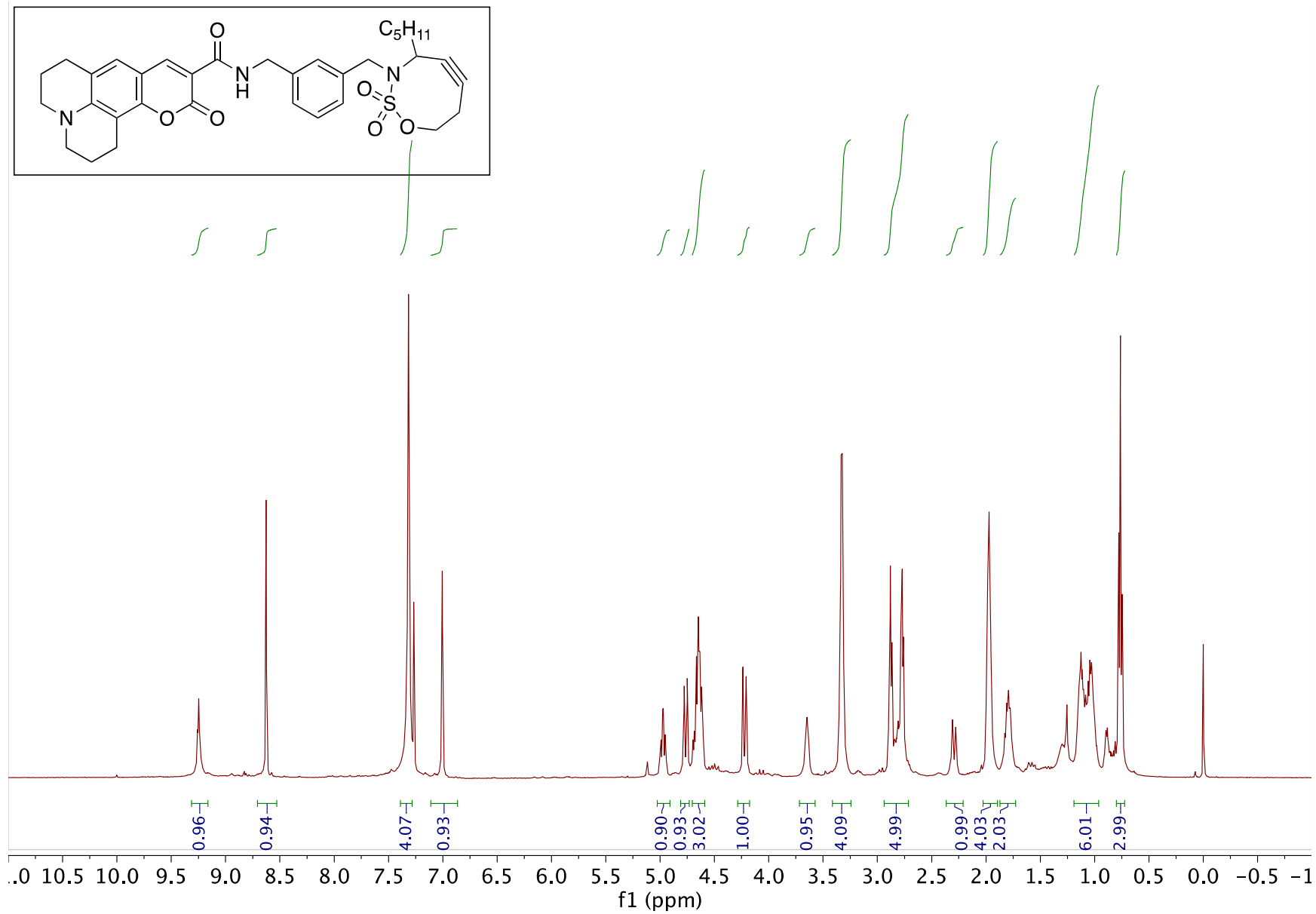
¹H NMR for Compound S6.



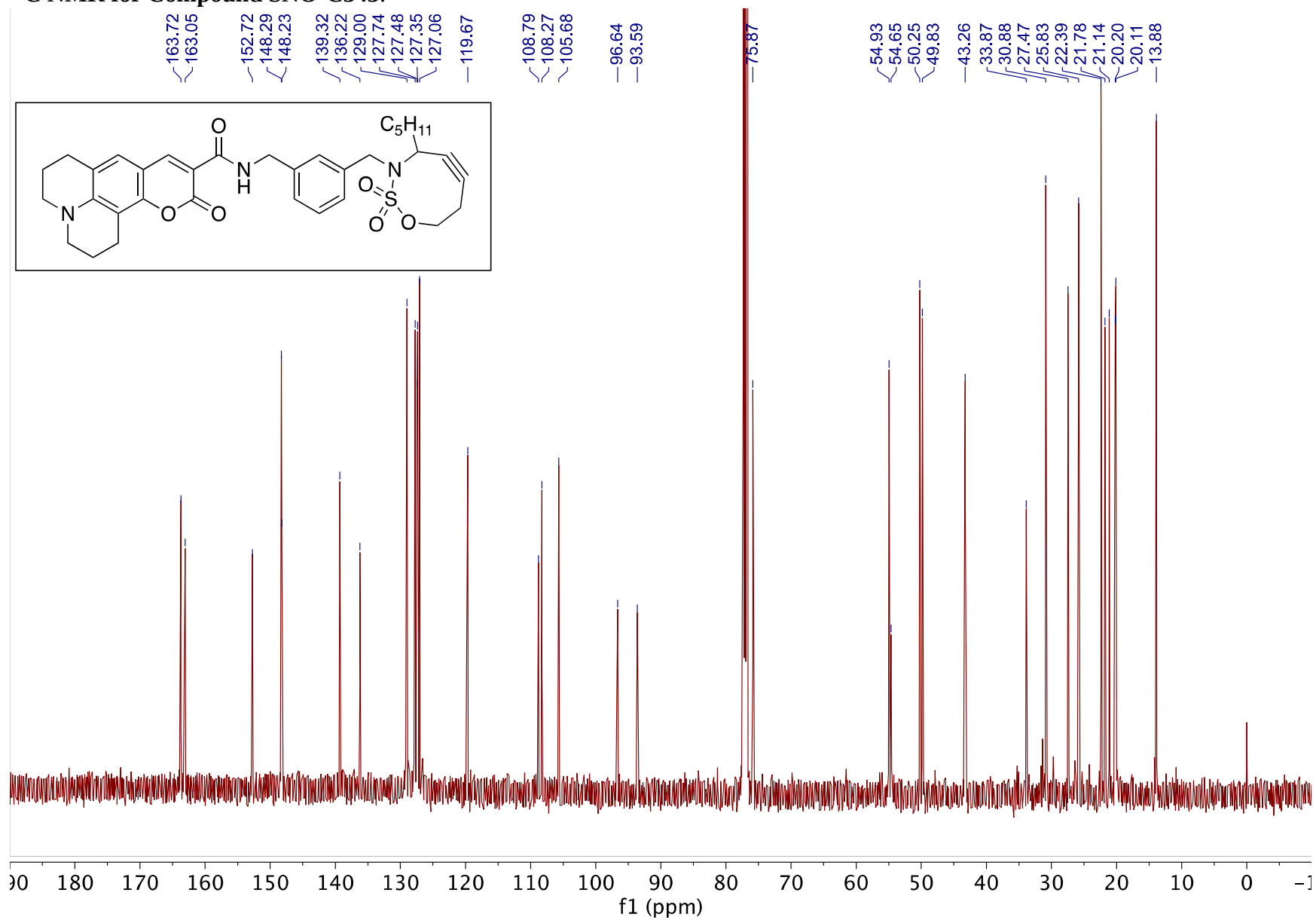
^{13}C NMR for Compound S6.



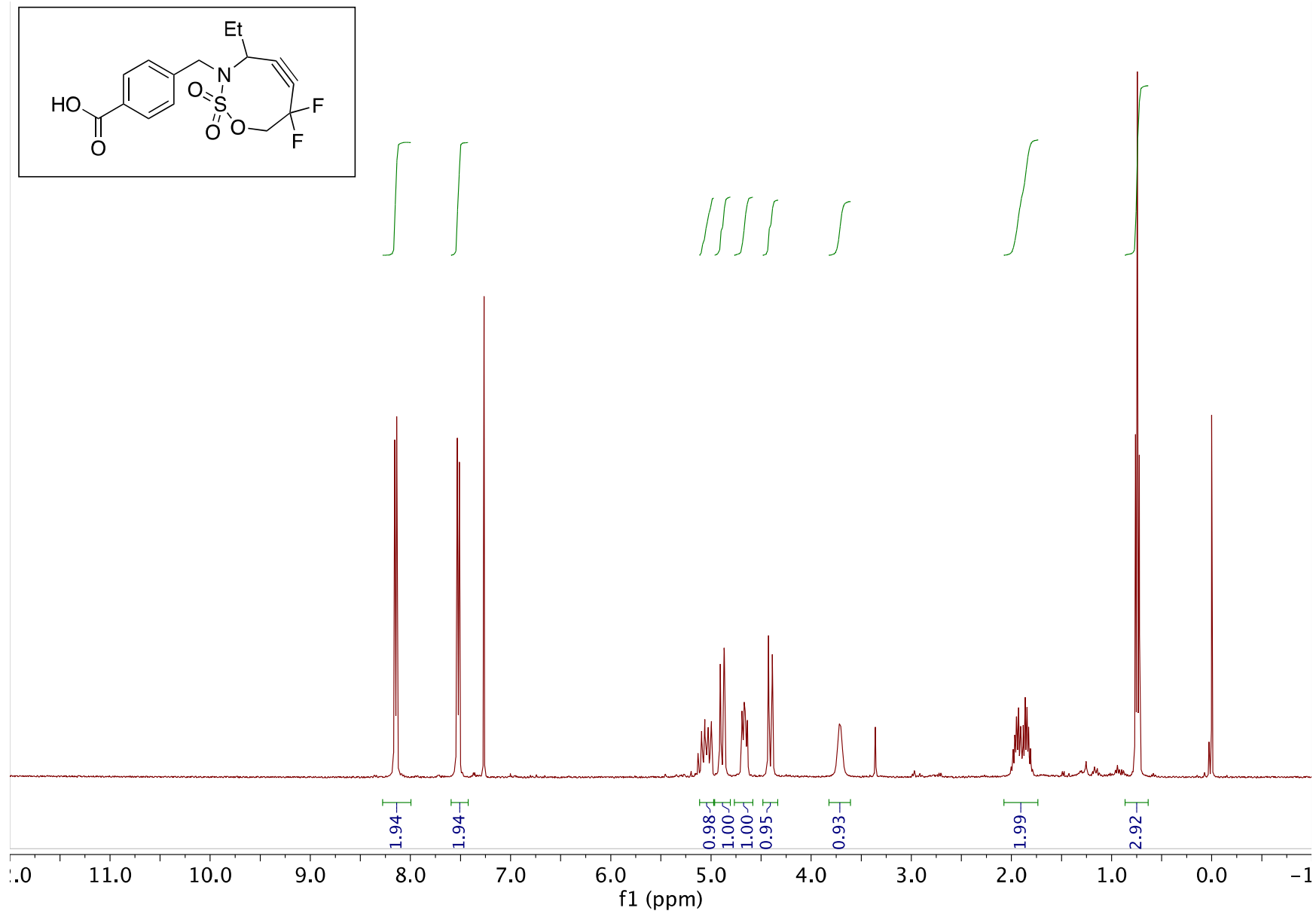
¹H NMR for Compound SNO-C343.



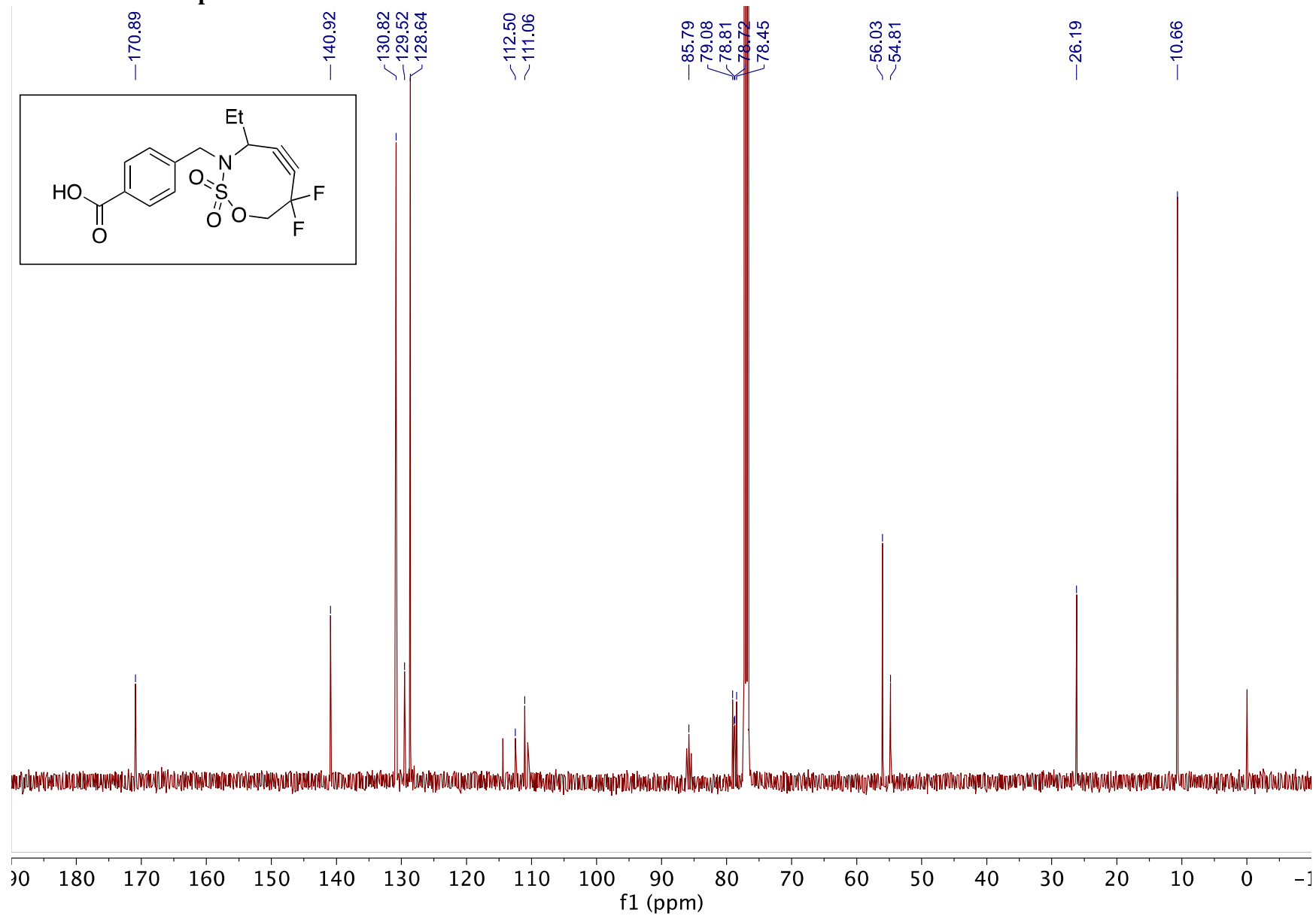
¹³C NMR for Compound SNO-C343.



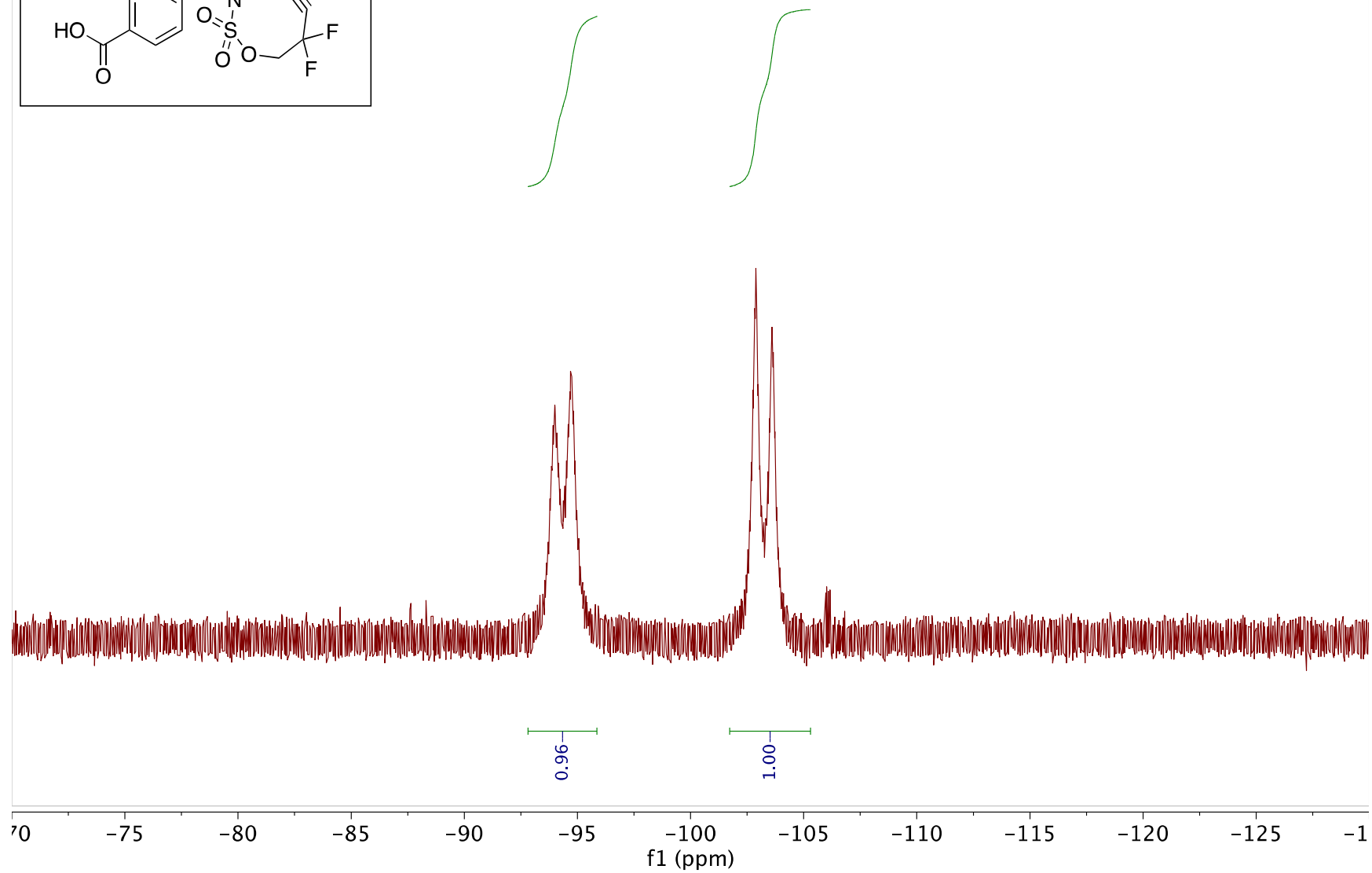
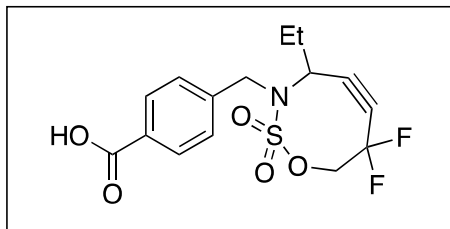
¹H NMR for Compound S7



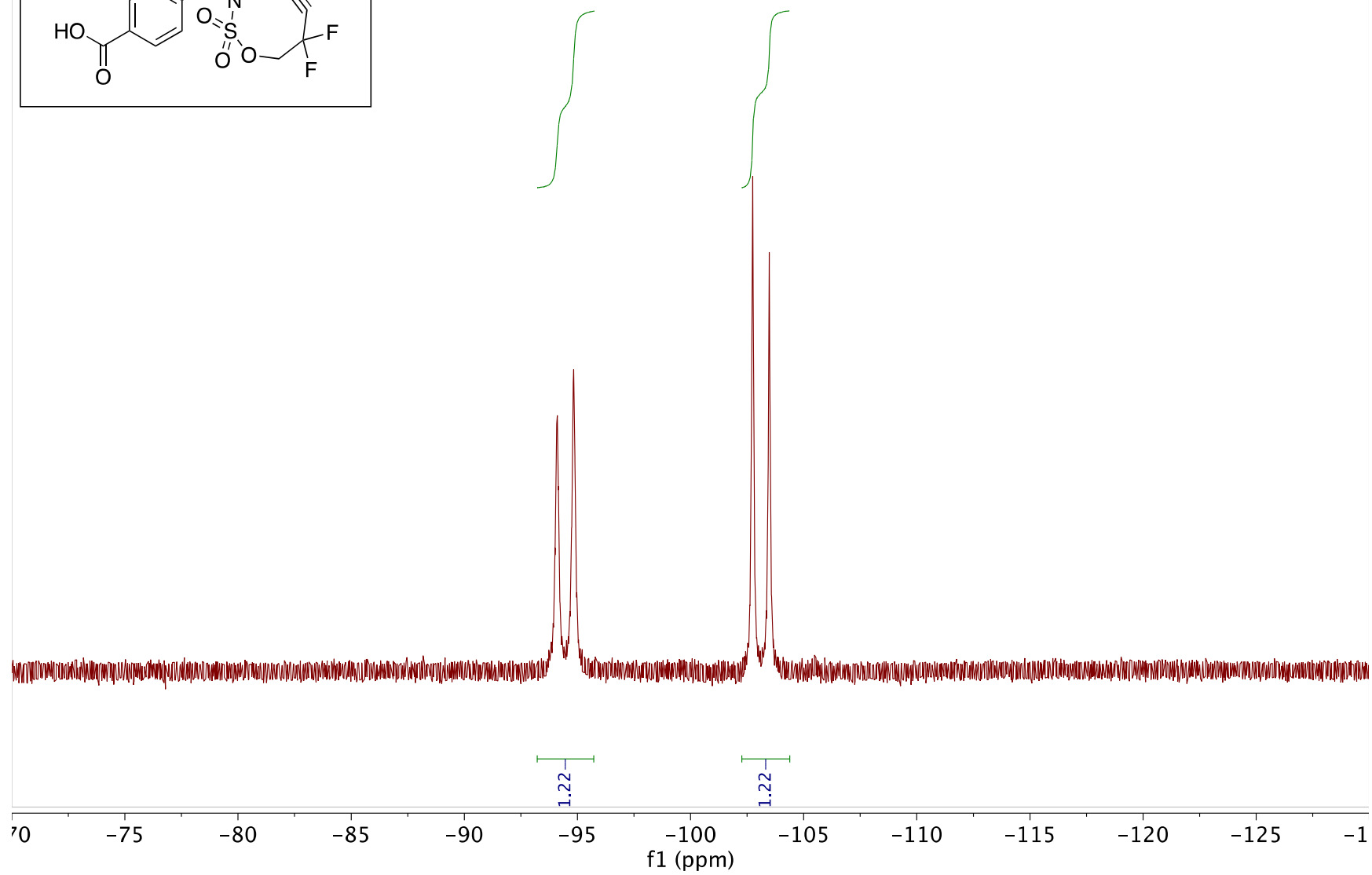
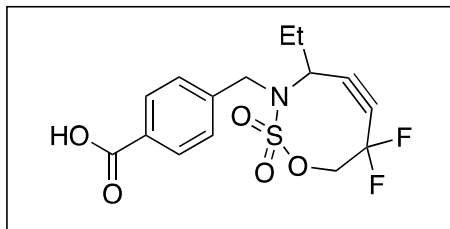
¹³C NMR for Compound S7



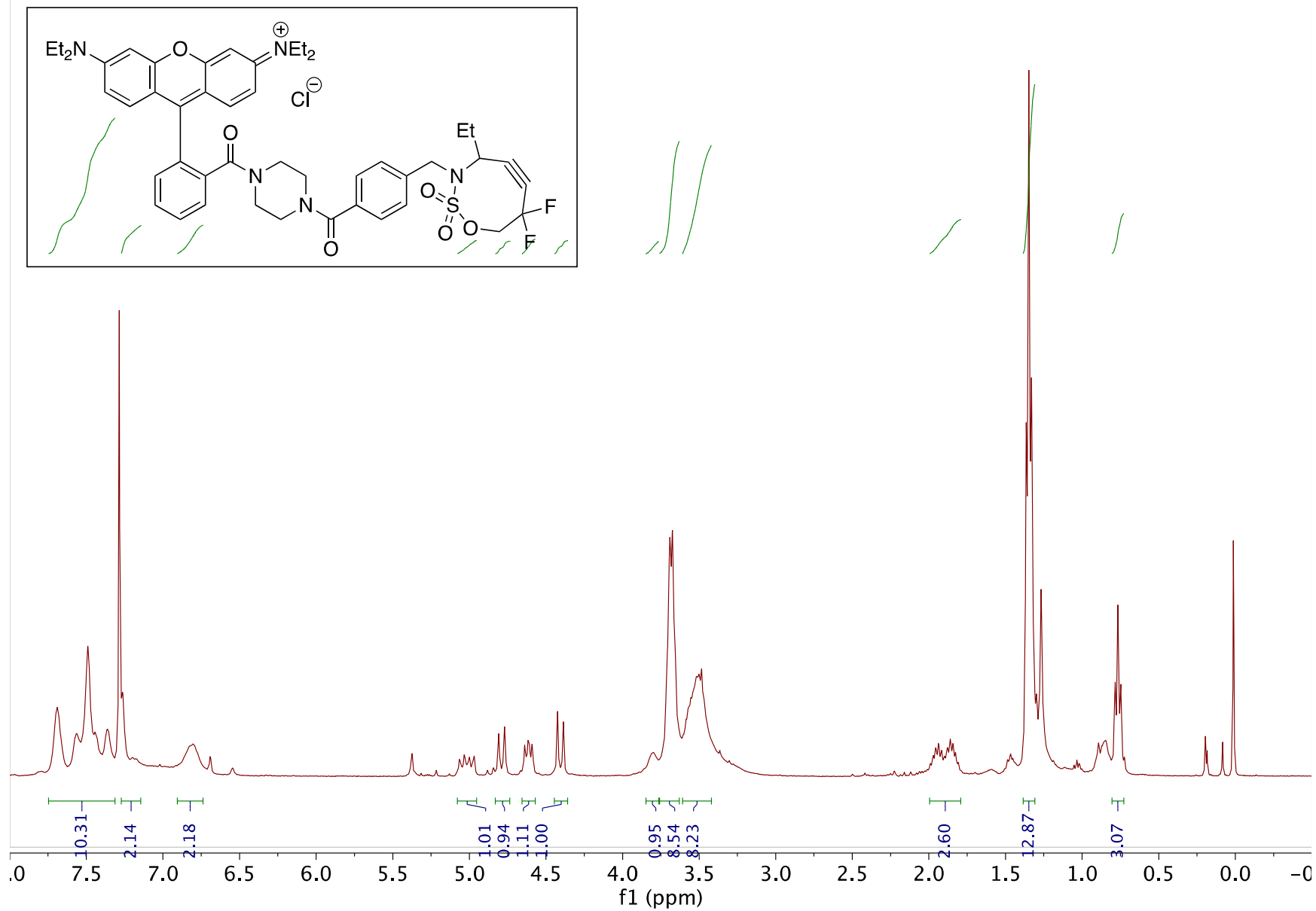
^{19}F NMR for Compound S7 (24°C)



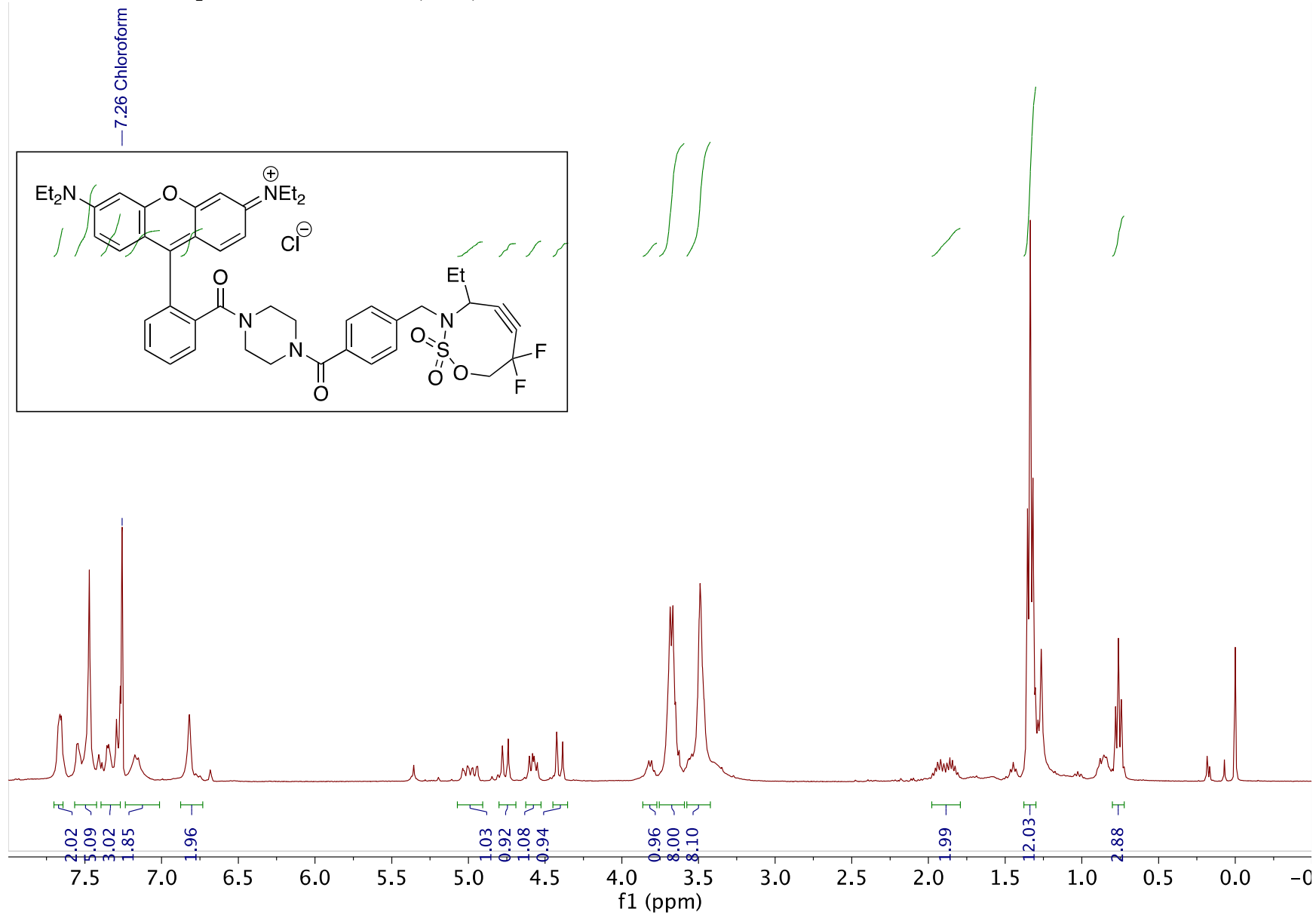
^{19}F NMR for Compound S7 (50°C setpoint)



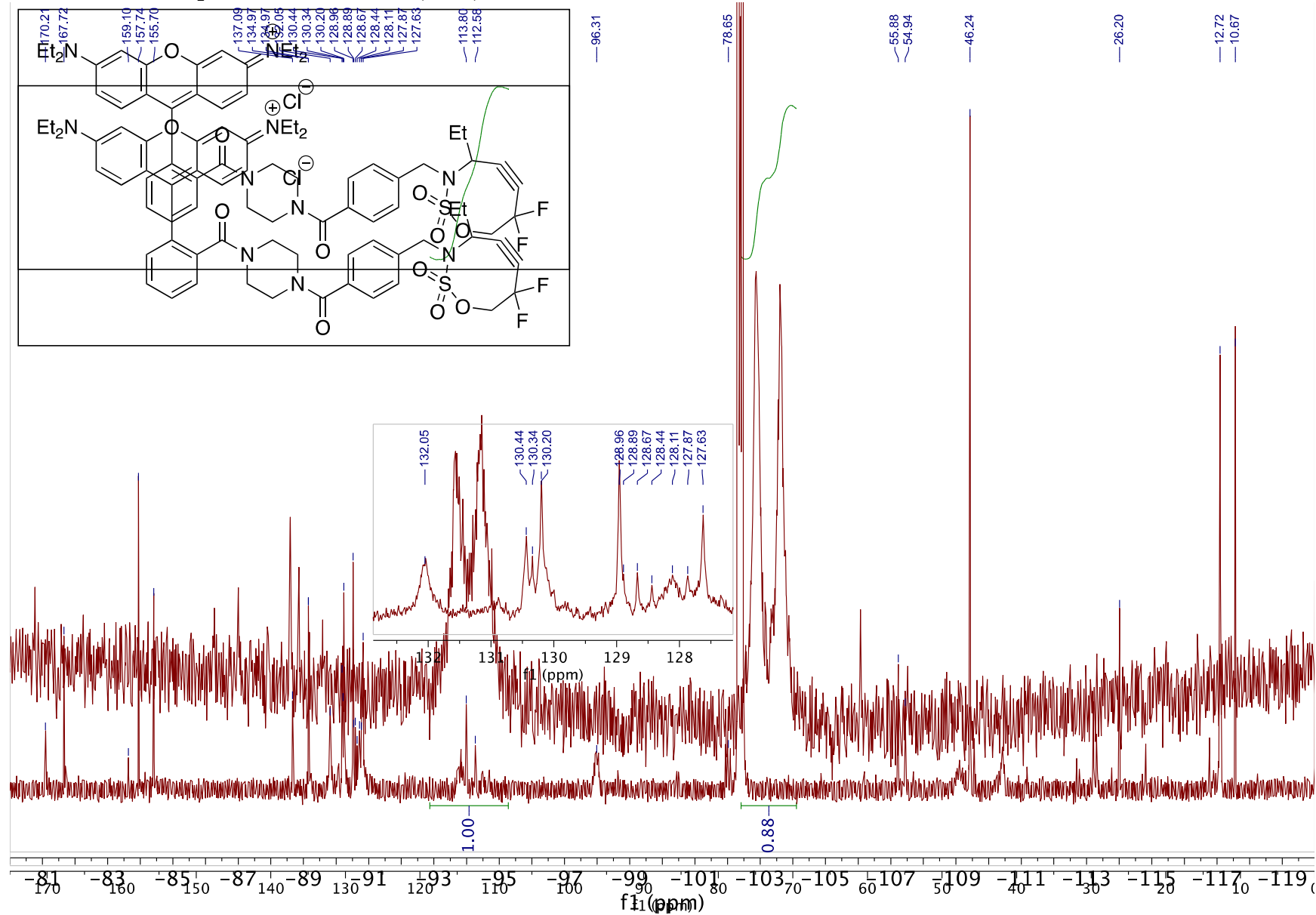
¹H NMR for Compound SNO-DF-Rho (24°C).



¹H NMR for Compound SNO-DF-Rho (55°C)



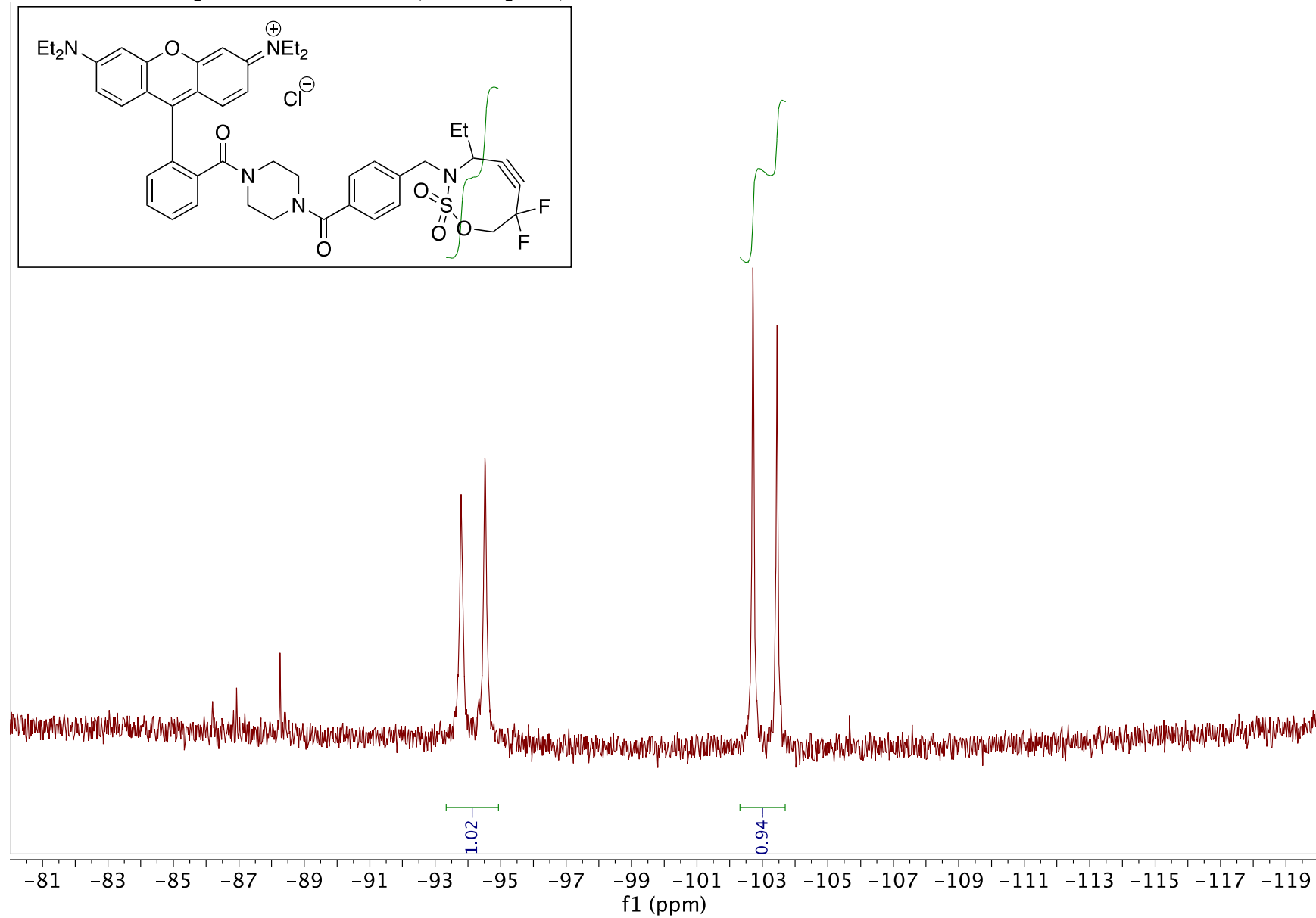
^{13}C NMR for Compound SNO-DF-Rho (24°C).



^{19}F NMR for Compound SNO-DF-Rho (24°C)

S2-100

^{19}F NMR for Compound SNO-DF-Rho (55°C setpoint)

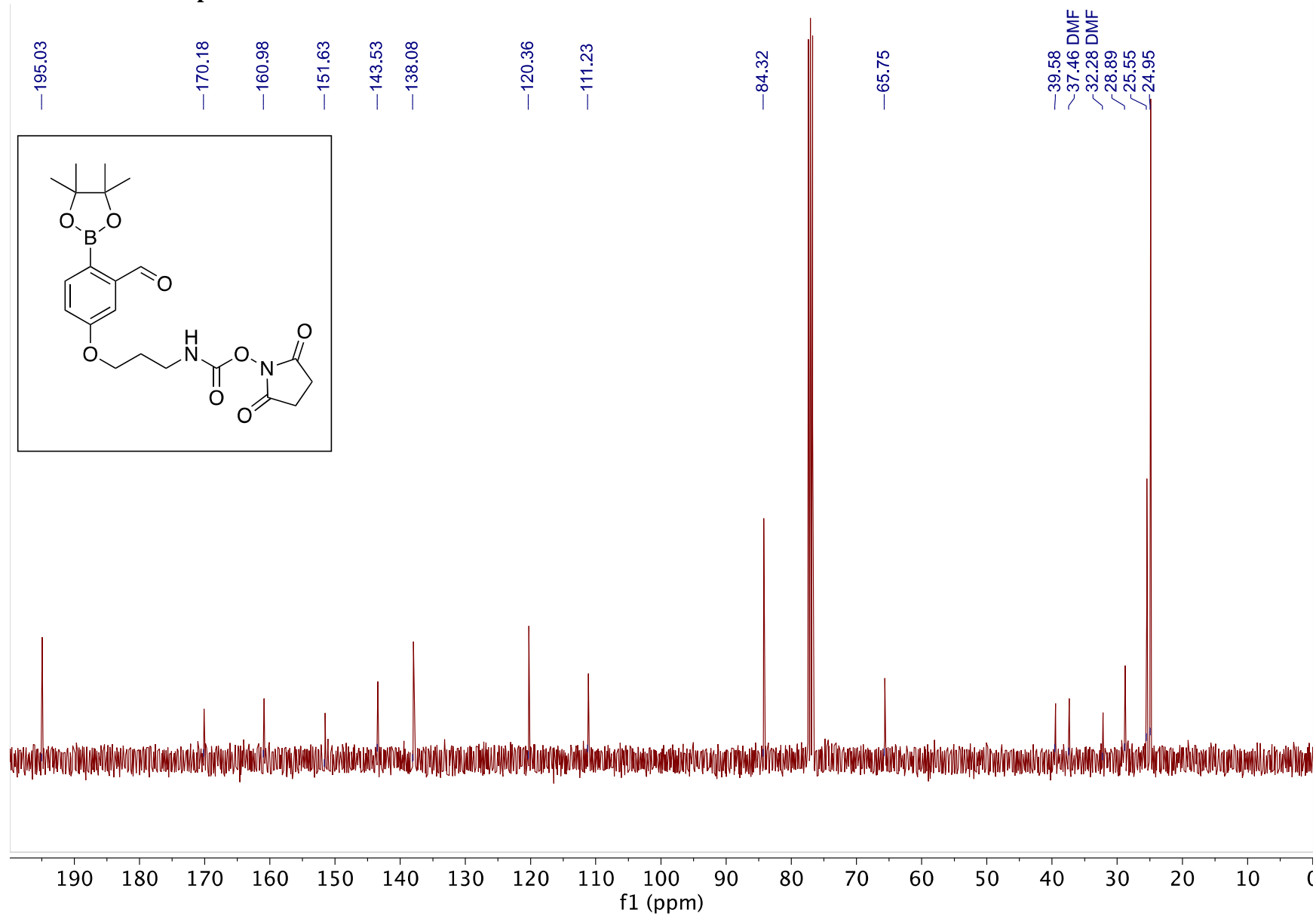


Chemical structure of compound 10 is shown in the inset. The structure consists of a 4-(4-(2,4,6-trimethyl-1,3,5-trioxane-2-yl)benzyl)phenyl group attached to a 2-oxo-1,3-dioxolane-5-carboxamide moiety.

¹H NMR spectrum (DMF-d₇) of compound 10. The x-axis represents the chemical shift in ppm (f1), ranging from -0.5 to 11.5. The spectrum shows several peaks, with integration values provided below the baseline. Key peaks are labeled with their chemical shifts and integration values:

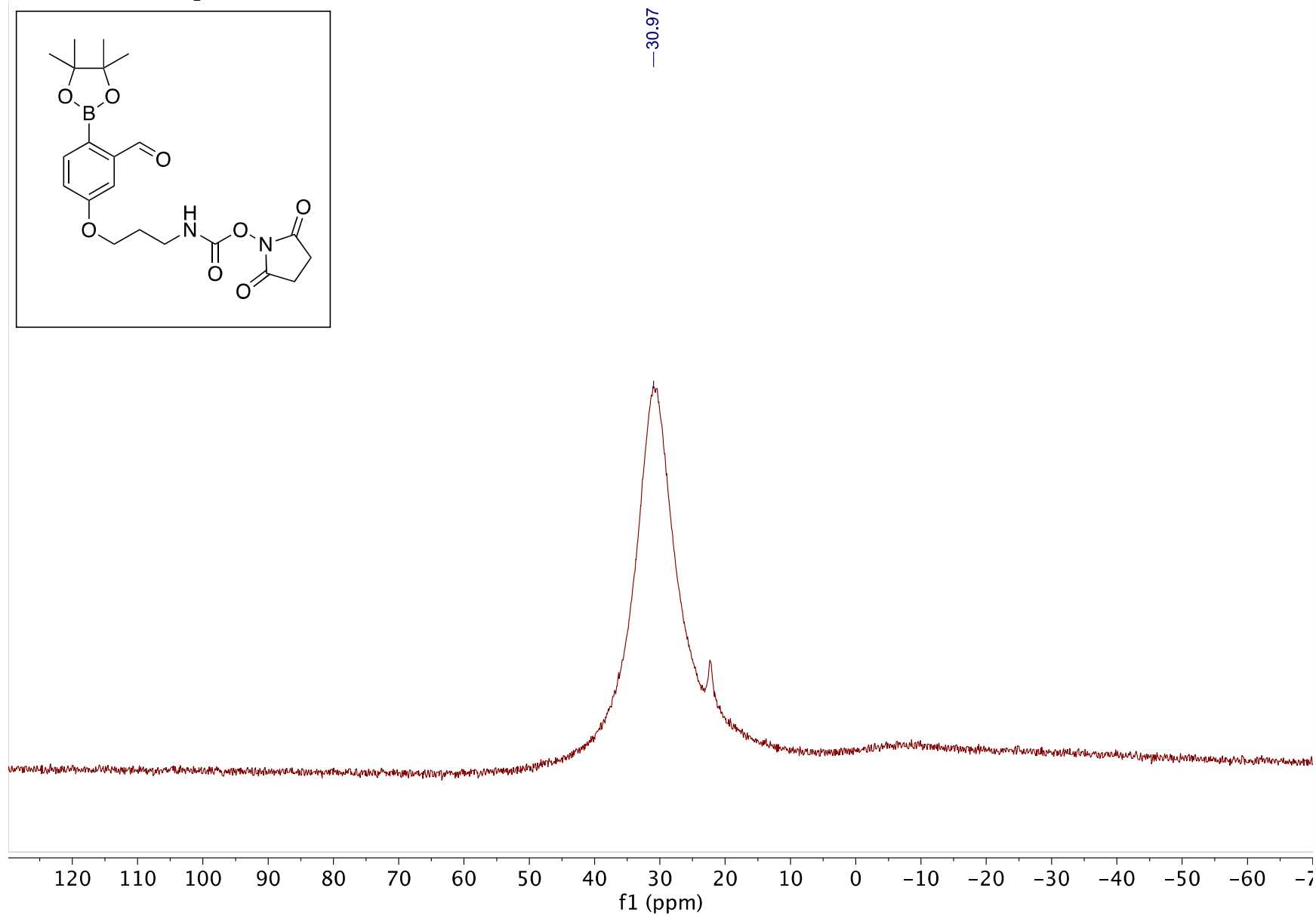
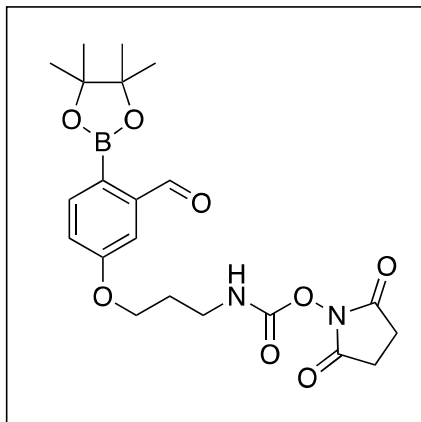
- 10.6 ppm (1.00)
- 8.0 ppm (0.80)
- 7.8 ppm (1.00)
- 7.5 ppm (1.01)
- 7.2 ppm (1.04)
- 5.7 ppm (0.98)
- 3.8 ppm (2.05)
- 3.5 ppm (2.02)
- 2.8 ppm (2.42, 2.40, 4.44)
- 2.5 ppm (2.51)
- 1.4 ppm (12.00)

¹³C NMR for Compound BE-NHS

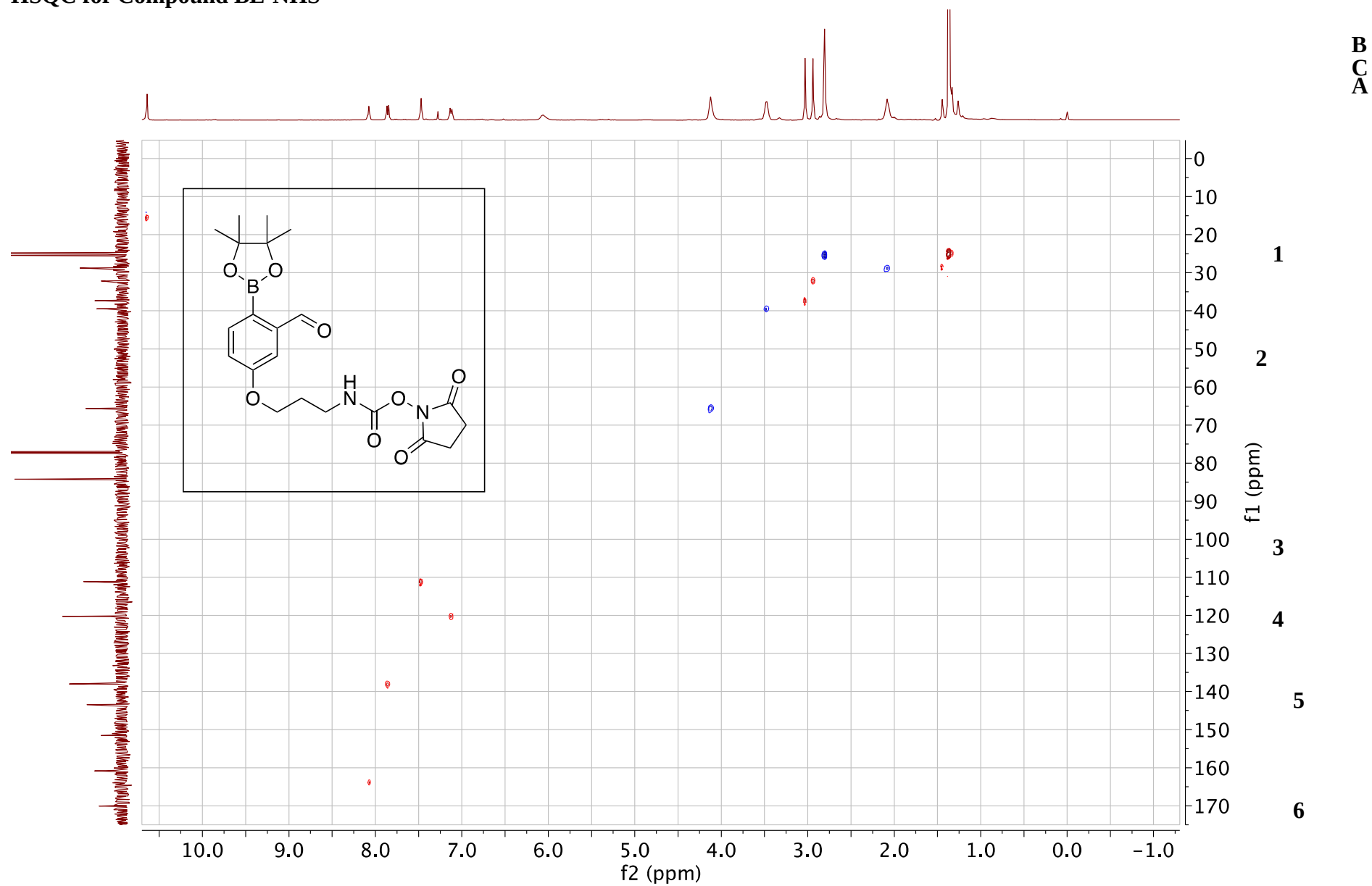


S2-103

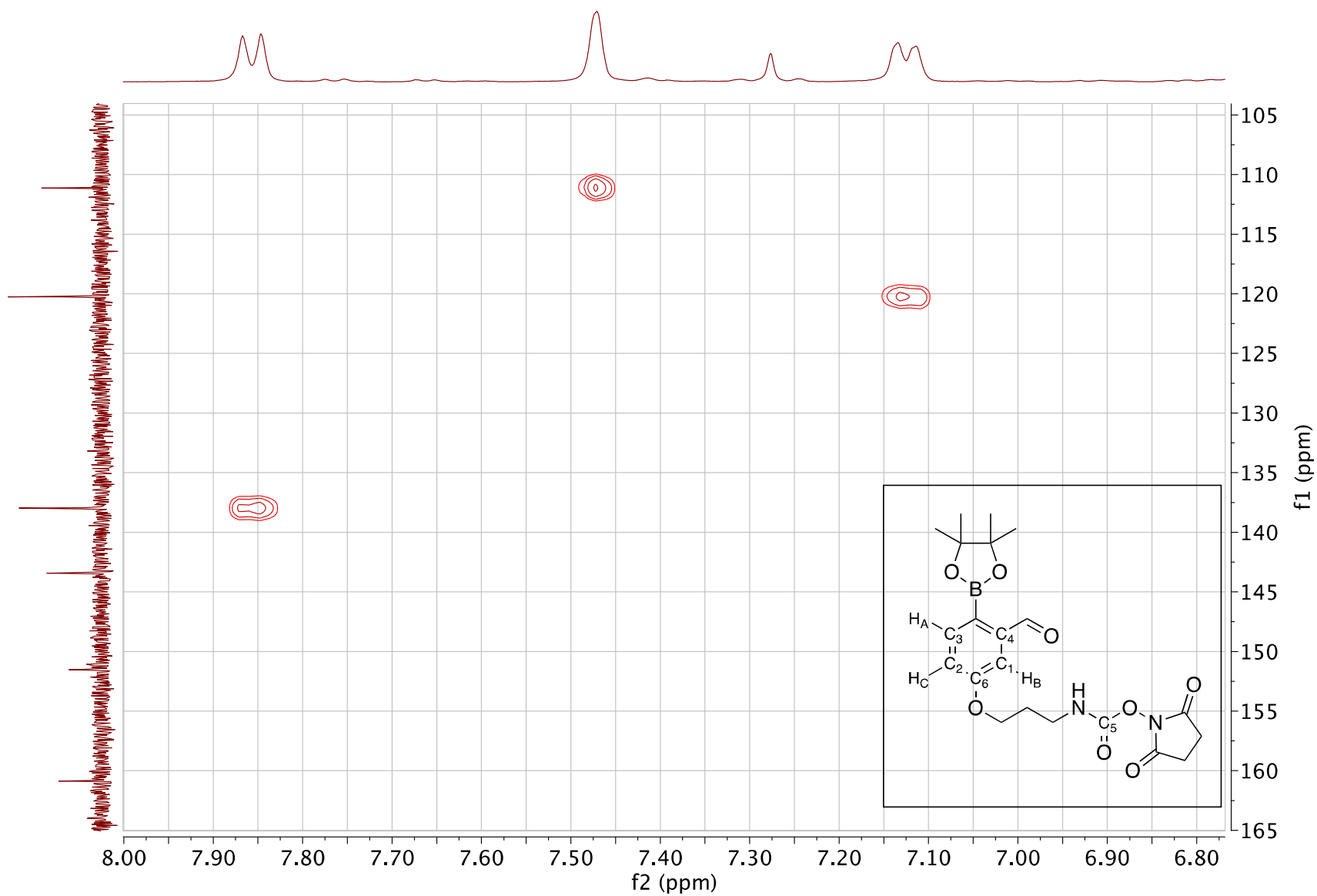
^{11}B NMR for Compound BE-NHS



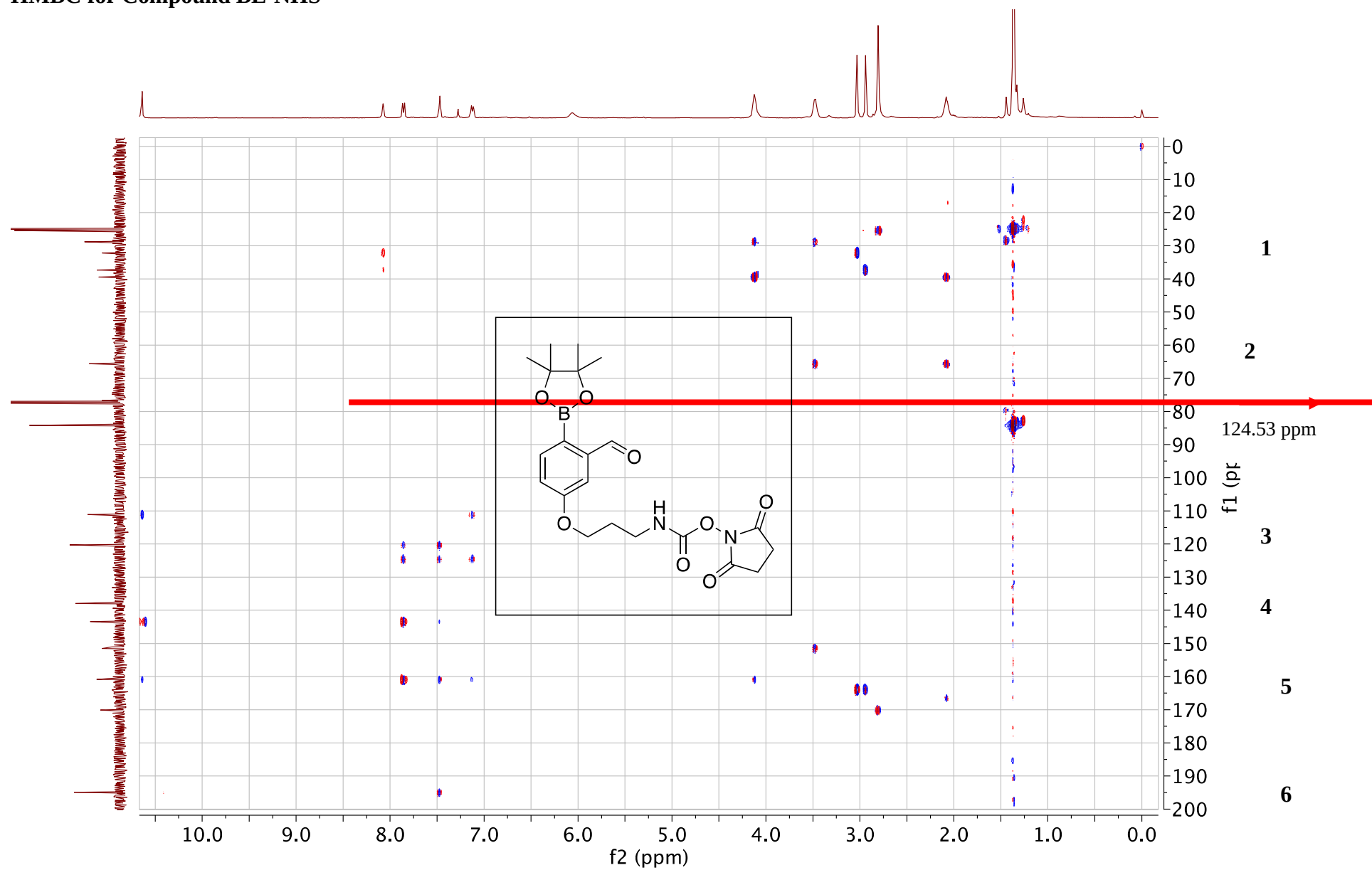
HSQC for Compound BE-NHS



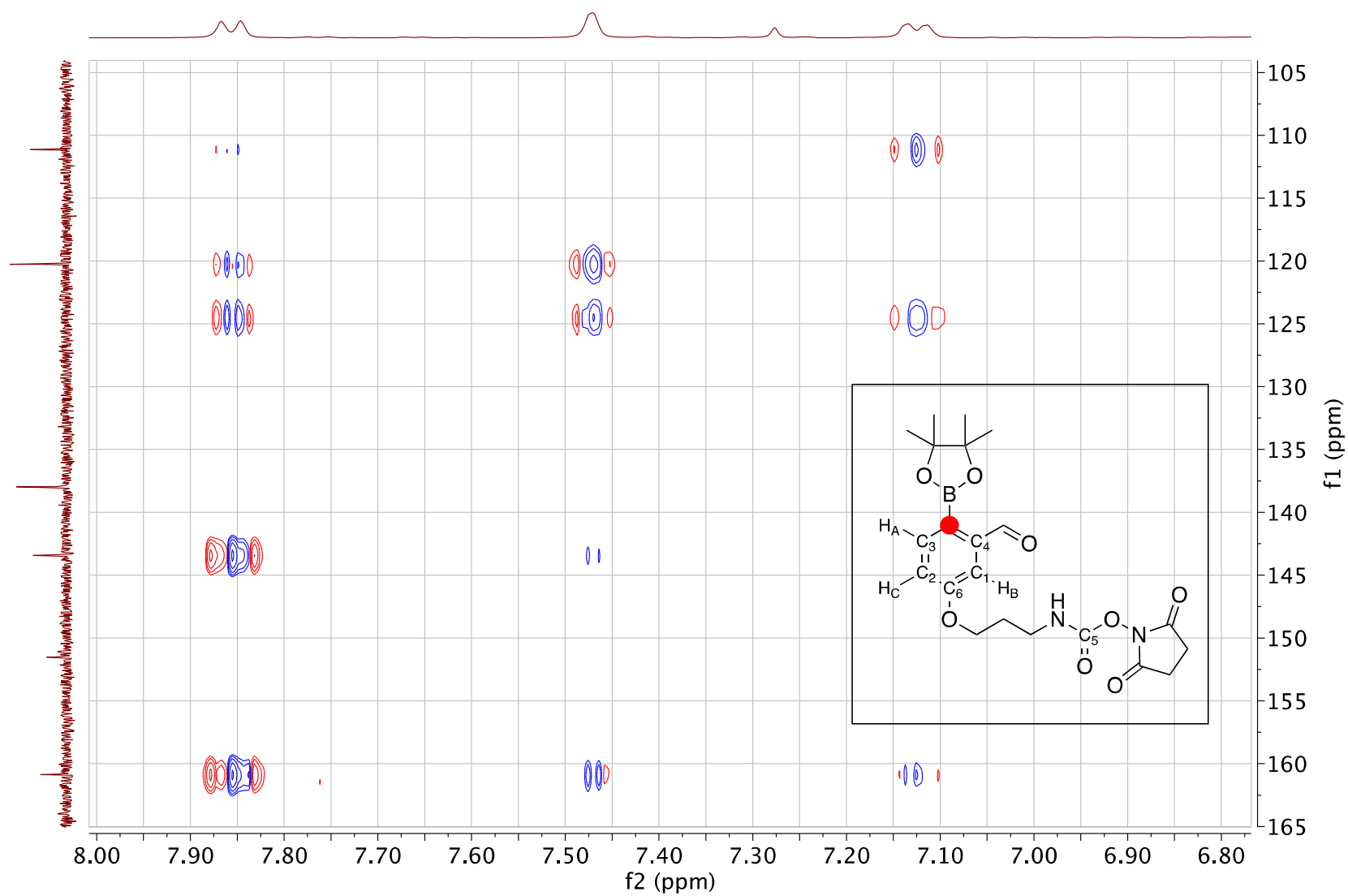
HSQC for Compound BE-NHS (Zoom)



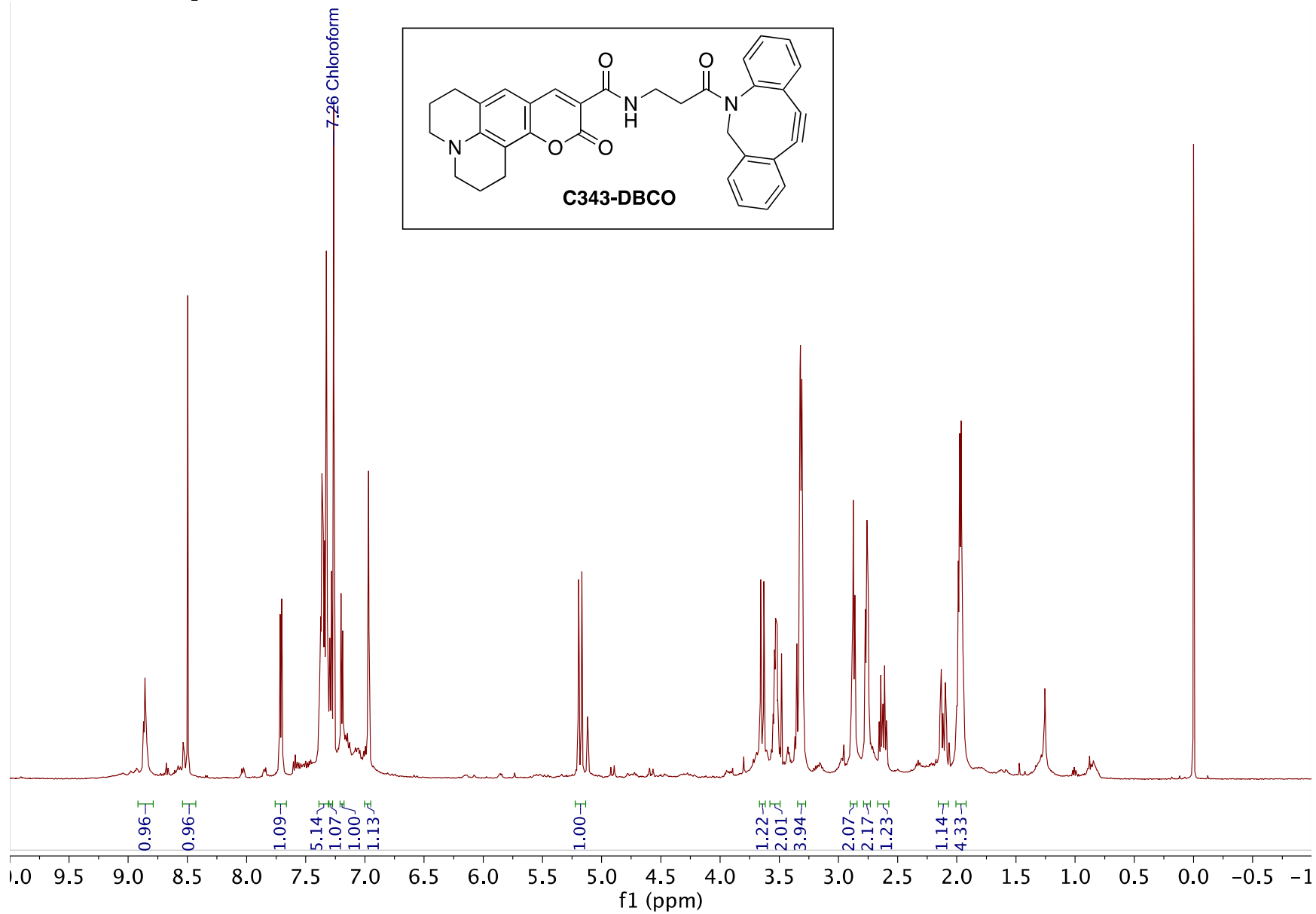
HMBC for Compound BE-NHS



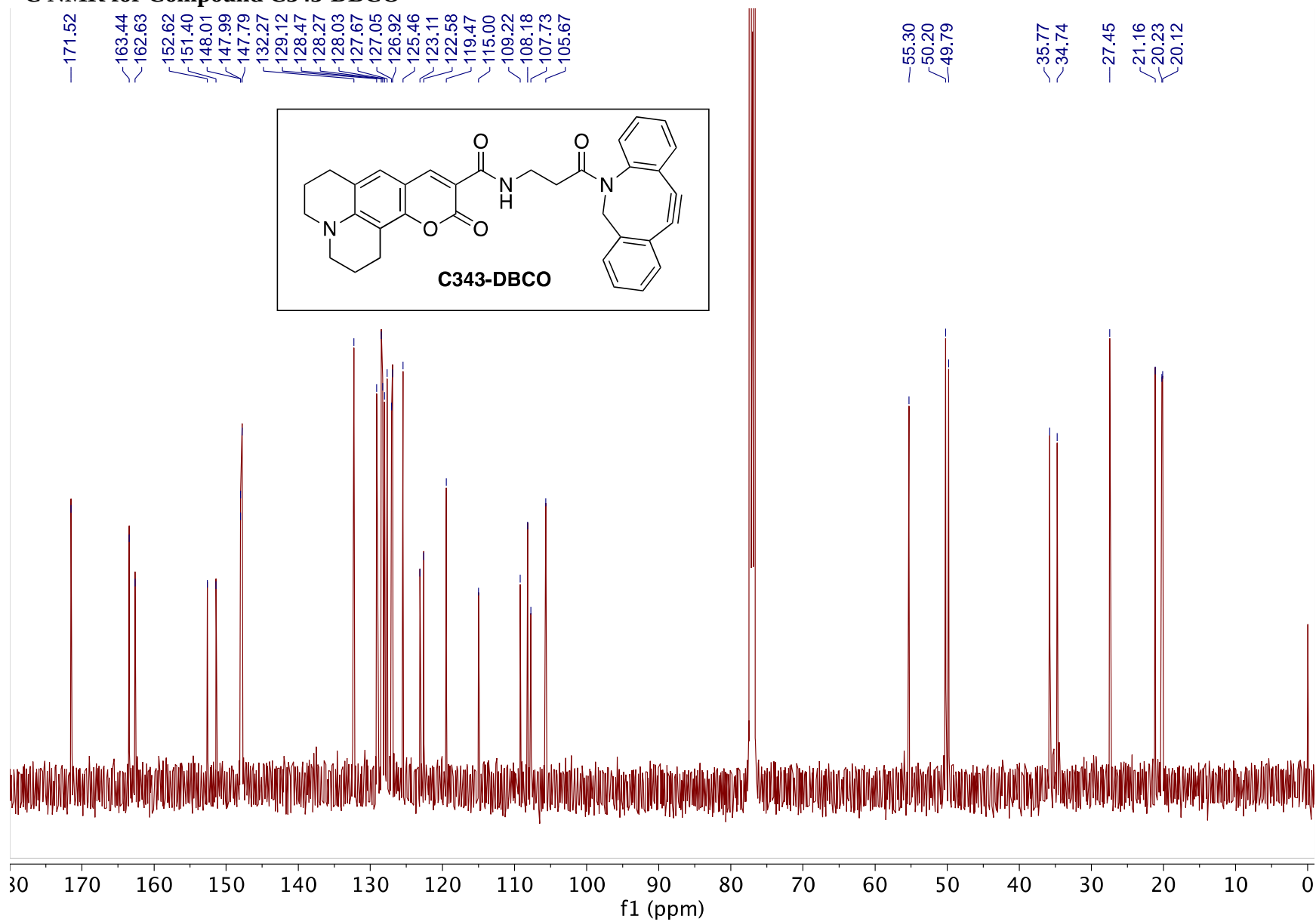
HMBC for Compound BE-NHS (Zoom)



¹H NMR for Compound C343-DBCO



¹³C NMR for Compound C343-DBCO



Triple, Mutually Orthogonal Cycloadditions Through the D... (25.71 MiB) [view on ChemRxiv](#) • [download file](#)
